Characterizing the Metabolic Fate of (2*S*, 4*R*)-4-[^{18}F]fluoroglutamine and its Applications in Cancer Imaging and Treatment Response Monitoring

NHAT THANH NGUYEN

Thesis submitted for the degree of

Doctor of Philosophy

of the

University of London

The Institute of Cancer Research

October 2020

Declaration

I, Nhat Thanh Nguyen, confirm that the work presented in this thesis is my own.

Date: 01/10/2020

Abstract

Glutaminolysis is a crucial pathway to provide the nitrogen source in addition to the carbon source from the glycolysis pathway for proliferating cells. (2S, 4R)-4-[^{18}F]fluoroglutamine (4-[^{18}F]fluoroglutamine) is potentially useful for Positron Emission Tomography (PET) imaging glutamine metabolism of cancer *in vitro* and *in vivo*. Despite initial promising results, including clinical trials, further metabolic characterisation of this probe is required to fully understand the metabolic fate of 4-[^{18}F]fluoroglutamine in cancer cells.

The overall aims of this project are to characterise the metabolic fate of 4-[^{18}F]fluoroglutamine, to investigate whether it can be used as a non-invasive PET imaging method for [^{18}F]FDG undetected tumours or for patients who have difficulty with the fasting requirement of [^{18}F]FDG and to apply 4-[^{18}F]fluoroglutamine for the monitoring of glutamine uptake changes in cancer following therapeutic strategies dual mTORC1/2 inhibitor AZD2014 and Paclitaxel, or Cdk2 kinase inhibitor CYC065.

In this study, we employed the stable isotope version of this PET tracer and [^{19}F]-Magnetic Resonance Spectroscopy (^{19}F-MRS) to evaluate the metabolic fate of the 4-[^{18}F]fluoroglutamine PET tracer. Similar to L-glutamine metabolism, glutaminase inhibition significantly increased the cellular 4-[^{19}F]fluoroglutamine concentration and decreased the cellular level of 4-[^{19}F]fluoroglutamate. Following alanine aminotransferase inhibition, the cellular concentration of 4-[^{19}F]fluoroglutamate increased in a similar way as L-glutamate. However, the rate of free F^- secretion increased, which is contrary to the hypothesis of the study. Therefore, this study proved that the metabolism of the 4-[^{18}F]fluoroglutamine PET tracer follows the same pathway as L-glutamine in cancer cells. There are more than one pathway for the defluorination of 4-[^{18}F]fluoroglutamine beside the catalysis by alanine aminotransferase enzyme. A comparison uptake study between 4-[^{18}F]fluoroglutamine and [^{18}F]FDG was performed in different cancer cell lines and tumour models. The results presented here indicate specific cancer cell types have a lower avidity for [^{18}F]FDG than for 4-[^{18}F]fluoroglutamine and suggest 4-[^{18}F]fluoroglutamine can have potential future application to patients who have difficulties with the fasting requirement of [^{18}F]FDG. Finally, the changes in *in vitro* 4-[^{18}F]fluoroglutamine uptake of which an increase following AZD2014 and a decrease following CYC065 treatments were achieved provide a necessary validation step towards establishing 4-[^{18}F]fluoroglutamine as a metabolic imaging radiotracer of treatment response in cancer.

Statement of COVID-19 impact on the thesis of NHAT THANH NGUYEN

This statement overviews the disruptions caused by COVID-19 and impact on the work of my thesis

Overview: The COVID-19 pandemic forced the Institute of Cancer Research (ICR) to enter the lockdown of laboratories starting from 26/03/2020 to 15/06/2020 which led to the cancellation of an *in vivo* experiment in chapter 5: **PI3K/AKT/mTOR pathway and Glutamine Metabolism** of my thesis.

The importance of the work: Following the promising results of *in vitro* 4-[^{18}F]fluoroglutamine uptake, the *in vivo* study would provide information on the application of 4-[^{18}F]fluoroglutamine in monitoring the treatment response in tumour following the treatment with mTOR inhibitor AZD2014 as a single agent and in combination with Paclitaxel chemotherapy.

Title of the experiment: Small animal PET imaging using 4-[^{18}F]fluoroglutamine to monitor the changes of ovarian tumour A2780 cisR glutamine uptake following the treatment with Vistusertib (AZD2014) and Paclitaxel.

- Upon the availability of the PET imaging facility in Centre of Cancer Imaging Sutton, the experiment was planned to be carried out from **01/04/2020** with the cancer cell injection of the animals. Ideally, the tumour expected to take 5-6 weeks to grow to appropriate size 80mm^3 for the treatment (planned date for starting the treatment **16/05/2020** (5 week tumour growth) or **23/05/2020** (6 week tumour growth)). The treatment would take 1 week to complete. After 1 week of treatment, the animals would be undergoing PET/CT scanning (planned date for the scanning **23/05/2020** (5 week tumour growth) or **30/05/2020** (6 week tumour growth)). If the experiment went well, the data analysis which normally takes around 7-10 days would be carried out (expected end date for the experiment (**08/06/2020**).

- Re-planning of this disrupted experiment and discussion on reducing the number of treatment groups were considered so that it could be performed in a shorter time for the remaining time of the PhD. However, it was not possible because the chosen conditions are optimal, and the omission of any treatment groups will lead to a lack of data for comparison and conclusion on the drug effect. The time after 08/06/2020 when the experiment was expected to finish was indeed planned for a second repeat if the first experiment did not go well. It would be very risky to plan the time for only one *in vivo* experiment because animal experiments can easily go wrong, especially with the failure of tumour growth which leads to an insufficient number of experimental animals.

- It was also not possible to perform the experiment when the ICR slowly reopened its labs at the end of June 2020 because of the strict rules on social distancing, number of people working on site, and shift working pattern. In addition, the ICR Biological Services Unit (BSU) which is the main venue for *in vivo* work limited the number of possible experiments per month. It took a long time for an experiment protocol to be approved by the BSU. In addition, the limit on the number of working people in the BSU and the shift working pattern

made the scheduled drug treatments of the animals become impossible. Hence, I and my supervisor's team have estimated the risks of not being able to finish the experiment in time of thesis submission deadline and decided not to carry out such a big experiment due to the insufficient remaining time and current strict regulations of social distancing.

Name of student: NHAT THANH NGUYEN
Signature:

Date: 25/08/2020

Name of supervisor: Dr. GRAHAM SMITH
Signature:

Date: 28/8/2020

Acknowledgements

I would first like to thank my supervisors for all their support, Dr. Graham Smith of the Division of Radiotherapy and Imaging for accepting me to his wonderful and inspiring research team, for the continuous support of my PhD study and related research and Dr. Yuen-Li Chung for all the time, guidance, patience, support and motivation. I would also like to thank Prof. Udai Banerji, Prof. Martin Leach, Dr. Anguraj Sadanandam, Prof. Jeffrey Bamber for their efforts in ensuring a smooth transition through this PhD project, and for helpful discussions at the beginning of this research.

I would also like to thank many people in the Division of Radiotherapy and Imaging that I had the pleasure of learning and working with, particularly Dr. Anne-Christine Wong her immense knowledge and excellent introduction to NMR, biochemistry and *in vivo* techniques. Her companionship in the laboratory was very helpful at the initial stage of my PhD. I wish to thank Dr. Harry Parkes for sharing his knowledge of magnetic resonance spectroscopy and for continuous help with 500 MHz NMR spectrometer, Drs. David Robert Turton and Andreas Doepner for providing ^{18}F and ^{19}F-fluoroglutamine, Drs. Gabriela-Kramer Marek and Florian Raes for continuous support with PET imaging, Drs. Igor Vivanco and Glori Lazaro for donating MYC dependent cancer cell lines Kelly and VMRC-LCD and sharing useful information on MYC pathway and its inhibitor CYC065, Dr. Alexis Barr for donating the HCT116 WT cell line, Dr. Paul Clarke for donating the HCT116 Bax-KO cell line, Dr. Anguraj Sadanandam for donating the TU8902, TU8988T, TU8988S, ASPC-1, T3M4, MIA PaCa-2, NCIH508, DAN-G cell lines, Dr. Carol Box for the SRB assay, STR, mycoplasma and PCR techniques.

Finally, I also wish to thank my family for the encouragement and their endless support and cheerleading.

The funding for this study is supported by the Institute of Cancer Research and Cancer Research UK.

Table of Contents

List of Figures 11
List of Tables 16
List of Abbreviations 17
1. Introduction 22
1.1. Cancer: Figures and Hallmarks 22
1.2. The metabolism of cancer cell 24
1.3. The cancer cell's requirement for glutamine 27
1.4. Glutamine transport in cancer cells 27
1.4.1. ASCT2 27
1.4.2. LAT1 28
1.5. Investigations into the relationship between the PI3K/ AKT/mTOR pathway and glutamine metabolism and the effects of mTORC1 pathway inhibitors on glutamine uptake and metabolism 31
1.5.1. Integration of ASCT2 and LAT1 with mTOR 31
1.5.2. Relationship between the PI3K/AKT/mTOR pathway and glutamine metabolism 31
1.5.3. Effect of glutamine uptake restriction on mTORC1 pathway 32
1.5.4. Effect of mTORC1 pathway inhibitors on glutamine uptake and metabolism 33
1.6. Investigations into the relationship between the Myc pathway and glutamine metabolism and the effects of Myc pathway inhibitors on glutamine uptake and metabolism 36
1.6.1. Relationship between the Myc pathway and glutamine metabolism 36
1.6.2. Triangle interactions among MYC, mTOR and glutamine metabolism..... 37
1.6.3. Cdk2 Kinase and Myc-repressed senescence: Potential target for cancer treatment 38
1.7. Imaging of cancer metabolism 39
1.7.1. Positron Emission Tomography 39
1.7.2. Magnetic Resonance Spectroscopy 45
1.8. Hypotheses and Aims of thesis 51
1.8.1. Hypotheses 51
1.8.2. Overall aims 51
1.9. Structure of the thesis 52
2. Materials and Methods 54
2.1. Cell culture and cellular assays 54
2.1.1. Maintenance of cell lines 54
2.1.2. Cytotoxicity assay of CB-839 and L-cycloserine 55
2.1.3. Determination of treatment schedules and optimal conditions for CB-839 and L-cycloserine studies 57

2.1.4. Cell treatment 57
2.1.5. Cell viability and count 57
2.1.6. *In vitro* cell uptake of [^{1}H]-Glutamine and [^{1}H]-Glucose 58
2.1.7. In vitro cell uptake of 4-[^{18}F]fluoroglutamine and [^{18}F]FDG 58
2.2. SDS-PAGE and immunoblotting 59
2.3. Magnetic Resonance Spectroscopy 60
2.3.1. Sample preparation 60
2.3.2. ^{1}H MRS of cell culture media and cell extract samples 61
2.3.3. ^{19}F-labelled glutamine MRS studies 62
2.3.4. MRS spectral acquisition and data processing 62
2.4. *In vivo* studies 70
2.4.1. Tumour growth in nude mice 70
2.4.2. Small animal PET imaging studies 70
2.4.3. *Ex vivo* biodistribution study in NCr-Foxn1nu male mice 71
2.4.4. Dual phase extraction of tumour tissues 72
2.4.5. ^{1}H MRS of tumour tissue extract samples 72
2.4.6. MRS spectral acquisition and data processing 72
2.5. Statistics 73
3. Evaluation of the metabolic pathways of 4-[^{18}F]fluoroglutamine PET tracer in cancer cells 74
3.1. Introduction 74
3.2. Experiments and Results 78
3.2.1. Cytotoxicity assay of CB-839 and L-cycloserine 78
3.2.2. Determination of treatment schedule and optimal condition for CB-839 or L-cycloserine treatment 78
3.2.3. Monitoring metabolic changes in HCT116 WT and HCT116 Bax-ko cells following CB-839 treatment by using ^{1}H-MRS 81
3.2.4. Monitoring metabolic changes in HCT116 WT and HCT116 Bax-ko cells following CB-839 treatment by using ^{19}F-MRS 81
3.2.5. Expression of glutaminase enzyme in HCT116 WT and HCT116 Bax-ko cells following CB-839 treatment 82
3.2.6. Monitoring metabolic changes in HCT116 WT and HCT116 Bax-ko cells following L-cycloserine treatment by using ^{1}H-MRS 88
3.2.7. Monitoring metabolic changes in HCT116 WT and HCT116 Bax-ko cells following L-cycloserine treatment by using ^{19}F-MRS 88
3.2.8. Expression of alanine aminotransferase enzyme in HCT116 WT and HCT116 Bax-ko cells following L-cycloserine treatment 89
3.3. Discussion 97
4. *In vitro* and *in vivo* uptake of 4-[^{18}F]fluoroglutamine and [^{18}F]FDG tracer in a panel cancer cell lines 101

4.1. Introduction 101
4.2. Experiments and Results 104
4.2.1. *In vitro* uptake studies of L-glutamine, D-glucose and ^{18}F- labelled glutamine and FDG in cancer cell lines 104
4.2.1.1. *In vitro* uptake of L-glutamine and D-glucose in cancer cell lines by ^{1}H-MRS 104
4.2.1.2. *In vitro* uptake of 4-[^{18}F]fluoroglutamine and [^{18}F]FDG 104
4.2.1.3. Correlations between ^{1}H-MRS and ^{18}F labelled *in vitro* uptake studies ... 105
4.2.1.4. Correlations between the intracellular level of L-glutamine and D-glucose measured by ^{1}H-MRS with the rates of ^{18}F labelled glutamine and glucose uptake in cancer cell lines 105
4.2.2. Time dependent in vitro uptake of 4-[^{18}F]fluoroglutamine and [^{18}F]FDG 114
4.2.3. *In vitro* uptake inhibition studies of 4-[^{18}F]fluoroglutamine and [^{18}F]FDG ... 114
4.2.4. *Ex vivo* biodistribution study of 4-[^{18}F]fluoroglutamine and [^{18}F]FDG in NCr-Foxn1nu male mice 117
4.2.5. Animal PET Studies in NCr-Foxn1nu male mice 120
4.3. Discussion 124
5. PI3K/AKT/mTOR pathway and Glutamine Metabolism 129
5.1. Introduction 129
5.2. Experiments and Results 134
5.2.1. A2780cisR and H520 cell growth inhibition following treatment with AZD2014 or Paclitaxel as a single agent and in a combination therapy 134
5.2.2. 4-[^{18}F]fluoroglutamine uptake changes in A2780cisR and H520 cells following treatment with AZD2014 or Paclitaxel as a single agent and in a combination therapy 134
5.2.3. Examination of glutamine transporter SLC1A5 (ASCT2) expression in A2780cisR and H520 cells following treatment with AZD2014 or Paclitaxel as a single agent and in a combination therapy 135
5.3. Discussion 140
6. Evaluating the effect of Cdk2 Kinase Inhibition on Glutamine Metabolism 143
6.1. Introduction 143
6.2. Experiments and Results 147
6.2.1. Kelly WT and Kelly CYC065R cell growth inhibition following treatment with Cdk2 inhibitor CYC065 147
6.2.2. ^{1}H-MRS study of metabolic changes in Kelly WT and Kelly CYC065R cells following CYC065 treatment 148
6.2.3. [^{18}F]FDG and 4-[^{18}F]fluoroglutamine uptake changes in Kelly WT and Kelly CYC065R following CYC065 treatment 156
6.2.4. Examination of glutamine transporter SLC1A5 (ASCT2), branched chain amino acid transporter SLC7A5 (LAT1) and glutaminase (GLS) enzyme expression following CYC065 treatment in Kelly WT and Kelly CYC065R cells 156

6.2.5. VMRC WT and VMRC CYC065R cell growth inhibition following treatment with Cdk2 inhibitor CYC065 160

6.2.6. ^{1}H-MRS study of metabolic changes in VMRC WT and VMRC CYC065R cells following CYC065 treatment 161

6.2.7. [^{18}F]FDG and 4-[^{18}F]fluoroglutamine uptake changes in VMRC WT and VMRC CYC065R following CYC065 treatment 169

6.2.8. Examination of glutamine transporter SLC1A5 (ASCT2), branched chain amino acid transporter SLC7A5 (LAT1) and glutaminase (GLS) enzyme expression following CYC065 treatment in VMRC WT and VMRC CYC065R cells 169

6.3. Discussion 173

7. Summary **177**

7.1. Objectives and summary of the studies 177

7.2. Overview of the chapters 178

7.2.1. Chapter 3: Evaluation of the metabolic pathways of 4-[^{18}F]fluoroglutamine PET tracer in cancer cells 178

7.2.2. Chapter 4: *In vitro* and *in vivo* uptake of 4-[^{18}F]fluoroglutamine and [^{18}F]FDG in a panel cancer cell lines 179

7.2.3. Chapter 5: PI3K/AKT/mTOR pathway and Glutamine Metabolism 182

7.2.4. Chapter 6: Evaluating the effect of Cdk2 Kinase Inhibition on Glutamine Metabolism 183

7.3. Conclusions and future work 184

References 190

List of Conferences and Meetings 224

List of Figures

Figure 1.1. Ten hallmarks of cancer.

Figure 1.2. Comparison between the metabolism of normal cells and tumour cells.

Figure 1.3. Structure of the ASCT2 transporter.

Figure 1.4. Relationship of ASCT2, LAT1 and mTOR in cancer cells.

Figure 1.5. Triangle interaction among MYC, mTOR and glutamine metabolism.

Figure 1.5. The interaction between Glutamine, PI3K/AKT/mTOR pathway and MYC.

Figure 1.6. Structures of glutamine based PET imaging agents.

Figure 1.7. The proposed metabolic pathways involved in the metabolism of (2S, 4R)-4-[^{18}F]fluoroglutamine in liver extracts using purified enzymes.

Figure 1.8. Structures of L-glutamine and glutamine based PET and MRS imaging agents.

Figure 1.9. ^{19}F – MRS of HCT116 Bax – ko cell extract and tumour extract.

Figure 2.1. Example ^{1}H MR spectrum of culture media.

Figure 2.2. Example ^{1}H MR spectrum of cellular extracts.

Figure 2.3. Example ^{19}F MR spectrum of culture media.

Figure 2.4. Example ^{19}F MR spectrum of cellular extracts

Figure 3.1. Cytotoxic effect of CB-839, and L-cycloserine on HCT116 WT and HCT116 Bax-ko cells.

Figure 3.2. Optimal treatment conditions for CB-839 and L-cycloserine on HCT116 WT and HCT116 Bax-ko cell lines.

Figure 3.3. Changes in glutamine metabolism measured by ^{1}H-MRS following CB-839 treatment in HCT116 WT and HCT116 Bax-ko cell lines.

Figure 3.4. Example ^{1}H-MRS spectra of cellular glutamine/glutamate changes in vehicle- (blue) and CB-839-treated (red) HCT116 WT cell extracts.

Figure 3.5. Changes in glutamine metabolism measured by ^{19}F-MRS following CB-839 treatment in HCT116 WT and HCT116 Bax-ko cell lines.

Figure 3.6. Example ^{19}F-MRS spectra showing cellular fluoroglutamine and fluoroglutamate changes in vehicle- (blue) and CB-839-treated (red) HCT116 WT cell extracts.

Figure 3.7. Changes in glutaminase enzyme expression level in HCT116 WT and HCT116 Bax-ko cell lines following CB-839 treatment.

Figure 3.8. Changes in glutamine metabolism measured by ^{1}H-MRS following L-cycloserine treatment in HCT116 WT and HCT116 Bax-ko cells.

Figure 3.9. Example ^{1}H-MRS spectra of alanine uptake/glutamate secretion and cellular alanine/glutamate changes in vehicle- and L-cycloserine-treated HCT116 WT.

Figure 3.10. Changes in glutamine metabolism measured by ^{19}F-MRS following L-cycloserine treatment in HCT116 WT and HCT116 Bax-ko cell lines.

Figure 3.11. ^{19}F-MRS of 4-[^{19}F]fluoroglutamine in clean media and clean media + L-cycloserine before incubation with the HCT116 WT and HCT116 Bax-ko cells

Figure 3.12. Example ^{19}F-MRS spectra of 4-[^{19}F]fluoroglutamate/free fluoride secretion and cellular 4-[^{19}F]fluoroglutamate changes in vehicle- and L-cycloserine-treated HCT116 WT.

Figure 3.13. Changes in alanine aminotransferase enzyme expression in HCT116 WT and HCT116 Bax-ko cell lines following L-cycloserine treatment.

Figure 4.1. *In vitro* ^{1}H-MRS uptake study of L-glutamine and D-glucose in thirteen different types of cell

Figure 4.2. Rates of 4-[^{18}F]fluoroglutamine and [^{18}F]FDG uptake in thirteen cell lines.

Figure 4.3. Correlations of L-glutamine and D-glucose uptake rates measured by ^{1}H-MRS with the rates of ^{18}F labelled glutamine and FDG uptake in thirteem cancer cell lines

Figure 4.4. Intracellular L-glutamine and D-glucose levels measured by ^{1}H-MRS in thirteen cancer cell lines.

Figure 4.5. Correlations of intracellular L-glutamine and D-glucose levels measured by ^{1}H-MRS with rates of ^{18}F labelled glutamine and FDG uptake.

Figure 4.6. Time dependent cell uptake studies of 4-[^{18}F]fluoroglutamine and [^{18}F]FDG in PC3 and HCT116 WT cell lines.

Figure 4.7. *In vitro* cell uptake inhibition studies of 4-[^{18}F]fluoroglutamine and [^{18}F]FDG in PC3 and HCT116 WT cell lines.

Figure 4.8. *Ex vivo* biodistribution of 4-[^{18}F]fluoroglutamine and [^{18}F]FDG in NCr-Foxn1nu male mice bearing HCT116 WT or PC3 tumour xenografts.

Figure 4.9. Imaging of 4-[^{18}F]fluoroglutamine and [^{18}F]FDG in HCT116 WT or PC3 tumour xenografts.

Figure 5.1. The mTORC1 and mTORC2 complexes.

Figure 5.2. Cellular response of A2780cisR and H520 cell lines following treatment with AZD2014 alone, Paclitaxel alone or the combination.

Figure 5.3. Changes in *in vitro* cell uptake of 4-[^{18}F]fluoroglutamine in A2780cisR and H520 cells following treatment with AZD2014 alone, Paclitaxel alone or the combination.

Figure 5.4. Changes in glutamine transporters SLC1A5 (ASCT2) expression in A2780cisR and H520 cell lines following treatment with AZD2014 alone, Paclitaxel alone or the combination.

Figure 6.1. The autostimulatory loop of MYC and RAS.

Figure 6.2. Cellular response of Kelly WT and Kelly CYC065R cell lines following treatment with CYC065

Figure 6.3. Metabolic changes in vehicle- and CYC065-treated Kelly WT cells measured by ^{1}H-MRS.

Figure 6.4. Changes in branch-chained amino acid metabolism in Kelly WT cells following vehicle or CYC065 treatment as measured by ^{1}H-MRS.

Figure 6.5. Metabolic changes in vehicle- and CYC065-treated Kelly CYC065R cells measured by ^{1}H-MRS.

Figure 6.6. Changes in branch-chained amino acid metabolism in Kelly CYC065R cells following vehicle or CYC065 treatment as measured by ^{1}H-MRS.

Figure 6.7. Example ^{1}H-MRS spectra of glutamine and branched chain amino acid (Leucine, iso-Leucine and Valine) uptake in Kelly WT cells.

Figure 6.8. Example ^{1}H-MRS spectra of glutamine and branched chain amino acid (Leucine, iso-Leucine and Valine) uptake in Kelly CYC065R cells.

Figure 6.9. Changes in *in vitro* cell uptake of [^{18}F]FDG and 4-[^{18}F]fluoroglutamine in Kelly WT and Kelly CYC065R following CYC065 treatment.

Figure 6.10. Changes in glutamine transporter SLC1A5 (ASCT2), branched chain amino acid transporter SLC7A5 (LAT1) and glutaminase enzyme expression in Kelly WT cell following CYC065 treatment.

Figure 6.11. Glutamine transporter SLC1A5 (ASCT2), branched chain amino acid transporter SLC7A5 (LAT1) and glutaminase enzyme expression in Kelly CYC065R cell following CYC065 treatment.

Figure 6.12. Cellular response of VMRC WT and VMRC CYC065R cell lines following treatment with CYC065.

Figure 6.13. Metabolic changes in vehicle- and CYC065-treated VMRC WT cells measured by ^{1}H-MRS.

Figure 6.14. Branch-chain amino acid changes in vehicle- and CYC065-treated VMRC WT cells measured by ^{1}H-MRS.

Figure 6.15. Metabolic changes in vehicle- and CYC065-treated VMRC CYC065R cells measured by ^{1}H-MRS.

Figure 6.16. Branch-chained amino acid changes in vehicle- and CYC065-treated VMRC CYC065R cells measured by ^{1}H-MRS.

Figure 6.17. Example ^{1}H-MRS spectra of glutamine and branched chain amino acid (Leucine, iso-Leucine and Valine) uptake in VMRC WT cells.

Figure 6.18. Example ^{1}H-MRS spectra of glutamine and branched chain amino acid (Leucine, iso-Leucine and Valine) uptake in VMRC CYC065R cells.

Figure 6.19. Changes in *in vitro* cell uptake of [^{18}F]FDG and 4-[^{18}F]fluoroglutamine in VMRC WT and VMRC CYC065R following CYC065 treatment.

Figure 6.20. Changes in glutamine transporter SLC1A5 (ASCT2), branched chain amino acid transporter SLC7A5 (LAT1) and glutaminase enzyme expression in VMRC WT cells following CYC065 treatment.

Figure 6.21. Glutamine transporter SLC1A5 (ASCT2), branched chain amino acid transporter SLC7A5 (LAT1) and glutaminase enzyme expression in VMRC CYC065R cells following CYC065 treatment.

Figure 7.1. The proposed metabolic pathways of (2S, 4R)-4-[^{18}F]fluoroglutamine (4-[^{18}F]fluoroglutamine).

List of Tables

Table 2.1. ^{1}H chemical shift of the assigned metabolites in culture media and cell extracts of HCT116 WT and HCT116 Bax-ko.

Table 2.2. ^{19}F chemical shift of the assigned metabolites in culture media and cell extracts of HCT116 WT and HCT116 Bax-ko.

Table 4.1. Summary of L-glutamine and D-glucose uptake rates measured by ^{1}H-MRS in thirteen cancer cell lines.

Table 4.2. Summary of *in vitro* uptake rates of 4-[^{18}F]fluoroglutamine and [^{18}F]FDG in thirteen cancer cell lines.

Table 4.3. Summary of intracellular L-glutamine and D-glucose levels measured by ^{1}H-MRS in thirteen cancer cell lines.

Table 4.4. Summary of *ex vivo* biodistribution of 4-[^{18}F]fluoroglutamine and [^{18}F]FDG in NCr-Foxn1nu male mice bearing HCT116 WT or PC3 tumour xenografts.

List of Abbreviations

[^{18}F]FDG: ^{18}F-Fluorodeoxyglucose

4EBP1: 4E binding protein 1

ACACA: acetyl-CoA carboxylase

ADP: Adenosine diphosphate

AMPK: AMP-activated protein kinase

ASCT1: Alanine-Serine-Cysteine transporter 2

ASCT2: Alanine-Serine-Cysteine transporter 2

ATCC: American Type Culture Collection

ATP: Adenosine triphosphate

BAT: brown adipose tissue

BCH: 2-aminobicyclo-(2,2,1)-heptane-2-carboxylic acid

BCH: 2-aminobicyclo-(2,2,1)-heptane-2-carboxylic acid

BSA: bovine serum albumin

Cdk2: Cyclin dependent kinase 2

CREB2: cAMP – responsive element binding 2

CT: computed tomography

Deptor: DEP-domain-containing mTOR-interacting protein

DHAP: Dihydroxyacetone phosphate

DMEM: Dulbecco's Modified Eagle Medium

DMSO: Dimethyl sulfoxide

DNP: Dynamic nuclear hyperpolarisation

DSMZ: Deutsche Sammlung von Mikroorganismen und Zellkulturen

EDTA: Ethylenediaminetetraacetic acid

eIF4E: eukaryotic translation initiation factor 4E

FASN: fatty acid synthetase

FBP: filtered back projection

FBS: Fetal Bovine Serum

FWHM: Full Width at Half Maximum

G6P: glucose 6-phosphate

GADP: D-glyceraldehyde 3-phosphate

GADPH: glyceraldehyde phosphate dehydrogenase

GLS: glutaminase

GLUT1: Glucose transporter 1

GPC: Glycerophosphocholine

GPE: Glycerophosphoethanolamine

GPNA: γ-glutamyl p-nitroanilide

GPT2: glutamic pyruvate transaminase 2

GS: glutamine synthetase

HPLC: High-performance liquid chromatography

HR-MAS: High-resolution magic angle spinning

HRP: Horseradish peroxidase

ID: injected dose

LAT1: large neutral amino acid transporter 1

m/z: mass/charge

MES: 2-(*N*-morpholino)ethanesulfonic acid

mLST8: mammalian lethal with Sec13 protein8

MOPS: 3-(*N*-morpholino)propanesulfonic acid

MRI: magnetic resonance imaging

MRS: magnetic resonance spectroscopy

MS: Mass spectrometry

MSI: Mass spectrometry imaging

mSIN1: mammalian stress-activated protein kinase interacting protein

mTOR: mammalian target of rapamycin

mTORC1/2: mammalian target of rapamycin complex 1/2

NADH: nicotinamide adenine dinucleotide hydrogen

NADP: Nicotinamide adenine dinucleotide phosphate

NADPH: Nicotinamide adenine dinucleotide phosphate hydrogen

NEAAs: non-essential amino acids

NMR: nuclear magnetic resonance

PBS: Phosphate-buffered saline

PCr: phosphocreatine

PCho: Phosphocholine

PET: Positron emission tomography

Peth: phosphoethanolamine

PFK-1: phosphofructokinase-1

PFK-2: phosphofructokinase-2

PGK: phosphoglycerate kinase

PGM: phosphoglycerate mutase

PI3K: Phosphoinositide 3-kinase

PKM2: pyruvate kinase M2

ppm: parts per million

PRAS40: prolinerich AKT substrate 40 kDa

Protor-1: protein observed with Rictor-1

Raptor: regulatory-associated protein of mTOR

Rictor: rapamycin-insensitive companion of mTOR

RIPA: Radioimmunoprecipitation assay

RNA: Ribonucleic acid

ROS: reactive oxygen species

rpm: rounds per minute

RPMI: Roswell Park Memorial Institute

RT: room temperature

SCD: stearoyl-CoA desaturase

SD: standard deviation

SDS-PAGE: sodium dodecyl sulphate-polyacrylamide gel electrophoresis

shRNA: short hairpin Ribonucleic acid

SIRT4: sirtuin 4

SNAT2: Solute neutral amino acid transporter 2

SNAT5: Solute neutral amino acid transporter 5

SRB: sulforhodamine B

STR: Short Tandem Repeat

TCA: tricarboxylic acid

TMS: tetramethylsilane

TSC2: tuberous sclerosis complex 2

TSP: 3-trimethylsilyl-2,2,3,3-tetradeuteropropionate

Chapter 1

Introduction

1.1. Cancer: Figures and Hallmarks

In economically developed countries, cancer is ranked as the leading cause of death. The burden of cancer is also now increasing in economically developing countries, making it the second cause of mortality in these places (World health Organisation 2011). The aging-population, smoking, fast food and westernized diets are linked to the development of cancer. Based on the GLOBOCAN 2018, the cancer diagnosed cases have raised from 14.1 million people in 2012 to 18.1 million people in 2018. 54.2% of these cases were in the economically developing world. The cancer mortality rate also increased from 8.2 million cases in 2012 to 9.6 million cases in 2018. 65% of the deaths occurred in the poor and developing states. It is estimated that breast cancer is the major cause of cancer death among females while lung cancer is the most frequently diagnosed cancer in males (Bray et al. 2018).

Cancer is a disease caused by an uncontrolled division of cells, leading to the malignant growth or tumour. In 2000, Hanahan and Weinberg described six hallmarks of cancer - “Limitless replicative potential, sustained angiogenesis, avoidance of apoptosis, self-sufficiency in growth signals, insensitivity to anti-growth signals and tissue invasion and metastasis” - which are the major cellular changes that lead to malignant transformation (Hanahan and Weinberg 2000) (Fig. 1.1). In 2011, the evasion of immune destruction, reprogramming of energy metabolism, tumour-promoting inflammation, and genome instability and mutation were also recognised as key characteristics that also contribute to malignant transformation (Hanahan and Weinberg 2011).

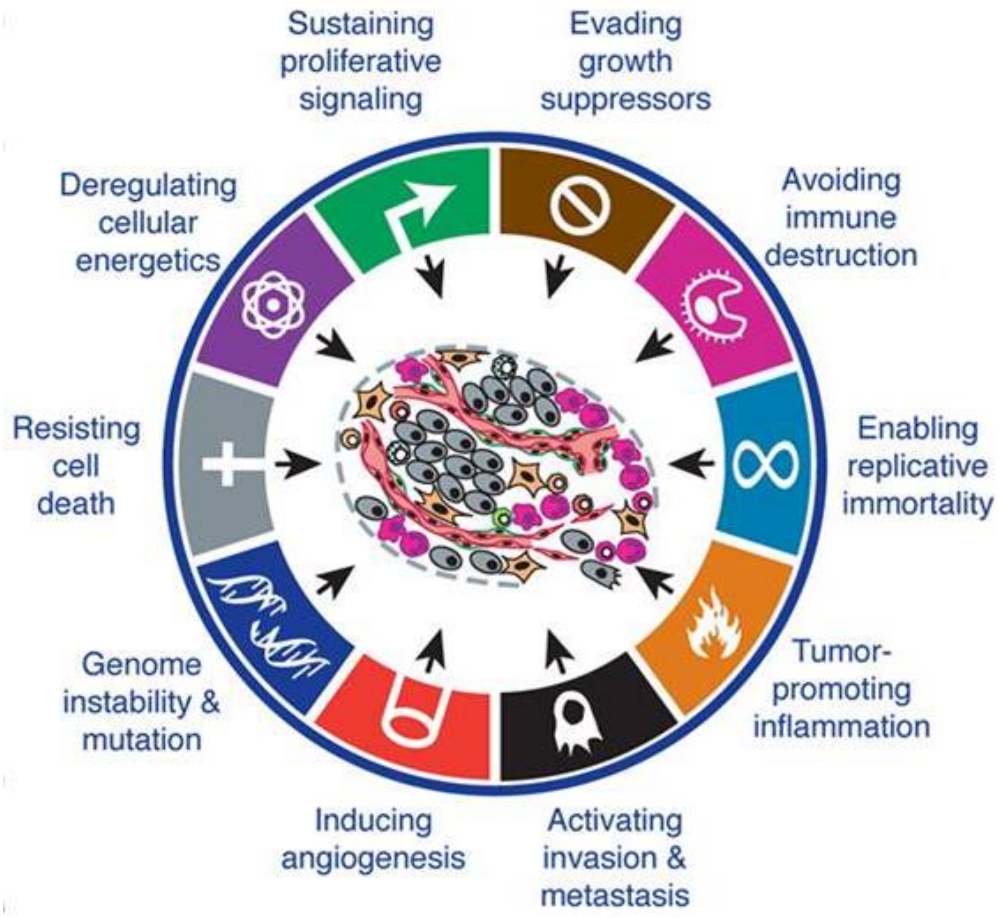

Figure 1.1. Ten hallmarks of cancer. This diagram illustrates ten distinctive but complementary hallmarks of cancer that support tumour growth and metastasis. Figure adapted from Hanahan and Weinberg (2011).

1.2. The metabolism of cancer cell

Glucose is the preferred substrate for cellular energy production in normal mammalian cells (Ozturk et al. 1997). Glucose is taken up via the glucose transporters GLUT-1 and GLUT-3 (Kasahara and Hinkle 1985; Mueckler et al. 1985; Thorens and Mueckler 1985; Brown and Wahl 1993; Reske et al. 1997; Brown et al. 1999) or through the sodium-glucose linked transporter 1 (SGLT1) (Casneuf et al. 2008). Each glucose molecule is metabolised in the glycolysis pathway via two phases: a preparatory phase and a harvesting phase (Alfarouk et al. 2014). In the first phase, glucose is phosphorylated by hexokinases to form glucose-6-phosphate (G6P). G6P is then isomerized into fructose-6-phosphate by glucose 6-phosphate isomerase. Fructose-6-phosphate is then phosphorylated further into fructose-1,6-diphosphate, and fructose-2,6-diphosphate by phosphofructokinase-1 (PFK-1) and phosphofructokinase-2 (PFK-2), respectively. By the activity of fructose-bisphosphate aldolase, fructose-1,6-disphosphate is transformed into D-glyceraldehyde 3-phosphate (GADP) and Dihydroxyacetone phosphate (DHAP). DHAP can be converted into GADP via the activity of triose phosphate isomerase. GADP then goes into the second phase of glycolysis pathway. GADP is converted into 1, 3-biphosphoglycerate by glyceraldehyde phosphate dehydrogenase (GADPH). 1,3-bisphosphoglycerate is then catalysed by phosphoglycerate kinase (PGK) to form 3-phosphoglycerate and produces ATP. The isomerization of 3-phosphoglycerate by phosphoglycerate mutase (PGM) produces 2–phosphoglycerate which is then converted into phosphoenolpyruvate by the enolase enzyme. Finally, phosphoenolpyruvate is converted into pyruvate by the pyruvate kinase enzymes. Another ATP molecule is produced at this stage (Ritter 1996). Each glucose molecule is metabolised in the glycolysis pathway to provide 2 pyruvate molecules, which then enter the Krebs cycle in the mitochondria to generate Nicotinamide adenine dinucleotide hydrogen (NADH), the electron donor of the oxidative phosphorylation pathway, which yields up to 36 ATP molecules (Baird et al. 2004; Lieberman and Marks 2009). Moreover, pyruvate, glutamate and fatty acids which are the intermediates of the Krebs cycle serve as building blocks for biosynthetic purposes and maintain the replenishment of carbon skeletons in this cycle (Kroemer and Pouyssegur 2008) (Fig. 1.2).

Cancer cells have an altered metabolism, a characteristic that was recognised nearly a century ago by Otto Warburg, termed Warburg effect or aerobic glycolysis (Hanahan and Weinberg 2011). Compared to normal cells, malignant transformation is associated with an increased glucose consumption rate, a higher rate of glycolysis together with a reduced pyruvate oxidation and a higher rate of lactate production, despite sufficient oxygen availability for complete aerobic oxidation of glucose. These altered metabolic features appear to be advantageous for cancer cells to survive under unfavourable conditions such as hypoxia (Sonveaux 2008). Higher risk of metastasis, treatment failure and increased mortality rate are associated with intratumoural hypoxia (Gort et al. 2008; Semenza 2008; Heddleston et al. 2010).

In addition to the Warburg effect or aerobic glycolysis, the glutaminolysis pathway in which large amounts of glutamine are consumed and metabolised by cancer cells plays an essential part in tumour metabolism (Fig. 1.2) (Wise and Thompson 2010). The main role of glutamine was pointed out to be the primary anaplerotic precursor in cancer cells (DeBerardinis et al. 2007). The replenishing mechanism of glutamine for TCA cycle is at the α-ketoglutarate level, and subsequently becomes the refill source for oxaloacetate and aspartate (Fig. 1.2) (DeBerardinis et al. 2007). A proportion of malate is secreted from the mitochondria to the cytosol in which malic enzymes transform it into pyruvate, simultaneously reducing NADP+ to NADPH. Pyruvate can then be converted into lactate and alanine. It is estimated that approximately 60% of glutamine is transformed to lactate (DeBerardinis et al. 2007).

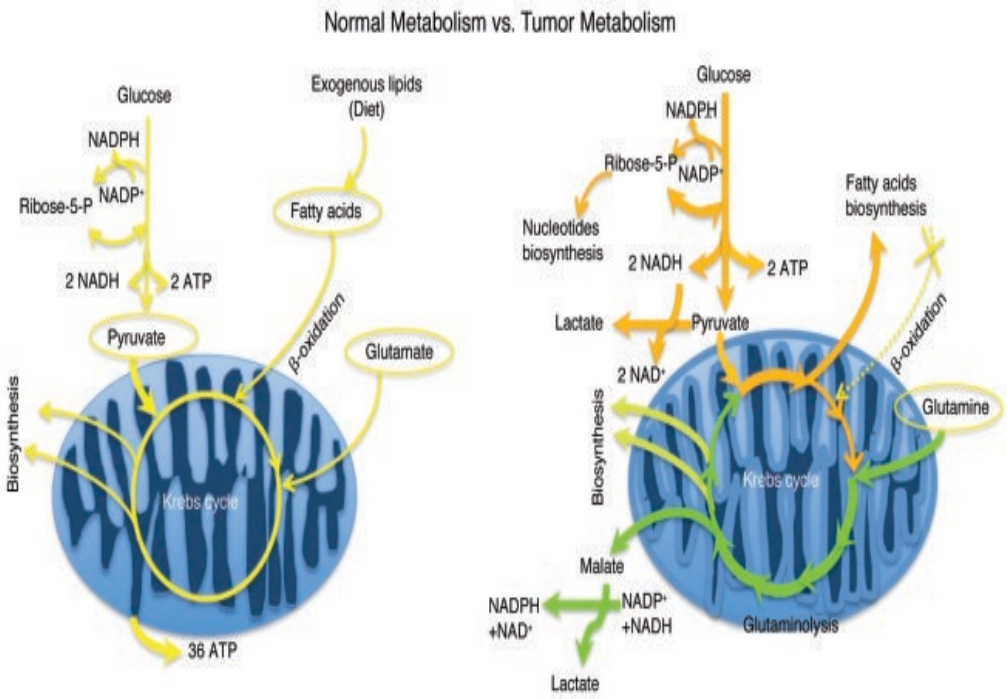

Figure 1.2. Comparison between the metabolism of normal cells (Left) and tumour cells (Right). In tumour cells, glycolysis is uncoupled from the respiratory chain and plays a role as the main ATP production source. Glucose consumption rate is increased together with a higher rate of glycolysis. The lactate dehydrogenase is overexpressed. The transport of pyruvate into the mitochondria is decreased, and pyruvate dehydrogenase activity is inhibited. This leads to a reduced pyruvate oxidation and a higher rate of lactate production. Glutamine contributes to the replenishment of the Krebs cycle, NADPH regeneration and lactate production. Extracellular glutamine is transported into cells and converted to glutamate by glutaminase enzyme. Subsequently, glutamate is converted to 2-keto-glutarate and enters the tricarboxylic acid (TCA) cycle in the mitochondria to be further utilised for protein, nucleotide and lipid synthesis. Figure adapted from Garcia et al. (2011).

1.3. The cancer cell's requirement for glutamine

Although the Warburg effect or aerobic glycolysis plays a key role in tumour growth, other nutrients are also required to provide substrates for the synthesis of essential building blocks for proliferating cells. Cancer cells require essential components containing nitrogen, sulphur, phosphorus and certain ions (DeBerardinis et al. 2008; Dang 2010); amino acids can provide the nitrogen source for the cells, whereas glucose provides the carbon source.

Glutamine is the most abundant amino acid and considered as non–essential in the human body, as many tissues have an enzyme called glutamine synthetase, which enables the synthesis of glutamine (Dang 2010). However, not all tissues have a high expression of glutamine synthetase, making these tissues depend on exogenous glutamine. Cancer is one of the most glutamine avid tissues, and cancer cells consume substantially excess glutamine (Dang 2010; Lu et al. 2010). In tumour cells, the metabolism of glutamine dominates any other non–essential amino acids and contributes to the anaplerosis of the Krebs cycle and NADPH regeneration through lactate production (Medina 2001; Szelina and Obara-Michlewska 2009, Tong et al. 2009). Moreover, the synthesis of purine, pyrimidine nucleotides, other amino acids and metabolites also requires glutamine as a nitrogen donor (Mates et al. 2009).

1.4. Glutamine transport in cancer cells

Glutamine metabolism of cancer cells takes place within the mitochondria. For this reason, glutamine must be transported from the extracellular medium into the mitochondria of tumour cells by specific transporters in the plasma and mitochondrial inner membranes. Neutral amino acid transporters ASCT2 (SLC1A5) and LAT1 (SLC7A5) have been implicated in tumour metabolism (Fuchs and Bode 2005; Nicklin et al. 2009).

1.4.1. ASCT2

ASCT2 (SLC1A5) is a sodium-dependent transporter located in the lung, kidney, intestines and testis where it plays a role in transporting small neutral amino acid

across the cell membrane (Mates et al. 2009). Yernool et al found a significant sequence similarity between ASCT2 and the glutamate transporter from Pyrococcus horikoshii, thus generated homology structure of ASCT2 as a bowl-shaped trimer with a concave aqueous basin facing the extracellular solution and a pointed base facing the cytoplasm (Yernool et al. 2004) (Fig. 1.3A). There are three independent binding sites at the bottom of the basin with each cradled by two helical hairpins, reaching from opposite sides of the membrane (Fig. 1.3B). It has been shown that ASCT2 is an amino acid transporter accepting small neutral amino acids, such as alanine, serine, cysteine and glutamine (Broer et al. 1999; Broer and Brookes 2001). The mechanism of ASCT2 has been described as being an amino acid antiport process (Fig. 1.3C). The uptake of neutral amino acids, e.g glutamine occurs only in exchange with intracellular amino acids, such as alanine. Nevertheless, the binding of Na+ is strictly required for the transport mechanism and multiple Na+ ions are exchanged during the transport of amino acids (Broer et al. 2000; Broer 2006; Oppedisano et al. 2006). Although the main substrate that ASCT2 can transport is neutral amino acid, it has been previously shown that the negatively charged amino acid glutamate can also be taken up weakly by ASCT2 at physiological pH 7.5 (Broer et al. 1999). ASCT2 expression levels are increased in various types of cancer, including breast, liver and brain tumours (Tennant et al. 2009). Hence, ASCT2 has been studied as a potential target of cancer treatment. L-γ-glutamyl-p-nitroanilide (GPNA) has been widely used among the ASCT2 inhibitors and shown tumour suppression effect in myeloma, non-small cell lung cancer and neuroblastoma (Hassanein et al. 2015; Ren et al. 2015; Bolzoni et al. 2016). Recently, the inhibition of ASCT2 by 2-amino-4-bis(aryloxybenzyl)aminobutanoic acids (AABA) showed promising results in osteosarcoma, and by V-9302 exerted tumour suppression effect in lung, breast and colorectal cancer (Broer et al. 2018; Schulte et al. 2018).

1.4.2. LAT1

LAT1 (SLC7A5) is a sodium-independent transporter located with high levels in brain, placenta, skeletal muscle and low levels in heart, colon, thymus, spleen, kidney, lung and leukocyte (Fuchs and Bode 2005). LAT1 belongs to the SLC7 family which is a member of the Amino acid-Polyamine-organo Cation (APC) superfamily (Christensen

1990). The SLC7 family is classified into two main subgroups: the cationic amino acid transporters and the light subunits (LATs) of the heterodimeric amino acid transporters. Both of subgroups have a common of 12 transmembrane domains. However, the cationic amino acid transporters have a duplication of the last two transmembrane domains, resulting in an addition of two more transmembrane domains (Verrey et al. 2004; Palacin et al. 2005; Fotiadis et al. 2013). The heterodimeric amino acid transporters compose two different subunits: the light subunits (LATs) and the heavy subunits (a membrane glycoprotein belonging to the SLC3 family). The interaction between the two subunits is via a disulphide bridge of the two cysteine residues of the proteins forming heterodimeric amino acid transporters (Bröer and Brookes 2001; Wagner et al. 2001; Palacín and Kanai 2004). In case of LAT1, the heavy subunit counterpart is the SLC3A2, also known as 4F2hc. A previous study by Kanai et al showed that when co-expressed with 4F2hc (the obligate chaperone), LAT1 transports neutral amino acids with large, branched or aromatic side chains like leucine, isoleucine, phenylalanine, methionine, tyrosine, histidine, tryptophan and valine (Kanai et al. 1998). Additional findings also revealed that LAT1 is able to transport glutamine and asparagine (Yanagida et al. 2001). The transport mechanism of LAT1 has been established that an obligatory pH and Na^+ independent antiport manner is mediated to transport tryptophan, phenylalanine, leucine and histidine with high affinity (Km for human isoform ranging from 5 to 50 μM) (Kanai et al. 1998; Mastroberardino et al. 1998; Prasad et al. 1999; Yanagida et al. 2001; Kim et al. 2002). The Na^+ independence characteristic of LAT1 leads to its low transport capacity when compared with other Na^+ gradient transporters, such as SNATs, ATB^0, and B^0AT1 (Pochini et al. 2014; Bröer and Bröer 2017). High expression level of LAT1 was detected in several leukaemia cell lines, RERF-LC-MA lung small cell carcinoma cells, HeLa uterine cervical carcinoma cells and T24 bladder carcinoma cells (Yanagida et al. 2001). Hence, targeting LAT1 has been considered as a potential cancer treatment. Inhibition of LAT1 with 2-aminobicyclo-(2,2,1)-heptane-2-carboxylic acid (BCH) has shown tumour suppression effect on the non-small cell lung cancer and the cholangiocarcinoma cancer (Imai et al. 2010; Janpipatkul et al. 2014)

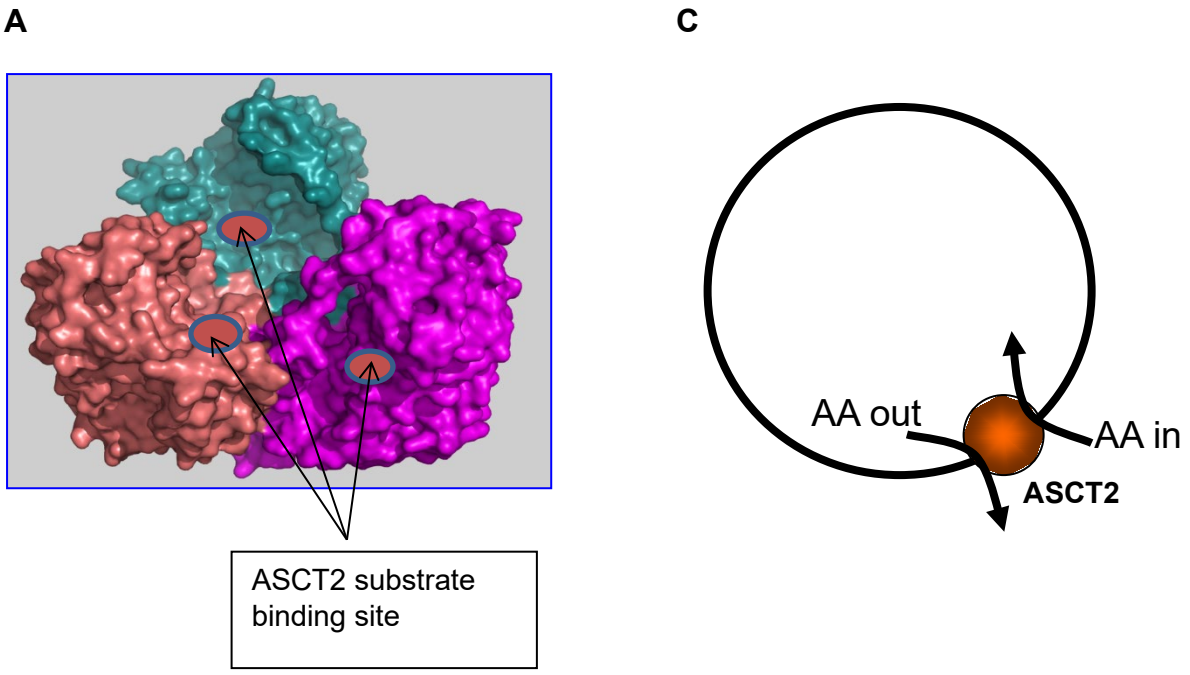

Figure 1.3. A. Structure of the ASCT2 transporter. ASCT2 is a bowl-shaped trimer with a concave aqueous basin facing the extracellular solution and a pointed base facing the cytoplasm. **B.** Ribbon representation of the protomer viewed in the plane of the membrane in which the transmembrane helices (1-8) and hairpins (HP1, HP2) are labelled. **C.** The amino acid antiport mechanism of ASCT2. The uptake of neutral amino acids occurs only in exchange with intracellular amino acids. Figure modified from Yernool et al. (2004).

1.5. Investigations into the relationship between the PI3K/ AKT/mTOR pathway and glutamine metabolism and the effects of mTORC1 pathway inhibitors on glutamine uptake and metabolism

1.5.1. Integration of ASCT2 and LAT1 with mTOR.

The mechanistic Target of Rapamycin (mTOR) is a serine/threonine kinase which plays a significant role in integrating signalling from growth factors, energy status and nutrients, especially amino acids (Fingar and Blenis 2004). Nicklin et al. identified the control of L-glutamine over mTOR signalling and concluded that cellular uptake and exchange of L-glutamine through the transporters ASCT2 and LAT1 is the rate limiting step for essential amino acid and growth factor regulation of mTORC1 (Nicklin et al. 2009). The regulation of mTORC1 by glutamine transport was illustrated as a two-step process. The first step involves the uptake of L-glutamine by ASCT2 leading to an increase in the intracellular concentration of L-glutamine. Secondly, the intracellular L-glutamine is used as an efflux substrate by LAT1 to regulate the uptake of extracellular L-leucine which subsequently leads to activation of mTORC1 (Nicklin et al. 2009) (Fig 1.4).

1.5.2. Relationship between the PI3K/AKT/mTOR pathway and glutamine metabolism.

The interactions between mTOR pathway and glutamine uptake and metabolism were examined previously. The growth of mammalian cells depends on the availability of nutrients and growth factors, which trigger mTOR activation through the PI3K/AKT pathway and MYC activation through the MEK/ERK pathway. MYC then stimulates the amino acid transporter genes and activates amino acid import (e.g. glutamine). Some of the imported glutamine is used to exchange for extracellular leucine, which further activates mTOR activity (Fuchs and Bode 2005; Nicklin et al. 2009; Duran et al. 2012; Csibi et al. 2013; Dang 2013; Csibi et al. 2014) (Fig 1.5). As mentioned in section 1.5.1, mTORC1 is regulated by a two-step amino acid transport mechanism with the first step involving the uptake of glutamine through the ASCT2 transporter and the second step consisting of the exchange of intracellular glutamine with extracellular leucine through the LAT1 transporter. L-leucine subsequently leads to the activation

of mTORC1 by disrupting the interaction between a GTPase activating protein GATOR2 and its interacting protein partner Sestrin2 (Nicklin et al. 2009; Wolfson et al. 2016). However, further study by Duran et al revealed that leucine alone was not sufficient to activate mTORC1 in glutamine-depleted cells and intracellular glutamine was a requirement for stimulation of mTORC1 by leucine (Duran et al. 2012). They also found that mTORC1 senses glutamine and leucine via glutaminolysis and, more specifically, through the glutaminolysis enzymes glutaminase and glutamate dehydrogenase. Glutamine is the substrate for glutaminase which converts glutamine into glutamate. Leucine directly binds and activates glutamate dehydrogenase which in turns deaminates glutamate and produces α-ketoglutarate (Sener and Malaisse 1980). The subsequent steps by which α-ketoglutarate leads to GTP loading of Rag and mTORC1 activation is still unknown.

The general mechanism of mTORC1 activation by L-glutamine and L-leucine through the glutaminolysis enzymes glutaminase and glutamate dehydrogenase has been shown. In addition, further studies by Yecies and Manning and Csibi et al. demonstrated that the activation of mTOC1 pathway has been able to promote the anaplerotic entry of glutamine into the TCA cycle through the activation of glutamate dehydrogenase enzyme (Yecies and Manning 2011; Csibi et al. 2013). To achieve this glutamate dehydrogenase activation, mTORC1 promotes the proteasome-mediated destabilization of cAMP – responsive element binding 2 (CREB2) which subsequently represses the mitochondrial – localized sirtuin SIRT4 that inhibits glutamate dehydrogenase. Csibi et al. also found that mTORC1 activation stimulates the uptake of glutamine through the positive regulation of glutaminase enzyme (Csibi et al. 2014). Mechanistically, mTORC1 regulates the level of glutaminase through the S6K1 dependent – regulation of c-Myc (Myc). S6K1 modulates the phosphorylation of eIF4B which subsequently enhances the Myc translation efficiency.

1.5.3. Effect of glutamine uptake restriction on mTORC1 pathway.

Recognising the correlation between the glutamine transporters ASCT2, LAT1 and mTORC1 pathway, it would be crucial to assess the effect of glutamine transport inhibition on mTORC1. It was reported that a direct inhibition of ASCT2 function by chemicals such as tamoxifen, raloxifene and γ-glutamyl p-nitroanilide (GPNA) or

shRNA decreases glutamine uptake and down regulates E2F transcription factor and mTORC1 pathway in lymph node carcinoma of prostate and PC-3 prostate cancer cell (Wang et al. 2015). Inhibition of LAT1 by 2-aminobicyclo-(2,2,1)-heptane-2-carboxylic acid (BCH) leads to a reduction of L-leucine uptake, and subsequently inhibits mTORC1 pathway activity in H1395 lung cancer cell and cholangiocarcinoma cells (Imai et al. 2010; Janpipatkul et al. 2014).

1.5.4. Effect of mTORC1 pathway inhibitors on glutamine uptake and metabolism.

Tanaka et al revealed that the levels of glutaminase and glutamate in glioblastoma multiforme cell lines are increased following mTOR inhibition with rapamycin or PP242 (Tanaka et al. 2015). The elevated glutaminase level increases the glutamine uptake, upregulates the glutamine metabolism via the TCA cycle and promotes resistance to mTOR kinase inhibitors. These results also highlight the close relationship between mTORC1 pathway and glutamine metabolism, and the critical role glutamine metabolism plays in mTOR inhibitor resistance. Tanaka et al also suggested that the mTOR inhibitor resistance could be suppressed by using a combination therapy of glutaminase inhibitor and mTOR-targeted treatments (Tanaka et al. 2015).

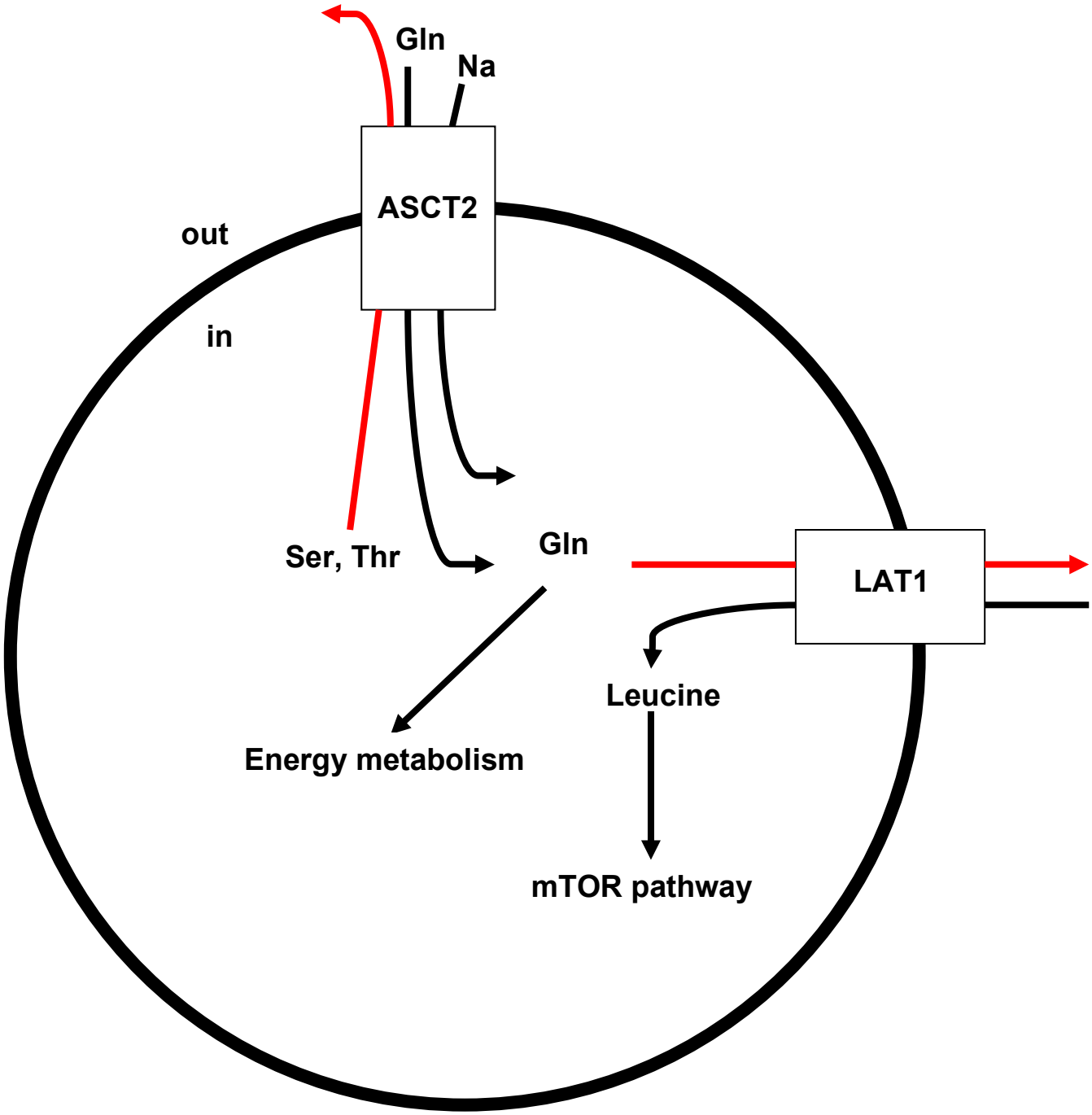

Figure 1.4. Relationship of ASCT2, LAT1 and mTOR in cancer cells. ASCT2 is a high affinity sodium dependent glutamine transporter that regulates the uptake of glutamine into intracellular environment. This uptake of glutamine requires an exchange of other neutral amino acid from inside the cell such as serine, threonine or alanine and also the binding of Na^+. LAT1 is a heterodimeric bidirectional antiporter that regulates the uptake of L-leucine in exchange for L-glutamine. The leucine uptake subsequently leads to the activation of mTOR pathway. A part of intracellular glutamine is used for the replenishment of TCA cycle and energy metabolism.

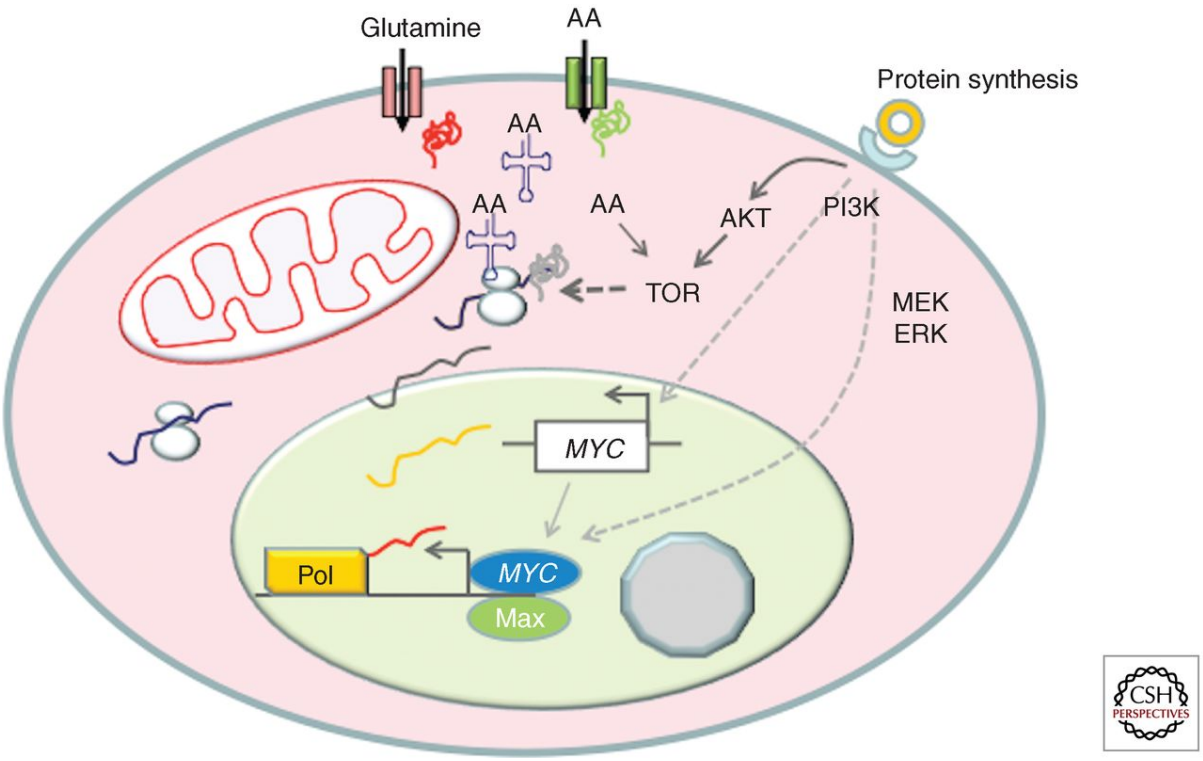

Figure 1.5. The interactions between Glutamine, PI3K/AKT/mTOR pathway and MYC. Growth factor receptor engagements signal mTOR activation through the PI3K/AKT pathway and MYC activation through the MEK/ERK pathway. MYC then stimulates the amino acid transporter genes and activates amino acid import (e.g. glutamine). Some of the imported glutamine is used to exchange for extracellular leucine, which further activates mTOR activity. Figure adapted from Dang (2013).

1.6. Investigations into the relationship between the Myc pathway and glutamine metabolism and the effects of Myc pathway inhibitors on glutamine uptake and metabolism

1.6.1. Relationship between the Myc pathway and glutamine metabolism

The MYC proto-oncogene which is a member of the MYC gene family (MYC, MYCN, MYCL) has been recognised to directly regulate many important cellular processes and be engaged in the interaction between the extracellular matrix and growth factor availability (Eilers and Eisenman 2008; Dang 2012). MYC has been documented to induce glycolysis and glutaminolysis pathways which provide essential ATP and building blocks for the cell's need, especially for cancer cells (Morrish et al. 2009; Hu et al. 2011; Yuneva et al. 2012; Dang 2013). The mechanism by which MYC stimulates genes involved in glutamine metabolism was found at both the transcriptional and post-transcriptional levels. MYC induction is able to elevate mitochondrial glutaminase (GLS) levels by repressing micro-RNAs, especially, miR23a, and miR23b, which suppress the synthesis of GLS (Wise et al. 2008; Gao et al. 2009; Chang et al. 2008). In addition, the expression of glutamine transporters ASCT2 (SLC1A5) and LAT1 (SLC7A5) was also induced by MYC stimulation (Deberardinis and Cheng 2010). Thus, glutamine consumption and metabolism can be stimulated by MYC induction to support the demand for protein and glutathione synthesis in cancer cells.

Metabolic tracking studies also reveal that MYC induction of glutaminolysis is important for cell survival under glucose or oxygen-derived environment (Le et al. 2012). The study indicated the ability of MYC-induced cancer cell to adapt to a glucose-independent cycle using glutamine as a substrate. Moreover, this study also highlighted a significant contribution of glutaminolysis to glutathione synthesis, under hypoxic environments. Glutathione which is a reducing agent plays a significant role in preventing damage to important cellular components mainly caused by an excess of reactive oxygen species (ROS) such as free radicals or peroxides (Pompella et al. 2003). Under hypoxia, a mismatch between NADH production and terminal oxidase activity can generate an excess level of ROS (Wu et al. 2007). MYC-induced cancer cell is able to overcome such an oxidative stress under hypoxia for survival by enhancing a conversion of glutamine to glutathione (Le et al. 2012).

1.6.2. Triangular interactions among MYC, mTOR and glutamine metabolism

The interaction between mTOR and glutamine metabolism has been shown in section 1.5.2 and the induction of MYC to glutaminolysis has also been documented in section 1.6.1. Together, these findings raised a question of a potentially common translational node between MYC and mTOR signalling pathway. It has been found that MYC indirectly activates mTOR activity by stimulating genes involved in amino acid import, such as glutamine and leucine (Dang 2013). Surprisingly, an unexpected and important link between MYC and mTOR has been uncovered by Pourdehnab et al through the tumour suppressor eukaryotic translation initiation factor 4E binding protein 1 (4EBP1) and oncogene eukaryotic translation initiation factor 4E (eIF4E) (Pourdehnab et al. 2013) (Fig 1.6). mTOR has been shown to control protein synthesis by directly phosphorylating 4EBP1. This phosphorylation of 4EBP1 which prevents its suppression on eIF4E is essential for cancer survival throughout MYC tumour development, tumour initiation and maintenance (Brown et al. 1995; Gingras et al. 1998; Gingras et al. 2001; Kim et al. 2002; Bader et al. 2005; Ruvinsky and Meyuhas 2006; Sonenberg and Hinnebusch 2009). Moreover, eIF4E is known to be transcriptionally activated by MYC (Schmidt 2004), and the overexpression of eIF4E is capable of promoting MYC tumorigenesis (Wendel et al. 2004). Importantly, it has been demonstrated that hyperactivation of eIF4E, through inhibition of 4EBP1, is essentially important for mTOR-dependent tumorigenesis (Hsieh et al. 2010; Dumstorf et al. 2010). In this regard, the mTOR-4EBP1-eIF4E-MYC axis appears to be a significantly common node and druggable target for future cancer therapy. Sapanisertib (MLN0128) which is a dual mTOR inhibitor has been tested in Myc-driven myeloma cells (Pourdehnab et al. 2013). The inhibitor was shown to effectively block mTOR-dependent 4EBP1 phosphorylation and cause cell death in Myc-driven myeloma cells. This provides evidence that mTOR inhibitors might have therapeutic efficacy on Myc-dependent tumour cell through the common node 4EBP1-eIF4E.

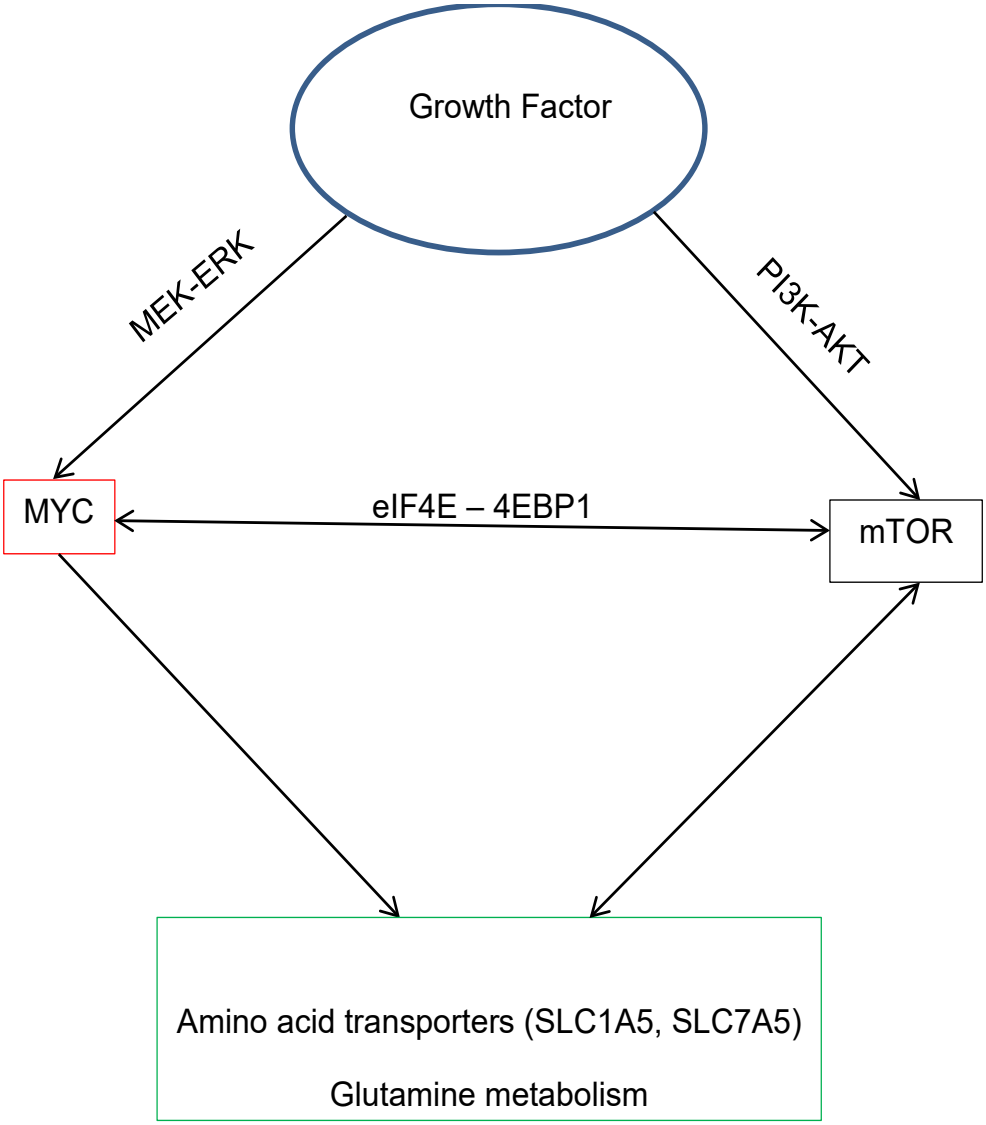

Figure 1.6. Triangular interaction among MYC, mTOR and glutamine metabolism. Growth factor receptor activates mTOR through PI3K and MYC through the MEK-ERK pathway. MYC stimulates the amino acid import, especially glutamine and leucine which further activate mTOR signalling pathway. mTOR phosphorylation of 4EBP1 prevents its suppression of eIF4E and is essential for MYC tumour development. MYC transcriptionally activates eIF4E which is essentially important for mTOR-dependent tumorigenesis.

1.6.3. Cdk2 Kinase and Myc-repressed senescence: Potential target for cancer treatment

Apoptosis and senescence are two main barriers of tumour development. Apoptosis which is a form of pre-programmed cell death functions in removal of damaged or pre-neoplastic cells (Green 2011). Senescence or permanent cell cycle arrest normally

happens in primary human cells in culture after undergoing a finite number of divisions (Hayflick and Moorhead 1961). Overactive MYC stimulates apoptosis, and Ras oncogene induces senescence (Serrano et al. 1997; Zindy et al. 1998). The co-expression of MYC and Ras has been found to suppress these barriers. Ras was known to inhibit MYC-induced apoptosis via the PI3K/Akt pathway (Land et al. 1983, Larsson and Henriksson 2010). It was then discovered that Cdk2-mediated phosphorylation of MYC suppresses Ras-induced senescence (Hydbring and Larsson 2010). Cdk2 and MYC are involved in an autostimulatory loop in suppression of senescence. MYC stimulates Cdk2, which, subsequently, phosphorylates MYC to supress senescence and promote tumour initiation. Hydbring and Larsson found that inhibition of Cdk2 prevents MYC-suppressed senescence and turns MYC into an inducer of senescence, and subsequently tumour suppressor (Hydbring and Larsson 2010). This represents Cdk2 as a potential target for the treatment of MYC driven tumours.

1.7. Imaging of cancer metabolism

1.7.1. Positron Emission Tomography

Positron Emission Tomography (PET) is a nuclear medicine functional imaging technique which is widely used for the monitoring of metabolic processes and the diagnosis of disease. Initially, a tracer which is made by attaching a radioisotope to a chemical substance used by a particular organ or tissue is injected into patient's body. The tracer then moves to and gets trapped in the tissue of interest. The positrons which are emitted from the unstable nucleus of the radioisotope collide with the electrons in the tissue in an annihilation reaction to produce two gamma-ray photons moving in opposite directions. A scanner then detects these two photons and a computer is used for the analysis and image construction (Bailey et al. 2005). The most commonly used radioisotope is fluorine-18, which is attached to the biologically active molecule of interest for introduction into the body. Depending on the purpose of study, different ligands can be used. PET imaging can be combined with X-ray computed tomography (CT) to isolate anatomic changes in the body in addition to the PET capability of detecting areas of molecular biology detail. PET has an advantage of assessing the biochemical changes which are altered in the earliest stages of

diseases. Hence, PET can detect these changes before anatomical or structural changes occur and are displayed by Magnetic Resonance Imaging (MRI) or CT. However, the spatial resolution is a drawback of PET (Full width at half maximum FWHM = 4 – 10 mm) when compared with MRI (FWHM = 1 – 2 mm) or CT (FWHM = 0.5 – 0.625 mm) (Lin and Alessio 2009; Zhu et al. 2011).

The Warburg effect or aerobic glycolysis demonstrates a higher glucose uptake in cancer cells. Based on this finding, the glucose analogue ^{18}F-Fluorodeoxyglucose ([^{18}F]FDG) is used in PET imaging to evaluate the *in vivo* glucose uptake of tumours. Currently, [^{18}F]FDG PET scans which can be routinely used for staging and restaging various malignant tumours such as lung, pancreatic, colorectal and ovarian cancers with a very high sensitivity and specificity of ~ 90% or even more are widely used to diagnose cancer in hospitals worldwide (Zhu et al. 2011).

The [^{18}F]FDG glucose analogue has been shown to be taken up by cells via glucose transporters such as GLUT1, be phosphorylated to [^{18}F]-Fluorodeoxyglucose-6-phosphate by hexokinase in the first step of glycolysis (Brown and Wahl 1993; Reske et al. 1997; Brown et al. 1999). This phosphorylation prevents the tracer from being released from the cell again. A significant difference between [^{18}F]FDG and normal D-glucose is the lack of 2-hydroxyl group (OH) in this glucose analogue which suppresses [^{18}F]FDG from being metabolized further in cells (Torizuka et al. 1995; Rempel et al. 1996; Caraco et al. 2000). The forming of [^{18}F]-Fluorodeoxyglucose-6-phosphate happens when [^{18}F]FDG enters the cell, thus, cannot move out of the cell before radioactive decay. As a consequence, the distribution of [^{18}F]FDG reflects both the glucose uptake and phosphorylation by cells in the organ of interest (Maschauer et al. 2004). The loss of cancer cells' viability can be measured by a decrease in [^{18}F]FDG signal. [^{18}F]FDG uptake can also be used to monitor treatment response of cancer cells to drugs that target glucose metabolism (Sunaga et al. 2008). Beside [^{18}F]FDG, other PET imaging agents which include ^{11}C-acetate, a precursor of acetyl-CoA, in various types of solid tumours (Grassi et al. 2012), ^{18}F-choline in prostate cancer (Vali et al. 2015), ^{11}C-methionine in brain tumours (Glaudemans et al. 2013) and ^{18}F-fluorothymidine as a proliferation marker for tumour response to therapy assessment (Barwick et al. 2009; Mankoff et al. 2005) have also been being used.

Despite the widely use of [^{18}F]FDG PET in clinical practice, a notable fraction of tumours was reported to be [^{18}F]FDG negative and could not be detected by [^{18}F]FDG PET (Robey et al. 2008). This phenomenon indicates these types of tumours may depend on nutrients other than glucose. Previous studies suggest that these [^{18}F]FDG negative tumours may have switched their metabolic pathway to glutaminolysis (Wise et al. 2008; Thompson 2009; Cheng et al. 2011; Rajagopalan and DeBerardinis 2011; Shanware et al. 2011; Gao et al. 2009). Non – invasive PET imaging of glutamine may be an alternative method for [^{18}F]FDG negative tumours. It could also provide measurable indicators for tumour response following therapies, such as inhibition of mTORC1 pathway or MYC. Another potential application of this glutamine based PET tracer is dose painting, which could provide spatial optimization of radiotherapy dose based on tumour areas that are, for example, more responsive or resistant to radiotherapy (Baumann et al. 2016).

To develop a glutamine based PET imaging agent, (2S)-5-[^{11}C]-glutamine ([^{11}C]-Gln) (Fig. 1.7A) which is the radiolabelled version of naturally occurring glutamine was developed and showed a high tumour cell uptake (Qu et al. 2011). However, there has been no reported human studies of [^{11}C]-Gln and this could be due to the short physical half-life of ^{11}C ($T_{1/2}$ = 20 min) and/or the complicated radiolabeling and purification. To overcome these obstacles of ^{11}C-Gln, a new ^{18}F-glutamine based PET tracer called (2S, 4R)-4-[^{18}F]fluoroglutamine (4-[^{18}F]fluoroglutamine), which has a half-life of 5.5 times longer than that of ^{11}C ($T_{1/2}$ of ^{18}F = 110 min), was synthesized and examined (Qu et al. 2011) (Fig. 1.7B). This tracer showed high uptake by cancer cells *in vitro* and *in vivo* (Liebermann et al. 2011) and is now being used in a phase I clinical trial NCT01697930 by the Memorial Sloan Kettering Cancer Center (NY, USA). This trial enrolled 25 patients bearing either solid malignancy (breast, colon, lung, pancreas cancer) or lymphoma which were confirmed and visualised with MRI, CT or [^{18}F]FDG PET. The results were very promising when 4-[^{18}F]fluoroglutamine PET imaging was able to depict tumours of different cancer cell types and produced comparable signal with [^{18}F]FDG PET. More importantly, an advantage of 4-[^{18}F]fluoroglutamine PET over [^{18}F]FDG PET found in this study was patients did not need to be fasted at least 8 hours before the imaging session. It would be beneficial for patients with metabolic diseases like diabetes (Dunphy et al. 2018).

A

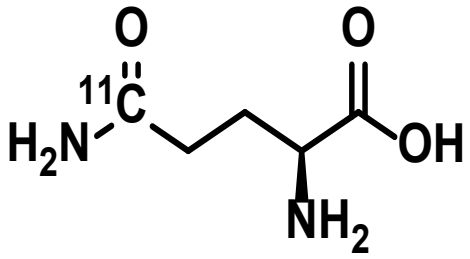

(2S)-5-[^{11}C]glutamine

[^{11}C] - Gln

B

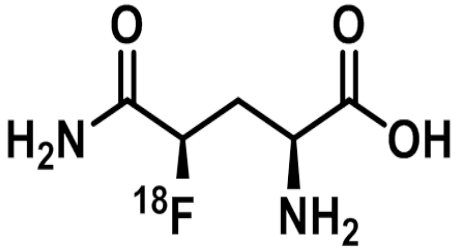

(2S, 4R)-4-[^{18}F]fluoroglutamine

4-[^{18}F]fluoroglutamine

Figure 1.7. Structures of glutamine-based PET imaging agents. A. 5 – ^{11}C – (2S) – glutamine. **B.** (2S, 4R)-4-[^{18}F]fluoroglutamine.

Further characterisation of 4-[^{18}F]fluoroglutamine is required, in order to gain a better understanding on the metabolic fate of this PET tracer and to confirm whether 4-[^{18}F]fluoroglutamine is a true surrogate for L-glutamine. The major concern is whether the replacement of an hydrogen atom with a highly electronegative fluorine atom in the 4 position of L-glutamine could result in the formation of a non-physiological L-amino acid and affect the biological properties of the 4-[^{18}F]fluoroglutamine and its metabolic activity *in vitro* and *in vivo*. Cooper et al suggested that by replacing a C-H with a C-F bond in this case only had minor effects on the binding and substrate processing of glutamine utilizing enzymes on this fluorinated glutamine analogue (Cooper et al. 2012). They reasoned that the van der Waal and atomic radii of F (1.47 Å, 0.42 Å, respectively) and H (1.2 Å, 0.53 Å, respectively) were relatively similar (Bondi 1964). Although there is a large difference in electronegativity of two atoms (F, 4; H, 2.1), they did not find any significant effect on the binding of 4-[^{18}F]fluoroglutamine to glutamine-utilising enzymes due to this difference (Cooper et al. 2012). Furthermore, they also found that 4-[^{18}F]fluoroglutamine was an even better substrate for glutaminase in rat kidney than L-glutamine. This was all due to the electron-withdrawing properties and negative inductive effect of the F atom on the C-F bond which result in the better affinity of 4-[^{18}F]fluoroglutamine to the active site of the glutaminase enzyme. It was suggested that 4-[^{18}F]fluoroglutamine may be

metabolized in a similar fashion to L-glutamine (Cooper et al. 2012). The proposed metabolic pathway of this tracer is summarized in Figure 1.8 (Cooper et al. 2012).

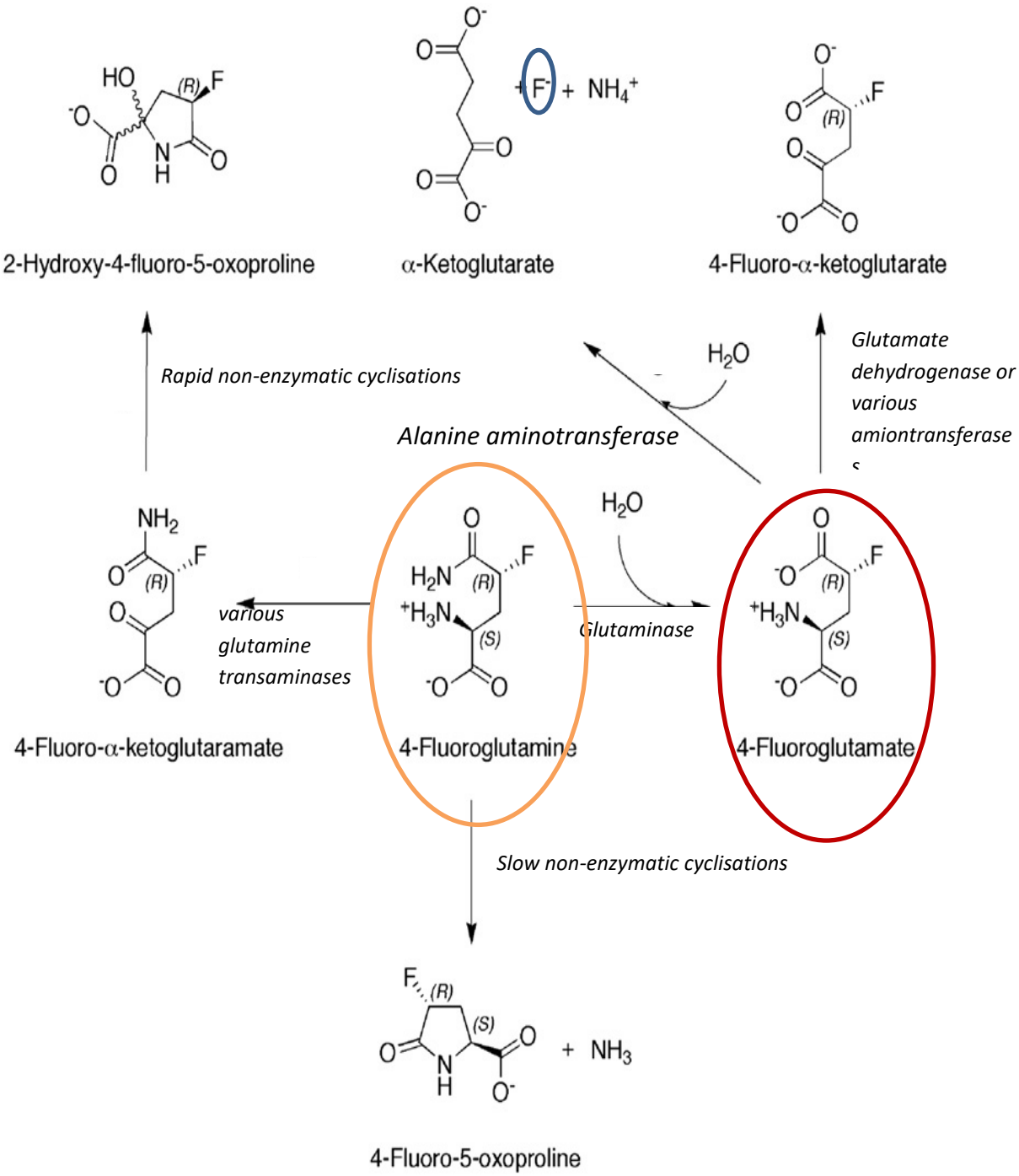

Figure 1.8. The proposed metabolic pathways involved in the metabolism of (2S, 4R)-4-[^{18}F]fluoroglutamine in liver extracts using purified enzymes. 4-Fluoroglutamine (orange circle) can be enzymatically hydrolyzed to 4-Fluoroglutamate (red circle) which can be metabolized further by glutamate dehydrogenase to 4-Fluoro-α-ketoglutarate. The detection of the free F^- (blue circle) in tumours exposed to 4-Fluoroglutamine in the study also revealed the coupling of a deamidase reaction with a γ-elimination reaction in which the enzyme alanine aminotransferase plays an important role. Slow and rapid non-enzymatic cyclisations can lead to the formation of 4-Fluoro-5-oxoproline and 2-Hydroxy-4-Fluoro-5-oxoproline, respectively. Diagram adapted from Cooper et al. (2012).

1.7.2. Magnetic Resonance Spectroscopy

The application of nuclear magnetic resonance (NMR) spectroscopy in biomedicine comprises two components: magnetic resonance imaging (MRI) and magnetic resonance spectroscopy (MRS). MRS can be applied as a research tool in diverse studies, ranging from isolated cells, body fluids or organs such as prostate (Thomas et al. 2014), or brain (Dowling et al. 2001). NMR spectroscopy is a term used to describe MRS *ex vivo* (high-resolution MRS) which is applied to study metabolism in cell, biofluids or tumour extracts (Michelli et al. 2006; DeBerardinis et al. 2007). High-resolution magic angle spinning (HR-MAS) MRS which is less sensitive than NMR is a method applied to measure metabolites in solid tumours and cell samples. The advantages of HR-MAS MRS include less sample preparation, no tissue destruction and easier application to the clinics (DeFeo and Cheng 2010). Dynamic nuclear hyperpolarisation (DNP) which enables a temporal enhancement of MRS signal from ^{13}C-labelled compounds (≥ 10,000 fold) is a method used to examine multiple metabolic pathways non-invasively *in vivo* (Wilson et al. 2010; Witney et al. 2011). *In vivo* MRS can be applied and guided by selecting the region of interest following a MRI scan to obtain information on the changes of metabolites in specific tissues. Total choline to creatine ratios have been used to monitor treatment response in squamous cell carcinoma (Mukherji et al. 1997). Reduced levels of citrate in prostate tumours and N-acetylaspartate in brain cancers were observed when compared with normal tissues (Dowling et al. 2001; Thomas et al. 2014). *In vivo* MRS has also been being used in clinical practice in combination with MRI on the whole-body MRI scanners to study the metabolism of specific regions of interest in the human body. The sensitivity of MRS (1.5 – 3.0 T) appears to be a limiting factor, especially for *in vivo settings*, However, this limitation can be overcome by using much higher magnetic field strengths (~11.7-14.1 T) (Tognarelli et al. 2015).

Chemical nuclei such as ^{1}H, ^{13}C, ^{31}P and ^{19}F can be detected by MRS based on a magnetic property they possess, which is called “spin”. This phenomenon was first discovered in 1946 by Bloch and Purcell (Belouche-Barbari et al. 2010; Tognarelli et al. 2015). The most abundant atom in living organisms is hydrogen. It uses high power magnetic fields on in vitro samples. When the stated nuclei are placed in a constant magnetic field, the orientation of the nucleus with respect to that field will decide the energy of the magnetic moment. The nuclei transitions between high and low energy

states can be stimulated by applying the electromagnetic radiation at a suitable frequency. The energy absorption detection and the transition in energy level provide the basis for NMR spectroscopy (Harwood et al. 2003; Higson 2004). The type of chemical nucleus and the chemical environment surrounding it will decide the interaction of the nuclei with the magnetic field, and hence the resonant radiofrequency. The resonant frequency of a nucleus relative to a standard in a magnetic field is termed the “chemical shift” which is expressed in units of parts per million (ppm). The structure of a molecule can often be diagnosed by the position and number of chemical shifts (Lin and Chung 2014).

MRS can be applied for *ex vivo* study such as interpretation of metabolism in cellular and tumour extracts, or biofluids. ^{1}H-MRS provides information on a wide range of metabolites from glucose, fatty acids to amino acids metabolites due to a high abundance of hydrogen in living organisms. ^{1}H-MRS has been used widely to study glucose metabolism in brain (Kaiser et al. 2016; Zhao et al. 2018; Lai et al. 2018; Roussel et al. 2019). ^{1}H-MRS has also been applied to measure the glutamine level and study the glutamine-glutamate cycle in brain (Pioro et al. 1999; Radaman et al. 2013; Świątkiewicz et al. 2017; Hasler et al. 2019). The glutamine metabolism in cancer cells was also examined by ^{1}H-MRS (Li et al. 2015; Zhou et al. 2017).

The application of ^{13}C-MRS is limited as the natural abundance of ^{13}C is too low for the measurements. Usually, only ^{13}C-MRS enriched metabolites are studied by this ^{13}C-MRS technique. Miccheli et al employed this technique to study the flux of ^{13}C-glucose in metabolism pathways such as glycolysis and the TCA cycle (Miccheli et al. 2006). Deberardinis et al also applied ^{13}C-MRS to study ^{13}C-Glutamine as a substrate to replenish the intermediates in the TCA cycle (Deberardinis et al. 2007). ^{13}C-Glutamine was also applied to show Myc-induced lymphoma was able to change its metabolism from glucose to glutamine dependence to survive under glucose depleted conditions (Le et al. 2012). ^{13}C-pyruvate is the most commonly used probe in DNP-MRS to measure pyruvate to lactate exchange in cancer cells (Day et al. 2007; Park et al. 2011; Chen et al. 2013)

The combination of ^{31}P-MRS and ^{1}H-MRS has been applied widely to study membrane phospholipid metabolism of which the elevation distinguishes cancer from normal cells (Glunde et al. 2011). Significant phospholipid metabolites include phosphocholine

(PCho), glycerophosphocholine (GPC), phosphoethanolamine (Peth), glycerophosphoethanolamine (GPE), inorganic phosphate (Pi) and ATP, ADP. In addition, ^{31}P-MRS can also be used in bioenergetic studies such as measuring phosphocreatine (PCr) recovery rate in skeletal muscle oxidative metabolism in sub-clinical thyroid dysfunction (Rana et al. 2012). ^{31}P-MRS can also measure the intracellular pH by examining the chemical shift difference between pH-dependent Pi and pH-independent reference peak in non-Hodgkin's lymphoma patients (Rata et al. 2014).

^{19}F-MRS can be used to study the structure and metabolism of drugs that contain a fluorine atom. ^{19}F-MRS has been applied to assist the synthesis of [^{18}F]FDG PET imaging tracer (Bida et al. 1984) and to study the metabolism of the drug 5-fluorouracil and compare its pharmacokinetics following intravenous and intraperitoneal administration (Wolf et al. 1990). In addition, [^{19}F]FDG has been used to identify pathological information such as neurological disorder or inflammatory response in animal and human studies (Stevens 1987). As ^{19}F-metabolites are not naturally present in mammalian cells, ^{19}F-labelled molecules or drugs can be easily traced in living systems by ^{19}F-MRS due to the low background (Glaholm et al. 1990; McIntyre et al. 2011). The favourable characteristics of ^{19}F-MRS include: 100% natural abundance, 84% sensitivity in comparison with ^{1}H-MRS, and a wide chemical shift range which is greater than 200 ppm (Wolf et al. 2000, Gadian 1996).

As mentioned in section 1.7.1, the metabolic fate of 4-[^{18}F]fluoroglutamine still requires further studies to confirm whether it is a true surrogate for L-glutamine. The limitation of PET imaging is the absence of chemical information because PET imaging can be used to measure the radiotracer uptake of 4-[^{18}F]fluoroglutamine but it cannot distinguish the metabolised molecules from the parent compound without the complex ex vivo radio-HPLC metabolite analysis. In this case, ^{19}F-MRS can be used to provide information about downstream metabolism of the tracer, as a complementary imaging strategy to validate the findings of the PET imaging and to assist early preclinical investigation using glutamine metabolism as a biomarker. To assist in the study of the metabolic profile of 4-[^{18}F]fluoroglutamine, a ^{19}F version of this PET tracer has been synthesized at ICR (Fig. 1.9). The fluorine – 19 is a stable isotope and also the second most abundant MRS nucleus, which can be detected by MRS. Therefore, ^{19}F-MRS can be used to study the downstream metabolic fate of 4-[^{18}F]fluoroglutamine.

The preliminary ^{19}F-MRS results obtained by members in the lab at ICR (Drs Gabriela Andrejeva and Yuen-Li Chung) showed that (2S, 4R)-4-[^{19}F]fluoroglutamine (4-[^{19}F]fluoroglutamine) was metabolised by colorectal carcinoma HCT116 Bax-ko cells and tumours (Fig. 1.10). The metabolite products were (2S, 4R)-4-[^{19}F]fluoroglutamate (4-[^{19}F]fluoroglutamate), ^{19}F-4-Fluoro-5-oxoproline and free F^-. These findings, which are consistent with some of the metabolic pathways proposed by Cooper et al. for the metabolism of 4-[^{19}F]fluoroglutamine in liver extracts using purified enzymes, support the hypothesis that glutaminase and alanine aminotransferase enzymes play important roles in the metabolism of 4-[^{19}F]fluoroglutamine (Cooper et al. 2012) (Fig. 1.7). Normal glutamine is taken up by cancer cells and tumours and metabolised to glutamate by glutaminase which is then further metabolised to α-ketoglutarate (by glutamine dehydrogenase) for use in the TCA cycle (Fig. 1.2). Similar to normal glutamine metabolism, 4-[^{19}F]fluoroglutamine is converted to 4-[^{19}F]fluoroglutamate in these studies. The 'free F^-' observed in the ^{19}F-MRS studies is likely due to the metabolism of 4-[^{19}F]fluoroglutamate to α-ketoglutarate catalysed by alanine aminotransferase as proposed by Cooper et al. The presence of 'free F^-' could be a marker for the formation of α-ketoglutarate from 4-[^{19}F]fluoroglutamate

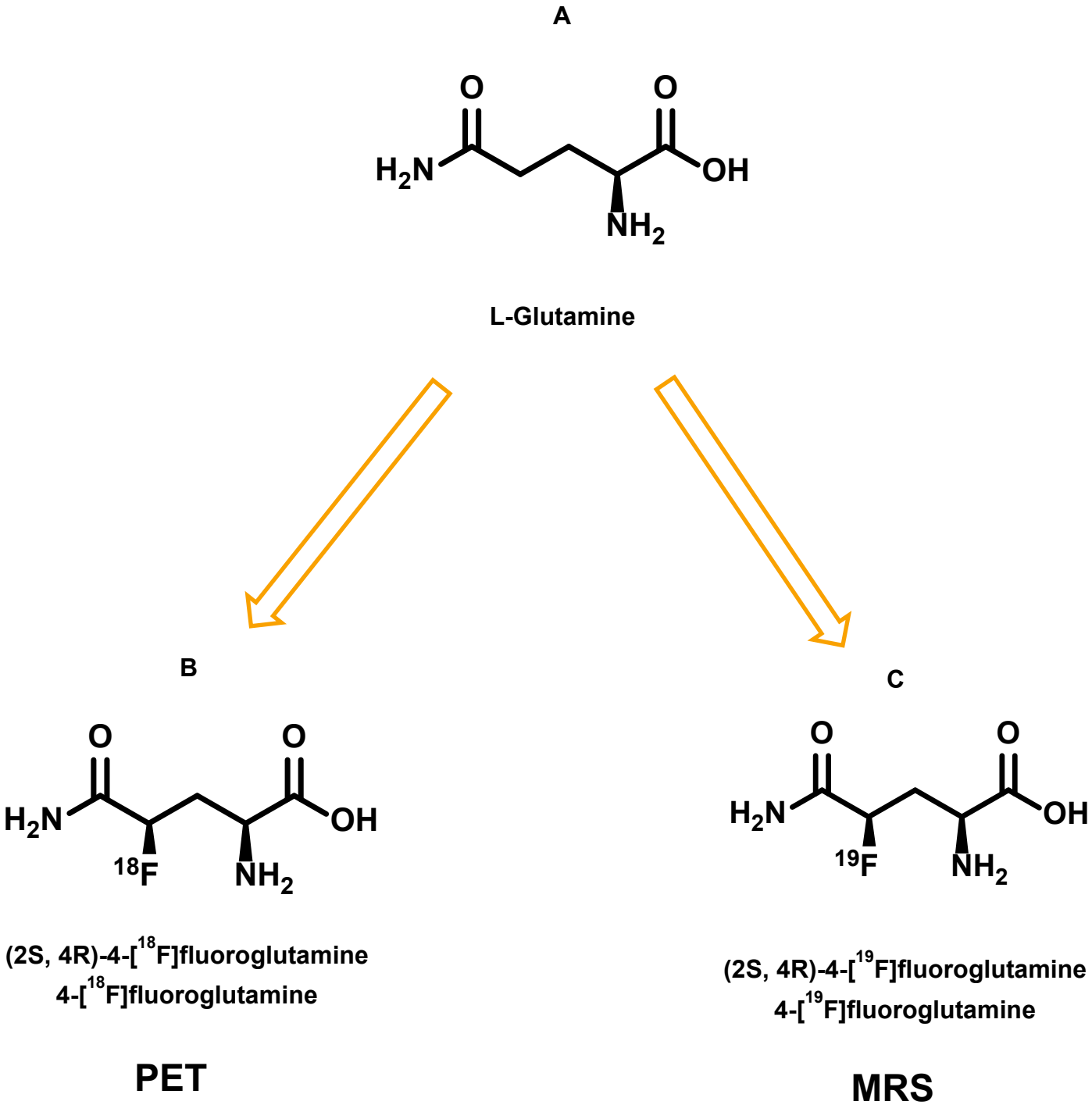

Figure 1.9. Structures of L-glutamine and glutamine based PET and MRS imaging agents. A. L-glutamine. **B.** (2S, 4R)-4-[^{18}F]fluoroglutamine. **C.** (2S, 4R)-4-[^{19}F]fluoroglutamine

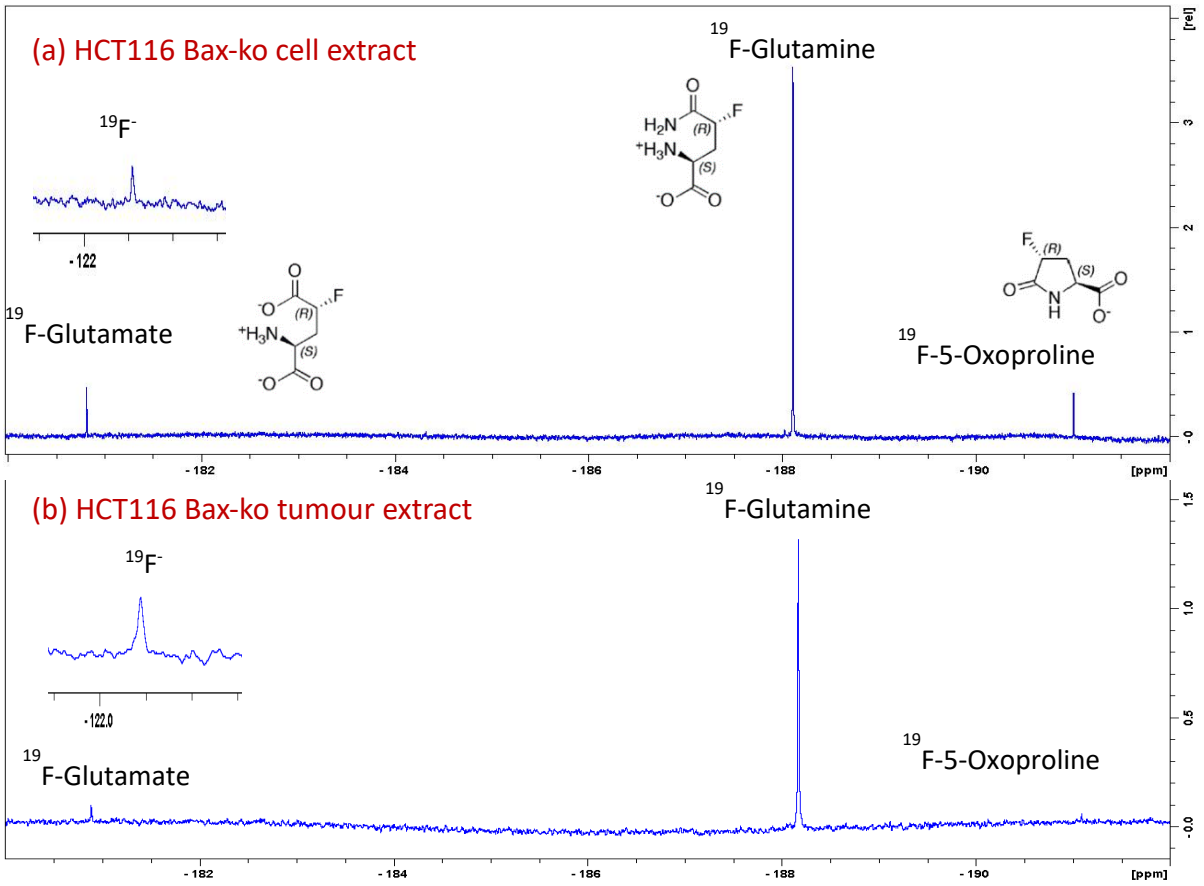

Figure 1.10. ^{19}F – MRS of (a) HCT116 Bax – ko cell extract after 6 h of incubation with (2S, 4R)-4-[^{19}F]fluoroglutamine; **(b)** HCT116 Bax – ko tumor extract after 2 h of (2S, 4R)-4-[^{19}F]fluoroglutamine injection. Figure kindly provided by Yuen-Li Chung (ICR, Sutton, United Kingdom).

1.8. Hypotheses and Aims of thesis

1.8.1. Hypotheses

a) 4-[^{18}F]fluoroglutamine follows the same metabolism pathway as L-glutamine.

b) 4-[^{18}F]fluoroglutamine can be used as an alternative PET tracer to [^{18}F]FDG for tumours which have a low uptake of [^{18}F]FDG.

c) 4-[^{18}F]fluoroglutamine can be used to monitor glutamine metabolism in cancer cells and tumours.

d) The quantitative information on treatment response following novel anti – cancer therapies that target PI3K/AKT/mTOR pathway and Cdk2 Kinase can be obtained by ^{1}H-MRS and the non – invasive PET imaging of glutamine using 4-[^{18}F]fluoroglutamine in relevant ovarian, lung cancer and neuroblastoma models. The collection of this information will enable the further application of the glutamine-based PET tracer in the clinic.

1.8.2. Overall aims

(i) examine the metabolism of 4-[^{18}F]fluoroglutamine in cancer cells by using 4-[^{19}F]fluoroglutamine and [^{19}F]-Magnetic Resonance Spectroscopy (MRS), in order to confirm whether the metabolic fate of this PET tracer is the same as L-glutamine (Chapter 3).

(ii) investigate the uptake of 4-[^{18}F]fluoroglutamine in comparison with [^{18}F]FDG in different cancer cell lines and tumour xenograft models, in order to confirm whether 4-[^{18}F]fluoroglutamine can be used as an alternative PET tracer to assess cellular metabolism in certain types of tumour with a low uptake of [^{18}F]FDG (Chapter 4).

(iii) evaluate the 4-[^{18}F]fluoroglutamine PET tracer for use in monitoring glutamine metabolism and therapeutic efficacy in cancer cells and tumour xenograft models following treatment with inhibitors that target mTOR (Chapter 5) or Cdk2 Kinase-MYC (Chapter 6).

1.9. Structure of the thesis

This thesis is presented as follows:

Chapter 1. Introduction. An overview picture of cancer metabolism, thorough details of glutamine transport metabolism in cancer cell, the interactions between PI3K/AKT/mTOR pathway and glutamine metabolism as well as between Myc signalling and glutamine metabolism are introduced. The effect of PI3K/AKT/mTOR pathway or Cdk2 Kinase-MYC inhibition on glutamine metabolism and tumour survival is also investigated in the literature. Current state-of-the-art methods of cancer metabolism imaging are described with a view on benefits and limitations. The overall hypotheses and aims are presented.

Chapter 2. Materials and Methods. This chapter is for a detailed description of the materials and methods used throughout this thesis.

Chapter 3. Evaluation of the metabolic pathways of 4-[^{18}F]fluoroglutamine PET tracer in cancer cells. This chapter characterizes the metabolic fate of 4-[^{18}F]fluoroglutamine to confirm the hypothesis that 4-[^{18}F]fluoroglutamine follows the same metabolism pathway as L-glutamine.

Chapter 4. *In vitro* and *in vivo* uptake of 4-[^{18}F]fluoroglutamine and [^{18}F]FDG in a panel cancer cell lines. This chapter compares the uptake of 4-[^{18}F]fluoroglutamine and [^{18}F]FDG in different cancer cells and tumour xenograft models and explores the hypothesis that 4-[^{18}F]fluoroglutamine can be used as an alternative PET tracer to [^{18}F]FDG for tumours which have a low uptake of [^{18}F]FDG.

Chapter 5. PI3K/AKT/mTOR pathway and Glutamine Metabolism. This chapter evaluates the value of 4-[^{18}F]fluoroglutamine PET imaging in monitoring cellular response and glutamine metabolism changes following the inhibition of mTOR pathway by using Vistusertib AZD2014 as a single agent, the treatment with Paclitaxel as a single agent and the combination treatment of AZD2014 and Paclitaxel. Paclitaxel monotherapy has been used in the treatment of many cancer types. However, resistance to Paclitaxel treatment was found in gynaecological cancer and activation of the PI3K/mTOR signalling pathway was shown to be one of the mechanisms behind treatment resistance. Based on these findings, the combinations of novel anticancer drugs, such as mTOR kinase inhibitors, with Paclitaxel were found to be effective in

cancer growth inhibition in ovarian cancer, pancreatic cancer, breast cancer and squamous non-small-cell lung cancer (Basu et al. 2015; Wong et al. 2017; Basu et al. 2018) when compared with the use of Paclitaxel as a monotherapy**.**

Chapter 6. Evaluating the effect of Cdk2 Kinase Inhibition on Glutamine Metabolism. This chapter evaluates the changes of cellular response and glutamine metabolism following the inhibition of Cdk2 Kinase and its subsequent MYC phosphorylation pathway by using CYC065.

Chapter 7. Summary. This chapter summarises main findings, presents conclusions and proposes future directions for this thesis.

Chapter 2

Materials and Methods

2.1. Cell culture and cellular assays

2.1.1. Maintenance of cell lines

All media and reagents for cell culture were purchased from Life Technologies and Sigma-Aldrich, UK, unless otherwise stated. HCT116 WT cells were a kind gift of Dr. Alexis Barr (the Institute of Cancer Research, London, UK), HCT116 Bax-ko cells were a kind gift of Dr. Paul Clarke (the Institute of Cancer Research, London, UK), PC3 cells were purchased from ATCC. Kelly and MDA-MB-231 cells were a kind gift from Dr. Gabriela Kramer-Marek (the Institute of Cancer Research, London, UK), and TU8902, TU8988T, TU8988S, ASPC-1, T3M4, MIA PaCa-2, NCI-H508, DAN-G cells were a kind gift from Dr. Anguraj Sadanandam (the Institute of Cancer Research, London, UK). Kelly WT, Kelly CYC065R, VMRC-LCD WT, VMRC-LCD CYC065R were a kind gift from Dr. Igor Vivanco (the Institute of Cancer Research, London, UK). A2780 cisR and H520 were purchased from ATCC, Teddington, UK. HCT116 WT, HCT116 Bax-ko, PC3, VMRC-LCD WT and VMRC-LCD CYC065R cells were grown in Dulbecco's Modified Eagle Medium (cat. 41965-039, Gibco, Life Technologies, UK) (DMEM with 3.97mM L-glutamine, 25 mM D-glucose, without sodium pyruvate) supplemented with 10% Fetal Bovine Serum (FBS), 1% non-essential amino acids (NEAAs) and 5,000 units of penicillin-streptomycin. Kelly WT and Kelly CYC065R cells were grown in RPMI media (cat. 61870-010, Gibco, Life Technologies, UK) supplemented with 10% FBS. A2780 cisR and H520 cells were grown in RPMI media (cat. 32404-014, Gibco, Life Technologies, UK) (without L-Glutamine and Phenol red indicator) supplemented with 10% Fetal Bovine Serum (FBS), 1% non-essential amino acids (NEAAs), and 2.2 mL of 200 mM L-Glutamine. The rest of cell lines was grown in DMEM+Glutamax (cat. 61965-026, Gibco, Life Technologies, UK) supplemented with 10% FBS. Cells were maintained subconfluently in flasks and culture media were changed every two days. Cells have been STR profiled (100% match with the reference profile of ATCC, DSMZ) and mycoplasma tested (no infection found).

2.1.2. Cytotoxicity assay of CB-839 and L-cycloserine

HCT116 WT and HCT116 Bax-ko were treated with the CB-839 (Calithera Biosciences) or L-cycloserine (Sigma-Aldrich) for 72 hours and the cytotoxicity was determined by the sulforhodamine B (SRB) assay. The method was adapted from Skehan et al. (1990).

Materials and solutions:

Fixative solution:

10% trichloroacetic acid (TCA) (store at room temperature (RT))

Prepare this solution by adding 227 mL of water to 500 g of TCA (BDH chemicals) to give a 100% solution weight/volume (w/v) and simply dilute total volume to 10% with double distilled (dd) water.

Stain solution:

Sulforhodamine B (Sigma S1402) dissolved to 0.4% (w/v) in 1% volume/volume (v/v) acetic acid.

Store at RT.

Wash solution:

1% acetic acid (v/v).

Store at RT.

Eluting solution:

10 mM Tris base, pH 10 approx.

Store at RT.

Methods:

Day 1: 2000 cells were seeded in 100 µL normal growth medium/well to inner 60 wells of a 96-well plate. 200 µL/well sterile phosphate-buffered saline (PBS)/water was added to outer wells.

*The seeding density must be carefully determined for each cell line in pilot experiments. Ensure the control cells are just sub-confluent before the assay is stopped. The control cells will slow down or stop proliferating if they are too confluent and the cells in drug treatment will continue to proliferate & 'catch up' with the control cells. This will artificially increase the GI_{50} value.

Day 2: Serial dilution of drugs were prepared allowing for 100 µL/well at 2x the desired final concentration. 6 replicate wells per drug concentration were used. The control wells contained DMEM media only (for L-cycloserine assay) or DMEM media supplemented with 0.1% (v/v) DMSO (for CB-839 assay). Different concentrations of CB-839 in DMEM media supplemented with final concentration of 0.1% (v/v) DMSO or various concentrations of L-cycloserine in DMEM media were placed in treatment wells. Cells were then incubated with drug or vehicle solutions for 72 hours. The drug concentrations used for CB-839 assay were 0, 0.0078, 0.0156, 0.03125, 0.0625, 0.125, 0.25, 0.5, 1 µM; and for L-cycloserine assay were 0, 3.90625, 7.8125, 15.625, 31.25, 62.5, 125, 250, 500, 1000 µM.

Day 5: Growth medium was discarded. Cells were fixed by adding 100 µL/well 10% TCA and incubated at RT for 1 hour. The plates were then washed twice with tap water to remove fixative and then dry completely in a low heat oven for 1 hour. Cells were then stained using 100 µL/well 0.4% SRB for 1 hour. After that, the plates were washed once with tap water and 3-4 times with acetic acid wash solution. Firm tap on the bottom of the plates over a dry paper towel were delivered to confirm the excess stain was removed completely. The plates were then kept in an oven for drying. The stain was eluted by adding 100 µL/well Tris buffer. The plates were tapped gently to encourage homogenous mixing of the solutions. Finally, the absorbance was measured at 570 nm using the FLUOstar® Omega microplate reader. The background reading consisted of empty wells that contain fixative, stain and Tris solutions. The plates can be kept at room temperature as cells can be restained at a later date if required.

2.1.3. Determination of treatment schedules and optimal conditions for CB-839 and L-cycloserine studies

The GI_{50} values for CB-839 and L-cycloserine were determined from the cytotoxicity assay (Section 2.1.2). The treatment schedule and optimal conditions were then determined as follow. HCT116 WT and HCT116 Bax-ko were seeded at a density of $1x10^6$ cells into each T25 flasks. The cells were treated with CB-839 or L-cycloserine at concentrations of 0, $1xGI_{50}$, $3xGI_{50}$, $5xGI_{50}$ and $10xGI_{50}$ for 24 hours. The cells were then collected by trypsinization and counted on a haemocytometer. The drug concentration that causes reduction in proliferation (with the number of treated cells approximately 50% of control cells) is chosen for further metabolic studies.

2.1.4. Cell treatment

HCT116 WT and HCT116 Bax-ko were seeded into T75 flasks, incubated overnight (37ºC, 5% CO2) and then treated for 24 hours with either $10xGI_{50}$ of CB-839 or L-cycloserine. A2780 cisR cells were treated for 24 hours with 303.5 nM or with 607 nM Vistusertib AZD2014 (AstraZeneca, UK) as a single agent , with 7.75 nM Paclitaxel (USBiological Life Sciences) as a single agent or with both AZD2014 (303.5 nM or 607 nM) and Paclitaxel (7.75 nM) as a combination treatment. H520 cells were treated for 24 hours with with 503.3 nM or with 1006.5 nM Vistusertib AZD2014 (Astra Zeneca, UK) as a single agent, with 7.95 nM Paclitaxel (US Biological Life Sciences) as a single agent or with both AZD2014 (503.3 nM or 1006.5 nM) and Paclitaxel (7.95 nM) as a combination treatment. Kelly WT, Kelly CYC065R, VMRC-LCD WT and VMRC-LCD CYC065R cells were treated for 24 hours with 250 nM of CYC065 (Cyclacel).

2.1.5 Cell viability and count

Cells were washed with phosphate-buffered saline (PBS) and collected by standard trypsin-EDTA (Sigma-Aldrich) treatment. Cell number and viability was determined by a haemocytometer and trypan blue stain, and with Guava® Muse® Cell Analyzer.

2.1.6. *In vitro* cell uptake of [^{1}H]-Glutamine and [^{1}H]-Glucose

Thirteen different cell lines (Kelly, DAN-G, PC3, TU8902, TU8988S, TU8988T, ASPC-1, HCT116 WT, HCT116 Bax-ko, NCI-H508, MDA-MB-231, MIA PaCa-2, T3M4) were seeded in T75 flasks. 2 flasks were seeded (1 flask for cell counting and 1 flask for dual phase extraction) for each cell line. The cells were grown in DMEM+Glutamax (cat. 61965-026, Gibco, Life Technologies, UK) supplemented with 10% FBS and DMEM (cat. 41965-039, Gibco, Life Technologies, UK) supplemented with 10% Fetal Bovine Serum (FBS), 1% non-essential amino acids (NEAAs) and 5,000 units of penicillin-streptomycin. The cells were then incubated for 48 hours (37^{o}C, 5% CO2). After 48 hours, the cells in the counting flask were collected by trypsinization and counted on a haemocytometer. The cell numbers were used to standardise the metabolite data. The dual phase extraction of cells was then carried out and analysed by ^{1}H-MRS. Cell culture media were also collected for ^{1}H-MRS analysis. (For complete procedure of dual phase extraction of cells see section 2.3.1).

2.1.7. *In vitro* cell uptake of 4-[^{18}F]fluoroglutamine and [^{18}F]FDG

Tumour cells were plated at a density of 2.0x10^{5} cells/well and incubated in culture media for 48 hours to achieve an 80% cellular confluency, which is suitable for the uptake experiment. After 48 hours of incubation, two plates of cells were used with 1 for cell counting and 1 for radiotracer uptake assay. For the radiotracer uptake plate, the media was aspirated and the cells were washed twice with 200 µL of PBS/well. (2S, 4R)-4-[^{18}F]fluoroglutamine (synthesised by the Smith lab, ICR, Sutton, UK, the purity of product was analysed by chiral high-performance liquid chromatography, radiochemical yield [decay-corrected], 14.9% ± 2.4%; radiochemical purity, 96.4% ± 1.1%; n = 8) or [^{18}F]FDG (obtained from Alliance Medical and The Royal Marsden Hospital, UK) was dissolved in DMEM media (cat. 31053-028, Gibco, Life Technologies, UK) without phenol red, and L-glutamine or DMEM media (cat. A1443001, Gibco, Life Technologies, UK) without D-glucose, respectively. 400 µL of this radiotracer solution was then added to each well (300KBq/well). The cells were incubated for 1 hour.

For the time dependent uptake study, 400 µL of this radiotracer solution was added to each well (300KBq/well). The cells were incubated at different time points 0, 30, 60, 90, 120 minutes.

For the competitive inhibition studies, 400 µL of this radiotracer solution was added to each well (300KBq/well) together with 0, 0.1, 0.3, 1, 3, or 5 mM of L-glutamine or D-glucose. The cells were incubated for 1 hour.

At the end of the incubation period, the cells were observed under the microscope to check for cell detachment. Then, the wells were aspirated and the cells were washed once with PBS. Trypsin was added at 500µL/well and the cells were then incubated for 1-2 minutes. The trypsin-cell suspension in each well was collected and added into appropriate scintillation vials. The wells were washed again with DMEM media (without phenol red and L-glutamine for the (2S, 4R)-4-[^{18}F]fluoroglutamine experiments or without D-glucose for the [^{18}F]FDG experiments) and the wash solution was added into the same scintillation vials for each sample. Samples were counted on a gamma counter (2480 WIZARD2; Perkin Elmer).

2.2. SDS-PAGE and immunoblotting

Harvested cells were washed with PBS, collected by centrifugation at 1200 rpm (258 x g) for 5 minutes and lysed in Cell lysis buffer (Cell Signalling) (specifically for phosphor-protein western blots) or RIPA Buffer (Cell Signalling) which contains protease inhibitor cocktail and phosphatase inhibitor cocktail (Roche Applied Bioscience). Total proteins were extracted through 15-minute incubation with these cell lysing buffer. Protein concentration in cell lysates was determined by using Detergent Compatible (DC) Protein Assay (BioRad) which is based on Lowry method (Bradford, 1976). The soluble cell extracts were then denatured in NuPage LDS Sample Buffer for 10 minutes (at 70^{o}C for phosphor-protein samples, 95^{o}C for all other proteins) and subjected to sodium dodecyl sulphate-polyacrylamide gel electrophoresis (SDS-PAGE) in NuPAGE™ 4-12% Bis-Tris Protein Gels, 1.0 mm in NuPAGE 3-(N-morpholino)propanesulfonic acid (MOPS) (for phosphoproteins) or 2-(N-morpholino)ethanesulfonic acid (MES) (for all other proteins) SDS running buffer (Life Technologies). The separated proteins were then electronically transferred onto

Immobilon-P membrane (Millipore) and blocked in wash buffer (10 mM Tris, 100 mM NaCl, 0.1% v/v Tween-20, pH 7.5) with 5% w/v non-fat milk powder or 5% w/v bovine serum albumin (BSA, for phosphorylated proteins). The membrane was then incubated overnight with the appropriate primary antibodies. The following primary antibodies were used for overnight incubation at 4^{o}C: β-actin (catalog #4970S, 1:2000), β-catenin (catalog #9562S, 1:2000), ASCT2 (catalog #8057S, 1:2000) (all from Cell Signalling), glutaminase antibody (catalog #ab156876, 1:2000) was obtained from Abcam. Alanine aminotransferase (catalog #sc-398383, 1:100), LAT1 (catalog #sc-374232, 1:200) antibody was obtained from Santa Cruz Biotechnology. Horseradish peroxidase (HRP)-conjugated polyclonal goat anti-rabbit (catalog #NA934V, 1:2000; GE Healthcare) or m-IgGκ BP-HRP anti-mouse (catalog #sc-516102, 1:2000; Santa Cruz Biotechnology) secondary antibodies were used for 1 hour incubation at room temperature. The protein-antibody interactions were then visualized using SuperSignal West Pico Chemiluminescent Substrate (Thermo Scientific) and exposed to KODAK BioMax XAR Film (Carestream Health) which was then scanned using X-RAY Processor & Peripheral Equipment SRX-101A (Konica Minolta, UK). For membrane stripping, ReBlot Plus Strong Antibody Stripping Solution (Millipore) was used. Densitometric analysis was performed using ImageJ (National Institutes of Health, USA). Data are represented as the mean ± SD (n = 3 independent experiments).

2.3. Magnetic Resonance Spectroscopy

2.3.1. Sample preparation

For cellular metabolite analysis, metabolites were extracted using a dual phase extraction method (Tyagi et al. 1996; Al-Saffar et al. 2014; Chung et al. 2017). Cells were grown in T75 or T175 culture flasks, or 6 well plates (for ^{19}F-MRS experiment). After a 24 hour incubation with either media only (control condition), or appropriate inhibitor, the flasks were taken out of the incubator. 1 mL of cell culture media was collected from each flask into appropriate Eppendorf tubes and stored at -20^{o}C (NOTE: 1 mL of clean media (starting media that hasn't been incubated with the cells) was also collected and stored at -20^{o}C. The cells were then washed three times with 10 mL ice-cold saline, and the saline was carefully removed after each wash. 3 mL of

ice-cold methanol was added into each flask to cover the cells. The flasks were kept on ice (5-10 minutes) to prevent methanol evaporation during manipulation of the flasks. The cells were scraped off from the culture flask surface into the added methanol using a cell scraper, and subsequently transferred to clean centrifuge tubes. 3 mL of ice-cold chloroform was added into each tube using a glass pipette, and the tubes were vortexed vigorously for 30 seconds. 3 mL of ice-cold de-ionised water was added into each tube and again the tubes were vortexed vigorously for 30 seconds. The samples were centrifuged @~ 3220 rpm (~ 1855 x g) for 20 mins at 4^{o}C for phase separation. The final chlorform:methanol:water ratio was approximately 1:1:1 (v/v/v). The upper methanol-water phase contains the water-soluble cellular metabolites, the middle phase contains the protein pellet and the bottom chloroform phase contains the cellular lipids. The cell pellets (the middle phase) were kept and stored at -80^{o}C (for protein concentration determination if necessary).

The water-soluble metabolite phase was collected and Chelex 100 (~1mg/1 mL) was added to remove divalent ions. The beads were then removed using centrifugation and the clear supernatants were collected and stored at -80^{o}C until freeze drying.

2.3.2. ^{1}H-MRS of cell culture media and cell extract samples

For cell culture media samples:

500 µL of the collected cell culture media was added to 5 mm NMR tubes and 50 µL D2O (Sigma---Aldrich) and 50 µL of 0.75% sodium 3-trimethylsilyl-2,2,3,3-tetradeuteropropionate (TSP) in D2O (Sigma---Aldrich) were also added for quantitation and chemical shift calibration.

For cellular water-soluble metabolite samples:

650 µL D2O (Sigma---Aldrich) and 50 µL of 0.75% sodium 3-trimethylsilyl-2,2,3,3-tetradeuteropropionate (TSP) in D2O (Sigma---Aldrich) (for quantitation and chemical shift calibration) were used to reconstitute freeze-dried cell extract samples (Section 2.3.1). 600 µL of these solutions were then put into 5 mm NMR tubes and the pH adjusted to pH 7 using 0.1 M KOH and 0.6% perchloric acid.

2.3.3. ^{19}F-labelled glutamine MRS studies

HCT116 WT and HCT116 Bax-ko cells were cultured and treated for 18 hours with control vehicle or inhibitors (CB-839 or L-cycloserine) as described in section 2.1.4. The treatment medium was then removed and substituted for medium containing (2S, 4R)-4-[^{19}F]fluoroglutamine (synthesised by Drs Andreas Doepner and Graham Smith, ICR, Sutton, UK based on the materials and methods as described in Qu et al. 2011) with the respective vehicle or inhibitors (CB-839 or L-cycloserine) treatment for a further 6 hours. The (2S, 4R)-4-[^{19}F]fluoroglutamine medium was prepared by using L-glutamine free DMEM media supplemented with 10% dialyzed FBS and 2 mM (2S, 4R)-4-[^{19}F]fluoroglutamine. The cells were then extracted using the dual phase extraction protocol in section 2.3.1. The water-soluble metabolite samples prepared as described in section 2.3.2.

2.3.4. MRS spectral acquisition and data processing

All spectra were acquired on a 500 MHz NMR machine (Bruker, Germany).

For cell culture media samples:

Spectra were acquired with 6,000 Hz spectral width using a water-suppressed pulse and collect sequence with a repetition time of 2.7s, 12 ppm spectral width, 32768 time domain points and 64 scans at 298K.

For water-soluble cellular extract samples:

Spectra were acquired with 6,000 Hz spectral width using a water-suppressed pulse and collect sequence with a repetition time of 2.7s, 12 ppm spectral width, 32768 time domain points and 512 scans at 298K.

For ^{19}F-MRS:

Spectra were acquired with 47,620 Hz spectral width using a pulse and collect sequence with repetition time of 3s, 101 ppm spectral width, 65536 time domain points, 2048 or 8192 scans for cell media and cell extract samples, respectively, at 298K. Quantification was performed by adding a solution of 20 mmol/L [^{19}F]fluorodeoxyglucose ([^{19}F]FDG) in D_2O as an internal reference standard to a final

concentration of 0.0005 mmol/L. This internal standard gives a peak at -199.5 ppm, and the concentration of fluorine-containing metabolite was measured by integrating the metabolite peak relative to the internal standard. Concentration of ^{19}F compounds in cell culture media samples and aqueous cell extracts was normalized to total cell numbers.

The spectra were phased and manually baseline corrected using Bruker Topspin 3.6 software package. ^{1}H-MR spectra of cell media and water-soluble cellular extract samples were referenced to TSP, and the ^{19}F-MR spectra were referenced to [^{19}F]FDG. Spectral assignments were based on literature values (Sze and Jardetzky 1990; Mancuso et al. 1994; Tyagi et al.1996; Govindaraju et al. 2000; Sitter et al. 2002; DeBerardinis et al. 2007; Wishart et al. 2009; Wishart et al. 2013).

For ^{1}H-MRS of water-soluble cellular extract samples, metabolite concentrations in the sample were calculated by relating the peak integrals of metabolites, corresponding to individual metabolite resonances, to the peak integrals and concentration of TSP (0.00000256 mmol/L), and then corrected for the number of protons. For ^{19}F-MRS of water-soluble extract samples, metabolite concentrations were calculated by relating the peak integrals of metabolites, corresponding to individual metabolite resonances, to the peak integrals and concentration of the internal reference [^{19}F]FDG (0.0005 mmol/L). Metabolite concentrations were then standardised to cell number. An equation showing the calculation of metabolite concentration is presented as follow:

$$[M]_{metabolite} = \frac{P_{REF} \times I_{MET} \times [REF]}{P_{MET} \times N \times I_{REF}}$$

where $[M]_{metabolite}$: concentration of metabolite; P_{REF}: number of proton or fluorine atoms giving rise to the signal integral of reference compounds TSP and [^{19}F]FDG (P_{TSP} = 9 for ^{1}H-MRS and $P_{[FDG]}$ = 1 for ^{19}F-MRS); P_{MET}: number of proton or fluorine atoms giving rise to the signal integral of metabolite; I_{REF}: signal integral of reference compounds (TSP for ^{1}H-MRS, [^{19}F]FDG for ^{19}F-MRS); I_{MET}: signal integral of metabolite; [REF]: concentration of reference compounds ([TSP] = 0.00000256 mmol/L, [FDG] = 0.0005 mmol/L); N: final cell number

The rates of cellular metabolite uptake from/secretion into culture media are calculated from the ^{1}H-MRS or ^{19}F-MRS spectrum of culture media that have been incubated with cells for a given incubation time and a specific final cell number with respect to the clean media (without cells). A positive rate value is considered as a metabolite uptake from the clean media by the cells. Meanwhile, a negative rate value is considered as a metabolite secretion into the clean media by the cells. An equation showing the calculation of metabolite uptake or secretion rate is presented as follow:

$$\text{Rate of metabolite uptake/secretion} = \frac{(I_{CM} - I_{IM}) \times P_{REF} \times V_{TOT} \times [REF]}{P_{MET} \times N \times I_{REF} \times V_{tube} \times T}$$

where I_{CM}: signal integral of metabolite in clean media (without cells); I_{IM}: signal integral of metabolite in incubated media with cells; I_{REF}: signal integral of reference compounds (TSP for ^{1}H-MRS, [^{19}F]FDG for ^{19}F-MRS); P_{REF}: number of proton or fluorine atoms giving rise to the signal integral of reference compounds TSP and [^{19}F]FDG (P_{TSP} = 9 for ^{1}H-MRS and $P_{[FDG]}$ = 1 for ^{19}F-MRS); P_{MET}: number of proton or fluorine atoms giving rise to the signal integral of metabolite; [REF]: concentration of reference compounds ([TSP] = 0.00000256 mmol/L, [FDG] = 0.0005 mmol/L); N: final cell number; V_{TOT}: total volume of media incubated with the cells; V_{tube}: volume of media placed into the NMR tube (500 µL, as described in section 2.3.2); T: given incubation time

A sample ^{1}H-MRS spectrum of HCT116 WT conditioned medium is shown in Figure (2.1). A sample spectrum of water-soluble cellular extract metabolites from an HCT116 WT cell extract is shown in Figure (2.2). The corresponding metabolites are indicated in Table 2.1. Nineteen different metabolites in culture media and twenty four metabolites in cell extract were assigned.

A sample ^{19}F-MRS spectrum of HCT116WT conditioned medium is shown in Figure (2.3). A sample ^{19}F-MRS spectrum of cellular extracts metabolites from an HCT116 WT cell extract is shown in Figure (2.4). The corresponding metabolites are indicated in Table 2.2. Five different metabolites in culture media and four different metabolites in cell extract were assigned.

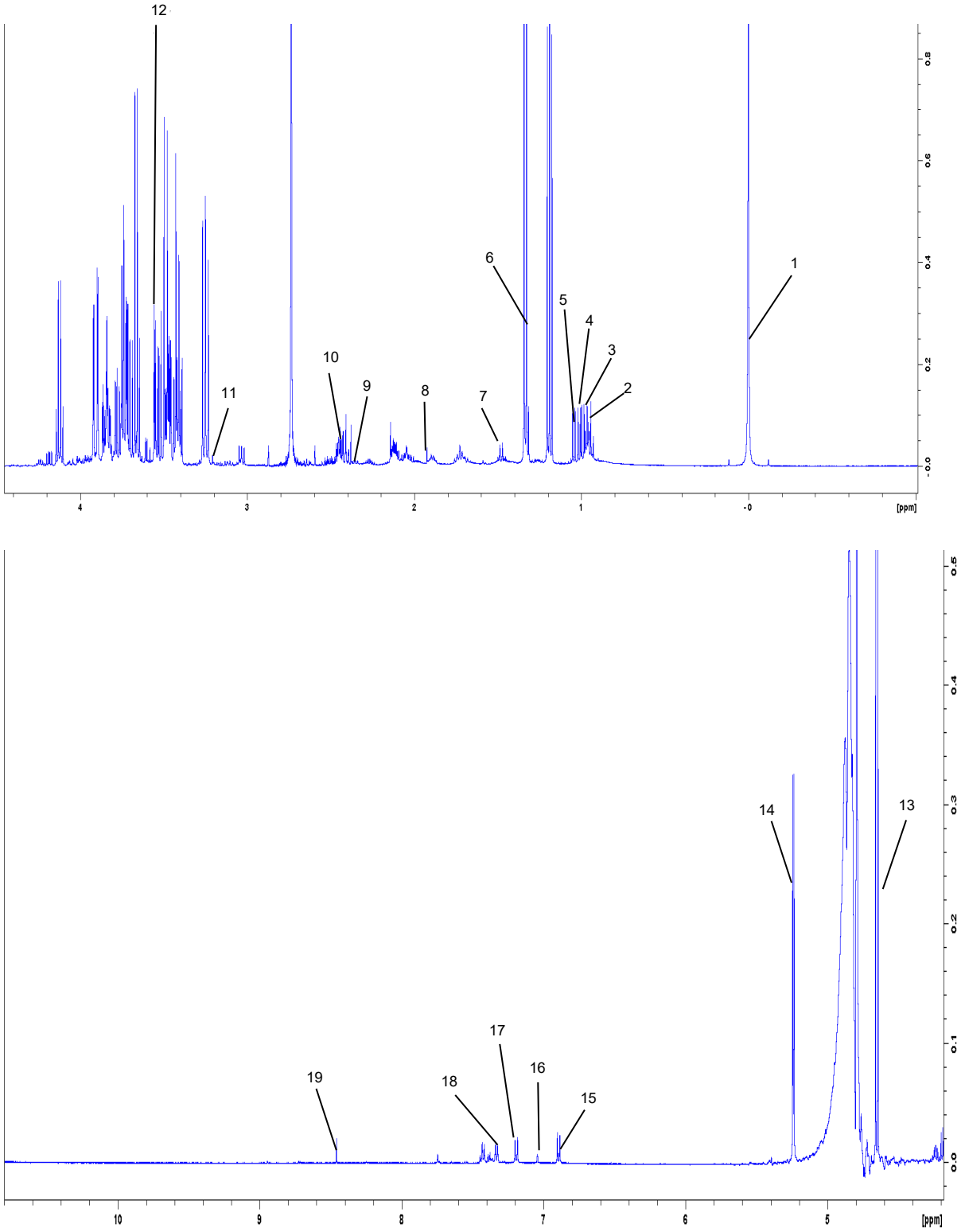

Figure 2.1. Example ^{1}H MR spectrum of culture media. Peak assigments were TSP (1) Leucine (2), Valine (3), Iso-leucine (4), Valine (5), Lactate (6), Alanine (7), Acetate (8), Glutamate (9), Glutamine (10), Choline (11), Glycine (12), β-Glucose (13), α-Glucose (14), Tyrosine (15), Histidine (16), Tyrosine (17), Phenylalanine (18), Formate (19).

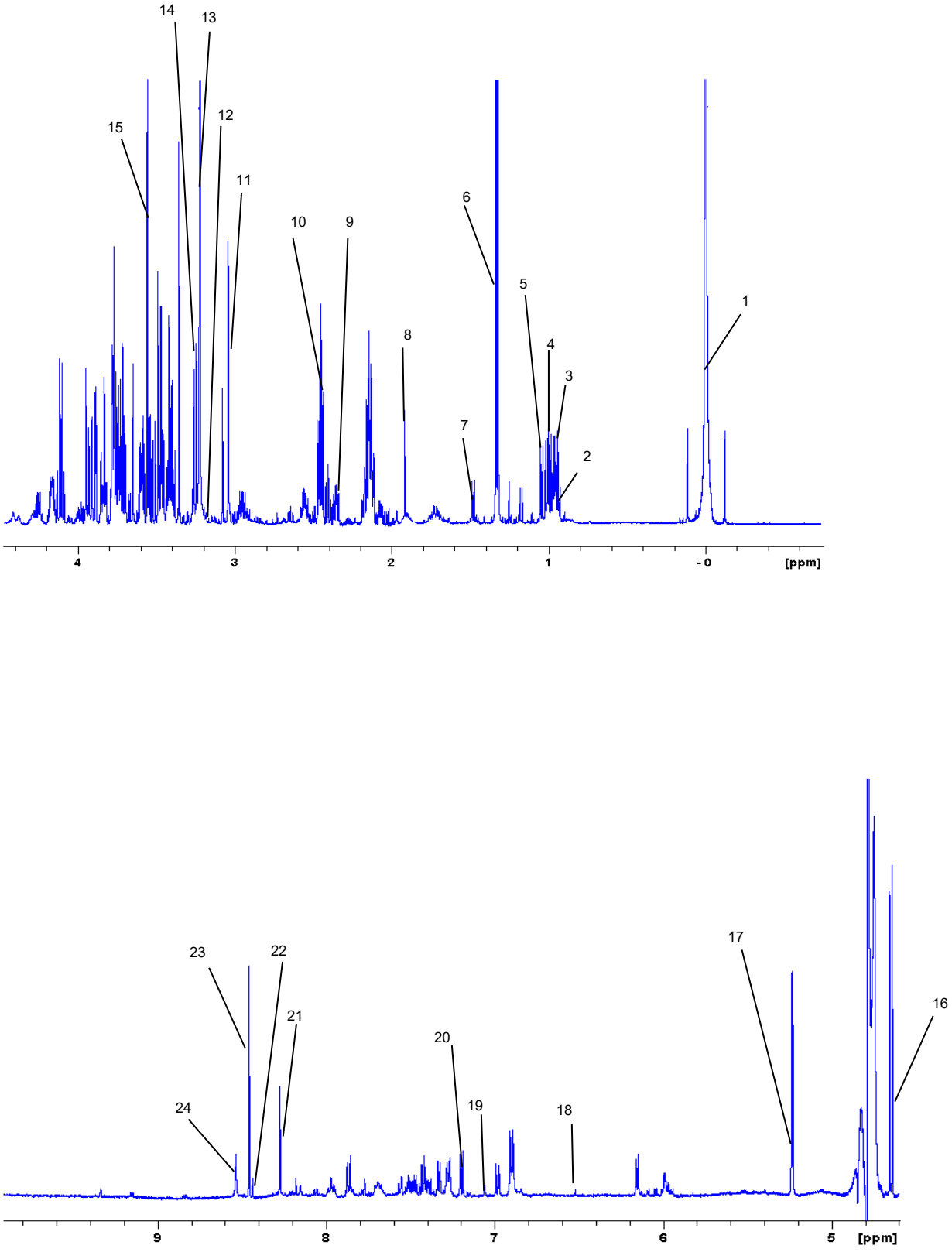

Figure 2.2. Example ^{1}H MR spectrum of cellular extracts. Peak assigments were TSP (1) Leucine (2), Valine (3), Iso-leucine (4), Valine (5), Lactate (6), Alanine (7), Acetate (8), Glutamate (9), Glutamine (10), Creatine (11), Choline (12), Phosphocholine (13), Glycerophosphocholine (14), Glycine (15), β-Glucose (16), α-Glucose (17), Fumarate (18), Histidine (19), Tyrosine (20), ATP+ADP (21), NAD^{+}+NADH (22), Formate (23), ATP+ADP (24).

Metabolite	Number of protons	^{1}H multiplet	Chemical Shift (ppm)
Leucine	δ'CH_3	d	0.96
Leucine	δCH_3	d	0.97
Valine	γCH_3	d	0.99
Isoleucine	γCH_3	d	1.02
Valine	γ'CH_3	d	1.05
Lactate	CH_3	d	1.33
Alanine	CH_3	d	1.48
Acetate	(CH_3)	s	1.92
Glutamate	γCH_2	t	2.34
Glutamine	γCH_2	m	2.45
Creatine	CH_3	s	3.04
Choline	N(CH_3)$_3$	s	3.21
Phosphocholine	N(CH_3)$_3$	s	3.23
Glycerophosphocholine	N(CH_3)$_3$	s	3.24
Glycine	αCH_2	s	3.56
β-Glucose	C1H	d	4.65
α-Glucose	C1H	d	5.24
Fumarate	CH	s	6.51
Tyrosine	C3H, 5H ring	d	6.90
Histidine	C4H, ring	s	7.07
Tyrosine	C2H, 6H ring	d	7.20
Phenylalanine	C2H, C6H, ring	m	7.33
ATP and ADP	C2 ring	s	8.27
NAD and NADH	A8H ring	s	8.43
Formate	HCOO'	s	8.46
ADP	C8 ring	s	8.53
ATP	C8 ring	s	8.54

Table 2.1. ^{1}H chemical shift of the assigned metabolites in culture media and cell extracts of HCT116 WT and HCT116 Bax-ko. ^{1}H multiplet is abbreviated as s = singlet, d = doublet, t = triplet, m = multiplet. Spectral assignments were based on literature values (Chung and Griffiths, 2011, De Castro et al. 2018).

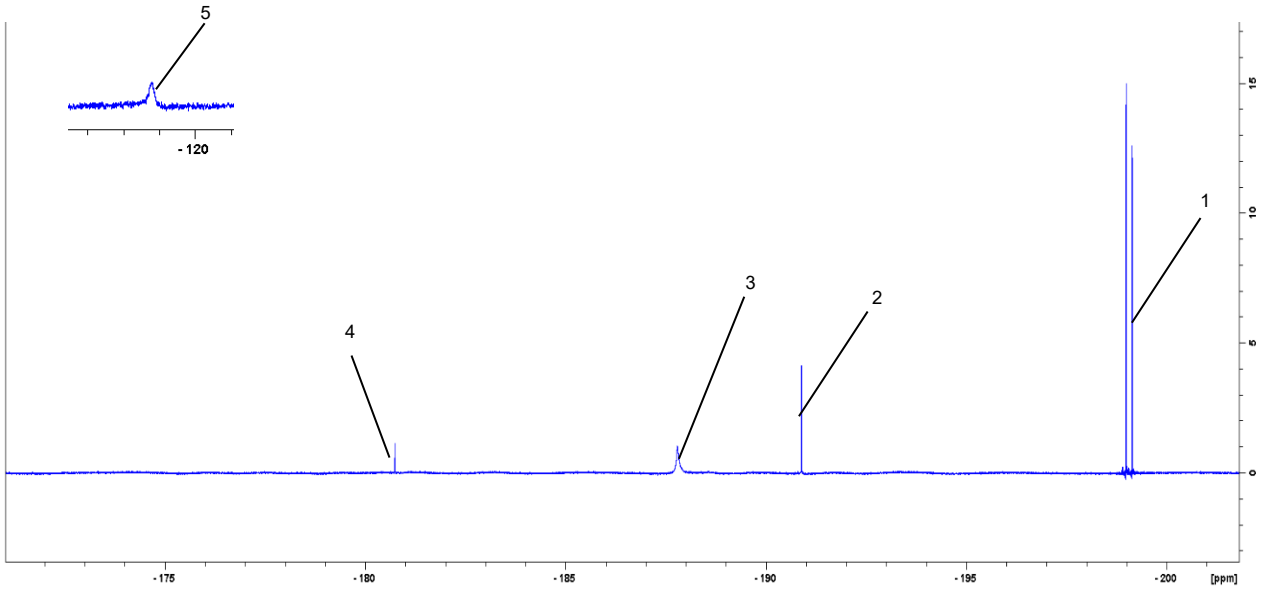

Figure 2.3. Example ^{19}F MR spectrum of culture media. Peak assigments were [^{19}F]FDG (1), ^{19}F-4-Fluoro-5-oxoproline (2), (2S, 4R)-4-[^{19}F]fluoroglutamine (3), (2S, 4R)-4-[^{19}F]fluoroglutamate (4), free fluoride (5)

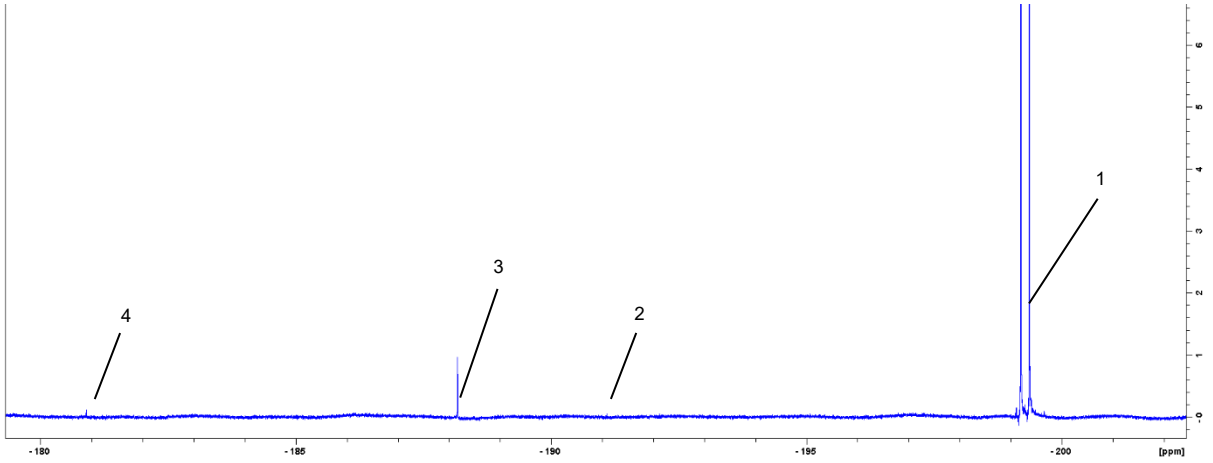

Figure 2.4. Example ^{19}F MR spectrum of cellular extracts. Peak assigments were [^{19}F]FDG (1), ^{19}F-4-Fluoro-5-oxoproline (2), (2S, 4R)-4-[^{19}F]fluoroglutamine (3), (2S, 4R)-4-[^{19}F]fluoroglutamate (4)

Metabolite	Chemical Shift (ppm)
[^{19}F]fluorodeoxyglucose	-199.5
^{19}F-4-Fluoro-5-oxoproline	-191
(2S, 4R)-4-[^{19}F]fluoroglutamine	-188
(2S, 4R)-4-[^{19}F]fluoroglutamate	-181
Free Fluoride	-122

Table 2.2. ^{19}F chemical shift of the assigned metabolites in culture media and cell extracts of HCT116 WT and HCT116 Bax-ko. Spectral assignments were based on literature values (Kanazawa et al. 1997; Cooper et al. 2012; Komarov et al. 2019).

2.4. *In vivo* studies

2.4.1. Tumour growth in nude mice

All animal studies were approved by the Animal Welfare and Ethical Review Body of the Institute of Cancer Research (ICR). HCT116 WT and PC3 cells grown to about 70% confluence were harvested by trypsinization, washed twice with PBS and then resuspended in PBS at a concentration of 5 million cells/100 µL. PC3 and HCT116 WT xenografts were established in NCr-Foxn1^{nu} mice (male, 5-6 weeks old; ICR). Briefly, 5 million PC3 or HCT116 WT cells in PBS were injected subcutaneously in the right shoulder of the mouse. Developing tumours were measured in two orthogonal directions using callipers, and the tumour volume was calculated using the formula: Tumour volume = (Length x Width x Width)/2. When the PC3 and HCT116 WT tumours measured at ~100 mm^3, 10-12 mice (depending on tumour growth) were used for PET imaging in which 5-6 mice were used for [^{18}F]FDG and 5-6 mice for 4-[^{18}F]fluoroglutamine. Mice that were injected with [^{18}F]FDG were fasted 12 hours before the PET scan.

2.4.2. Small animal PET imaging studies

Small-animal PET imaging studies were conducted with 4-[^{18}F]fluoroglutamine or [^{18}F]FDG on a dedicated animal PET scanner (Albira tri-modal PET/SPECT/CT pre-clinical scanning system) (Bruker, UK). NCr-Foxn1nu male mice with HCT116 WT or PC3 xenografts were used for the imaging studies. Mice were put under anaesthesia with the use of isoflurane (2 - 3%). 0.1 mL saline solution containing 7 MBq of either 4-[^{18}F]fluoroglutamine or [^{18}F]FDG was injected intravenously and the mice were then placed back into cages for recovery. 60 minutes after the administration of the radiotracer, the mice were then placed on a heating pad to maintain body temperature and anaesthetised throughout the imaging procedure (20 minutes). Animals were visually monitored for breathing and any other signs of distress throughout the entire imaging period. The mice were sacrificed at the end of the imaging study under anaesthesia. The organs and tumour tissues of PC3 and HCT116 WT were collected for subsequent *ex vivo* biodistribution and dual phase extraction studies

For the HCT116 WT and PC3 xenografts, the mice were separated into two groups in which one group is used for 4-[^{18}F]fluoroglutamine PET imaging and the other is for [^{18}F]FDG PET. The mice in the [^{18}F]FDG group were fasted for 12 hours prior to the PET measurements. Each mouse was injected with 7 MBq of either 4-[^{18}F]fluoroglutamine or [^{18}F]FDG. Whole body PET static images were acquired 1 hour post radionuclide injection for the duration of 10 minutes with a 358 to 664 keV energy window, followed by CT acquisition.

The imaging data were normalized to correct for PET non-uniformity, dead-time count losses, positron branching ratio, and physical decay to the time of injection. No attenuation or partial-volume averaging corrections were applied. The PET images were reconstructed using a MLEM algorithm (12 iterations) with a voxel size of 0.5 × 0.5 × 0.5 mm^3. Whole body standard high resolution CT scans were performed with the X-ray tube set-up at a voltage of 45 kV, current of 400 µA, 250 projections (1 sec per projection) and a voxel size of 0.5 × 0.5 × 0.5 mm^3. The CT images were reconstructed using a filtered back projection (FBP) algorithm. Image analysis was performed using the PMOD software package (PMOD Technologies Ltd, CH). Tumor segmentation was performed using a 50% threshold. The mean counts (PET Mean) and the PET Peak (mean of the 500 voxels with highest counts within the tumor volume) were recorded per mouse and converted into percentage of the injected dose per gram of tissue (%ID/g) by means of a calibration factor (MBq/g/counts) determined from scanning a ^{18}F source of known activity and volume.

2.4.3. *Ex vivo* biodistribution study in NCr-Foxn1nu male mice

The organs and tumour tissues of PC3 and HCT116 WT were collected from the PET scan studies. The organs of interest and tumours were removed, weighed and the radioactivity was counted with a gamma counter (2480 WIZARD2; Perkin Elmer). The percent dose per gram of tissue was calculated by comparing tissue activity counts with counts of 1.0 % of the initial dose. The initial dose consisted of 14 times diluted aliquots of the injected material measured at the same rate (1 min/sample, 80% efficiency).

2.4.4. Dual phase extraction of tumour tissues

The tumour tissues of PC3 and HCT116 WT were collected from the PET scan studies. The tumours were removed and weighed. Half of the tumour was used for the *ex vivo* biodistribution study (section 2.4.3). The other half was snap frozen for the ^{1}H-MRS dual phase extraction study. The freeze-clamped or snap frozen tissue sample were weighed and the wet tissue weight was recorded. The tissue sample was then ground into fine powder in liquid nitrogen using a pestle and mortar. The ground tissue sample was transferred into a clean centrifuge tube. 3 mL of ice-cold methanol was added into a clean centrifuge tube with the ground tissue sample and the tube was vortexed vigorously for 30 sec. The extraction procedures were then continued from the step of adding 3 mL of ice-cold chloroform as described in Section 2.3.1.

2.4.5. ^{1}H MRS of tumour tissue extract samples

650 µL D2O (Sigma---Aldrich) and 50 µL of 0.75% sodium 3-trimethylsilyl-2,2,3,3-tetradeuteropropionate (TSP) in D2O (Sigma---Aldrich) (for quantitation and chemical shift calibration) were used to reconstitute freeze-dried tumour tissue extract samples. 600 µL of these solutions were then put into 5 mm NMR tubes and the pH adjusted to pH 7 using 0.1 M KOH and 0.6% perchloric acid.

2.4.6. MRS spectral acquisition and data processing

^{1}H-MR spectra were acquired with 6,000 Hz spectral width using a water-suppressed pulse and collect sequence with a repetition time of 2.7s, 12 ppm spectral width, 32768 time domain points, 512 scans at 298K. The spectra were phased and manually baseline corrected using Bruker Topspin 3.6 software package.

Metabolite amounts in the sample were calculated by relating the peak integrals of metabolites, corresponding to individual metabolite resonances, to the peak integrals of internal reference TSP and then corrected for the number of protons. Metabolite levels were then standardised to protein concentration or tissue wet weight.

2.5. Statistics

Statistical calculations were performed using Prism software (GraphPad Software v8.0) and Microsoft Excel 2016. All assays were performed at least in triplicate and data presented as Mean ± S.D. Student's two-tailed unpaired t-test was used in all statistical analysis unless otherwise stated, with a p value of ≤ 0.05 considered significant. Five PC3 or HCT116 WT xenografts per group were used for the *in vivo* 4-[^{18}F]fluoroglutamine and [^{18}F]FDG imaging. Sample size was calculated with 90% power and 5% significance level. The mice were randomized before imaging session. No data were excluded from the analysis, including all outliers. Correlation analysis was performed using Pearson's rank correlation, with linear regression, 95% confidence intervals, and statistical significance determined using Prism software.

Chapter 3

Evaluation of the metabolic pathways of 4-[^{18}F]fluoroglutamine PET tracer in cancer cells

3.1. Introduction

The discovery by Otto Warburg and colleagues in the 1920s found a strong reliance of cancerous cell on glycolysis, even in an oxygen rich environment (Levine and Puzier-Kuter 2010). However, it has been noticed that aerobic glycolysis does not provide enough substrates and energy for the synthesis of essential building blocks for proliferating cells (DeBerardinis et al. 2008; Dang 2010). Many previous studies revealed L-glutamine is an important source for nitrogen supply and energy generation for many cancer cell types (Blau et al. 2008; Szeliga and Obara-Michlewska 2009; Erickson and Cerione 2010; Hu et al. 2010; Levine and Puzio-Kuter 2010; Suzuki et al. 2010; Wang et al. 2010; Chatterjee et al. 2011; Dang et al. 2011; Koppenol et al. 2011).

Based on this glutamine addiction phenomenon, metabolic imaging methods have been developed to monitor glutamine metabolism in tumours. One approach is the application of isotopically labelled glutamine in mass spectrometry or MRS to analyse the glutamine uptake and glutaminolysis in cancer and tumour models. ^{1}H, or ^{13}C labelled glutamine is incubated with the cancer cell lines of interest or administered to patients or preclinical models for a certain period of time prior to cell extraction or surgery and tumour collection or MRI session to study the metabolism of specific regions of interest in the human body (Pioro et al. 1999; Deberardinis et al. 2007; Radaman et al. 2013; Świątkiewicz et al. 2017; Hasler et al. 2019).

PET imaging can also be a suitable strategy to monitor glutaminolysis non-invasively. Glutamine is labelled with a positron-emitting isotope, instead of a stable isotope as in MRS. ^{11}C ($T_{1/2}$ = 20 min) or ^{13}N ($T_{1/2}$ = 9.96 min) labelled glutamine was developed initially for the PET imaging of glutamine metabolism. Some initial attempts which used ^{13}N-amide-glutamine and ^{13}N-glutamate to image sarcomas in patients or provide metabolic information on the glutamine metabolism in rat liver have been reported in earlier studies (Gelbard et al. 1979; Reiman et al. 1981; Reiman et al. 1982; Cooper et al. 1988). However, the short half life of ^{13}N-Glutamine or complicated chemical

synthesis and separation of ^{11}C-Glutamine (Vaalburg et al. 1992) restrict the systematic use of these isotopes in human or rodent PET imaging studies (Cooper et al. 2012).

^{18}F-labelled imaging agents could overcome these limitations due to the relatively long half-life of ^{18}F isotope ($T_{1/2}$ = 110 min) and 4-[^{18}F]fluoroglutamine (Fig. 1.6B) was developed for glutamine PET imaging (Qu et al. 2011). Qu et al developed a method for the rapid chemical synthesis of 4-[^{18}F]fluoroglutamine and reasoned that the replacement of a hydrogen atom in the 4 position of L-glutamine structure with a fluorine atom, which results in a glutamine analogue of 4-[^{18}F]fluoroglutamine, did not significantly change the biological and metabolic characteristics of this radiotracer when compared with L-glutamine (Qu et al. 2011). It was also shown in the study by Qu et al that 4-[^{18}F]fluoroglutamine was taken up in glutamine addicted 9L tumour cells and xenograft models at a similar rate to [^{18}F]FDG, but at a greater rate than [^{18}F]FDG in glutamine avid SF188-Bcl-x_L cancer models (Qu et al. 2011). Different types of cancer such as breast, pancreas, renal, lung, colon, or glioma have been shown to be detected by 4-[^{18}F]fluoroglutamine PET imaging in a clinical trial, NCT01697930, carried out by Dunphy et al (Dunphy et al. 2018). The signal intensity obtained from 4-[^{18}F]fluoroglutamine PET imaging was comparable to the standard [^{18}F]FDG imaging. More importantly, the authors have concluded that fasting did not have significant effect on 4-[^{18}F]fluoroglutamine biodistribution and no adverse effects were found on patients (Dunphy et al. 2018).

Despite all of these promising results, it is poorly understood how 4-[^{18}F]fluoroglutamine is metabolised in cancer cells and tumours. Therefore, it is important to investigate the metabolic fate of this PET tracer to confirm whether it is a true surrogate for L-glutamine. Cooper et al utilised different animal enzymes in the glutamine metabolic pathway, such as rat kidney glutaminase, sheep brain glutamine synthetase, or pig heart alanine aminotransferase, to investigate the enzymatic transformation of 4-[^{18}F]fluoroglutamine and 4-[^{18}F]fluoroglutamate (Cooper et al. 2012). 4-[^{18}F]fluoroglutamate has been previously shown as a potential metabolic product of 4-[^{18}F]-Fluoroglutamine (Fig. 1.7) (Lieberman et al. 2011, Qu et al. 2011, Ploessl et al. 2012). The results indicated that 4-[^{18}F]fluoroglutamine is a substrate of rat kidney glutaminase (Cooper et al. 2012). This is interesting since most human cancer cells have been shown to express the kidney form of glutaminase (glutaminase

K, GLS 1) (Dang et al. 2011). Hence, 4-[^{18}F]fluoroglutamine can be a potential substrate for glutaminase enzyme in human cancer cells. However, the study of 4-[^{18}F]fluoroglutamine metabolism by glutaminase enzyme by Cooper et al is still not broad enough to cover a full range of different glutaminase enzymes. It has been shown in previous studies that some cancer cells can express the liver form (glutaminase L, GLS 2) (Hu et al. 2010), or a spliced variant of the kidney form (GAC) (DeLaBarre et al. 2011).

Another important finding in the Cooper et al study is the ability of pig heart alanine aminotransferase to catalyse the conversion of 4-[^{18}F]fluoroglutamate into α-ketoglutarate (Fig. 1.7) (Cooper et al. 2012). This catalytic function of pig heart alanine aminotransferase has also been illustrated in the transformation of L-glutamate (Babu and Johnston 1976; Cooper 1976). This finding may provide a potential mechanism to explain the γ-elimination of F^- from 4-[^{18}F]fluoroglutamate (Fig. 1.7). However, further studies are required to confirm this conversion. 4-[^{18}F]fluoroglutamate was found to be a strong inhibitor of sheep brain glutamine synthetase enzyme (Cooper et al. 2012), whereas L-glutamate has been confirmed as the substrate of synthetase reaction catalysed by this enzyme (Wellner et al. 1966). These observations confirm that 4-[^{18}F]fluoroglutamate cannot be converted back to 4-[^{18}F]fluoroglutamine. Finally, a minor side reaction, which involves the intramolecular attack of either 4-[^{18}F]fluoroglutamine or its intermediates, for the formation of 5-oxoproline was also illustrated (Fig 1.7) (Cooper et al. 2012).

Most of the Cooper et al study focused primarily on the action of individual mammalian enzymes and depicted a general picture of 4-[^{18}F]fluoroglutamine metabolism. However, this work should be expanded wider, especially in a complex cellular system. The aim of the study in this chapter is to characterize the metabolic fate of 4-[^{18}F]fluoroglutamine in glutamine dependent colorectal cancer cell lines with a high expression of glutaminase enzyme HCT116 WT and HCT116 Bax-ko. HCT116 Bax-ko cell line which has an apoptosis accelerator Bax gene knocked out has an impaired apoptosis pathway and makes them a good model for the evaluation of 4-[^{18}F]fluoroglutamine metabolism with minimal apoptosis signal following treatment with the inhibitors. Herein, the two main metabolic pathways of 4-[^{18}F]fluoroglutamine proposed by Cooper et al were examined. The conversion of 4-[^{18}F]fluoroglutamine to 4-[^{18}F]fluoroglutamate by glutaminase enzyme was examined by using a glutaminase

inhibitor CB-839 (Calithera Biosciences) and the γ-elimination of F^- from 4-[^{18}F]fluoroglutamate by alanine aminotransferase enzyme was investigated by an alanine aminotransferase inhibitor L-cycloserine (Sigma-Aldrich). The use of ^{1}H-MRS confirms the effectiveness of chosen inhibitors on L-glutamine metabolism in cancer cells. Subsequently, ^{19}F-MRS of 4-[^{19}F]fluoroglutamine, an isotopically stable version and MRS-detectable analogue of 4-[^{18}F]fluoroglutamine PET tracer, were also utilised to fully confirm the metabolic fate of the glutamine PET tracer.

3.2. Experiments and Results

3.2.1. Cytotoxicity assay of CB-839 and L-cycloserine

The sulforhodamine B (SRB) cytotoxicity assay was used to determine a suitable dose of CB-839 and L-cycloserine which can be used to evaluate the metabolism of 4-[^{19}F]fluoroglutamine without significant effects on the cell viability.

The percentage of cell growth which corresponds to the increasing compound concentration is shown in Figure 3.1. A reduction in proliferation was observed in both HCT116 WT and HCT116 Bax-ko cells when incubated with CB-839 (Fig. 3.1A). The GI_{50} values of CB-839 measured for the HCT116 WT and HCT116 Bax-ko cell lines are 50 nM and 90 nM, respectively. Figure 3.1B illustrates the antiproliferative activity of L-cycloserine in the corresponding colorectal cancer cell lines. The GI_{50} values of L-cycloserine for HCT116WT and HCT116 Bax-ko cell lines are 47 μM and 122 μM, respectively.

The GI_{50} values of tested compounds were then used to determine the treatment schedule and optimal condition for the evaluation of 4-[^{19}F]fluoroglutamine metabolism.

3.2.2. Determination of treatment schedule and optimal condition for CB-839 or L-cycloserine treatment.

HCT116 WT and HCT116 Bax-ko were seeded at a density of $1x10^6$ cells per T25 flask and then treated with CB-839 or L-cycloserine for 24 hours at concentration of 0, 1xGI_{50}, 3x GI_{50}, 5x GI_{50} and 10x GI_{50} (Fig. 3.2). In order to examine the effect of these two inhibitors on cellular metabolism, the required inhibitor concentrations to induce a cytostatic effect on the treated cells were established (about 50% of treated cell number relative to control) without causing significant cell kill.

There is an approximately 50% of viable HCT116WT (58%, $p<0.01$) and HCT116 Bax-ko (52%, $p<0.05$) cells following 24 hour treatment with 10xGI_{50} CB839 when compared with vehicle-controls (Fig. 3.2A). Figure 3.2B shows the effect of L-cycloserine on cells at different treatment concentrations. After 24 hours of treatment, about 50% of viable treated HCT116 WT (52%, $p<0.001$) and HCT116 Bax-ko (52%,

p<0.01) cells were observed following treatment with 10xGI_{50} of L-cycloserine when compared with vehicle-treated controls. Therefore, 10xGI_{50} of CB839 and 10xGI_{50} of L-cycloserine were used in our subsequent studies.

A.

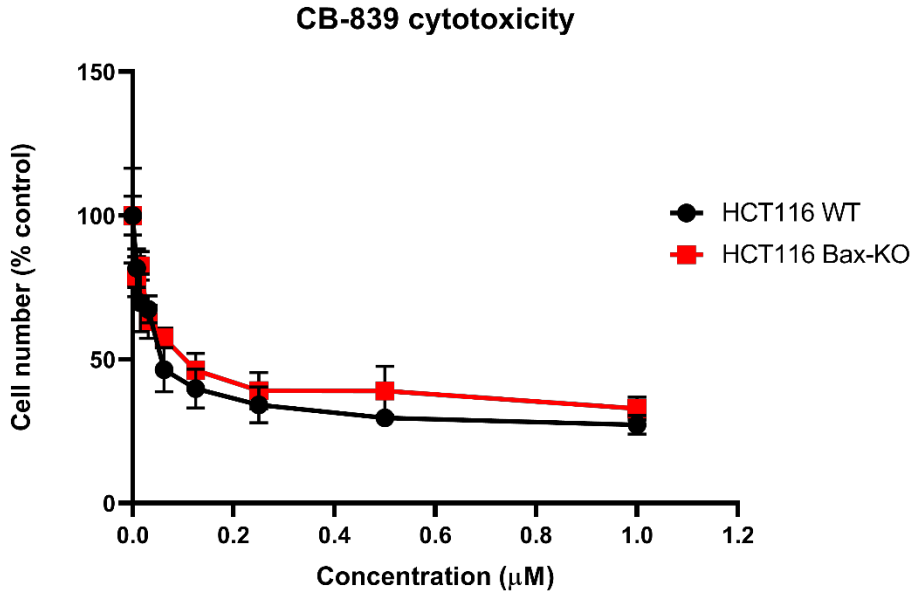

B.

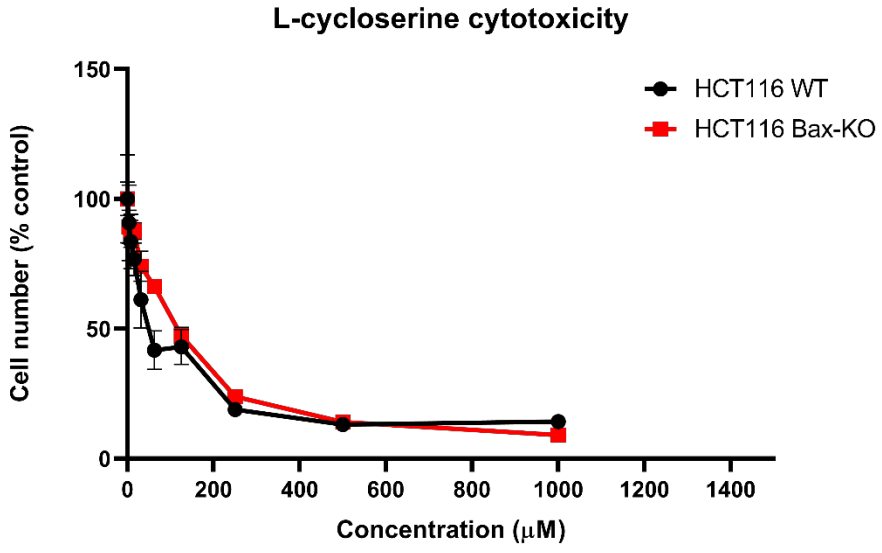

Figure 3.1. Cytotoxic effect of CB-839 **(A)**, and L-cycloserine **(B)** on HCT116 WT **(black)** and HCT116 Bax-ko **(red)** cells. The diagram showing the antiproliferative effect of increasing concentrations of CB – 839 from 0 to 1 μM and L-cycloserine from 0 to 1000 μM on HCT116 WT and KO cells. Data are expressed as mean ± SD, n = 3. Error bars represent ± SD for 3 replicates.

A.

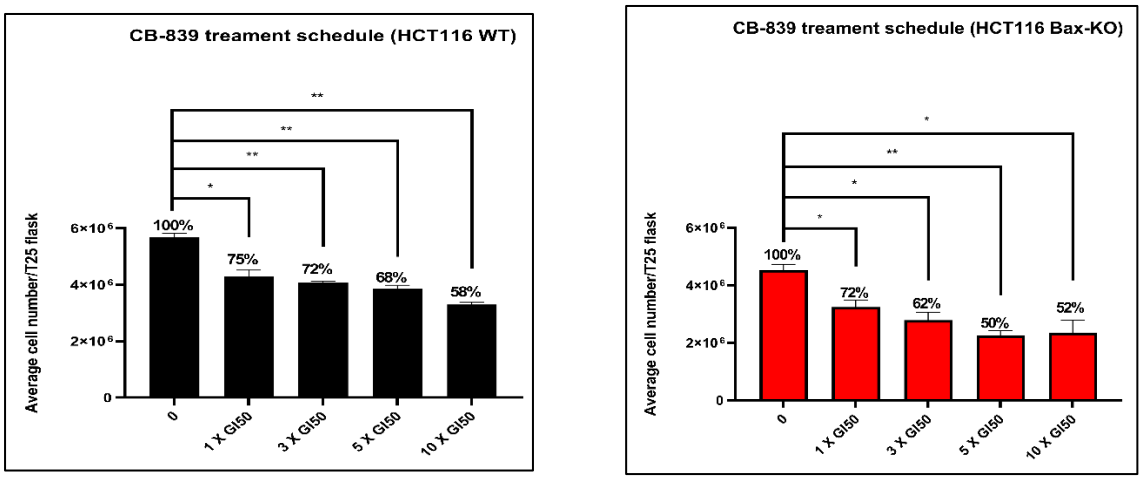

B.

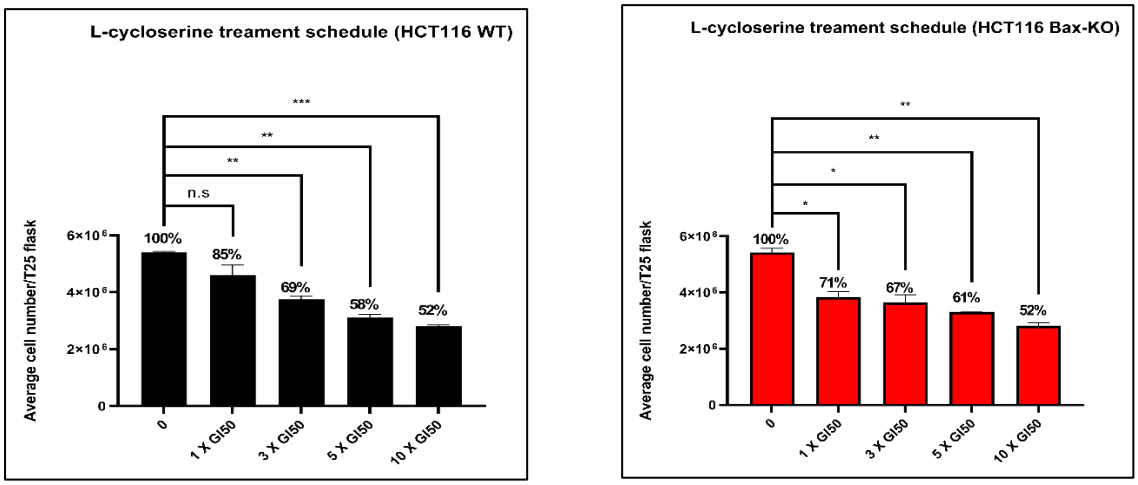

Figure 3.2. Optimal treatment conditions for CB-839 **(A)** and L-cycloserine **(B)** on HCT116 WT and HCT116 Bax-ko cell lines. The diagram showing the number of viable cell following treatment with 5 different concentrations (0, 1xGI_{50}, 3x GI_{50}, 5x GI_{50} and 10x GI_{50}) of CB-839 and L-cycloserine. Data are expressed as mean +/- SD, n = 3. Error bars represent +/- SD for 3 independent measurements. The significance level was assessed using 2-tailed Student's t-test. P values: * - <0.05, ** - <0.01, *** - <0.001, n.s = not significant, n = 3.

3.2.3. Monitoring metabolic changes in HCT116 WT and HCT116 Bax-ko cells following CB-839 treatment by using ^{1}H-MRS

To examine the potential involvement of glutaminase enzyme in the metabolism of 4-[^{19}F]fluoroglutamine, HCT116 WT and HCT116 Bax-ko cells were treated for 24 hours with 10xGI_{50} of CB-839, a glutaminase inhibitor, and ^{1}H-MRS spectroscopy was used to analyse the cell culture media and cellular extracts. The rates of glutamine uptake and glutamate secretion were calculated as described in section 2.3.4. No changes were observed in glutamine uptake and glutamate secretion following the drug treatment (Figure 3.3) in both cell lines. A significant increase in cellular glutamine was found in the CB-839-treated groups when compared with vehicle-treated controls (≈1.8-folds, $p<0.01$ for HCT116 WT; ≈1.7-folds, $p<0.05$ for HCT116 Bax-ko; Fig. 3.3). This increase in intracellular glutamine coupled with no change in glutamine uptake indicated that the accumulation of intracellular glutamine was mainly caused by the inhibition of glutaminase following CB-839 treatment, as the cells are unable to convert glutamine to glutamate. A significant decrease in cellular glutamate was found in CB-839-treated cells when compared with vehicle-treated controls (≈2.1-folds, $p<0.01$ for HCT116 WT; ≈1.7-folds, $p<0.05$ for HCT116 Bax-ko; Fig. 3.3). The increase in cellular glutamine and decrease in cellular glutamate are consistent with glutaminase inhibition, as the cells are unable to convert cellular glutamine to glutamate and subsequently cause a reduction in cellular glutamate and an accumulation of glutamine inside the cells. An example of ^{1}H-MRS spectra which illustrates the changes of cellular glutamine/glutamate level following CB-839 treatment is shown in Fig. 3.4.

3.2.4. Monitoring metabolic changes in HCT116 WT and HCT116 Bax-ko cells following CB-839 treatment by using ^{19}F-MRS

Next, the role of glutaminase in the metabolism of 4-[^{19}F]fluoroglutamine was tested. HCT116 WT and HCT116 Bax-ko cells were treated with 10xGI_{50} of the glutaminase inhibitor CB-839 for 24 hours. The cells were labelled with 4-[^{19}F]fluoroglutamine, which is the stable isotope version of the PET tracer, for the last 6 hours of the 24 hour treatment and the cell culture media and cellular extracts were analysed by ^{19}F-MRS. The rates of metabolite uptake/secretion were calculated as described in section 2.3.4.

Similar to the ^{1}H-MRS data, there were no changes in the 4-[^{19}F]fluoroglutamine uptake and 4-[^{19}F]fluoroglutamate secretion following the drug treatment in HCT116 WT cell line (Fig. 3.5A). However, a significant decrease in 4-[^{19}F]fluoroglutamate secretion was observed following the drug treatment in HCT116 Bax-ko cell line (≈3.1-folds, $p<0.05$; Fig. 3.5B). This might be a survival response of HCT116 Bax-ko cells from the effect of CB-839 on glutaminase activity by preserving the amount of intracellular 4-[^{19}F]fluoroglutamate to fuel the TCA cycle. A significant increase in cellular 4-[^{19}F]fluoroglutamine (≈2.6-folds, $p<0.01$ for HCT116 WT; ≈2.5-folds, $p<0.01$ for HCT116 Bax-ko; Fig 3.5) and a decrease in cellular 4-[^{19}F]fluoroglutamate were found by ^{19}F-MRS following CB-839 treatment when compared with vehicle-treated controls (≈2.4-folds, $p<0.0001$ for HCT116 WT; ≈1.6-folds, $p<0.05$ for HCT116 Bax-ko; Fig. 3.5). The results suggest that 4-[^{19}F]fluoroglutamine can be metabolised by glutaminase enzyme in the same way as L-glutamine in cancer cells. A significant increase in [^{19}F]-4-Fluoro-5-oxoproline secretion was found following the drug treatment in both cell lines (≈2.7-folds, $p<0.05$ for HCT116 WT; ≈2.3-folds, $p<0.05$ for HCT116 Bax-ko; Fig 3.5). This result indicates a significant effect of CB-839 on the non-enzymatic cyclisation of 4-[^{19}F]fluoroglutamine. Example ^{19}F-MRS spectra which illustrate the changes in cellular 4-[^{19}F]fluoroglutamine and 4-[^{19}F]fluoroglutamate levels following CB-839 treatment are shown in Fig. 3.6.

3.2.5. Expression of glutaminase enzyme in HCT116 WT and HCT116 Bax-ko cells following CB-839 treatment.

In order to confirm whether the results obtained from the ^{1}H-MRS and ^{19}F-MRS studies are due to the effect of CB-839 on the glutaminase enzyme, the glutaminase protein was probed in CB-839 treated cells after 24h of the treatment. Following the drug treatment, a decrease in the expression of glutaminase enzyme was found when compared with vehicle-treated controls (≈2-folds for HCT116 WT, ≈2.4-folds for HCT116 Bax-ko, $p<0.01$; Fig. 3.7). These results showed that the glutaminase enzyme was inhibited by CB-839 and reaffirmed the effective working mechanism of the drug.

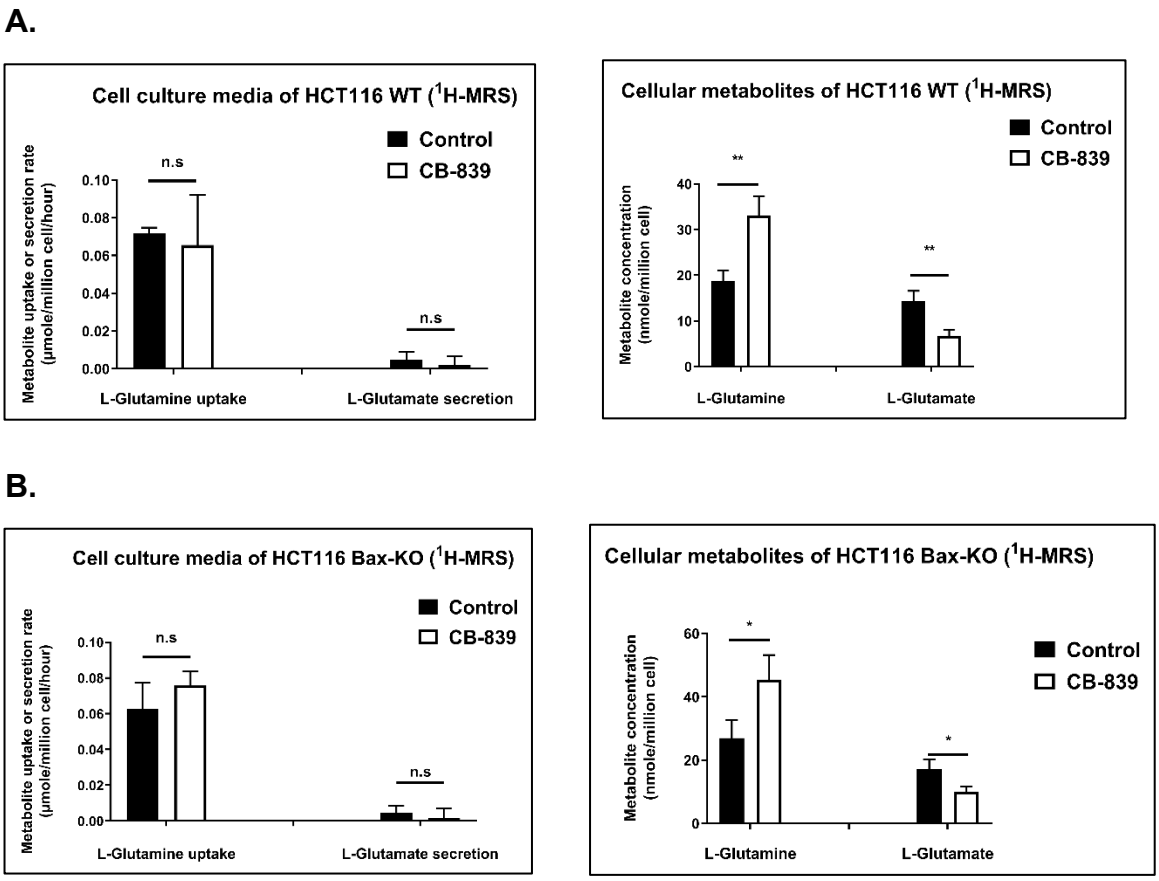

Figure 3.3. Changes in glutamine metabolism measured by ^{1}H-MRS following CB-839 treatment in HCT116 WT and HCT116 Bax-ko cell lines. A. ^{1}H-MRS metabolic profiling of cell culture media and cell extracts from vehicle- and CB-839-treated HCT116 WT cells**. B.** ^{1}H-MRS metabolic profiling of cell culture media and cell extracts from vehicle- and CB-839-treated HCT116 Bax-ko cells**.** The rates of metabolite uptake/secretion were calculated as described in section 2.3.4. Data are expressed as mean +/- SD, n = 3. The significance level was assessed using 2-tailed Student's t-test. P values: * - <0.05, ** - <0.01, n.s = not significant.

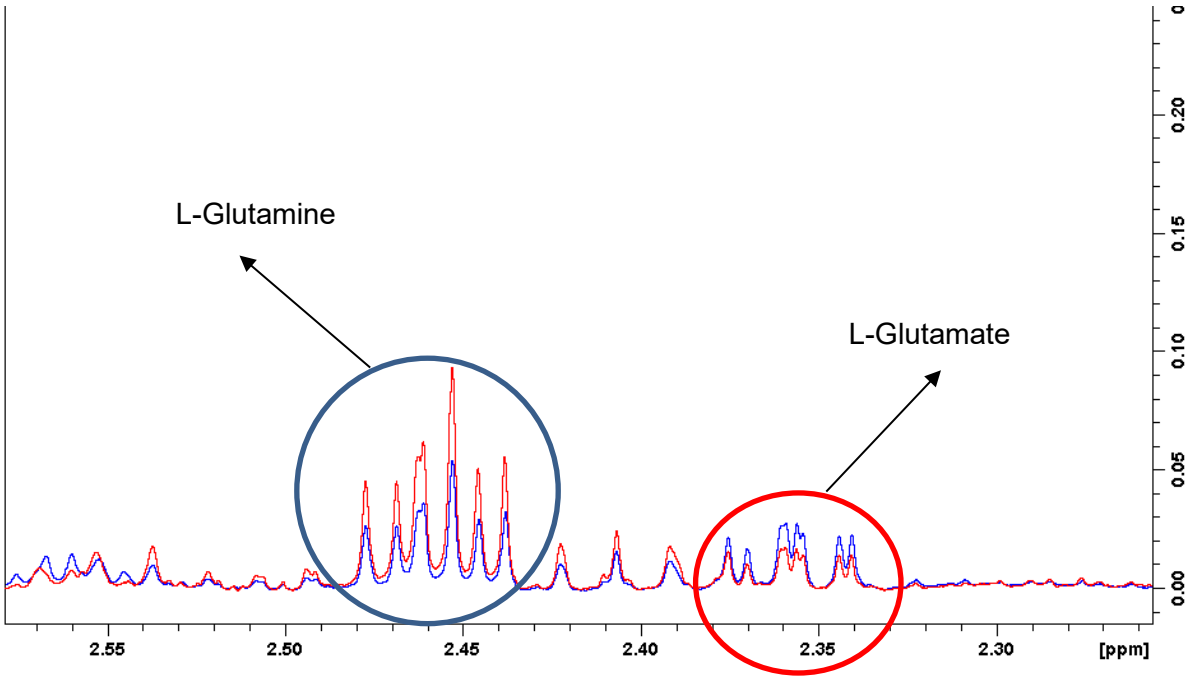

Figure 3.4. Example ^{1}H-MRS spectra of cellular glutamine/glutamate changes in vehicle- (blue) and CB-839-treated (red) HCT116 WT cell extracts. Intracellular glutamine level significantly increased and glutamate level decreased following CB-839 treatment

A.

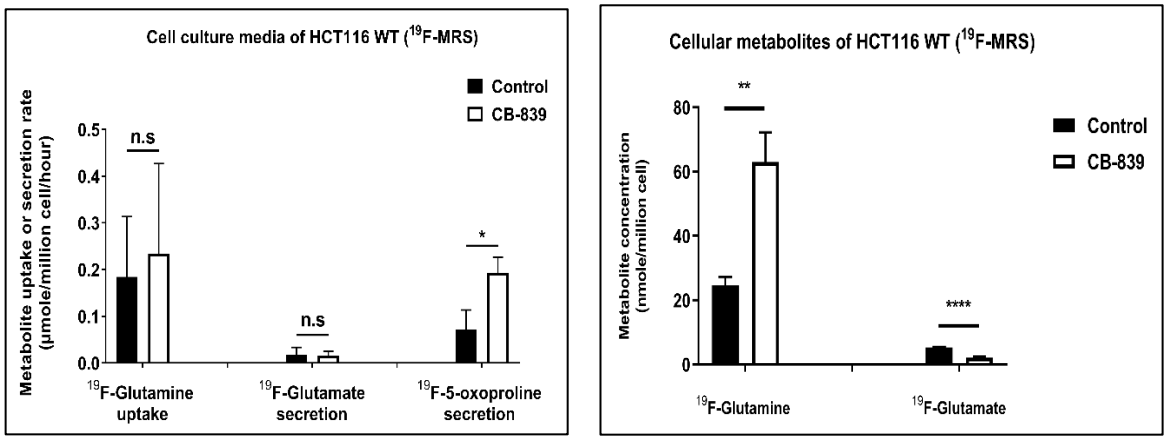

B.

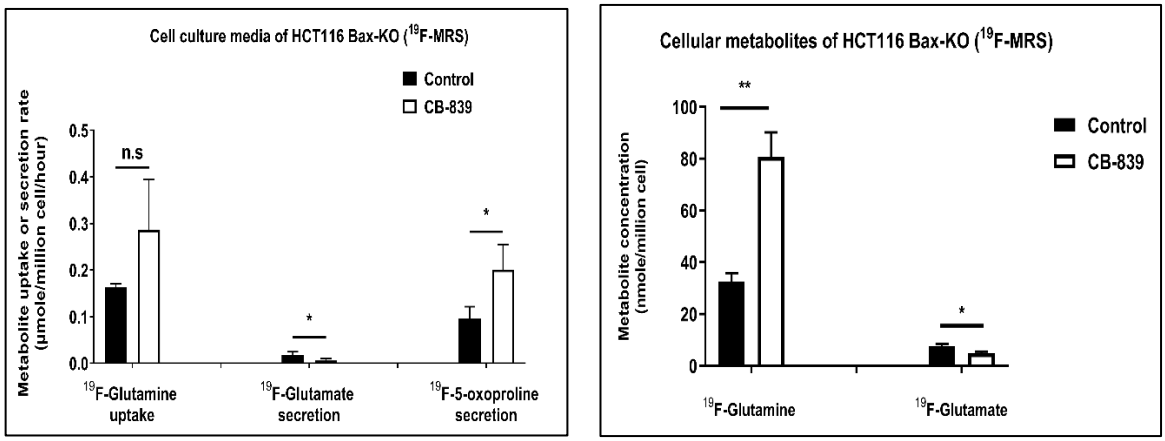

Figure 3.5. Changes in glutamine metabolism measured by ^{19}F-MRS following CB-839 treatment in HCT116 WT and HCT116 Bax-ko cell lines. A. ^{19}F-MRS metabolic profiling of cell culture media and cell extracts from vehicle- and CB-839-treated HCT116 WT cells**. B.** ^{19}F-MRS metabolic profiling of cell culture media and cell extracts from vehicle- and CB-839-treated HCT116 Bax-ko cells**.** Data are expressed as mean +/- SD, n = 3. The significance level was assessed using 2-tailed Student's t-test. P values: * - <0.05, ** - <0.01, **** - <0.0001, n.s = not significant.

A.

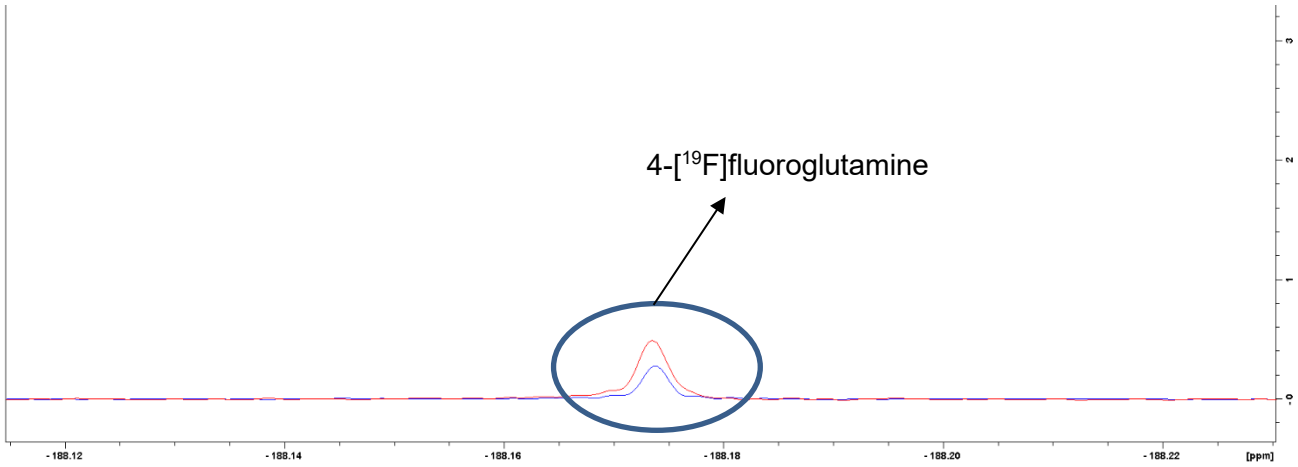

B.

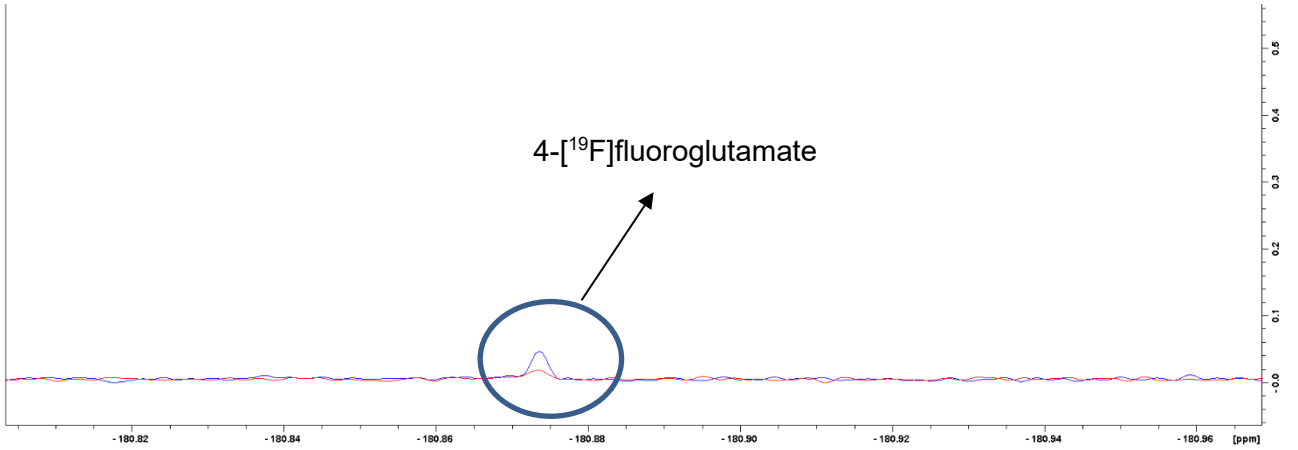

Figure 3.6. Example ^{19}F-MRS spectra showing cellular fluoroglutamine and fluoroglutamate changes in vehicle- (blue) and CB-839-treated (red) HCT116 WT cell extracts. Intracellular 4-[^{19}F]fluoroglutamine level significantly increased and 4-[^{19}F]fluoroglutamate level decreased following CB-839 treatment.

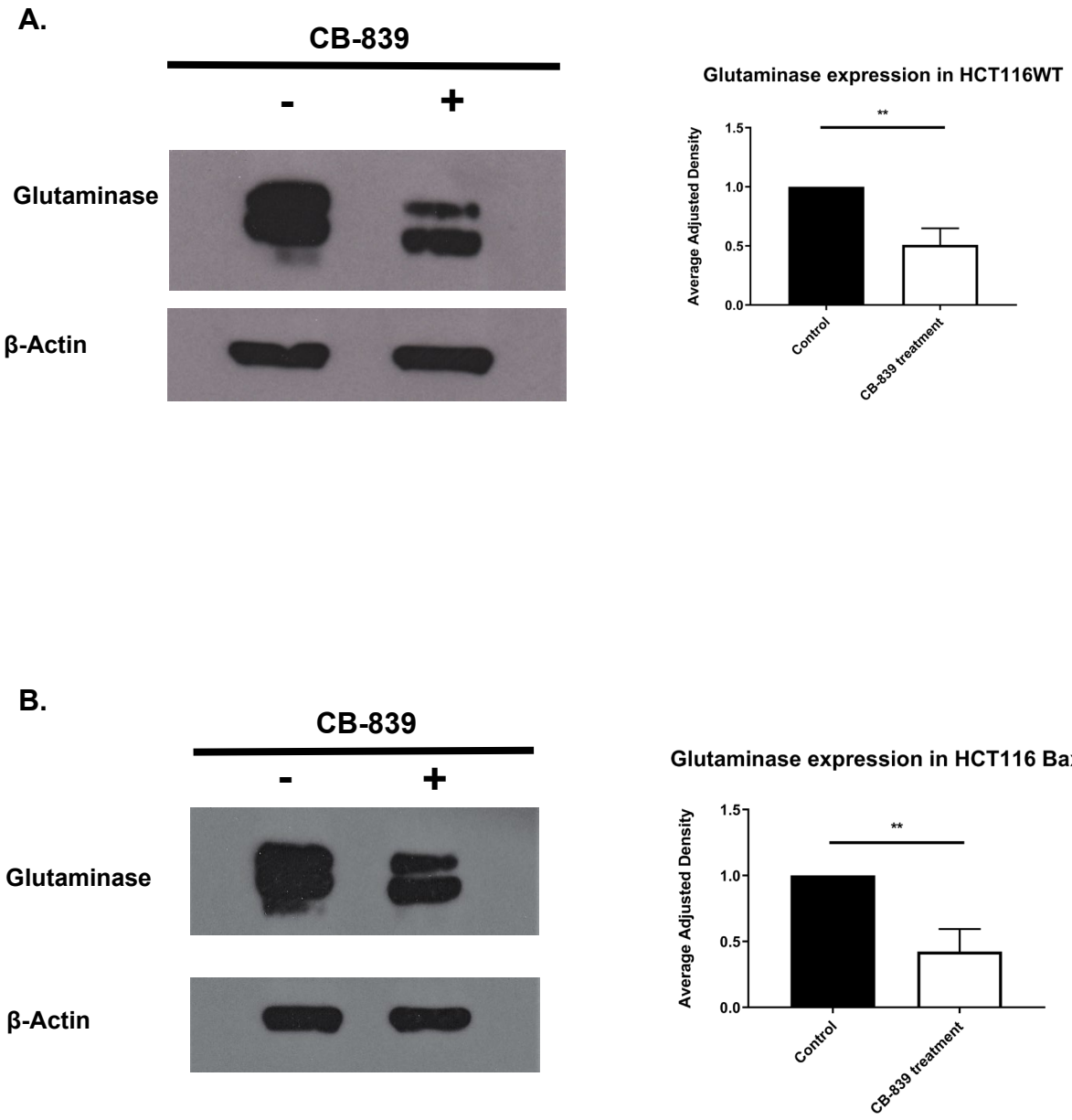

Figure 3.7. Changes in glutaminase enzyme expression level in HCT116 WT and HCT116 Bax-ko cell lines following CB-839 treatment. A. HCT116 WT cells were exposed to 10 x GI_{50} of CB-839 (0.5 μM) for 24 hours. Figure representative of western blot analysis was done in triplicate. Total protein was normalised to β-Actin as a loading control. There is a reduction in level of glutaminase expression following CB-839 treatment. **B.** HCT116 Bax-ko cells were exposed to 10 x GI_{50} of CB-839 (0.9 μM) for 24 hours. Figure representative of western blot analysis was done in triplicate. Total protein was normalised to β-Actin as a loading control. There is a reduction in level of glutaminase expression following CB-839 treatment. Data are expressed as mean ± SD, n = 3. The significance level was assessed using 2-tailed Student's t-test. P values: ** - <0.01.

3.2.6. Monitoring metabolic changes in HCT116 WT and HCT116 Bax-ko cells following L-cycloserine treatment by using ^{1}H-MRS

To examine the potential involvement of alanine aminotransferase enzyme in the metabolism of 4-[^{19}F]fluoroglutamine, HCT116 WT and HCT116 Bax-ko cells were treated for 24 hours with 10xGI_{50} of L-cycloserine, an alanine aminotransferase inhibitor, and ^{1}H-MRS spectroscopy was used to analyse cell culture media and cellular extracts. It was noticeable that the cells significantly changed from alanine secretion to alanine uptake and no significant changes in cellular alanine level following drug treatment ($p<0.05$) when compared to vehicle controls (Fig.3.8). This phenomenon allowed the cell to maintain cellular alanine level during L-cycloseine treatment. Significant increases in glutamate secretion (≈2.4-folds, $p<0.05$ for HCT116 WT; ≈5.4-folds, $p<0.05$ for HCT116 Bax-ko; Fig. 3.8) and cellular glutamate level (≈1.9-folds, $p<0.01$ for HCT116 WT; ≈3.3-folds, $p<0.05$ for HCT116 Bax-ko; Fig. 3.8) were observed following the treatment with L-cycloserine when compared with vehicle-treated controls . No significant changes in either glutamine uptake or cellular glutamine were observed, consistent with the inhibition mechanism of L-cycloserine on alanine aminotransferase enzyme. The cells are unable to convert cellular glutamate to alanine which leads to an accumulation of intracellular glutamate level. The cells then change the metabolism from alanine secretion to alanine uptake to maintain cellular alanine level. Example ^{1}H-MRS spectra illustrating the changes of alanine uptake and glutamate secretion and cellular alanine and glutamate levels following L-cycloserine treatment are shown in Fig. 3.9.

3.2.7. Monitoring metabolic changes in HCT116 WT and HCT116 Bax-ko cells following L-cycloserine treatment by using ^{19}F-MRS

Next, the role of alanine aminotransferase in the metabolism of 4-[^{19}F]fluoroglutamine was examined. HCT116 WT and HCT116 Bax-ko cells were treated with 10xGI_{50} of L-cycloserine for 24 hours and the cells were labelled with 4-[^{19}F]fluoroglutamine for the last 6 hours of the 24 hours experiment. The cell culture media and cellular extracts were then analysed by ^{19}F-MRS. Similar changes to ^{1}H-MRS were observed in the ^{19}F-MRS study. Significant increases in 4-[^{19}F]fluoroglutamate secretion (≈2.2-folds for HCT116 WT, ≈2.4-folds for HCT116 Bax-ko, $p<0.01$, Fig. 3.10) and cellular 4-[^{19}F]fluoroglutamate (≈3.4-folds, $p<0.0001$ for HCT116 WT; ≈2.9-fold, $p<0.001$ for HCT116 Bax-ko, Fig. 3.10) were found following L-cycloserine treatment when

compared with vehicle controls. There was no significant change in either 4-[^{19}F]fluoroglutamine uptake or cellular 4-[^{19}F]fluoroglutamine. In the study by Cooper et al, it was proposed that alanine aminotransferase might be a potential enzyme for the γ-elimination of F^- ion from 4-[^{18}F]fluoroglutamate (Cooper et al. 2012). Hence, it was expected that the free F^- secretion would decrease following the L-cycloserine treatment in this study. However, an opposite trend was found in this study where the free fluoride secretion increased significantly following the drug treatment when compared with vehicle-treated controls (≈1.5-folds, $p<0.001$ for HCT116 WT, ≈1.6-folds, $p<0.05$ for HCT116 Bax-ko; Fig. 3.10). There was no significant changes in [^{19}F]-4-Fluoro-5-oxoproline secretion following the cycloserine treatment in HCT116 WT cells (Fig. 3.10). However, a significant increase in [^{19}F]-4-Fluoro-5-oxoproline secretion was found in cycloserine-treated HCT116 Bax-ko cells (≈1.9-folds, $p<0.05$ for HCT116 Bax-ko; Fig. 3.10). This result indicates a significant effect of L-cycloserine on the non-enzymatic cyclisation of 4-[^{19}F]fluoroglutamine in HCT116 Bax-ko cells.
The results obtained from this study also showed that 4-[^{19}F]fluoroglutamate, a product of 4-[^{19}F]fluoroglutamine, is stable in the cell culture media and can be metabolised by alanine aminotransferase in the same way as L-glutamate. The origin of free F^- release from 4-[^{19}F]fluoroglutamine is yet not fully determined. 4-[^{19}F]fluoroglutamine and 4-[^{19}F]fluoroglutamate were found to be stable in cell culture media, as no free F^- was detected before cell incubation (Fig. 3.11A & B). The free F^- was only detected when 4-[^{19}F]fluoroglutamine was incubated with cells (Fig. 3.11C) and the γ-elimination of F^- from this glutamine analogue might be due to a spontaneous cellular degradation or other enzymatic pathways, in addition to the alanine aminotransferase catalytic pathway. Example ^{19}F-MRS spectra which illustrates the changes of free fluoride secretion and 4-[^{19}F]fluoroglutamine uptake and 4-[^{19}F]fluoroglutamate secretion and cellular 4-[^{19}F]fluoroglutamine and 4-[^{19}F]fluoroglutamate level following L-cycloserine treatment are shown in Fig. 3.12.

3.2.8. Expression of alanine aminotransferase enzyme in HCT116 WT and HCT116 Bax-ko cells following L-cycloserine treatment.

In order to confirm whether the results obtained from ^{1}H-MRS and ^{19}F-MRS are due to the effect of L-cycloserine on the alanine aminotransferase enzyme, the alanine aminotransferase protein was probed in L-cycloserine treated cells after 24 hours of

the treatment. Following L-cycloserine treatment, a decrease in the expression of alanine aminotransferase enzyme was found when compared with vehicle-treated controls (≈3.5-folds, $p<0.01$ for HCT116 WT, ≈8.7-folds, $p<0.0001$ for HCT116 Bax-ko, Fig. 3.13). These results showed alanine aminotransferase was inhibited by L-cycloserine and reaffirmed the effective working mechanism of the drug.

A.

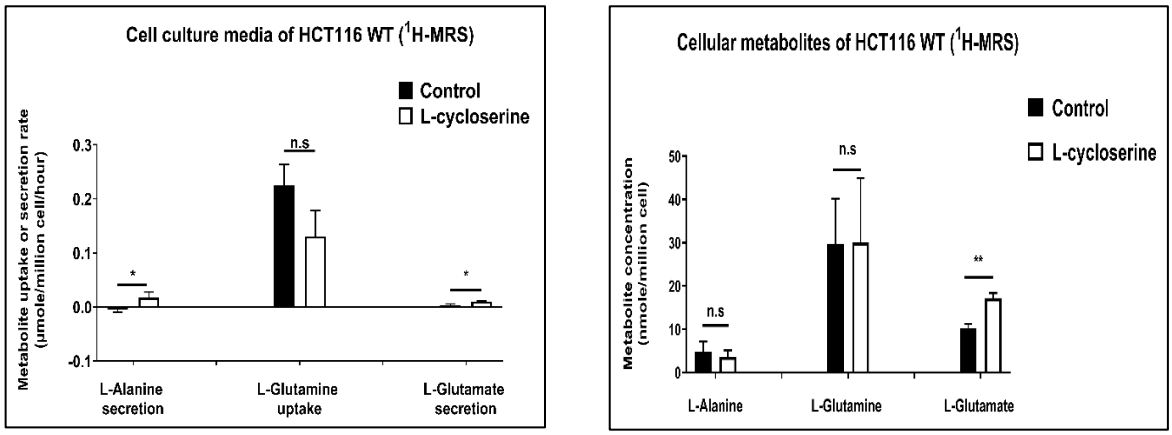

B.

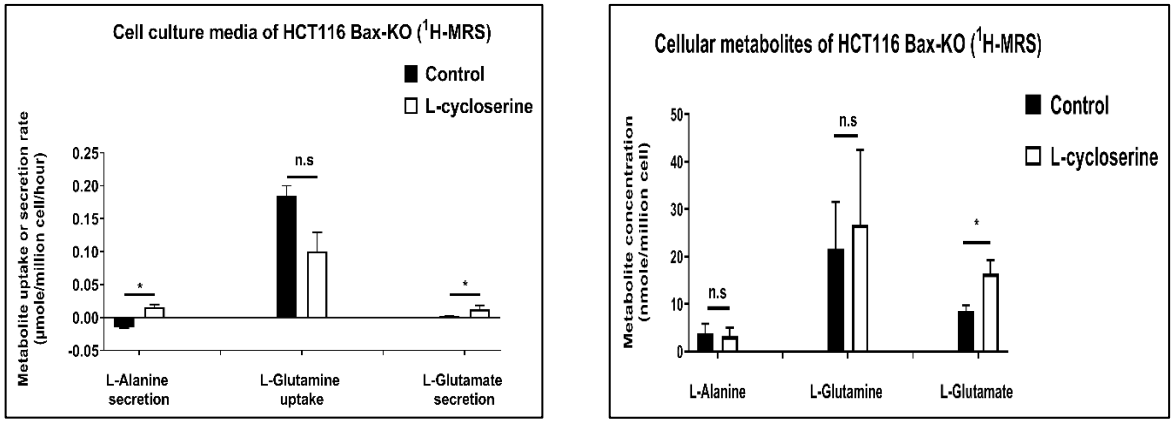

Figure 3.8. Changes in glutamine metabolism measured by ^{1}H-MRS following L-cycloserine treatment in HCT116 WT and HCT116 Bax-ko cells. A. ^{1}H-MRS metabolic profiling of cell culture media and cell extracts from vehicle- and L-cycloserine-treated HCT116 WT cells**. B.** ^{1}H-MRS metabolic profiling of cell culture media and cell extracts from vehicle- and L-cycloserine-treated HCT116 Bax-ko cells**.** Data are expressed as mean +/- SD, n = 3. The significance level was assessed using 2-tailed Student's t-test. P values: * - <0.05, ** - <0.01, n.s = not significant.

A.

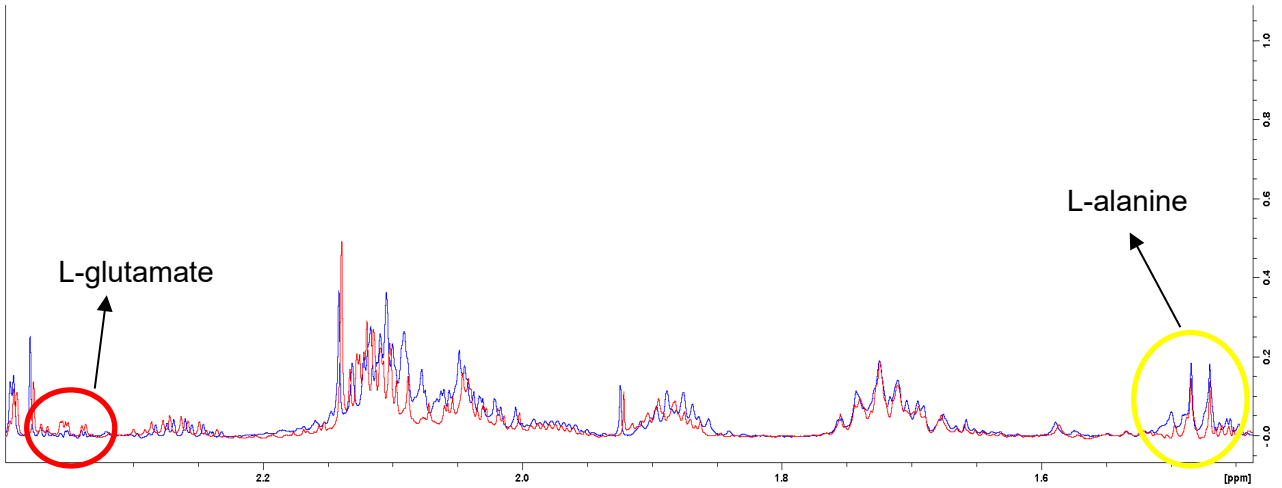

B.

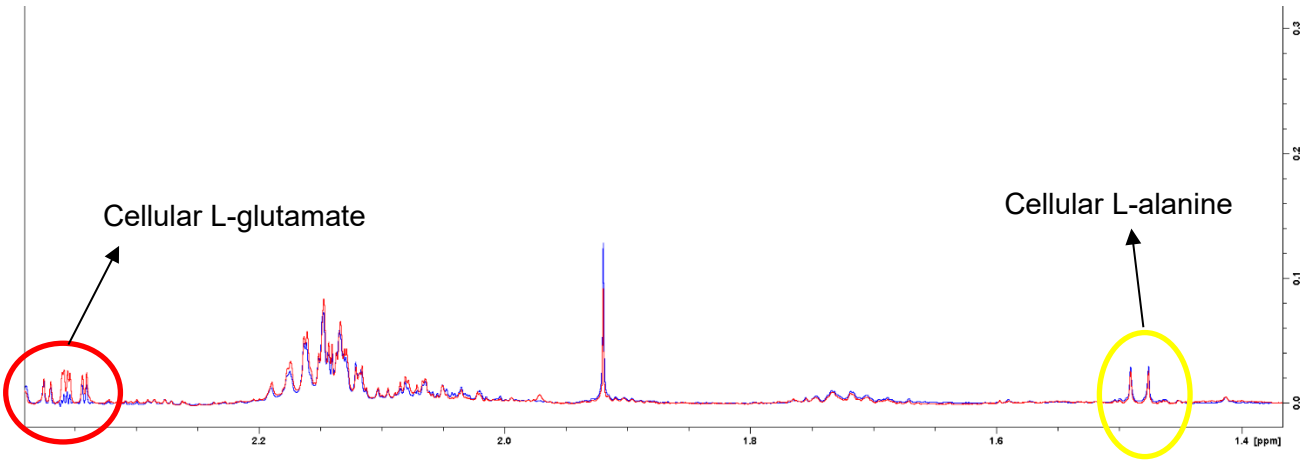

Figure 3.9. Example ^{1}H-MRS spectra. A. Changes of alanine uptake/glutamate secretion in culture media from vehicle- (blue) and L-cycloserine-treated (red) HCT116 WT cells. **B.** Changes of cellular alanine/glutamate in vehicle- (blue) and L-cycloserine-treated (red) HCT116 WT cell extracts.

A.

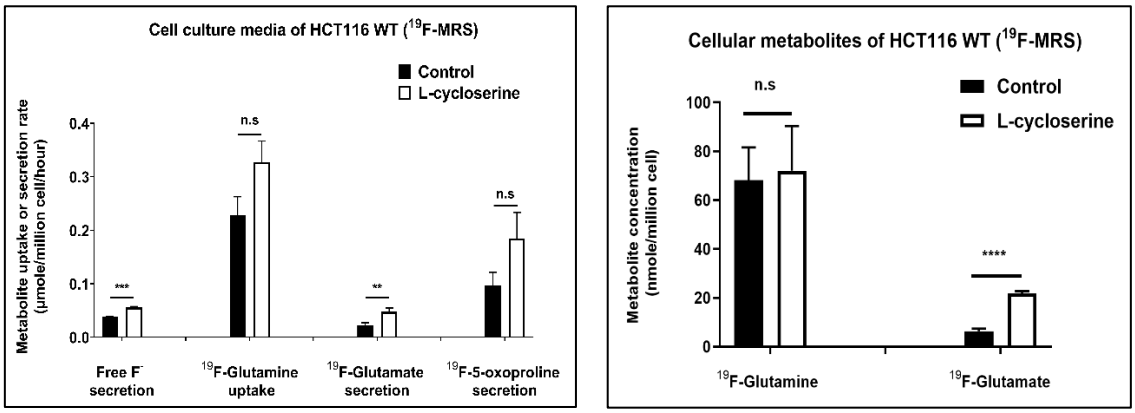

B.

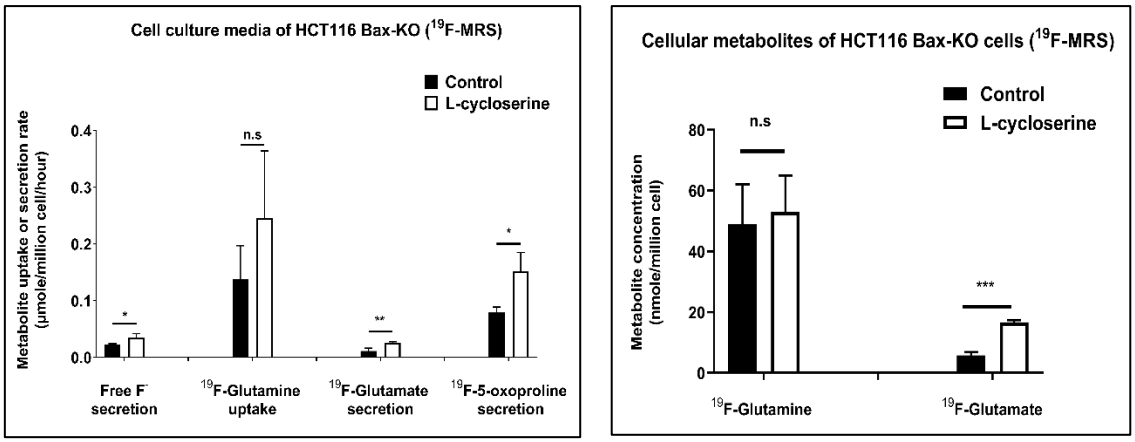

Figure 3.10. Changes in glutamine metabolism measured by ^{19}F-MRS following L-cycloserine treatment in HCT116 WT and HCT116 Bax-ko cell lines. A. ^{19}F-MRS metabolic profiling of cell culture media and cell extracts from vehicle- and L-cycloserine-treated HCT116 WT cells**. B.** ^{19}F-MRS metabolic profiling of cell culture media and cell extracts from vehicle- and L-cycloserine-treated HCT116 Bax-ko cells**.** Data are expressed as mean +/- SD, n = 3. The significance level was assessed using 2-tailed Student's t-test. P values: * - <0.05, ** - <0.01, *** - <0.001, **** - <0.0001, n.s = not significant.

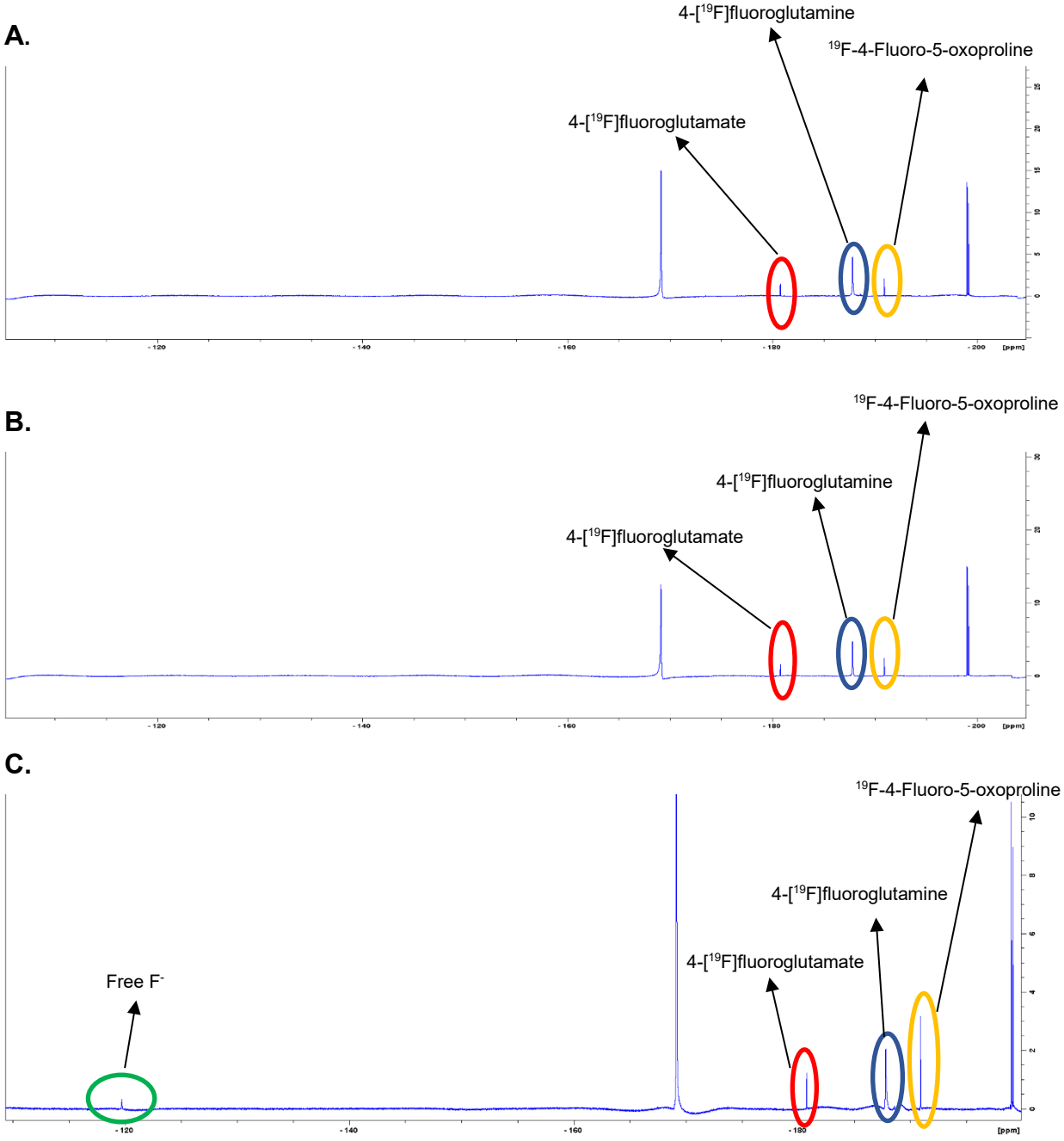

Figure 3.11. ^{19}F-MRS of 4-[^{19}F]fluoroglutamine in (A) clean media and (B) clean media + L-cycloserine before incubation with the HCT116 WT and HCT116 Bax-ko cells. Only ^{19}F-4-Fluoro-5-oxoproline (-191 ppm), 4-[^{19}F]fluoroglutamine (-188 ppm) and 4-[^{19}F]fluoroglutamate (-181 ppm) peaks were detected. The free fluoride signal (-122 ppm) was not detected in the clean media ± L-cycloserine. Hence, it indicates that 4-[^{19}F]fluoroglutamine is quite stable in cell media and not affected by L-cycloserine**. (C) incubated media with the HCT116 WT cells.** ^{19}F-4-Fluoro-5-oxoproline (-191 ppm), 4-[^{19}F]fluoroglutamine (-188 ppm), 4-[^{19}F]fluoroglutamate (-181 ppm) and free F^- (-122ppm) were all detected in the incubated media with HCT116 WT cells

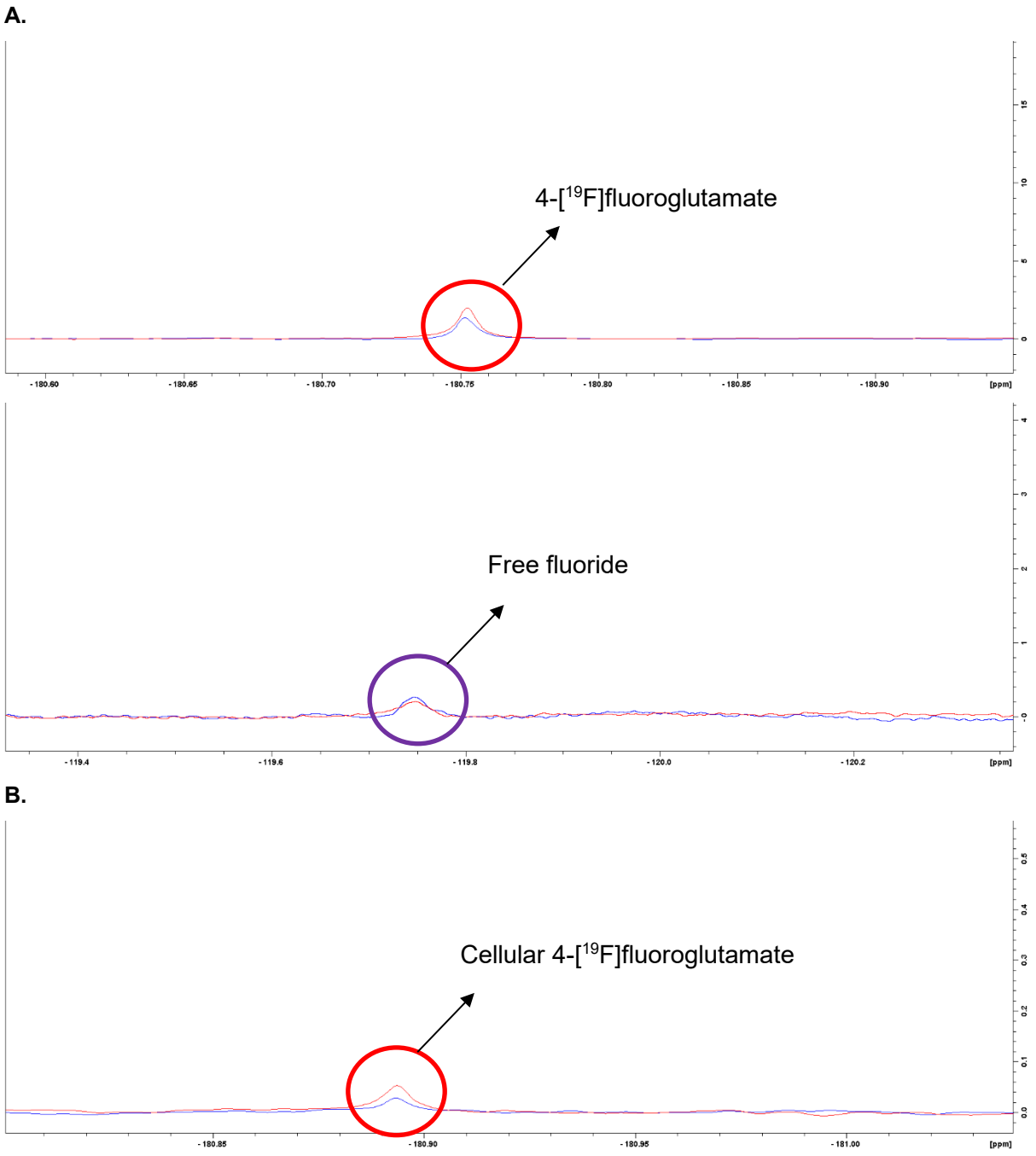

Figure 3.12. Example ^{19}F-MRS spectra. A. Changes of 4-[^{19}F]fluoroglutamate/free fluoride secretion in culture media from vehicle- (blue) and L-cycloserine-treated (red) HCT116 WT cells**.** The free fluoride secretion in culture media from vehicle- (blue) and L-cycloserine-treated (red) cells was shown at a similar level. Following a metabolite standardisation to cell number in which the cell number following L-cycloserine treatment was lower than the one from vehicle treatment, the quantified concentration of free fluoride was significantly higher following L-cycloserine treatment. **B.** Changes of cellular 4-[^{19}F]fluoroglutamate in vehicle- (blue) and L-cycloserine-treated (red) HCT116 WT cell extracts**.**

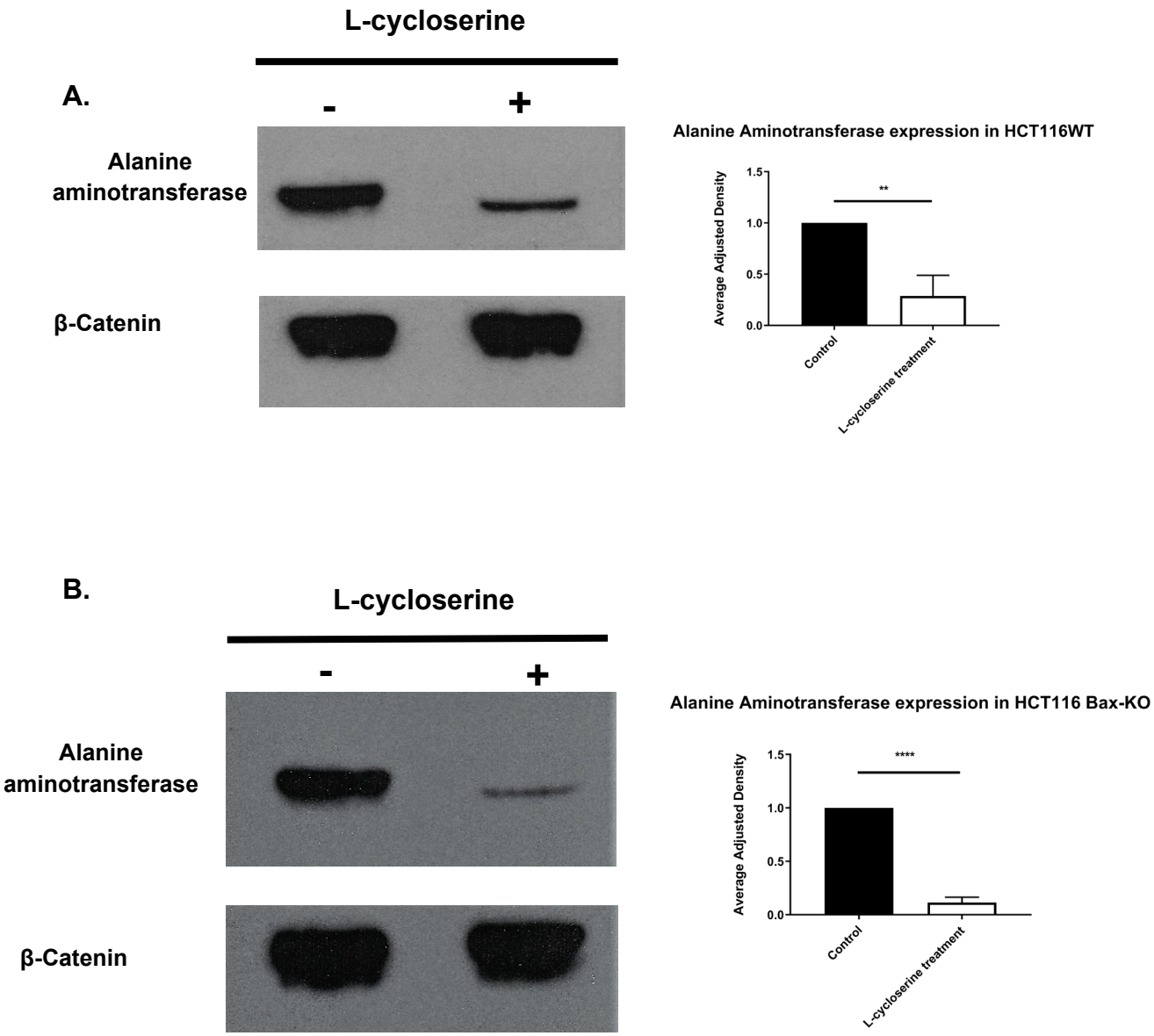

Figure 3.13. Changes in alanine aminotransferase enzyme expression in HCT116 WT and HCT116 Bax-ko cell lines following L-cycloserine treatment. A. HCT116 WT cells were exposed to 10 x GI_{50} of L-cycloserine (470 μM) for 24 hours. Figure representative of western blot analysis was done in triplicate. Total protein was normalised to β-Catenin as a loading control. There is a reduction in level of alanine aminotransferase expression following L-cycloserine treatment. **B.** HCT116 Bax-ko cells were exposed to 10 x GI_{50} of L-cycloserine (1220 μM) for 24 hours. Figure representative of western blot analysis was done in triplicate. Total protein was normalised to β-Catenin as a loading control. There is a reduction in level of alanine aminotransferase expression following L-cycloserine treatment. Data are expressed as mean ± SD, n = 3. The significance level was assessed using Student's t-test. P values: ** - <0.01, **** - <0.0001.

3.3. Discussion

The glutaminolysis pathway, in which large amounts of glutamine are consumed and metabolised by cancer cells, has been shown to play an essential part in tumour metabolism (Wise and Thompson 2010). Due to the importance of glutamine in tumour, the tracer 4-[^{18}F]fluoroglutamine was developed for use in non-invasive PET imaging of glutamine metabolism (Lieberman et al. 2011; Qu et al. 2011). Previous characterization studies of 4-[^{18}F]fluoroglutamine support that this tracer might be metabolised in the same way as L-glutamine (Cooper et al. 2012). The present study used CB-839 (a glutaminase inhibitor) and L-cycloserine (an alanine aminotransferase inhibitor) to investigate the metabolism of 4-[^{19}F]fluoroglutamine, an isotopically stable version of 4-[^{18}F]fluoroglutamine, in human colorectal cancer cell lines HCT116 WT and HCT116 Bax-ko. 24 hour treatment was applied with either 10 x GI_{50} of CB-839 or L-cycloserine and ^{1}H- and ^{19}F-MRS were used to examine the metabolic effects of these drugs on cellular metabolism.

It is necessary to firstly investigate the drug effect on cellular metabolism and specifically on L-glutamine uptake and consumption before carrying out the ^{19}F-MRS study of 4-[^{19}F]fluoroglutamine. Hence, ^{1}H-MRS is the best method to use in this context. It is known that glutamine is one of the key nutrients that fuel the proliferation of many cancers (DeBerardinis et al. 2007, Wise and Thompson 2010). The conversion of glutamine to glutamate by the mitochondrial glutaminase (Gao et al. 2009, Wang et al. 2010) is a critical step at the start of glutamine metabolism.

$$\text{L-Glutamine} + H_2O \xrightarrow{\textbf{Glutaminase}} \text{L-Glutamate} + NH_4^+$$

It was hypothesised that cells treated with a glutaminase inhibitor CB-839, would accumulate glutamine inside the cells due to the inhibition of glutaminase and subsequent reduction of glutamine conversion to glutamate. A significant increase in cellular glutamine and decrease in cellular glutamate were observed in both cell lines in the current study following CB-839 treatment when compared to controls, which supports the above hypothesis and is consistent with the mechanism of drug action. Similar results were also observed with 4-[^{19}F]fluoroglutamine in which a significant increase of cellular 4-[^{19}F]fluoroglutamine and a decrease of cellular 4-[^{19}F]fluoroglutamate were found in HCT116 cell lines following CB-839 treatment when

compared with vehicle-treated controls. A recent study by Zhou et al found that glutaminase inhibition by CB-839 increase the L-glutamine pool size and also the signal intensity of 4-[^{18}F]fluoroglutamine PET imaging in triple-negative breast cancer (Zhou et al. 2017). This solidifies the findings of higher accumulation of intracellular glutamine after treatment in our study.

Contrary to the confirmation in previous studies (Qu et al. 2011; Liebermann et al. 2011; Copper et al. 2012; Ploessl et al. 2012; Dunphy et al. 2018) and our observed conversion of 4-[^{19}F]fluoroglutamine to 4-[^{19}F]fluoroglutamate in cancer cells, the study by Zhou et al reported that 4-[^{18}F]fluoroglutamine was minimally or even not metabolized in tumours (Zhou et al. 2017). However, there are some differences in experimental design with our studies when compared to the Zhou et al report (Zhou et al. 2017). We incubated the HCT116 cells with 4-[^{19}F]fluoroglutamine for 6 hours before the cells were harvested and analysed by ^{19}F-MRS, whereas, their study used radio-HPLC to characterise the metabolites of 4-[^{18}F]fluoroglutamine in tumours after 30 minutes post injection of the radiotracer. This length of time may not be long enough for the tumours to metabolise this glutamine tracer fully. Zhou et al also found that the 4-[^{18}F]fluoroglutamate signal, which was confirmed as the metabolic product of 4-[^{18}F]fluoroglutamine (Cooper et al. 2012), starting to appear at this time point (Zhou et al. 2017). The reason of choosing such a short time point for carrying out the invasive radio-HPLC procedure of metabolic analysis in the mentioned study is due to the short half-life of the positron (β^+) emitter ^{18}F ($T_{1/2}$ = 110 minutes), which can obstruct the exploitation and distinction of chemical compounds. Hence, the use of ^{19}F isotopically stable version of the glutamine PET tracer in the ^{19}F-MRS study, allows a longer time period for tumour metabolism of 4-[^{19}F]fluoroglutamine (ca. 6 hours of cancer cell incubation with 4-[^{19}F]fluoroglutamine in the work of this thesis), emerges to be essential. Overall, the findings in the current study confirm that 4-[^{19}F]fluoroglutamine can be enzymatically hydrolysed by glutaminase enzyme in the same way as L-glutamine.

Alanine aminotransferase or glutamic pyruvate transaminase is another important target in the metabolic study of 4-[^{19}F]fluoroglutamine. It catalyses a reversible transamination reaction by transferring an amino group from L-glutamate to pyruvate to yield α-ketoglutarate and L-alanine. The metabolic pathways of 4-[^{19}F]fluoroglutamine proposed by Cooper et al indicate a potential involvement of the

alanine aminotransferase enzyme in the detection of free F^- (Cooper et al. 2012). The presence of 'free F^-' could be a marker for the formation of α-ketoglutarate from 4-[^{19}F]fluoroglutamate which is catalysed by alanine aminotransferase.

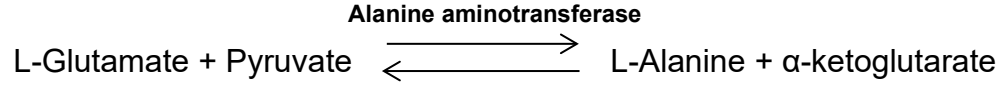

It was hypothesised that when cells were treated with L-cycloserine, an alanine aminotransferase inhibitor, there would be an increase of glutamate and decrease in alanine levels inside the cells due to the inhibition of the enzyme and subsequent reduction of glutamate conversion to alanine. A significant increase in cellular glutamate was observed in the ^{1}H-MRS study following L-cycloserine treatment when compared with the control group, which is consistent with the mechanism of drug action. However, the intracellular alanine concentration remains at a similar level in both vehicle-treated and L-cycloserine-treated groups. This result is not surprising because it was observed in this study that the cells changed metabolism from alanine secretion to alanine uptake following L-cycloserine treatment. A previous study pointed out that when alanine aminotransferase is inhibited and the cellular alanine synthesis is downregulated, cancer cells will switch to a complete dependence on environmental alanine (Parker et al. 2020). Cancer cells can upregulate alanine transporters SLC1A4 (ASCT1), SLC1A5 (ASCT2) and SLC38A2 (SNAT2) to rapidly replenish the depletion of cellular alanine following inhibitor treatment and maintain alanine concentration in cells (Parker et al. 2020). Since the inhibition of alanine aminotransferase by L-cycloserine is irreversible and non-competitive with the substrate (i.e glutamate or alanine) (Wong et al. 1973), the flexible utilization of different transporter systems can support cancer cell survival in adverse conditions.

Similar trends were also observed in the 4-[^{19}F]fluoroglutamine study in which a significant increase of cellular 4-[^{19}F]fluoroglutamate was found following L-cycloserine treatment. Contrary to the hypothesis of this study, an increase rather than a decrease in free F^- secretion was found following alanine aminotransferase inhibition. This finding suggests that the γ-elimination of F^- ion from 4-[^{19}F]fluoroglutamate might be originated from more than one pathway, in addition to the catalysis by alanine aminotransferase as proposed by Cooper et al (2012). Since 4-[^{19}F]fluoroglutamine and 4-[^{19}F]fluoroglutamate are quite stable in cell culture media

with no free F^- detected before cell incubation, the release of free F^- might come from a spontaneously non-enzymatic cellular degradation of 4-[^{19}F]fluoroglutamate or other enzymatic pathways. Cooper et al also proposed that 4-[^{19}F]fluoroglutamate may be metabolised by glutamate dehydrogenase (converting normal mitochondrial glutamate to α-ketoglutarate) to form 4-Fluoro-α-ketoglutarate which might be another source for the γ-elimination of F^- ion (Cooper et al. 2012). It has been found in this study that higher level of free F^- was generated when a higher concentration of 4-[^{19}F]fluoroglutamate was accumulated and 4-[^{19}F]fluoroglutamate could be a substrate of glutamate dehydrogenase enzyme. Further experiments will need to be carried out to fully determine whether the release of free F^- from the PET tracer 4-[^{18}F]fluoroglutamine comes from an enzymatic or non-enzymatic reaction.

Taken together, the changes observed in this study indicate that similar to L-glutamine, 4-[^{19}F]fluoroglutamine can be metabolised in cancer cells by the glutaminase enzyme to yield 4-[^{19}F]fluoroglutamate, which can be subsequently catalysed by the alanine aminotransferase enzyme analogous to L-glutamate. Besides the alanine aminotransferase pathway, the elimination of free F^- from 4-[^{19}F]fluoroglutamate may result from a spontaneous cellular degradation of the compound or other enzymatic pathways.

Chapter 4

In vitro and *in vivo* uptake of 4-[^{18}F]fluoroglutamine and [^{18}F]FDG in a panel cancer cell lines

4.1. Introduction

The Warburg effect or aerobic glycolysis is a classical feature of cancer cells where the cells depend on glycolysis to meet their energy demand for tumour growth and maintenance (Hanahan and Weinberg 2011). This increase in glucose utilization in tumour cells provides the biochemical basis for the development of PET imaging radiotracer [^{18}F]FDG for use in tumour diagnosis and staging (Zhu et al. 2011). Even though this PET tracer is being widely used as a gold standard for the detection and monitoring of malignant tumours, there were many reported cases of [^{18}F]FDG unable to detect certain types of tumour (Robey et al. 2008; Tsunoda et al. 2008; Almuhaideb et al. 2011; Brush et al. 2011; Yu et al. 2016; Bae et al. 2018; Kim et al. 2019). Previous studies have found the limitations of [^{18}F]FDG in detecting and diagnosing small-sized breast tumours (Wahl et al. 1991; Rostom et al. 1991; Avril et al. 2000; van der Hoeven et al. 2002; Eubank and Mankoff 2005), non-invasive carcinomas (Yu et al. 2016), metastatic lymph nodes associated with rectal cancer (Bae et al. 2018) and colorectal cancer with Kras mutation (Kim et al. 2019). It has also been shown that [^{18}F]FDG imaging exhibited a low sensitivity in detecting primary prostate cancer and yielded unsatisfactory results (Liu et al. 2001; Salminen et al. 2002; Jadvar 2012). These limitations of using [^{18}F]FDG to image prostate cancer stem from a low avidity of this tracer in a majority of prostate cancers, false positive signal from benign prostate hyperplasia and the influence of [^{18}F]FDG excretion into the urinary bladder (Shen et al. 2018). In addition to the inability of [^{18}F]FDG to detect some tumour types, the issue with false positive and false negative findings of [^{18}F]FDG imaging is also a major concern. For example, the increased uptake of [^{18}F]FDG is not specific to tumours: benign or infectious diseases such as fungal, mycobacterial, bacterial infection, sarcoidosis, or even post-operative surgical conditions could also cause false positive results in [^{18}F]FDG imaging (Goo et al. 2000; Kostakoglu et al. 2003; Chang et al. 2006; Lawal and Sathekge 2016; Viglianti et al. 2018; Vöö and Bomanji 2019; Saranovic and Stojiljkovic 2020). Furthermore, false negative results were recorded in tumours with low glycolytic activity (such as, adenomas, low-grade lymphomas and

carcinoid tumours) or tumours with a diameter of less than 1.0 cm (Goo et al. 2000; Turkington and Coleman 2002; Yu et al. 2016).

Limitation of [^{18}F]FDG imaging in tumours with low glycolytic activity or small size, indicates certain types or stages of tumours may depend on nutrients other than glucose. It has been shown that glucose-derived carbon alone is not sufficient for cancer cell growth and survival (DeBerardinis et al. 2008; Dang 2010). Glutamine is an important nitrogen source, which is essential for the biosynthesis of nucleotides and hexosamine (Mathew and White 2011). Previous studies suggest that the [^{18}F]FDG negative tumours may depend upon glutaminolysis to support their growth and survival (Wise et al. 2008; Thompson 2009; Cheng et al. 2011; Rajagopalan and DeBerardinis 2011; Shanware et al. 2011; Gao et al. 2009). Hence, non-invasive PET imaging with 4-[^{18}F]fluoroglutamine (its metabolic fate has been investigated in Chapter 3) may provide an alternative method to study the [^{18}F]FDG negative tumours. Furthermore, the use of 4-[^{18}F]fluoroglutamine PET tracer might be beneficial for imaging diabetic patients, as fasting is an essential requirement for [^{18}F]FDG imaging and it is not needed for 4-[^{18}F]fluoroglutamine imaging (Dunphy et al. 2018). This is because [^{18}F]FDG competes with blood glucose for tumour cell uptake and the increase in blood glucose level will decrease the intracellular transport of [^{18}F]FDG. Furthermore, insulin accelerates the skeletal muscle and myocardium uptake of [^{18}F]FDG and lowers the biodistribution of [^{18}F]FDG to cancer cells (Wahl et al. 1992; Langen et al. 1993; Torizuka et al. 1997). Therefore, fasting prior to [^{18}F]FDG imaging is required to lower the influence of blood glucose and insulin on [^{18}F]FDG biodistribution and to enhance the tumour uptake of tracer and image contrast.

The aim of this chapter is to investigate whether 4-[^{18}F]fluoroglutamine can be used as an alternative PET tracer to [^{18}F]FDG for studying tumours that have a low uptake of [^{18}F]FDG and whether 4-[^{18}F]fluoroglutamine can produce comparable signal intensity and tumour detection ability to [^{18}F]FDG without the need of fasting. To investigate these hypotheses, ^{1}H-MRS was firstly used to assess the uptake of L-glutamine and D-glucose in thirteen cancer cell lines (HCT116 WT, HCT116 Bax-ko, PC3, Kelly, MDA-MB-231, TU8902, TU8988T, TU8988S, ASPC-1, T3M4, MIA PaCa-2, NCIH508, DAN-G). These cell lines have been chosen based on their wide ranging glucose and/or glutamine dependencies and they would be the ideal tools for investigating the relationships between these substrate dependencies and the uptake

of 4-[^{18}F]fluoroglutamine and [^{18}F]FDG PET tracers. Some of these cell lines have been shown to be dependent on glutamine, such as Kelly neuroblastoma (Qing et al. 2012) and prostate cancer (White et al. 2017), and they would be useful for examining the uptake of 4-[^{18}F]fluoroglutamine PET tracer. On the other hand, the colorectal cancer cell lines, HCT116 WT and HCT116 Bax-ko, were found to have a higher glucose uptake and they would be useful for demonstrating the high uptake of [^{18}F]FDG. A number of pancreatic cancer cell lines were also studied in this study, as it was previously shown that pancreatic cancer can be highly glutamine avid, such as TU8902, TU8988 cell lines (Bott et al. 2019, Nelson et al. 2020), or be glucose dependent, such as T3M4 cell line (Kiss et al. 2015), depending on the cancer subtypes. Subsequently, the *in vitro* uptake assays of 4-[^{18}F]fluoroglutamine and [^{18}F]FDG were carried out in these cell lines to determine whether the results from these radiotracer uptake studies can be correlated to the L-glutamine and D-glucose uptake measured by ^{1}H-MRS. *In vivo* uptake study of these two radiotracers were also performed on HCT116 WT (glucose dependent) and PC3 (glutamine dependent) xenograft models.

4.2. Experiments and Results

4.2.1. *In vitro* uptake studies of L-glutamine, D-glucose and ^{18}F- labelled glutamine and FDG in cancer cell lines

4.2.1.1. *In vitro* uptake of L-glutamine and D-glucose in cancer cell lines by ^{1}H-MRS

^{1}H-MRS was firstly used to assess the uptake of L-glutamine and D-glucose in thirteen different cancer cell lines: pancreatic cancer cells (TU8902, TU8988T, TU8988S, ASPC-1, T3M4, MIA PaCa-2, DAN-G), colorectal cancer cells (HCT116 WT, HCT116 Bax-ko, NCIH508), prostate cancer (PC3), breast cancer (MDA-MB-231) and neuroblastoma (Kelly). Cells were grown in cell culture media containing an L-glutamine alternative, Glutamax. Glutamax is an L-alanyl-L-glutamine dipeptide with increased stability than L-glutamine. It was found that cancer cell types displayed different trends of glutamine and glucose uptake: the Kelly cell line has the highest rate of glutamine uptake and HCT116 WT, HCT116 Bax-ko and Kelly cells have the highest rate of glucose uptake (Figure 4.1A). Cancer cells that originate from the same organ, such as pancreas and colon, also have different rates of glutamine and glucose uptake. For example, TU8988S (red) is more glutamine avid while T3M4 (green) is more glucose dependent (Figure 4.1B and C) (Table 4.1).

4.2.1.2. *In vitro* uptake of 4-[^{18}F]fluoroglutamine and [^{18}F]FDG

The *in vitro* uptake assays of 4-[^{18}F]fluoroglutamine and [^{18}F]FDG in the same cell lines were subsequently carried out to investigate whether the results from these radiotracer uptake studies can be correlated to L-glutamine and D-glucose uptake measured by ^{1}H-MRS. A similar trend of radiotracer uptake rates in these cells lines were found when compared with L-glutamine and D-glucose uptake rates measured by ^{1}H-MRS, with the Kelly cell line also has the highest rate of 4-[^{18}F]fluoroglutamine uptake and the HCT116 WT and HCT116 Bax-ko cells exhibited a high rate of [^{18}F]FDG uptake. Pancreatic and colorectal cancer cell lines again displayed different avidity for 4-[^{18}F]fluoroglutamine and [^{18}F]FDG. For example, TU8902 and TU8988S have a higher uptake of 4-[^{18}F]fluoroglutamine while T3M4 displays a similar uptake level of 4-[^{18}F]fluoroglutamine and [^{18}F]FDG (Fig. 4.2) (Table 4.2). This suggests that

4-[^{18}F]fluoroglutamine could potentially be used as an alternative imaging agent for some tumour types that have a low rate of [^{18}F]FDG uptake, hence, cannot be detected by [^{18}F]FDG imaging.

4.2.1.3. Correlations between ^{1}H-MRS and ^{18}F labelled *in vitro* uptake studies

Here, we compared the rates of L-glutamine uptake measured by ^{1}H-MRS (section 4.2.1.1) with the rates of 4-[^{18}F]fluoroglutamine uptake (section 4.2.1.2) in thirteen different cancer cell lines. We found a significant Pearson correlation between the rates of 4-[^{18}F]fluoroglutamine and L-Glutamine uptake in these cell lines (R^2 = 0.58, p=0.0026) (Fig 4.3A). When we compared the rates of D-glucose uptake (section 4.2.1.1) with the rates of [^{18}F]FDG uptake (section 4.2.1.2) in these cell lines, we observed a trend correlation but it did not reach statistical significance (R^2 = 0.3, p=0.06) (Fig. 4.3B) and this was due to the large standard deviation (0.24 ± 0.33 µmole/million cell/hour) seen in D-glucose uptake in the Kelly cell line. A significant correlation between the rates of [^{18}F]FDG and D-glucose uptake was obtained when the uptake value from the Kelly cell line was omitted (R^2 = 0.79, p=0.0001) (Fig. 4.3C).

4.2.1.4. Correlations between the intracellular level of L-glutamine and D-glucose measured by ^{1}H-MRS with the rates of ^{18}F labelled glutamine and glucose uptake in cancer cell lines

Additionally, the intracellular level of normal glutamine and glucose in these thirteen cell lines was also evaluated by using ^{1}H-MRS. Similar to the glutamine and glucose uptake study by ^{1}H-MRS (section 4.2.1.1), the Kelly cell line has the highest level of intracellular glutamine, whereas the NCI-H508, HCT116 WT and HCT116 KO cells have the highest level of intracellular glucose (Fig. 4.4) (Table 4.3).

No significant correlation was found between the rates of 4-[^{18}F]fluoroglutamine uptake and intracellular glutamine levels (R^2 = 0.1873, p=0.14) (Fig. 4.5A). Significant correlation was found between [^{18}F]FDG uptake rates and intracellular glucose levels (R^2 = 0.32, p=0.04) (Fig. 4.5B).

A.

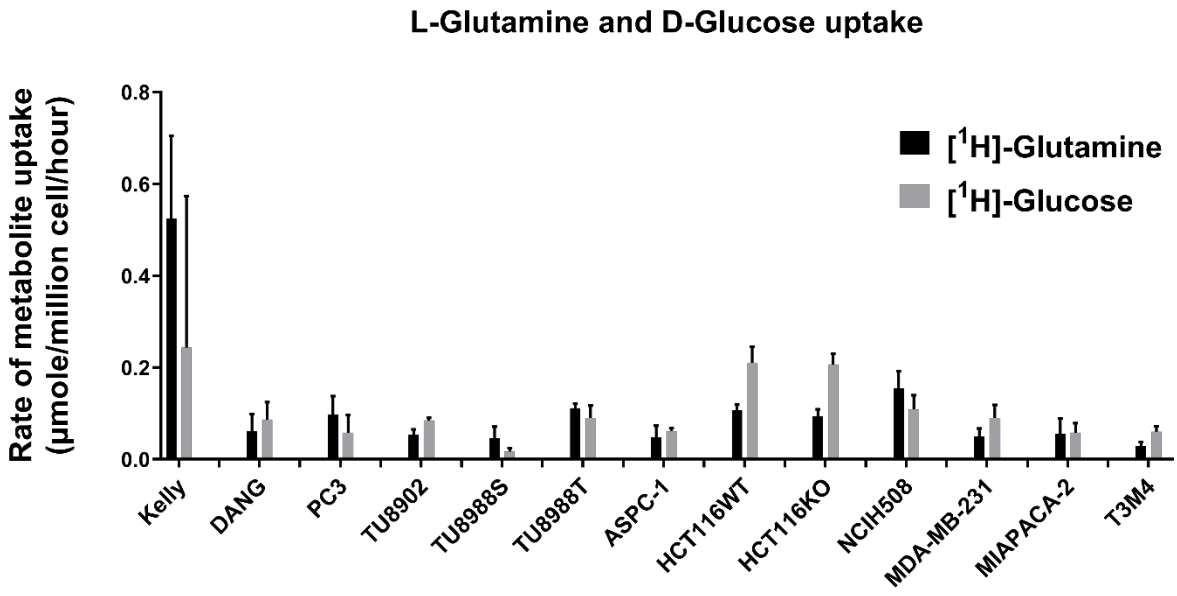

B.

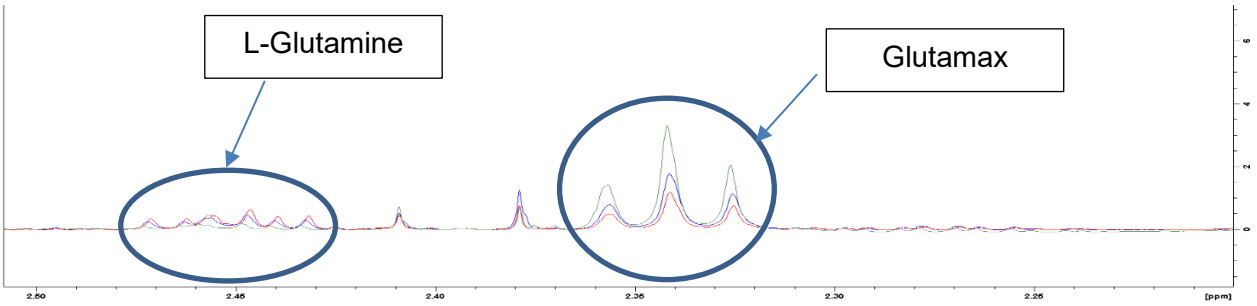

C.

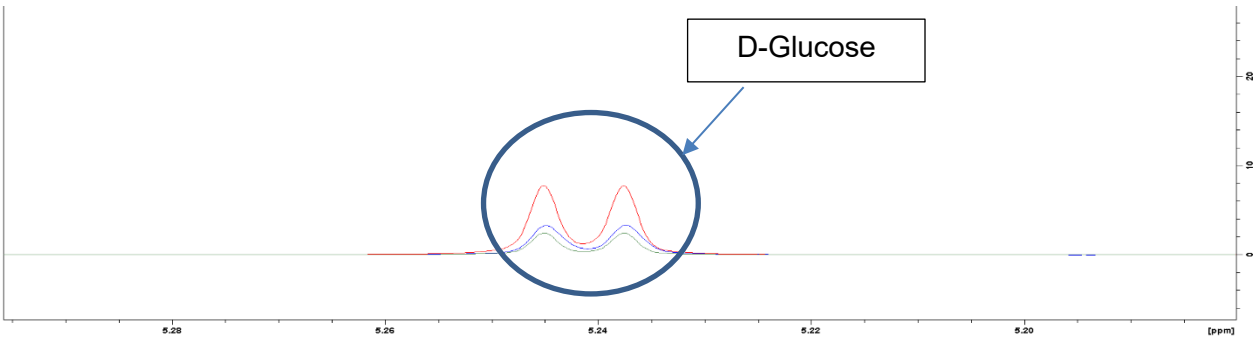

Figure 4.1. ***In vitro*** **^{1}H-MRS uptake study of L-glutamine and D-glucose in thirteen different types of cell. A**. Comparison of glutamine and glucose uptake rates measured by ^{1}H-MRS in thirteen different cell lines. Rates of L-glutamine and D-glucose uptake are expressed as µmole/million cell/hour and the bars represent mean ± SD (n=3). **B.** Example NMR spectra of cell culture media showing the L-glutamine uptake in three pancreatic cancer cell lines TU8902 (blue), TU8988S (red) and T3M4 (green).

Cells were grown in cell culture media containing an L-glutamine alternative, Glutamax. Glutamax is an L-alanyl-L-glutamine dipeptide with increased stability than L-glutamine. TU8902 and TU8988S are more glutamine dependent and release more aminopeptidases to hydrolyse Glutamax into L-glutamine for the cellular uptake. Hence, the amount of Glutamax is less in cell media in these two cell lines. **C.** Example NMR spectra of cell culture media showing the D-glucose uptake in three pancreatic cancer cell lines TU8902 (blue), TU8988S (red) and T3M4 (green). T3M4 and TU8902 consume more glucose. Hence, less amount of D-glucose was shown in media in these two cell lines.

Substrate / Cell line	L-Glutamine	D-Glucose
Kelly	0.53 ± 0.18	0.24 ± 0.33
DAN-G	0.06 ± 0.04	0.09 ± 0.04
PC3	0.10 ± 0.04	0.06 ± 0.04
TU8902	0.05 ± 0.01	0.08 ± 0.01
TU8988S	0.05 ± 0.03	0.02 ± 0.01
TU8988T	0.11 ± 0.01	0.09 ± 0.03
ASPC-1	0.05 ± 0.03	0.06 ± 0.01
HCT116 WT	0.11 ± 0.01	0.21 ± 0.04
HCT116 Bax-ko	0.09 ± 0.02	0.21 ± 0.02
NCI-H508	0.15 ± 0.04	0.11 ± 0.03
MDA-MB-231	0.05 ± 0.02	0.09 ± 0.03
MIA PaCa-2	0.06 ± 0.03	0.06 ± 0.02
T3M4	0.03 ± 0.01	0.06 ± 0.01

Table 4.1. Summary of L-glutamine and D-glucose uptake rates measured by ^{1}H-MRS in thirteen cancer cell lines. Rates of L-glutamine and D-glucose uptake are expressed as µmole/million cell/hour and the data are presented as mean ± SD (n=3).

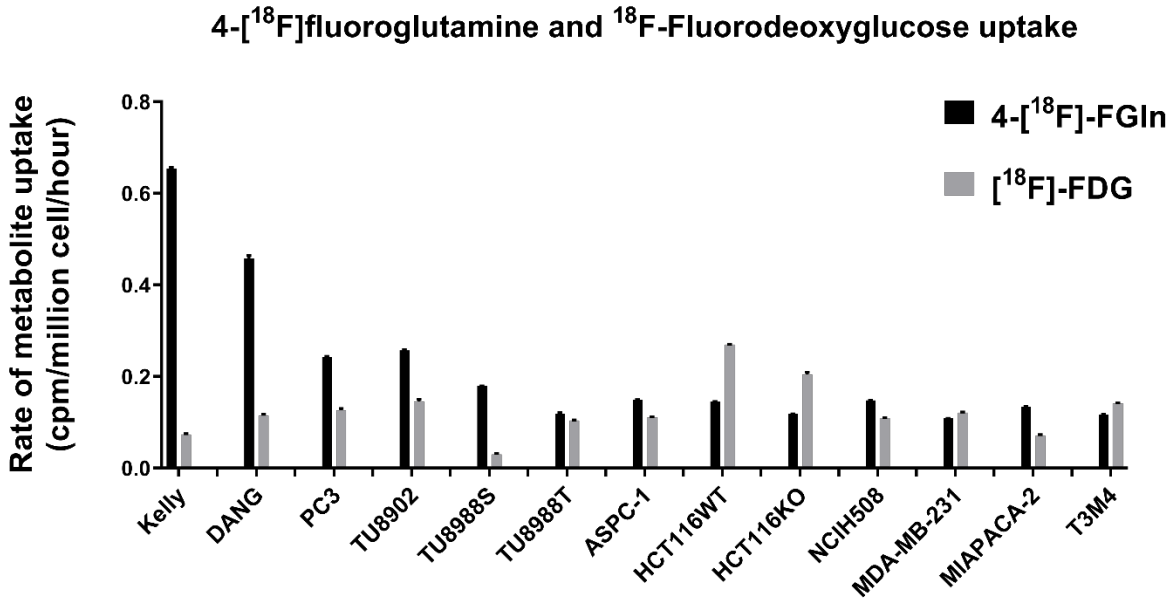

Figure 4.2. Rates of 4-[^{18}F]fluoroglutamine and [^{18}F]FDG uptake in thirteen cell lines. Comparison of 4-[^{18}F]fluoroglutamine and [^{18}F]FDG uptake rates in 13 different cell lines. Rates of 4-[^{18}F]fluoroglutamine and [^{18}F]FDG uptake are expressed as cpm/million cell/hour and the bars represent mean ± SD (n=3).

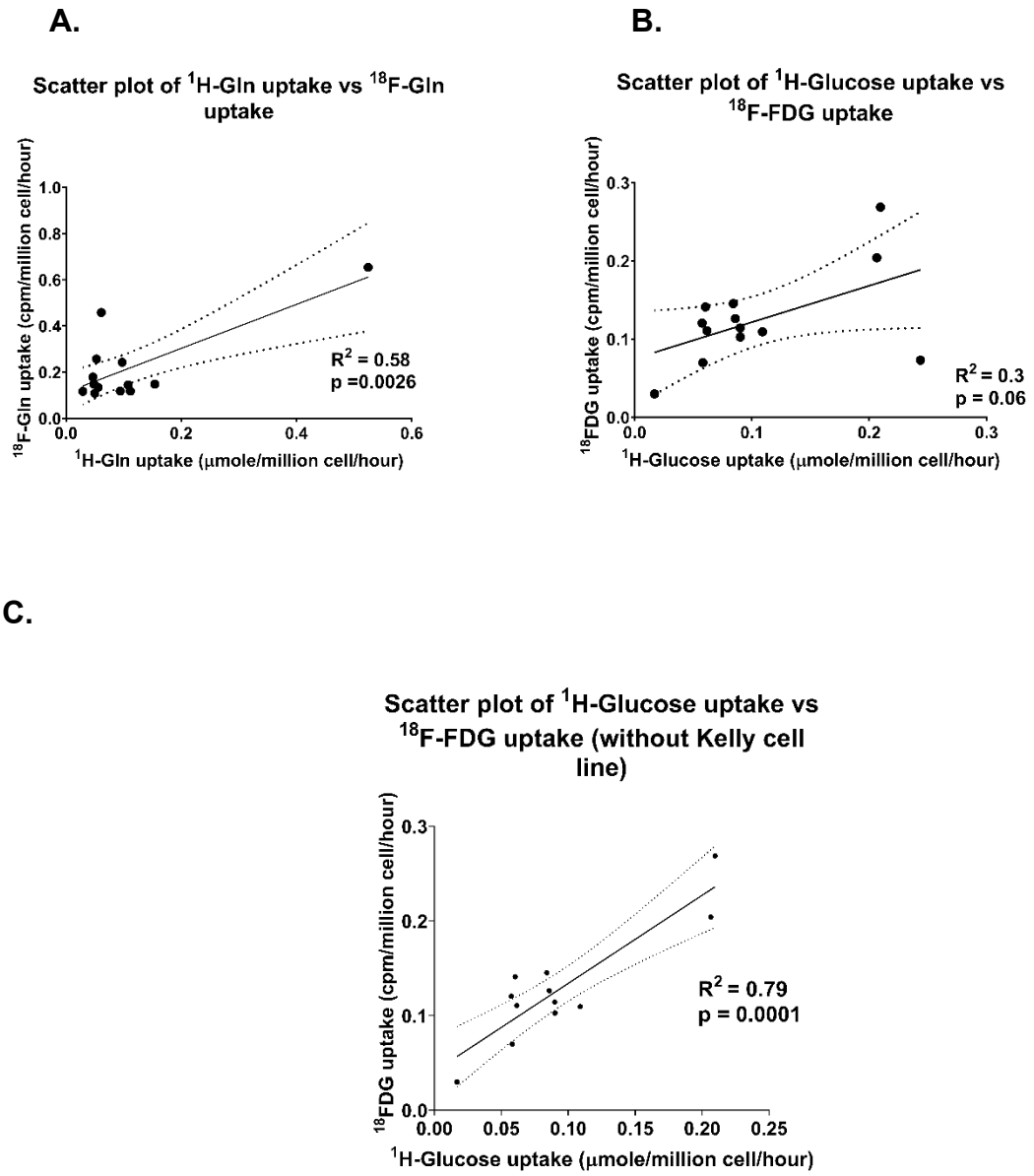

Figure 4.3. Correlations of L-glutamine and D-glucose uptake rates measured by ^{1}H-MRS with the rates of ^{18}F labelled glutamine and FDG uptake in thirteen cancer cell lines. (A) Correlation of L-glutamine (^{1}H-Gln) and 4-[^{18}F]fluoroglutamine (^{18}F-Gln) uptake rates**. (B)** Correlation of D-glucose (^{1}H-Glucose) and ^{18}F-Fluorodeoxyglucose (^{18}F-FDG) uptake rates. **(C)** Correlation of D-glucose (^{1}H-Glucose) and ^{18}F-Fluorodeoxyglucose (^{18}F-FDG) uptake rates (without Kelly cell line). Each dot represents a cell line. Pearson correlation was used to perform the comparisons. R^2 values are the correlation coefficients. $p \leq 0.05$ is considered statistically significant.

Substrate / Cell line	4-[^{18}F]fluoroglutamine	[^{18}F]FDG
Kelly	0.65 ± 0.002	0.07 ± 0.002
DAN-G	0.46 ± 0.01	0.11 ± 0.003
PC3	0.24 ± 0.002	0.13 ± 0.004
TU8902	0.26 ± 0.002	0.15 ± 0.01
TU8988S	0.18 ± 0.001	0.03 ± 0.002
TU8988T	0.12 ± 0.003	0.10 ± 0.002
ASPC-1	0.15 ± 0.001	0.11 ± 0.002
HCT116 WT	0.15 ± 0.001	0.27 ± 0.002
HCT116 Bax-ko	0.12 ± 0.0003	0.20 ± 0.005
NCI-H508	0.15 ± 0.001	0.11 ± 0.001
MDA-MB-231	0.11 ± 0.0003	0.12 ± 0.002
MIA PaCa-2	0.13 ± 0.001	0.07 ± 0.003
T3M4	0.12 ± 0.001	0.14 ± 0.002

Table 4.2. Summary of *in vitro* uptake rates of 4-[^{18}F]fluoroglutamine and [^{18}F]FDG in thirteen cancer cell lines. Rates of 4-[^{18}F]fluoroglutamine and [^{18}F]FDG uptake are expressed as cpm/million cell/hour and the data are presented as mean ± SD (n=3).

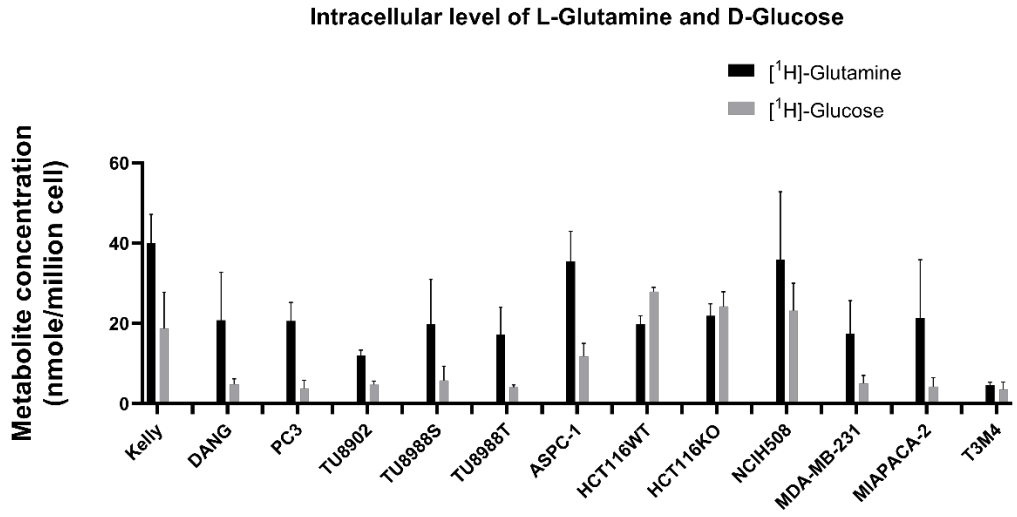

Figure 4.4. Intracellular L-glutamine and D-glucose levels measured by ^{1}H-MRS in thirteen cancer cell lines. Comparison of intracellular level of L-glutamine and D-glucose in 13 different cell lines. Cellular L-glutamine and D-glucose levels are expressed as nmole/million cell and the bars represent mean ± SD (n=3).

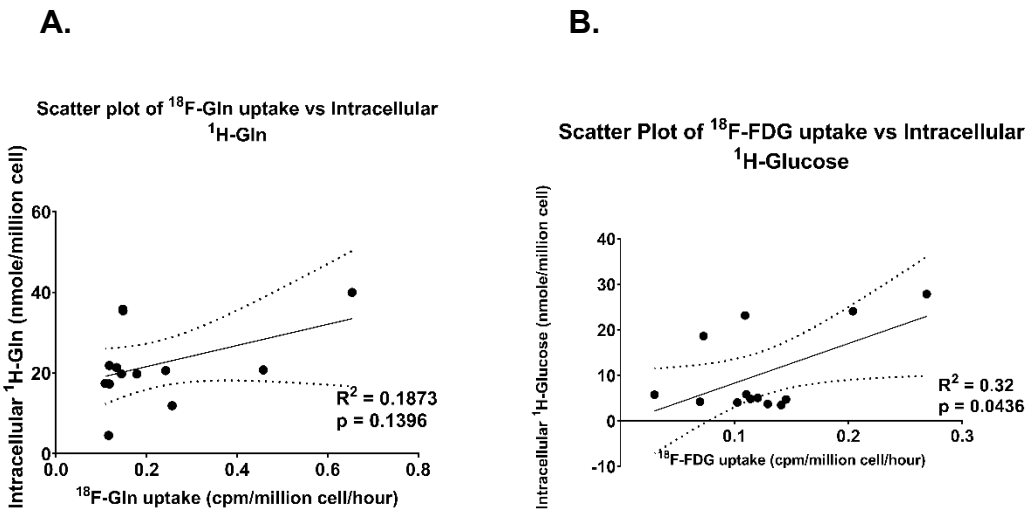

Figure 4.5. Correlations of intracellular L-glutamine and D-glucose levels measured by ^{1}H-MRS with rates of ^{18}F labelled glutamine and FDG uptake. (A) Correlation of intracellular glutamine level (^{1}H-Gln) and 4-[^{18}F]fluoroglutamine (^{18}F-Gln) uptake rates. **(B)** Correlation of intracellular glucose levels and ^{18}F-Fluorodeoxyglucose (^{18}F-FDG) uptake rates. Each dot represents a cell line. Pearson correlation was used to perform the comparisons. R^2 values are the correlation coefficients. $p \leq 0.05$ is considered statistically significant.

Substrate / Cell line	Intracellular L-Glutamine	Intracellular D-Glucose
Kelly	39.99 ± 7.19	18.65 ± 9.14
DAN-G	20.77 ± 11.93	4.85 ± 1.30
PC3	20.59 ± 4.63	3.73 ± 2.11
TU8902	11.91 ± 1.39	4.73 ± 0.88
TU8988S	19.76 ± 11.22	5.76 ± 3.55
TU8988T	17.29 ± 6.74	4.06 ± 0.61
ASPC-1	35.43 ± 7.53	5.88 ± 1.63
HCT116 WT	19.79 ± 2.08	27.86 ± 1.11
HCT116 Bax-ko	21.88 ± 2.97	24.11 ± 3.78
NCI-H508	35.81 ± 17.01	23.16 ± 6.88
MDA-MB-231	17.45 ± 8.25	5.08 ± 1.96
MIA PaCa-2	21.36 ± 14.51	4.20 ± 2.29
T3M4	4.52 ± 0.83	3.49 ± 1.89

Table 4.3. Summary of intracellular L-glutamine and D-glucose levels measured by ^{1}H-MRS in thirteen cancer cell lines. Cellular L-glutamine and D-glucose levels are expressed as nmole/million cell and the data are presented as mean ± SD (n=3).

4.2.2. Time dependent *in vitro* uptake of 4-[^{18}F]fluoroglutamine and [^{18}F]FDG

Cellular uptake of 4-[^{18}F]fluoroglutamine and [^{18}F]FDG were evaluated further in a time dependent manner by using the method stated in section 2.1.7 in HCT116 WT and PC3 cell lines. These two cell lines were selected because of their opposite avidity for 4-[^{18}F]fluoroglutamine and [^{18}F]FDG. The main purpose of this experiment was to examine the radiotracer retention level at different time points in the chosen cell lines. The glutamine dependent PC3 cell line has a higher rate of 4-[^{18}F]fluoroglutamine uptake than [^{18}F]FDG. The level of 4-[^{18}F]fluoroglutamine reached maximum (0.26 cpm/million cell) at 1 hour and it declined rapidly after that point (Fig. 4.6A). On the other hand, the level of [^{18}F]FDG was half of 4-[^{18}F]fluoroglutamine at the 1 hour time point, but it remained constant after 1 hour (Fig. 4.6A).

Under the same *in vitro* incubation conditions, the glucose dependent HCT116 WT cell line has a higher rate of uptake and retention of [^{18}F]FDG than 4-[^{18}F]fluoroglutamine (Fig. 4.6B), an approximate 50% difference. Similar to the 4-[^{18}F]fluoroglutamine uptake study in PC3 cells, the uptake of 4-[^{18}F]fluoroglutamine (0.14 cpm/million cell) reached a maximum at the 1 hour time-point in the HCT116 WT cells and the signal then declined after this time point, while the [^{18}F]FDG signal remained stable after 1 hour (Fig. 4.6B). These results are consistent with the observations in the study by Zhu et al which compared the uptake of 4-[^{18}F]fluoroglutamine and [^{18}F]FDG in similar experimental conditions (Zhu et al. 2017).

4.2.3. *In vitro* uptake inhibition studies of 4-[^{18}F]fluoroglutamine and [^{18}F]FDG

In vitro uptake inhibition studies were also conducted in PC3 and HCT116 WT cell lines by using the method described in section 2.1.7, in order to confirm the specificity of the radiotracers for glutamine and glucose transporters. Previous studies have confirmed that 4-[^{18}F]fluoroglutamine and [^{18}F]FDG can enter the cells via the same transporters as L-glutamine and D-glucose (Broer et al. 1999; Chaudhry et al. 1999, Brown and Wahl 1993; Reske et al. 1997; Brown et al. 1999, Liebermann et al. 2011, Qu et al. 2011). The results clearly demonstrate a competition for transporter binding of natural substrates L-glutamine and D-glucose with the radiotracers 4-[^{18}F]fluoroglutamine and [^{18}F]FDG, respectively, by the dose-dependent response of

4-[^{18}F]fluoroglutamine to L-glutamine (Fig. 4.7A and B) and of [^{18}F]FDG to D-glucose (Fig. 4.7C and D).

A.

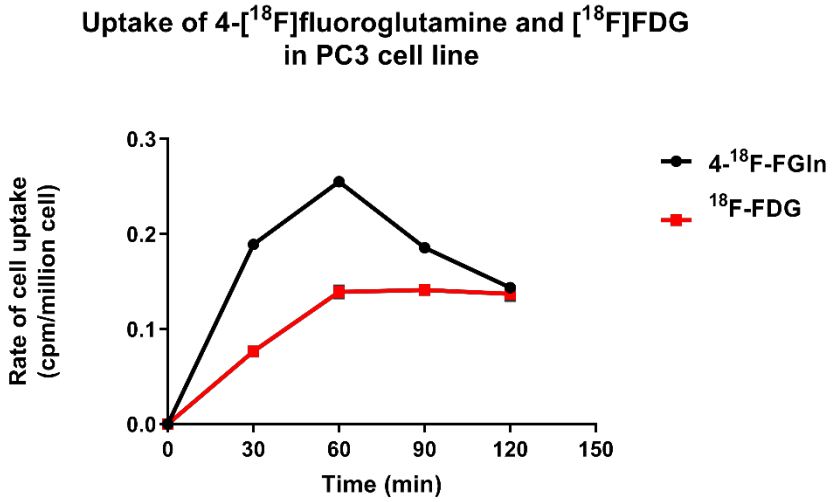

B.

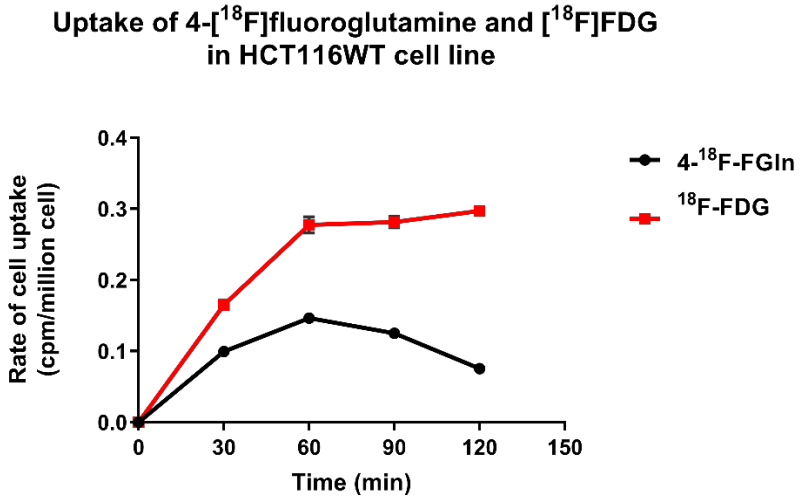

Figure 4.6. Time dependent cell uptake studies of 4-[^{18}F]fluoroglutamine and [^{18}F]FDG in PC3 and HCT116 WT cell lines. A. Time dependent cell uptake study of 4-[^{18}F]fluoroglutamine and [^{18}F]FDG in glutamine dependent PC3 cell line. **B.** Time dependent cell uptake study of 4-[^{18}F]fluoroglutamine and [^{18}F]FDG in glucose dependent HCT116 WT cell line. The cell uptake studies were carried out at five different time points at 0, 30, 60, 90 and 120 min. 4-[^{18}F]fluoroglutamine and [^{18}F]FDG levels are expressed as cpm/million cell and the data are presented as mean ± SD (n=3).

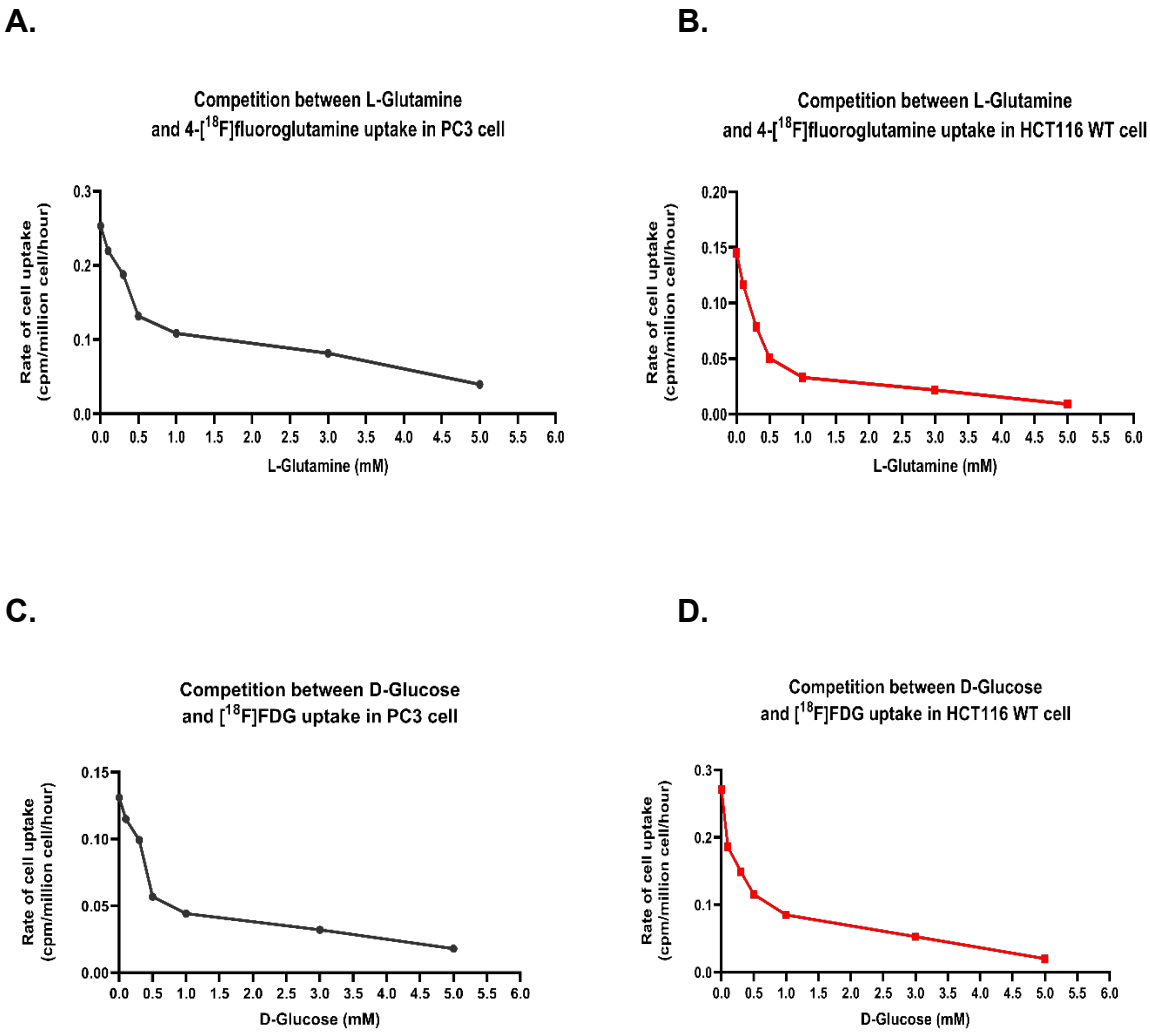

Figure 4.7. *In vitro* cell uptake inhibition studies of 4-[^{18}F]fluoroglutamine and [^{18}F]FDG in PC3 and HCT116 WT cell lines. A. *In vitro* cell uptake study of 4-[^{18}F]fluoroglutamine in PC3 cell line with various concentrations of L-glutamine. **B.** *In vitro* cell uptake study of 4-[^{18}F]fluoroglutamine in HCT116 WT cell line with various concentrations of L-glutamine. **C.** *In vitro* cell uptake study of [^{18}F]FDG in PC3 cell line with various concentrations of D-glucose. **D.** *In vitro* cell uptake study of [^{18}F]FDG in HCT116 WT cell line with various concentrations of D-glucose**.** Six different concentrations of L-Glutamine and D-Glucose ranging at 0.1, 0.3, 0.5, 1, 3, 5 mM were used. Rates of 4-[^{18}F]fluoroglutamine and [^{18}F]FDG uptake are expressed as cpm/million cell/hour and the data are presented as mean ± SD (n=3).

4.2.4. *Ex vivo* biodistribution study of 4-[^{18}F]fluoroglutamine and [^{18}F]FDG in NCr-Foxn1nu male mice

Based on results obtained from the *in vitro* radiotracer uptake study in section 4.2.1.2 in which HCT116 WT cells showed a higher uptake of [^{18}F]FDG than 4-[^{18}F]fluoroglutamine and PC3 cells displayed a higher uptake of 4-[^{18}F]fluoroglutamine than [^{18}F]FDG, these cell lines were chosen to compare the biodistribution of these radiotracers in xenograft models. Consistent with the results of the *in vitro* cell uptake study (Fig. 4.2), the HCT116 WT tumours showed a significantly higher uptake of [^{18}F]FDG than 4-[^{18}F]fluoroglutamine (7.93% dose/g and 3.37% dose/g, respectively, $p<0.001$) (Fig. 4.8A) (Table 4.4). However, no significant difference in the uptake of these two radiolabelled tracers was found in the PC3 tumours (5.57% dose/g for [^{18}F]FDG and 4.31% dose/g for 4-[^{18}F]fluoroglutamine) (Fig. 4.8B) (Table 4.4), which is different to the results in the *in vitro* uptake study where the PC3 cells showed a higher uptake of 4-[^{18}F]fluoroglutamine than [^{18}F]FDG (Fig. 4.2).

Ex vivo biodistribution of 4-[^{18}F]fluoroglutamine in HCT116WT and PC3 xenograft models showed a similar and expected behaviour of the radiolabelled amino acid with significant uptake in the pancreas (15.3% dose/g and 14.8% dose/g at 60 min, respectively). High uptake of 4-[^{18}F]fluoroglutamine was also observed in small intestine and liver of both models (5.59% dose/g and 5.39% dose/g for small intestine, 3.48% dose/g and 3.51% dose/g for liver at 60 min, respectively). Bones also showed a strong uptake of 4-[^{18}F]fluoroglutamine which suggests possible *in vivo* defluorination of 4-[^{18}F]fluoroglutamine (7.67% dose/g and 7.86% dose/g at 60 minutes, respectively). This observation highlights a common stability issue of fluorine 18 radiotracer *in vivo* (Lieberman et al. 2011; Kuchar and Mamat 2015). The C-F bond cleavage in 4-[^{18}F]fluoroglutamine and the rejection of free F^- often lead to a high background signal and radiotracer accumulation in the skeleton, which can hinder the analysis of tumours that are situated close to the bones (Kuchar and Mamat 2015; Grkovski et al. 2019).

The most noticeable uptake of [^{18}F]FDG was in the brown adipose tissue (BAT) in both xenograft models (3.96% dose/g and 3.57% dose/g, respectively) (Fig. 4.8) (Table 4.4). This observation is consistent with a previous report that brown fat has high glucose metabolism and [^{18}F]FDG uptake (Mullen et al. 2011). A high uptake of

[^{18}F]FDG in BAT can cause false positive or false negative results and prevent clinicians from making a precise tumour diagnosis (Steinberg et al. 2017).

A.

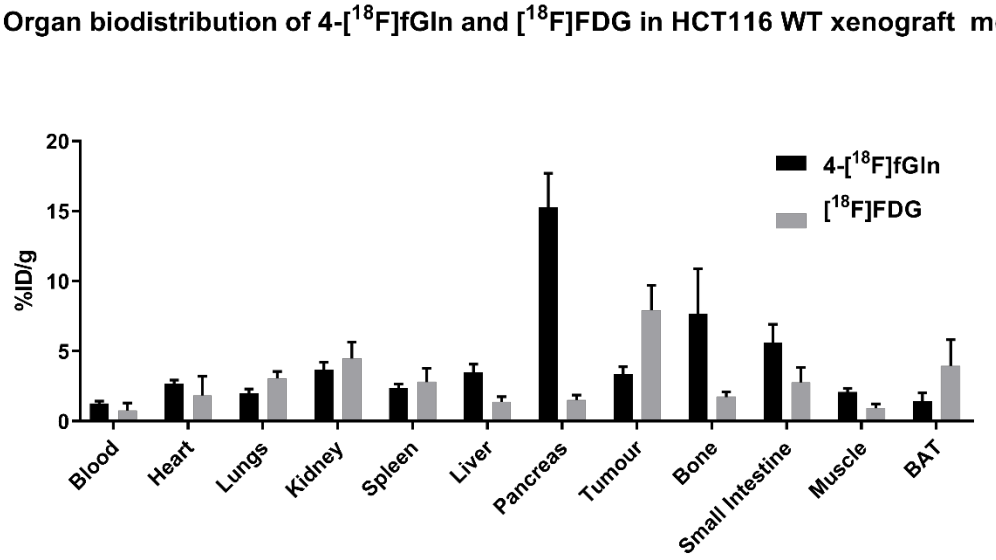

B.

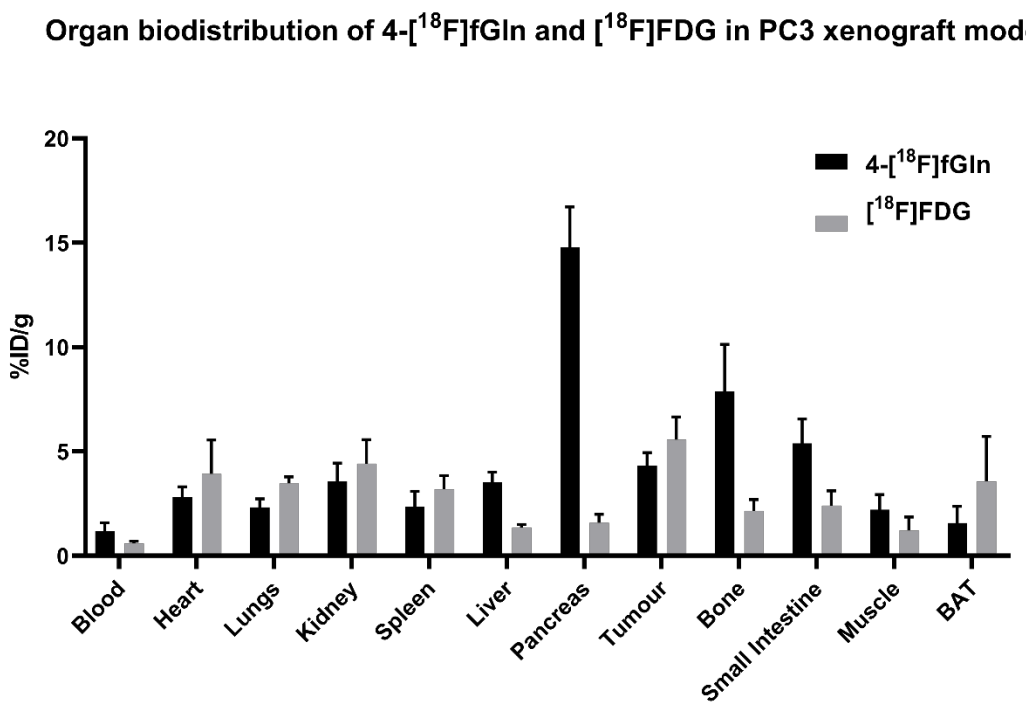

Figure 4.8. *Ex vivo* biodistribution of 4-[^{18}F]fluoroglutamine and [^{18}F]FDG in NCr-Foxn1nu male mice bearing HCT116 WT or PC3 tumour xenografts after 1 hour of intravenous injection. 4-

[^{18}F]fluoroglutamine and [^{18}F]FDG signals are expressed as %ID/g and the data are presented as mean ± SD (5 mice for 4-[^{18}F]fluoroglutamine, 5 mice for [^{18}F]FDG in each tumour xenograft model).

	HCT116 WT		PC3	
Tracer / Organ	4-[^{18}F]FGln	[^{18}F]FDG	4-[^{18}F]FGln	[^{18}F]FDG
Blood	1.28 ± 0.16	0.78 ± 0.54$^{n.s}$	1.19 ± 0.39	0.59 ± 0.11*
Heart	2.67 ± 0.27	1.84 ± 1.37$^{n.s}$	2.81 ± 0.51	3.93 ± 1.63$^{n.s}$
Lungs	1.98 ± 0.34	3.06 ± 0.49**	2.33 ± 0.41	3.47 ± 0.31***
Kidney	3.69 ± 0.52	4.48 ± 1.18$^{n.s}$	3.56 ± 0.88	4.42 ± 1.14$^{n.s}$
Spleen	2.36 ± 0.30	2.79 ± 0.98$^{n.s}$	2.36 ± 0.72	3.19 ± 0.65$^{n.s}$
Liver	3.48 ± 0.59	1.38 ± 0.37***	3.51 ± 0.49	1.35 ± 0.15****
Pancreas	15.3 ± 2.41	1.52 ± 0.36****	14.8 ± 1.94	1.58 ± 0.41****
Tumour	3.37 ± 0.53	7.93 ± 1.78***	4.31 ± 0.64	5.57 ± 1.09$^{n.s}$
Bone	7.67 ± 3.22	1.73 ± 0.36**	7.86 ± 2.27	2.16 ± 0.54***
Intestine	5.59 ± 1.34	2.78 ± 1.06**	5.39 ± 1.17	2.39 ± 0.72***
Muscle	2.09 ± 0.25	0.93 ± 0.32***	2.20 ± 0.73	1.21 ± 0.65*
BAT	1.46 ± 0.57	3.96 ± 1.86*	1.57 ± 0.80	3.57 ± 2.15*

Table 4.4. Summary of *ex vivo* biodistribution of 4-[^{18}F]fluoroglutamine and [^{18}F]FDG in NCr-Foxn1nu male mice bearing HCT116 WT or PC3 tumour xenografts after 1 hour intravenous injection. 4-[^{18}F]fluoroglutamine and [^{18}F]FDG levels are expressed as %ID/g and the data are presented as mean ± SD (5 mice for 4-[^{18}F]fluoroglutamine, 5 mice for [^{18}F]FDG in each tumour xenograft model). The significance was assessed with 2-tails Student's t-test. P values: * - <0.05, ** - <0.01, *** - <0.001, **** - <0.0001, n.s = not significant, n = 5.

4.2.5. Animal PET Studies in NCr-Foxn1nu male mice

Based on the results obtained from the *in vitro* radiotracer uptake study in section 4.2.1.2 in which HCT116 WT showed a higher uptake of [^{18}F]FDG than 4-[^{18}F]fluoroglutamine and PC3 displayed a higher uptake of 4-[^{18}F]fluoroglutamine than [^{18}F]FDG, in vivo PET studies on NCr-Foxn1nu male mice bearing HCT116 WT and PC3 tumour xenografts were performed to compare tumour uptake of the radiotracers. Whole body PET static images were acquired 1 hour post radiopharmaceutical injection for the duration of 10 min with a 358 to 664 keV energy window, followed by CT acquisition. Animal PET images of coronal sections were selected for visualisation. As the images demonstrate, higher tumour uptake of [^{18}F]FDG is visualised in the HCT116 WT tumour model when compared to 4-[^{18}F]fluoroglutamine uptake (Fig. 4.9A). Tumour uptake reached 12.17 ± 1.7% dose/g for [^{18}F]FDG and 8.14 ± 1.11% dose/g for 4-[^{18}F]fluoroglutamine ($p<0.01$) (Fig. 4.9B). However, no significant difference in tumour uptake of 4-[^{18}F]fluoroglutamine and [^{18}F]FDG was found in the PC3 model (9.16 ± 0.92 dose/g for [^{18}F]FDG and 9.06 ± 0.99% dose/g for 4-[^{18}F]fluoroglutamine, $p= 0.89$) (Fig. 4.9 C and D). High brain and brown adipose tissue uptake of [^{18}F]FDG was observed in both models. High uptake of 4-[^{18}F]fluoroglutamine is apparent in organs such as the pancreas, liver and small intestine regions (Figs. 4.9A and C). These data are consistent with the results obtained from the *ex vivo* biodistribution study.

A.

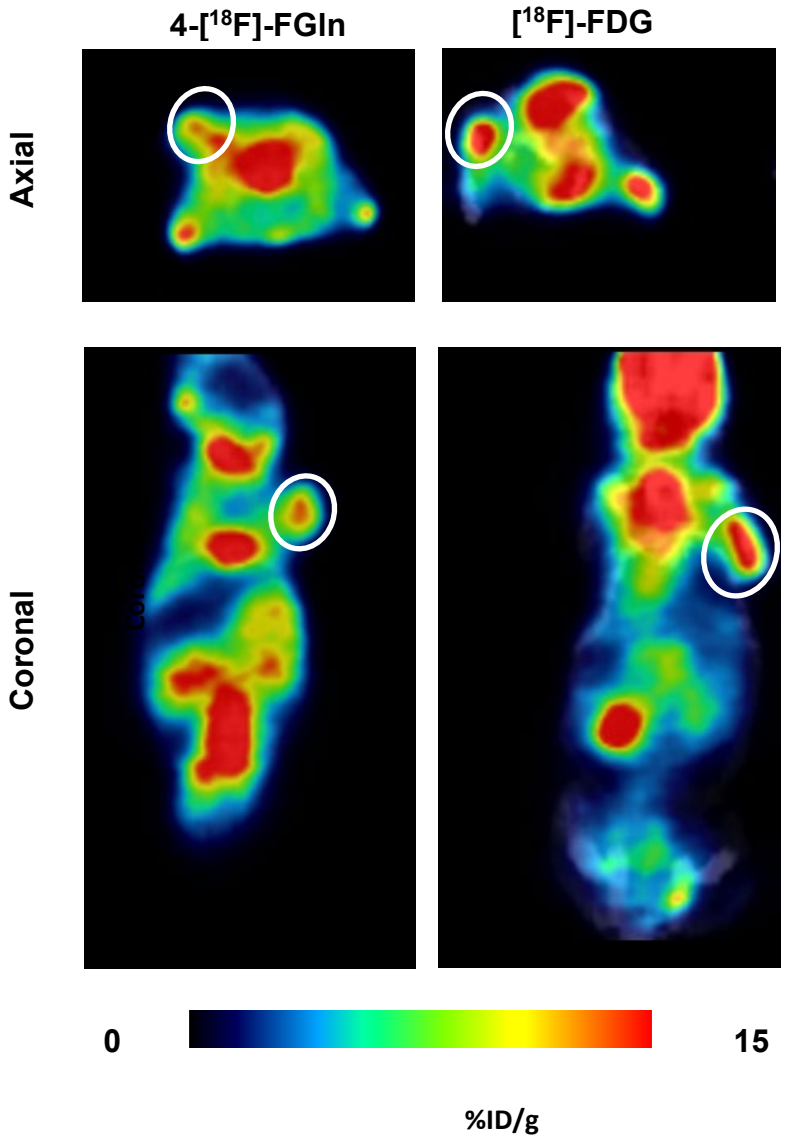
4-[18F]-FGln
[18F]-FDG
Axial
Coronal
0
15
%ID/g

B.

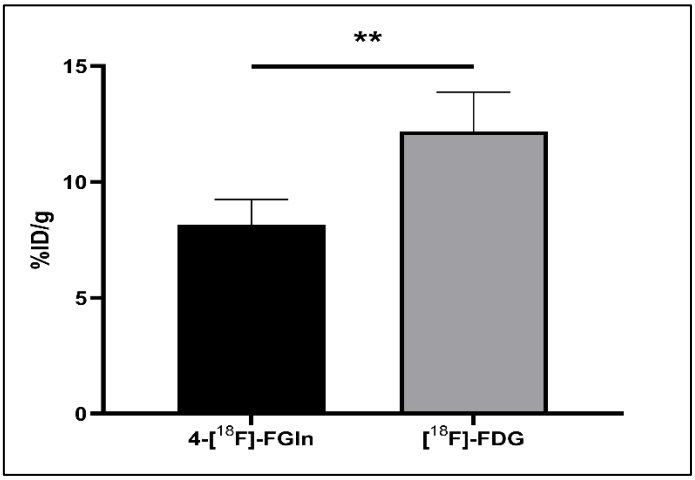
**
15
10
5
0
%ID/g
4-[18F]-FGln
[18F]-FDG

C.

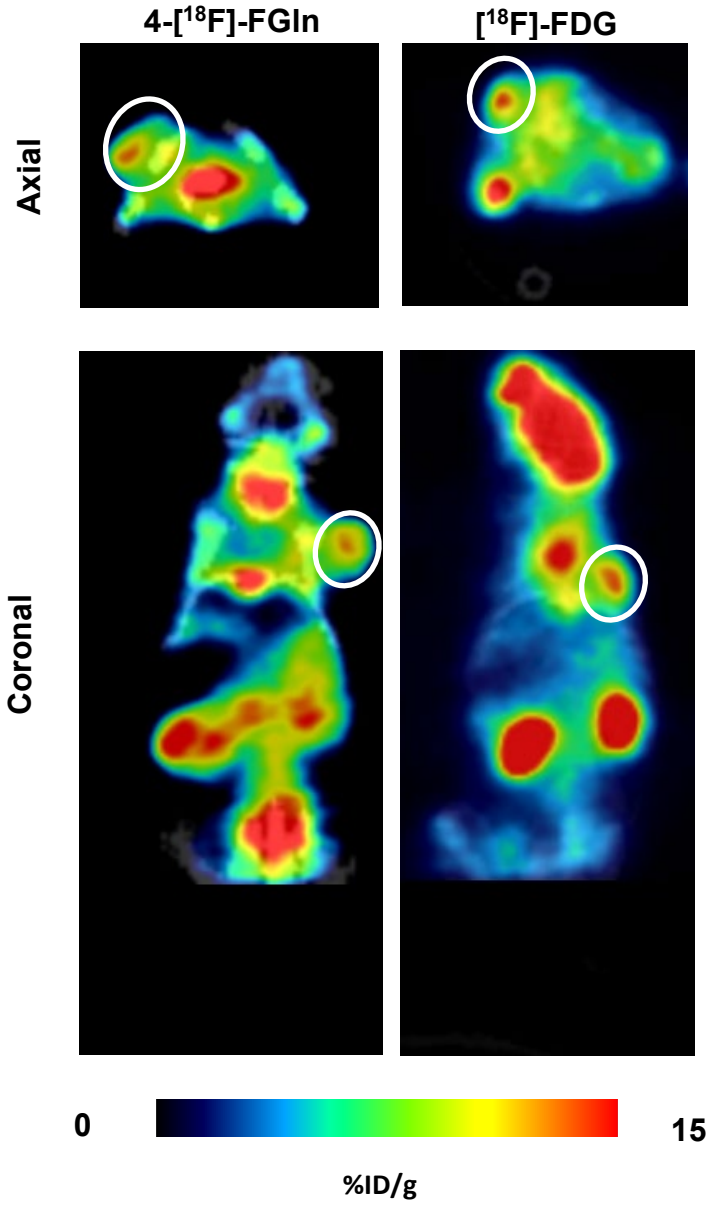
4-[18F]-FGln
[18F]-FDG
Axial
Coronal
0
15
%ID/g

D.

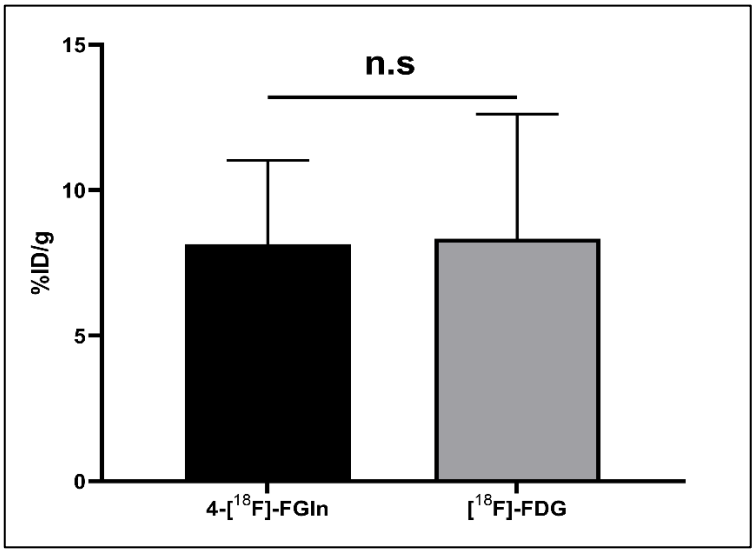
n.s
15
10
5
0
%ID/g
4-[18F]-FGln
[18F]-FDG

Figure 4.9. Imaging of 4-[^{18}F]fluoroglutamine and [^{18}F]FDG in HCT116 WT or PC3 tumour xenografts. Whole body PET static images were acquired 1 h post radionuclide injection for the duration of 10 min with a 358 to 664 keV energy window, followed by CT acquisition. **A**. Representative axial and coronal PET/CT images for 4-[^{18}F]fluoroglutamine and [^{18}F]FDG in HCT116 WT tumour bearing mice. White circles indicate tumour, identified from CT image. **B**. Quantitative tumour uptake values of 4-[^{18}F]fluoroglutamine and [^{18}F]FDG in HCT116 WT tumours**. C.** Representative axial and coronal PET/CT images for 4-[^{18}F]fluoroglutamine and [^{18}F]FDG in PC3 tumour bearing mice. **D.** Quantitative tumour uptake values of 4-[^{18}F]fluoroglutamine and [^{18}F]FDG in PC3 tumours. Data are expressed as mean ± SD (n = 5 per group of 4-[^{18}F]fluoroglutamine or [^{18}F]FDG). The significance was assessed with Student's t-test. P values: **- <0.01 and n.s = not significant.

4.3. Discussion

This part of the project investigated the feasibility of using 4-[^{18}F]fluoroglutamine PET tracer as an alternative method for studying [^{18}F]FDG undetected tumours which are thought to depend on other nutrients to glucose, such as glutamine (DeBerardinis et al. 2008; Dang 2010). The uptake of 4-[^{18}F]fluoroglutamine and [^{18}F]FDG was measured in thirteen cell lines with different avidity for glutamine and glucose and similar results were observed in a parallel study using ^{1}H-MRS to measure the uptake of L-glutamine and D-glucose in these cell lines.

Firstly, some cell types exhibited a high glutamine and 4-[^{18}F]fluoroglutamine intake but low glucose and [^{18}F]FDG uptake (Kelly, PC3, TU8988S); these results suggest certain cell lines prefer glutamine metabolism to glucose. Previous studies have found that some genetic alterations might drive tumours to become glutamine avid, such as MYC (Wise et al. 2008; Gao et al. 2009; Qing et al. 2012), P53 (Qing et al. 2012), EGFR, PIK3CA, GLUD, MTOR (Yang et al. 2009; Chen et al. 2014), and SDH (Yang et al. 2009).

Secondly, significant correlation was found between the rates of 4-[^{18}F]fluoroglutamine and L-glutamine uptake, which suggested that cellular uptake of 4-[^{18}F]fluoroglutamine behaves in a similar manner to L-glutamine. On the other hand, the rates of [^{18}F]FDG and D-glucose uptake showed a trend correlation but it did not reach statistical significance. This was due to the large standard deviation obtained in the Kelly cell line for the D-glucose uptake study by ^{1}H-MRS. A significant correlation between the rates of [^{18}F]FDG and D-glucose uptake was obtained when the uptake value from the Kelly cell line was omitted.

The intracellular level of L-glutamine did not correlate with the uptake rates of 4-[^{18}F]fluoroglutamine. On the other hand, significant correlation was found between the intracellular level of D-glucose and [^{18}F]FDG uptake. These results are not unexpected, as cellular metabolite levels are influenced by the rate of metabolite catabolism as well as the rate of metabolite uptake. Overall, these findings show a more consistent correlation between cellular uptake of 4-[^{18}F]fluoroglutamine and L-glutamine than the one between [^{18}F]FDG and D-Glucose. These data support the first necessary step toward establishing 4-[^{18}F]fluoroglutamine as an alternative imaging tracer for tumour types which cannot be detected by [^{18}F]FDG.

To investigate the intracellular level of radiotracers 4-[^{18}F]fluoroglutamine and [^{18}F]FDG over time, uptake studies were performed in the glutamine dependent PC3 and the glucose dependent HCT116 WT cell lines. The results showed a common trend that the 4-[^{18}F]fluoroglutamine signal reached a maximum level at 1 hour and then declined after this time point in both cell types. The drop in 4-[^{18}F]fluoroglutamine signal after 1 hour in these two cell lines can be explained by two main reasons. It was confirmed in chapter 3 and the study by Cooper et al that 4-[^{18}F]fluoroglutamine follows a similar metabolic pathway as L-glutamine, suggesting that the cellular metabolism of 4-[^{18}F]fluoroglutamine which involves an elimination of F^- from 4-[^{18}F]fluoroglutamine and an excretion of free F^- out of cell might contribute to such a decline in the signal count. The second reason might be due to the efflux of 4-[^{18}F]fluoroglutamine to exchange for other amino acids. Consistent to the studies by Qu et al and Lieberman et al (Lieberman et al. 2011; Qu et al. 2011), the current study on dose dependent response to L-glutamine indicated that 4-[^{18}F]fluoroglutamine can enter the cell via the same transporters as L-glutamine, which are known as the substrate of glutamine import/export transporter systems N (SNAT5) and ASC (ASCT2) (Broer et al. 1999; Chaudhry et al. 1999; Lieberman et al. 2011; Qu et al. 2011). On the other hand, the [^{18}F]FDG signal remained at a constant level after 1 hour in both cell lines. This is because [^{18}F]FDG is transported by the same transporters GLUT-1 and GLUT-3 as D-glucose (Brown and Wahl 1993; Reske et al. 1997; Brown et al. 1999). This was again confirmed by the *in vitro* cell uptake inhibition assay performed in this chapter. Upon entering the cell, [^{18}F]FDG is trapped by the phosphorylation process. Unlike D-glucose, [^{18}F]FDG cannot be metabolized further due to the lack of the 2-hydroxyl group (OH) which is needed for normal glycolysis pathway (Torizuka et al. 1995; Rempel et al. 1996; Caraco et al. 2000). Hence, the intracellular level of [^{18}F]FDG is built up inside in the cells and remained at the maximum level while radioactivity decays.

Consistent to the in vitro cell uptake studies, higher tumour uptake of [^{18}F]FDG relative to 4-[^{18}F]fluoroglutamine was found in HCT116 WT xenograft model in both ex vivo biodistribution and in vivo PET studies. However, no significant difference in the uptake of these two radiolabelled tracers was found in the PC3 tumours. This result is not consistent with the *in vitro* cell uptake studies in which PC3 cells was shown to have a higher rate of 4-[^{18}F]fluoroglutamine than [^{18}F]FDG uptake and a higher 4-

[^{18}F]fluoroglutamine than [^{18}F]FDG signal intensity was expected in the PC3 tumours. The observed inconsistent results between the cells and tumour experiments in the PC3 model could be due to the competition of 4-[^{18}F]fluoroglutamine uptake against the abundance of L-glutamine (in the bloodstream) uptake into the tumours, as 4-[^{18}F]fluoroglutamine is transported into cancer cells via the same transporter systems N and ASC as L-glutamine as shown in this chapter and in previous reports (Lieberman et al. 2011, Qu et al. 2011, Venneti et al. 2015). Hence, the uptake of 4-[^{18}F]fluoroglutamine into tumours will decrease substantially due to the presence of abundant L-glutamine in the blood stream. The efflux of 4-[^{18}F]fluoroglutamine via these transporters will also affect the signal intensity retention. In addition, it was confirmed in this thesis (Chapter 3) and by Cooper et al that 4-[^{18}F]fluoroglutamine can be metabolised further upon entering the cells. Taken together, the competition of L-glutamine, the influx/efflux rate and the tumour metabolism of 4-[^{18}F]fluoroglutamine might substantially affect the level of this radiotracer in tumours over time.

Another possible cause of lowering in vivo uptake of 4-[^{18}F]fluoroglutamine into the PC3 tumours, could be due to the very high uptake of this tracer into the pancreas which in turn might significantly alter the amount of 4-[^{18}F]fluoroglutamine distributed to the tumours. The high pancreas uptake of 4-[^{18}F]fluoroglutamine was also found in a previous study (Lieberman et al. 2011) and could be explained based on the pancreas's exocrine function and high use of amino acids as precursors for protein and peptide synthesis.

In contrast to the glutamine PET tracer, a built up of [^{18}F]FDG signal levels was found in cells over time and remained stable for a period of time (Section 4.2.2). This is because [^{18}F]FDG was trapped in the cells following phosphorylation as the cells were unable to metabolise the phosphorylated [^{18}F]FDG (Torizuka et al. 1995; Rempel et al. 1996; Caraco et al. 2000). This may attribute to the higher level of [^{18}F]FDG seen in PC3 tumours.

The size and developmental stage of the tumour is another factor that might contribute to the higher *in vivo* uptake of [^{18}F]FDG in PC3 model and requires careful consideration. Previous studies noted an inconsistent uptake trend of [^{18}F]FDG in prostate cancer patients (Liu et al. 2001, Salminen et al. 2002; Chang et al. 2003; Jadvar et al. 2013). The overall results of [^{18}F]FDG application in the diagnosis and

staging of primary prostate tumour were unsatisfactory and showed low tracer uptake in the tumours (Liu et al. 2001; Salminen et al. 2002), whereas the uptake of [^{18}F]FDG was shown to increase in the later stage or more aggressive prostate cancer (Chang et al. 2003, Jadvar et al. 2013). In addition, it was also found that prostate cancer with high Gleason score which has an overexpression of glucose transporters tend to consume more glucose and therefore take up more [^{18}F]FDG (Effert et al. 2004, Stewart et al. 2008). Based on these findings, it would suggest that [^{18}F]FDG may have limitations in primary prostate cancer diagnosis but this tracer may be useful for imaging aggressive prostate cancer (recurrent or metastatic lesions). Therefore, 4-[^{18}F]fluoroglutamine may be useful as an alternative PET tracer to [^{18}F]FDG for imaging primary prostate cancer or small prostate tumours.

Although 4-[^{18}F]fluoroglutamine did not produce a higher signal intensity than [^{18}F]FDG in the glutamine dependent PC3 tumour model, this PET tracer could still be useful for patients with glutamine dependent tumour like the PC3 prostate cancer model who might have difficulties with the fasting requirement, such as diabetics. The fasting requirement prior to [^{18}F]FDG PET imaging is intended to lower the influence of blood glucose and insulin on [^{18}F]FDG biodistribution and in turn enhance tumour uptake of the tracer. Herein, 4-[^{18}F]fluoroglutamine was able to detect all tumour lesions when compared with [^{18}F]FDG in the PC3 xenograft model without the need of acute fasting. Previous studies from Dunphy et al and Zhu et al also showed that 4-[^{18}F]fluoroglutamine produced a comparable but not higher signal intensity and tumour detection ability when compared with [^{18}F]FDG in *in vivo* tumour models and clinical trials (Dunphy et al. 2018; Zhu et al. 2019) . They reasoned that it is necessary to take into consideration the competitive effect of L-glutamine on 4-[^{18}F]fluoroglutamine tumour uptake. One might argue that whether fasting (which has been applied in the [^{18}F]FDG PET imaging) would also be helpful to lower the blood glutamine level. Dunphy et al also showed that 4-[^{18}F]fluoroglutamine PET is not affected by fasting because glutamine is a non-essential amino acid which means the body is able to synthesize a sufficient amount of this substrate for its use and does not primarily rely on diet (Dunphy et al. 2018). It has been shown that skeletal muscle produces 90% of glutamine for the body; brain and lungs were also found to synthesize a small amount of glutamine (Newsholme et al. 2003). These glutamine synthesising organs possess an enzyme called glutamine synthetase (GS) which catalyses the formation of

glutamine from glutamate and ammonia (Listrom et al. 1997, Hawkins 2009, Cooper 2012, Hawkins and Viña 2016). Taken together, 4-[^{18}F]fluoroglutamine PET imaging was not affected by fasting, produced comparable signal and was able to detect tumours when compared to [^{18}F]FDG in the glutamine avid PC3 cancer model. Hence, 4-[^{18}F]fluoroglutamine can be used as an alternative tracer to [^{18}F]FDG for patients who might have difficulties with the fasting requirement of [^{18}F]FDG imaging. Further *in vivo* studies is required to compare the uptake of 4-[^{18}F]fluoroglutamine and [^{18}F]FDG in different stages of tumour growth , in order to predict the correct stage of tumour growth which may affect or alleviate the uptake of 4-[^{18}F]fluoroglutamine and [^{18}F]FDG. Alternatively, sequential PET scanning at different time points which correspond to different stages of tumour growth can be applied on the same cohort of animals to reflect on the changes of cancer metabolism and radiotracer uptake.

Chapter 5

PI3K/AKT/mTOR pathway and Glutamine Metabolism

5.1. Introduction

The mechanistic Target of Rapamycin (mTOR) is a serine/threonine kinase which plays a significant role in a variety of cellular processes such as protein synthesis, lipid synthesis, autophagy, cell growth and proliferation, ion transport and survival (Laplante and Sabatini 2009). mTOR kinase links with other protein and forms a core of two distinct multi-protein complexes: mTOR complex 1 (mTORC1) and mTOR complex 2 (mTORC2) (Guertin and Sabatini 2007).

In particular, mTORC1 comprises of five protein components: mTOR is the centre of the complex, mammalian lethal with Sec13 protein8 (mLST8), proline-rich AKT substrate 40 kDa (PRAS40), DEP-domain-containing mTOR-interacting protein (Deptor) and regulatory-associated protein of mTOR (Raptor) (Peterson et al. 2009). mTORC2 has six protein components: the core mTOR, mammalian stress-activated protein kinase interacting protein (mSIN1), protein observed with Rictor-1 (Protor-1), mLST8, Deptor and rapamycin-insensitive companion of mTOR (Rictor) (Frias et al. 2006; Jacinto et al. 2006). The Rictor component modulates mTORC2 sensitivity to Rapamycin – the very first generation of mTOR inhibitor; by contrast mTORC1 can be inhibited by rapamycin completely. mTORC1 functions as a master regulator of divergent components of cellular metabolism. It controls protein and lipid synthesis (Kim and Chen 2004; Porstmann et al. 2008; Ma and Blenis 2009) and promotes ribosome biogenesis (Mayer et al. 2004); stimulation of mTORC1 can also reduce autophagy (Codogno and Meier 2005). Meanwhile, the investigation of mTORC2 functions is relatively unexplored when compared with mTORC1. Its main functions are controlling cell growth and proliferation (Sarbassov et al. 2005; Manning and Cantley 2007; Calnan and Brunet, 2008), cytoskeletal remodelling (Jacinto et al. 2004; Sarbassov et al. 2004) and ion transport (Lang and Pearce 2016) (Fig 5.1).

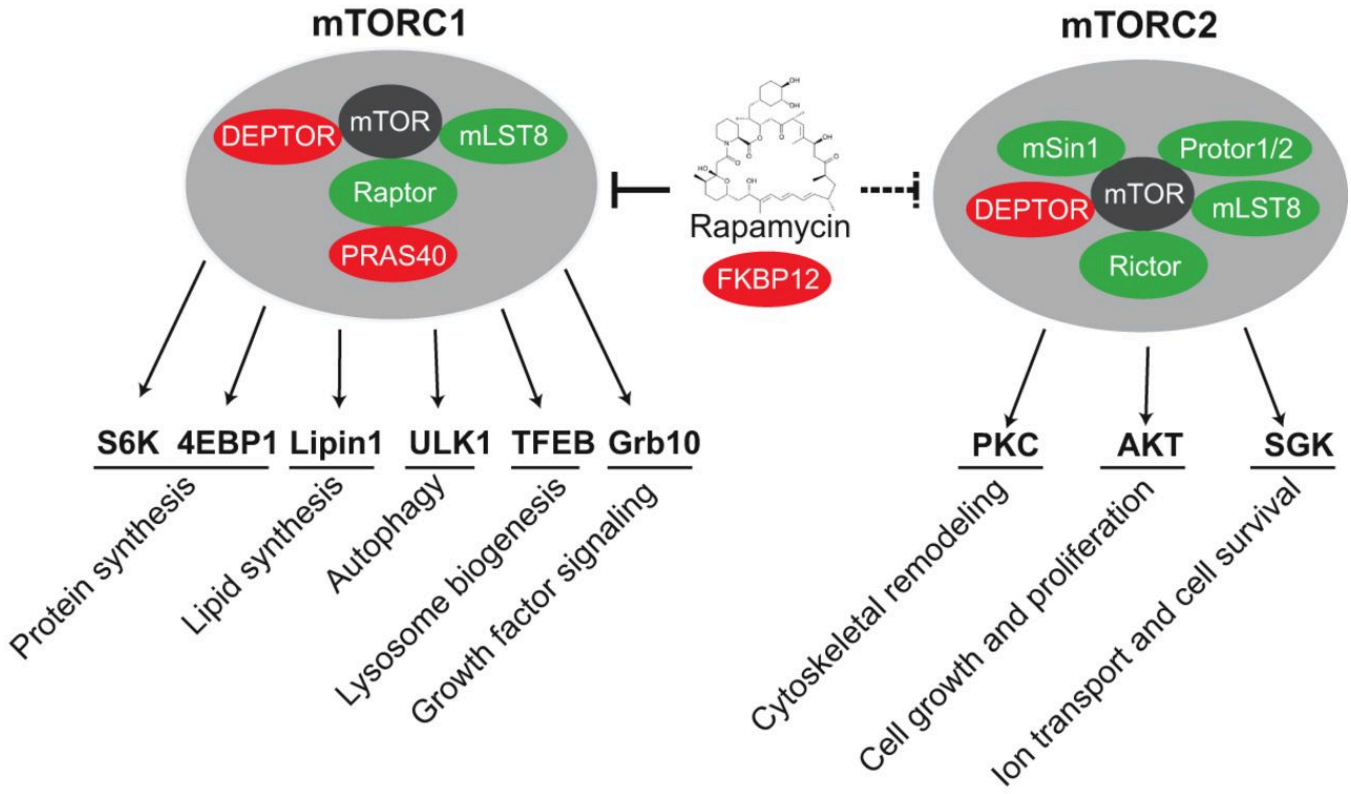

Figure 5.1. The mTORC1 and mTORC2 complexes. (Left): mTORC1 comprises of 5 components: mTOR, mLST8, PRAS40, DEPTOR and Raptor. The main functions of mTORC1 are to regulate protein synthesis, lipid synthesis, autophagy, lysosome, ribosome biogenesis and growth factor signalling by phosphorylating the respective proteins S6K, 4EBP1, lipin 1, ULK1, TFEB and Grb10. **(Right):** mTORC2 comprises of 6 components: mTOR, mLST8, mSin1, DEPTOR, Protor1/2 and Rictor. The main functions of mTORC2 are to regulate cytoskeletal remodelling, cell growth, proliferation, ion transport and cell survival by phosphorylating the respective proteins PKC, AKT and SGK. Figure adapted from Meng et al. 2018.

The PI3K/AKT/mTOR pathway is an important intracellular signalling pathway that controls and regulates the cell cycle. This signalling pathway also plays a significant role in multiple cellular processes, such as cellular proliferation, quiescence and cancer development. The general mechanism of this pathway involves a stimulation of PI3K by the engagement of growth factor and its receptor, then PI3K signals Akt activation by phosphorylation and plasma membrane localisation. Akt then exerts a downstream effect on mTOR signalling. The activation of mTOR by Akt is by phosphorylating and inhibiting tuberous sclerosis complex 2 (TSC2) – a negative regulator of mTOR (Castro et al. 2003; Garami et al. 2003; Inoki et al. 2003). The whole process of Akt mediated mTOR activation was reported to rely on the cellular ATP level and the inhibition of AMP-activated protein kinase (AMPK), which is an activator of TSC2 (Dennis et al. 2001; Inoki et al. 2003;Hahn-Windgassen et al. 2005). Depletion of ATP level was found to stimulate AMPK which phosphorylates TSC2 and lead to mTOR inhibition (Inoki et al. 2003).

The mTOR pathway was revealed to have a mutual interaction with glutamine metabolism. Nicklin et al found the glutamine uptake and exchange plays a critical role in controlling mTOR signalling (Nicklin et al. 2009). In particular, the exchange of L-glutamine/leucine via the ASCT2 and LAT1 transporters is considered to be the rate limiting step for essential amino acid and growth factor regulation of mTORC1. This activity involves a two-step process in which glutamine is firstly taken up by ASCT2 transporter and then used as an efflux substrate of LAT1 transporter to exchange for leucine which subsequently leads to the activation of mTORC1. In addition, Csibi et al also showed that mTORC1 activation also stimulates the uptake of glutamine through the positive regulation of glutaminase enzyme (Csibi et al. 2013). The relationship between the ASCT2 and LAT1 transporters and mTORC1 activation were reported in previous studies (Nicklin et al. 2009; Csibi et al. 2013). Therefore, unsurprisingly it was found that mTORC1 activity decreased significantly following the inhibition of ASCT2 with tamoxifen, raloxifene or γ-glutamyl p-nitroanilide (GPNA) (Wang et al. 2015) or inhibition of LAT1 with 2-aminobicyclo-(2,2,1)-heptane-2-carboxylic acid (BCH) (Imai et al. 2010; Janpipatkul et al. 2014). These findings solidify the importance of these transporters on mTORC1 activity.

Furthermore, Tanaka et al revealed that mTOR inhibition with rapamycin or PP242 also had an effect on glutamine metabolism. Elevated glutaminase level increases

glutamine uptake, upregulates glutamine metabolism via the TCA cycle and promotes resistance to mTOR kinase inhibitors (Tanaka et al. 2015). These observations also highlight the close relationship between mTORC1 pathway and glutamine metabolism and the critical role glutamine metabolism plays in mTOR inhibitor resistance. It was also demonstrated the first generation mTOR inhibitors (such as rapamycin and rapalogs) were not sufficient to achieve a robust anticancer effect (Brachmann et al. 2009; Tanneeru and Guruprasad 2011; Zhang et al. 2011). The main drawback of these drugs is the lack of a mechanism that can inhibit the mTOR signalling pathway completely. Rapamycin and rapalogs are known to inhibit mTORC1 but they cause a hyper-activation of mTORC2, Akt phosphorylation (Rodrik-Outmezguine et al. 2011) and incomplete inhibition of 4EBP1 phosphorylation (Kang et al. 2013). Therefore, new therapies that can target both mTORC1 and mTORC2 are needed. The second generation of mTOR inhibitors were then developed in the form of ATP competitive mTOR kinase inhibitors (Zaytsevaa et al. 2012). Dual mTORC1/2 inhibitors, which compete with ATP for binding to the catalytic site of mTOR kinase, were shown to effectively inhibit both mTORC1 and mTORC2 and the PI3K/Akt signalling. Vistusertib (AZD2014) is a dual mTORC1/2 inhibitor which was shown to exhibit good anti-tumour effect (Pike et al. 2013; Basu et al. 2015; Guichard et al. 2015). It was found to block S6K and Akt signalling by inhibiting mTORC1 and mTORC2, respectively (Basu et al. 2015)

The aim of the study in this chapter is to investigate the potential of 4-[^{18}F]fluoroglutamine PET imaging in monitoring cellular and tumour response and glutamine metabolic changes in cisplatin-resistant ovarian (A2780cisR) and lung (H520) cancer cell lines following mTOR pathway inhibition by using AZD2014 as a single agent, Paclitaxel as a single agent or a combination of AZD2014 with Paclitaxel. Paclitaxel chemotherapy has been used in the treatment of many cancer types, especially ovarian cancer (Baird et al. 2010; Chan et al. 2016). However, resistance to Paclitaxel treatment were found in gynaecological cancer, such as uterine and ovarian cancers (Holzmayer et al. 1992; Schneider et al. 1993; Kamazawa et al. 2002), and activation of the PI3K/mTOR signalling pathway was shown to be one of the mechanisms behind treatment resistance (Foster et al. 2010; Brasseur et al. 2016). Based on these findings, multiple clinical trials combining novel anticancer drugs, such as mTOR kinase inhibitors, with Paclitaxel have been performed. The synergistic

effect of combining Paclitaxel with AZD2014 was found to be effective in tumour growth inhibition (Le et al. 2003; Sun et al. 2011; Pujade-Lauraine et al. 2014; Wong et al. 2017). The *in vitro* uptake assay of 4-[^{18}F]fluoroglutamine was carried out in cisplatin-resistant ovarian and lung cancer cell lines A2780cisR and H520 to investigate the changes of glutamine uptake following treatment with AZD2014 alone, Paclitaxel alone or a combination of AZD2014 with Paclitaxel. The results obtained from this *in vitro* uptake assay will serve as the first necessary step to establish the potential use of 4-[^{18}F]fluoroglutamine PET imaging to monitor the tumour response *in vivo* in A2780cisR and H520 xenograft models following AZD2014 treatment and in Vistusertib clinical trials.

5.2. Experiments and Results

5.2.1. A2780cisR and H520 cell growth inhibition following treatment with AZD2014 or Paclitaxel as a single agent and in a combination therapy

Cisplatin-resistant ovarian cancer cell line A2780cisR were treated for 24 hours with 2.5xGI_{50} (303.5 nM) or with 5x GI_{50} (607 nM) Vistusertib (AZD2014) as a single agent, with 2.5x GI_{50} (7.75 nM) Paclitaxel as a single agent or with either 2.5xGI_{50} (303.5 nM) or 5x GI_{50} (607 nM) AZD2014 and 2.5xGI_{50} (7.75 nM) Paclitaxel as a combination treatment. Following the treatments, there was a 12% - 17% decrease of cell number in the 2.5xGI_{50} and 5xGI_{50} AZD2014 treated group when compared with the vehicle-treated controls ($p<0.0001$; Fig. 5.2A). On the other hand, there was no significant changes of cell growth in the 2.5xGI_{50} Paclitaxel treated group. A 20% - 21% decrease of cell number was also found in the combination treatment groups of AZD2014 and Paclitaxel) when compared with the vehicle control group ($p<0.0001$; Fig. 5.2A).

Cisplatin-resistant lung cancer cell line H520 cells were treated for 24 hours with 2.5xGI_{50} (503.3 nM) or with 5xGI_{50} (1006.5 nM) Vistusertib AZD2014 as a single agent, with 2.5xGI50 (7.95 nM) Paclitaxel as a single agent or with either 2.5xGI_{50} (503.3 nM) or 5x GI_{50} (1006.5 nM) AZD2014 and 2.5xGI_{50} (7.95 nM) Paclitaxel (7.95 nM) as a combination treatment. Following the treatments, there was a 13% - 22% decrease of cell number in the 2.5xGI_{50} and 5xGI_{50} AZD2014 treated groups when compared with the vehicle controls ($p<0.0001$; Fig. 5.2B). On the other hand, there was no significant changes of cell growth in the 2.5xGI_{50} Paclitaxel treated group. A 17% - 25% decrease of cell number was also found in the combination treatment groups of AZD2014 and Paclitaxel when compared with the vehicle control group ($p<0.0001$; Fig. 5.2B).

5.2.2. 4-[^{18}F]fluoroglutamine uptake changes in A2780cisR and H520 cells following treatment with AZD2014 or Paclitaxel as a single agent and in a combination therapy

The *in vitro* uptake assay of 4-[^{18}F]fluoroglutamine was carried out to investigate the changes in glutamine uptake in A2780cisR and H520 cancer cells following treatment with Paclitaxel alone, AZD2014 alone or in combination. Following the treatment with 2.5x GI_{50} or 5x GI_{50} of AZD2014, a significant increase in 4-[^{18}F]fluoroglutamine uptake

was observed in the treated group in both cell types when compared with vehicle controls (A2780cisR: ≈2.1-fold increase, $p<0.0001$ for $2.5xGI_{50}$ AZD2014 and ≈2.4-fold increase, $p<0.0001$ for $5xGI_{50}$ AZD2014; H520: ≈2.3-fold increase, $p<0.0001$ for $2.5xGI_{50}$ AZD2014 and ≈2.7-fold increase, $p<0.0001$ for $5xGI_{50}$ AZD2014; Fig. 5.3). On the other hand, there was no changes in 4-[^{18}F]fluoroglutamine uptake in the $2.5xGI_{50}$ Paclitaxel-treated group in both cell types when compared with vehicle controls (Fig. 5.3). A significant increase in 4-[^{18}F]fluoroglutamine uptake was also found in the combination treatment group in both cell types when compared with the vehicle groups (A2780cisR: ≈2.3-fold increase, $p<0.0001$ for $2.5xGI_{50}$ AZD2014 + $2.5xGI_{50}$ Paclitaxel and ≈2.8-fold increase, $p<0.0001$ for $5xGI_{50}$ AZD2014 + $2.5xGI_{50}$ Paclitaxel; H520: ≈2.4-fold increase, $p<0.0001$ for $2.5xGI_{50}$ AZD2014 + $2.5xGI_{50}$ Paclitaxel and ≈3-fold increase, $p<0.0001$ for $5xGI_{50}$ AZD2014 + $2.5xGI_{50}$ Paclitaxel; Fig. 5.3).

5.2.3. Examination of glutamine transporter SLC1A5 (ASCT2) expression in A2780cisR and H520 cells following treatment with AZD2014 or Paclitaxel as a single agent and in a combination therapy

In order to understand whether the increased rate of glutamine uptake following the treatment with AZD2014 as a single agent and in combination with paclitaxel is due to an upregulated expression of SLC1A5 (ASCT2) glutamine transporter, the expression of ASCT2 was probed in A2780cisR and H520 cells following 24 hours of AZD2014 treatment, either as a single agent or in combination with Paclitaxel. Following the treatment with $2.5xGI_{50}$ or $5xGI_{50}$ of AZD2014, a significant increase in ASCT2 expression was observed in the treated group in both cell types when compared with controls (A2780cisR: ≈13.2-fold increase, $p<0.001$ for $2.5xGI_{50}$ AZD2014 and ≈16.1-fold increase, $p<0.001$ for $5xGI_{50}$ AZD2014; H520: ≈3.7-fold increase, $p<0.001$ for $2.5xGI_{50}$ AZD2014 and ≈3.8-fold increase, $p<0.0001$ for $5xGI_{50}$ AZD2014; Fig. 5.4). On the other hand, there was no significant changes in ASCT2 expression in the $2.5xGI_{50}$ Paclitaxel treated group in both cell types when compared with vehicle controls (Fig. 5.4). A significant increase in ASCT2 expression was also found in the combination group in both cell types when compared with the vehicle groups (A2780cisR: ≈17.5-fold increase, $p<0.0001$ for $2.5xGI_{50}$ AZD2014 + $2.5xGI_{50}$

Paclitaxel and ≈14.5-fold increase, $p<0.0001$ for $5xGI_{50}$ AZD2014 + $2.5xGI_{50}$ Paclitaxel; H520: ≈3.6-fold increase, $p<0.01$ for $2.5xGI_{50}$ AZD2014 + $2.5xGI_{50}$ Paclitaxel and ≈3.3-fold increase, $p<0.0001$ for $5xGI_{50}$ AZD2014 + $2.5xGI_{50}$ Paclitaxel; Fig. 5.4). These changes in ASCT2 expression are consistent with the trend of 4-[^{18}F]fluoroglutamine uptake data and could explain, at least in part, the increase of glutamine uptake in cells following treatment with AZD2014 both as a single agent and in combination with Paclitaxel.

A.

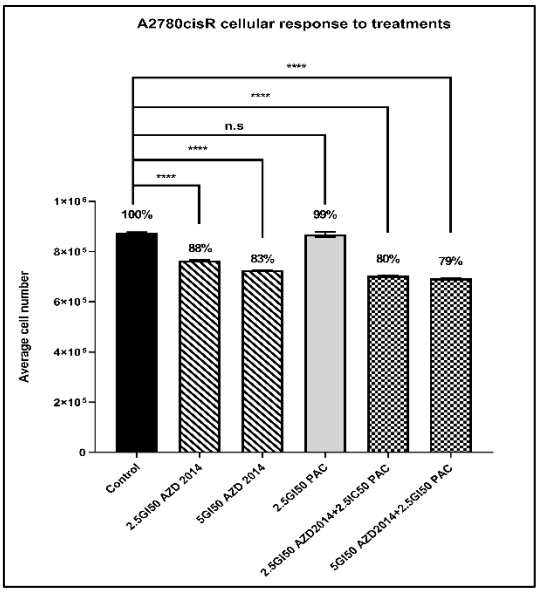

B.

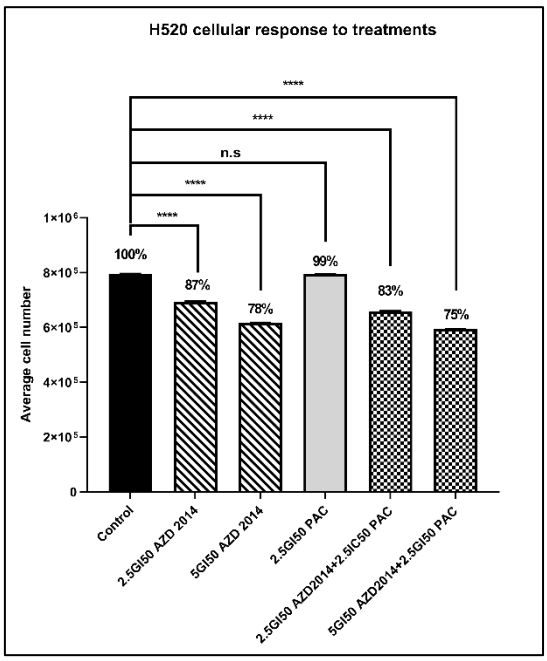

Figure 5.2. Cellular response of A2780cisR and H520 cell lines following treatment with AZD2014 alone, Paclitaxel alone or the combination. A. Cell growth response of A2780cisR cell line following treatment with AZD2014 alone, Paclitaxel alone or the combination. **B.** Cell growth response of H520 cell line following treatment with AZD2014 alone, Paclitaxel alone or the combination. Data are expressed as mean ± SD, n = 3. Statistically significant changes are indicated. P values: **** - <0.0001, n.s = not significant.

A.

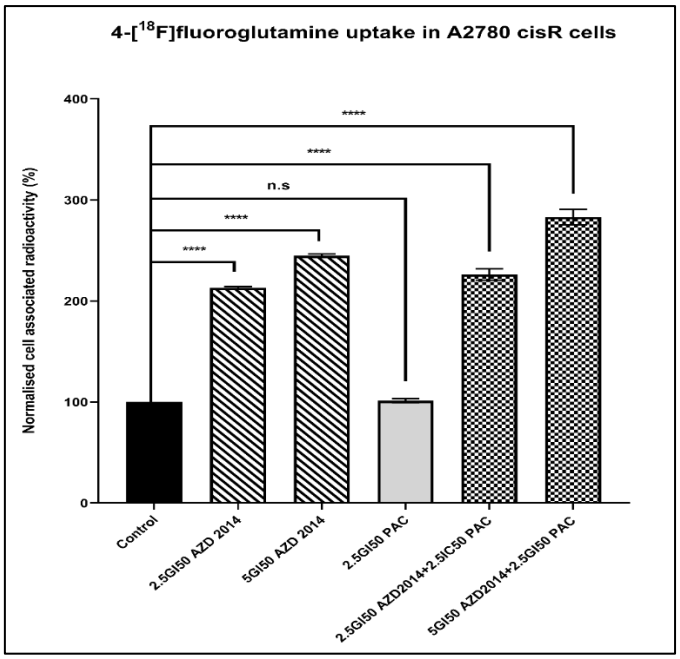

B.

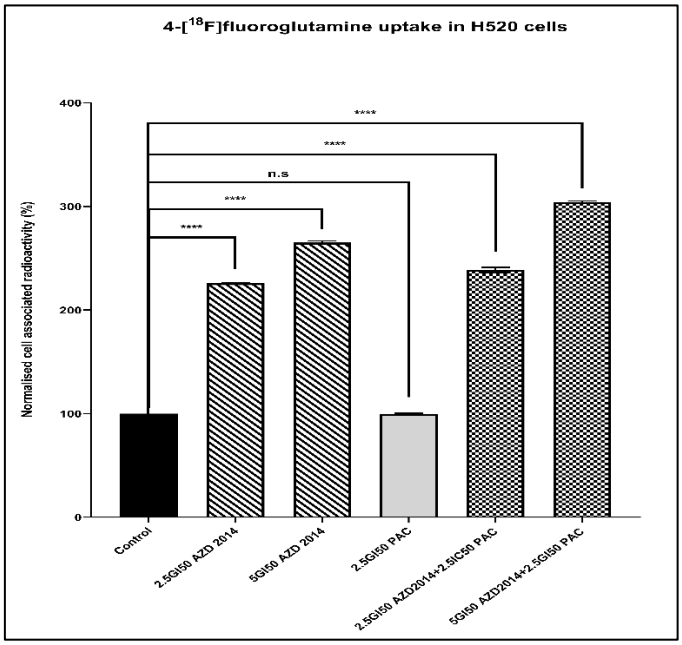

Figure 5.3. Changes in *in vitro* cell uptake of 4-[^{18}F]fluoroglutamine in A2780cisR and H520 cells following treatment with AZD2014 alone, Paclitaxel alone or the combination. A. 4-[^{18}F]fluoroglutamine uptake changes in A2780cisR cells following treatment with AZD2014 alone, Paclitaxel alone or the combination. **B.** 4-[^{18}F]fluoroglutamine uptake changes in H520 cells following treatment with AZD2014 alone, Paclitaxel alone or the combination . Data are expressed as mean ± SD, n = 3. Statistically significant changes are indicated. P values: **** - <0.0001, n.s = not significant.

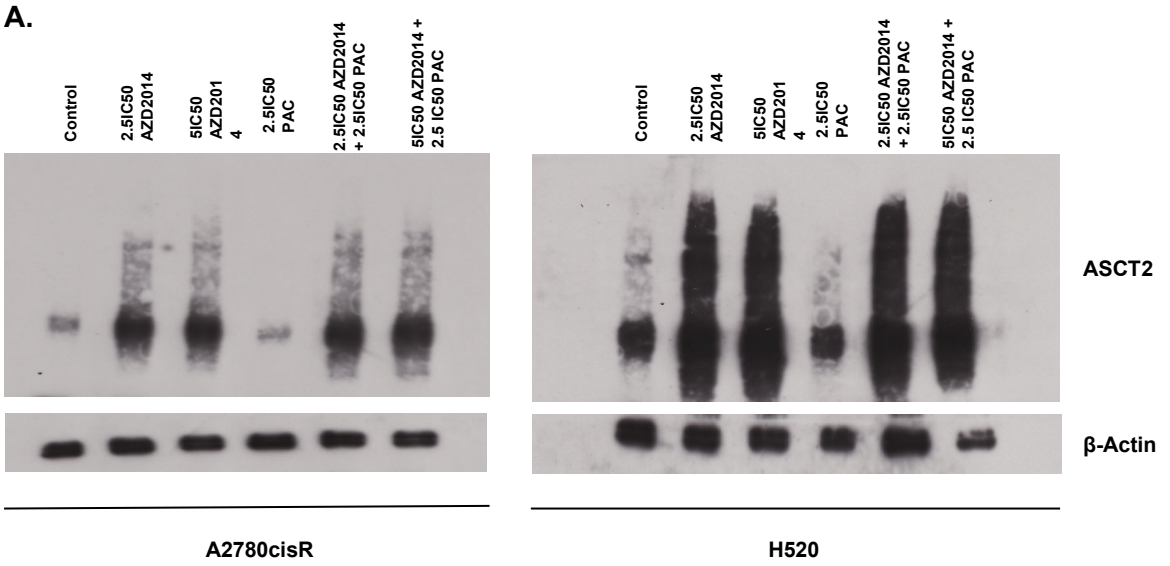

B.

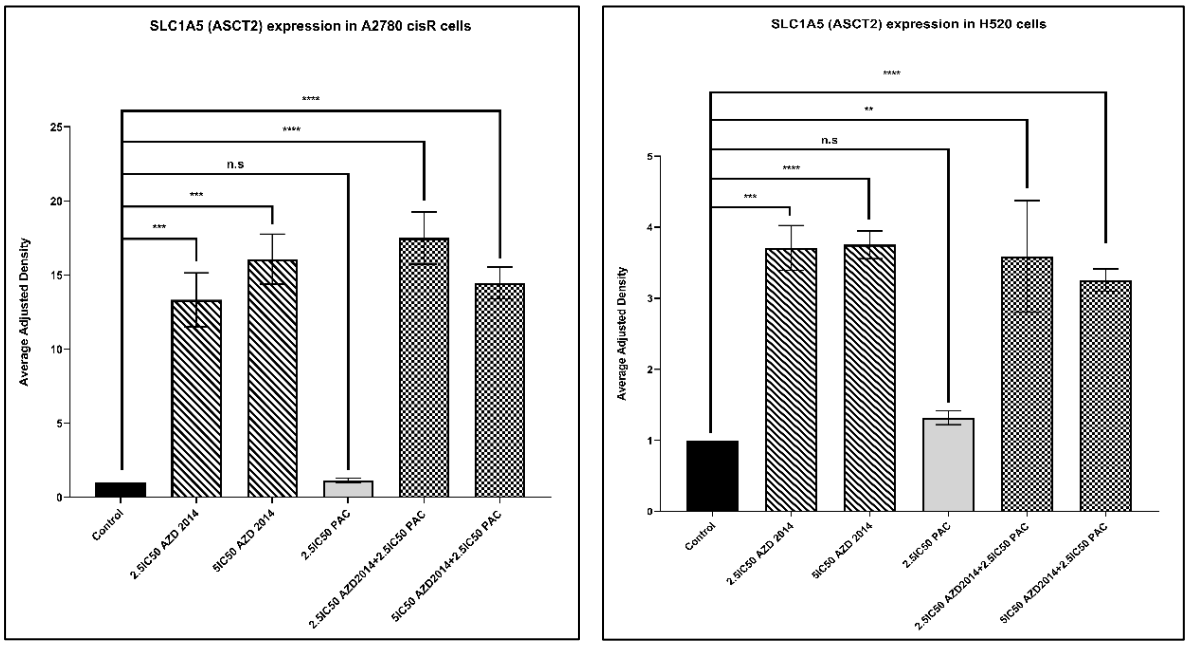

Figure 5.4. Changes in glutamine transporters SLC1A5 (ASCT2) expression in A2780cisR and H520 cell lines following treatment with AZD2014 alone, Paclitaxel alone or the combination. A. A2780cisR and H520 cells were exposed to treatment with vehicle control, AZD2014 alone, Paclitaxel alone or the combination for 24 hours. Figure representative of western blot analysis was done in triplicate. Total protein was normalised to β-Actin as a loading control. There is an increase in level of ASCT2 expression following the treatments with AZD2014 alone and the combination. **B.** Densitometry graphs showing the changes in ASCT2 expression following treatment with vehicle control, AZD2014 alone, Paclitaxel alone or the combination. Data are expressed as mean ± SD, n = 3. Statistically significant changes are indicated. P values: ** - <0.01, *** - <0.001, **** - <0.0001, n.s = not significant.

5.3. Discussion

The mTOR signalling pathway has a critical role in multiple cellular processes, especially in glutamine metabolism (Nicklin et al. 2009; Csibi et al. 2013). Previous studies have found a mutual interaction between mTOR pathway and glutamine uptake and metabolism (Nicklin et al. 2009; Csibi et al. 2013). Glutamine uptake and exchange via the ASCT2/LAT1 transporter directly controls the mTOR signalling (Nicklin et al. 2009). mTORC1 activation then stimulates the uptake of glutamine through the positive regulation of glutaminase enzyme (Csibi et al. 2013). The upregulated glutamine uptake and metabolism has also been shown to play an important part in mTOR inhibitor resistance in cancer (Tanaka et al. 2015).

This chapter aims at exploiting the potential use of 4-[^{18}F]fluoroglutamine PET imaging to monitor tumour response following treatment with AZD2014 and Paclitaxel in future clinical trials. Firstly, it was necessary to study the response of the tested cancer cell lines: ovarian cisplatin resistant A2780cisR cell line and lung cancer H520 cell line following the treatments with AZD2014 alone, Paclitaxel alone or the combination. Paclitaxel chemotherapy has been used in the treatment of many cancer types, especially in ovarian cancer (Baird et al. 2010; Chan et al. 2016). However, resistance to Paclitaxel treatment was found in gynaecological cancers such as uterine and ovarian cancers (Holzmayer et al. 1992; Schneider et al. 1993; Kamazawa et al. 2002). In this study, it was shown that Paclitaxel did not effectively inhibit the growth of tested cancer cell lines. The activation of the PI3K/mTOR signalling pathway was found to be one of the mechanisms behind the Paclitaxel treatment resistance (Foster et al. 2010; Brasseur et al. 2016). Based on this finding, multiple combined therapies of mTOR kinase inhibitors with Paclitaxel have been carried out. It was documented in previous studies that the combination of Paclitaxel with AZD2014 was effective in tumour growth inhibition in ovarian cancer, pancreatic cancer, breast cancer and squamous non-small-cell lung cancer (Le et al. 2003; Sun et al. 2011; Pujade-Lauraine et al. 2014; Basu et al. 2015; Wong et al. 2017; Basu et al. 2018), especially in the A2780cisR xenograft models (Wong et al. 2017). These studies support the findings in this chapter that the cell growth of A2780cisR and H520 which was not affected by the treatment of Paclitaxel alone but was significantly decreased by the use of AZD2014 either as a single treatment or in combination with Paclitaxel.

The *in vitro* uptake assay of 4-[^{18}F]fluoroglutamine was carried out to investigate the changes of glutamine uptake following the AZD2014 treatment of cancer cells. This cell uptake experiment is a first step to confirm the effect of AZD2014, Paclitaxel and combination treatment (as single agent or combined therapy) on glutamine metabolism and the ability of 4-[^{18}F]fluoroglutamine PET radiotracer to detect these changes. It is necessary to perform the *in vitro* uptake study of the radiotracer on cell lines before proceeding to *in vivo* studies and subsequent clinical trials. Herein, the results showed 4-[^{18}F]fluoroglutamine uptake increased substantially in both A2780cisR and H520 cell lines following treatment with AZD2014 alone or in combination with Paclitaxel. As mentioned in Chapters 3 and 4, 4-[^{18}F]fluoroglutamine can enter the cells via the ASCT2 transporter system and further metabolised in the TCA cycle in the same way as L-glutamine. In this study, it was confirmed that the expression of ASCT2 was significantly increased in cells following AZD2014 treatment both as a single agent and in combination with paclitaxel but not in cells treated with Paclitaxel alone. This result is consistent with the trend of 4-[^{18}F]fluoroglutamine uptake following the treatments with AZD2014 and Paclitaxel and again supports the finding that 4-[^{18}F]fluoroglutamine can enter the cells via the ASCT2 transporter system as L-glutamine. Overall, this study showed that treatment with AZD2014 as a monotherapy or in combination with Paclitaxel causes significant growth inhibition in A2780cisR and H520 cells when compared with vehicle- or Paclitaxel- treated groups. In addition, the use of AZD2014 either as a single agent or in combination with Paclitaxel also stimulates a higher 4-[^{18}F]fluoroglutamine uptake in A2780cisR and H520 cells when compared with vehicle- or Paclitaxel-treated cells.

There have been multiple trials of combination therapy, such as concurrent targeting mTOR kinase and glutaminase enzyme, which yielded massive tumour cell death and growth inhibition (Tanaka et al. 2015). Combined Paclitaxel chemotherapy with mTOR kinase inhibitors, such as AZD2014, was also applied as a potential treatment regimen and produced promising results in certain tumour types, e.g., ovarian cancer, pancreatic cancer, breast cancer and squamous non-small-cell lung cancer (Basu et al. 2015; Wong et al. 2017; Basu et al. 2018). Paclitaxel has been used to treat many cancer types, especially ovarian cancer (Baird et al. 2010; Chan et al. 2016); it binds to β-tubulin in cancer cells and interferes with mitosis through microtubule over-stabilisation (Orr et al. 2003; Jordan and Wilson 2004). Paclitaxel is commonly used

in a combination treatment with platinum chemotherapy (Baird et al. 2010; Chan et al. 2016). However, this type of treatment is not as effective as expected in certain tumour types, such as ovarian cancers and resistance to Paclitaxel is now established (Holzmayer et al. 1992; Schneider et al. 1993; Kamazawa et al. 2002). Several mechanisms have been suggested for this resistance to Paclitaxel (Foster et al. 2010; Brasseur et al. 2016) and the activation of PI3K/mTOR signalling pathway was shown to be directly related to the development of paclitaxel resistance. As a result, the utilization of mTOR inhibitors, such as AZD2014, in a combination therapy with Paclitaxel was considered to be a potential cancer treatment.

The study by Wong et al found that the combined treatment of AZD2014 and Paclitaxel yields superior tumour growth inhibition compared to Paclitaxel alone in the A2780cisR xenograft models (Wong et al. 2017). In this chapter, it was also found that the cell growth of A2780cisR and H520 lines, which was not affected by Paclitaxel treatment, decreased following the treatment of AZD2014 alone or the combined treatment of AZD2014 and Paclitaxel. The 4-[^{18}F]fluoroglutamine uptake was found to increase significantly following the AZD2014 treatment both as a single agent and in combination with paclitaxel. On the other hand, there was no changes in 4-[^{18}F]fluoroglutamine uptake in cells following treatment with Paclitaxel alone. Based on these findings, the observed increase in 4-[^{18}F]fluoroglutamine uptake in the combination groups is solely due to mTOR inhibition by AZD2014. As mentioned in the previous studies, an elevation of glutaminase enzyme and subsequent increase in glutamine uptake following mTOR inhibition is most likely due to an induction of the glutamine transporter ASCT2 transporter (Nicklin et al. 2009; Csibi et al. 2013). This study confirmed that the expression of ASCT2 was significantly increased in cells following AZD2014 treatment both as a single agent and in combination with paclitaxel but not in cells treated with Paclitaxel alone.

Further *in vivo* PET imaging can now be developed to examine the application of 4-[^{18}F]fluoroglutamine in monitoring the treatment response in tumours following the treatment with AZD2014 or paclitaxel alone or as combination therapy. The *in vivo* experiment was originally planned for this chapter but it was not feasible to perform the study at the end due to the COVID-19 pandemic.

Chapter 6

Evaluating the effect of Cdk2 Kinase Inhibition on Glutamine Metabolism

6.1. Introduction

This chapter evaluates the cellular changes and glutamine metabolism in MYC overexpressing Kelly (neuroblastoma) and VMRC-LCD (non-small cell lung) cancer cell lines (Kohl et al. 1983; Schwab et al. 1983; Rapp et al. 2009) following the inhibition of Cdk2 Kinase and its subsequent MYC phosphorylation pathway by CYC065.

The balance between proto-oncogenes and tumour suppressor genes plays a critical role in regulating cell growth. Any disrupting mutations or epigenetic changes may lead to cancer formation or tumorigenesis (Lowe et al. 2004). MYC is one of the two classical oncogenes beside Ras, which regulates cell growth and many important cellular processes at the transcriptional level (Grandori et al. 2000; Lowe et al. 2004; Larsson and Henriksson 2010). One of the key mechanisms of MYC is activating the glucose metabolism pathway. MYC stimulates many glycolytic genes by binding to MYC consensus E-boxes (CACGTG) (Osthus et al. 2000; Kim et al. 2004).

In addition to the stimulatory ability of MYC to glycolysis pathway, MYC was also found to induce genes in the glutamine metabolism pathway transcriptionally and posttranscriptionally (Wise et al. 2008; Gao et al. 2009). The induction of glutaminolysis was shown to be essential for cell survival under glucose or oxygen-deprived environment (Le et al. 2012). MYC is able to suppress micro-RNAs, such as, miR23b which block the synthesis of mitochondrial glutaminase (GLS) enzyme (Chang et al. 2008). Beside the suppression of micro-RNAs, MYC also appears to directly induce GLS mRNA at a transcriptional level (Wise et al. 2008; Gao et al. 2009). Furthermore, MYC also has the ability to increase the transcription of genes required for glutamine uptake, specifically, ASCT2 (SLC1A5) and LAT1 (SLC7A5) mRNAs by binding to the promoter elements of these glutamine transporter genes (Wise et al. 2008; Deberardinis and Cheng 2010).

The induction of both glycolysis and glutaminolysis pathways appears to be important in fulfilling cellular requirements of ATP and building blocks generation (Morrish et al. 2009; Hu et al. 2011; Yuneva et al. 2012; Dang 2013). These cellular building blocks

are essential for the subsequent nucleotide biosynthesis and metabolism (Liu et al. 2008; Mannava et al. 2008). Both glucose and glutamine have also been proven to be essential for fatty acid synthesis (Robertson et al. 1982; DeBerardinis et al. 2007). Glucose/Glutamine generates citrate via the TCA cycle in the mitochondria. The resultant citrate is then exported back into the cytosol for the conversion to acetyl-CoA, a starting material of lipid synthesis. It has been documented that the enzymes involved in the lipid synthesis pathway, such as ACACA (acetyl-CoA carboxylase), FASN (fatty acid synthetase), and SCD (stearoyl-CoA desaturase), are also activated by MYC (Zeller et al. 2003; Loven et al. 2012).

The link between the two master regulators, MYC and mTOR, has been shown in two pathways. The first pathway is by growth factor and its receptor interaction. Growth factor engagement activates mTOR signalling pathway through PI3K/AKT and MYC through MEK-ERK pathways (Dang et al. 2006; Wang and Proud 2006; Zoncu et al. 2010). MYC activation increases the expression of genes involved in amino acid transport. The most prominent transporter system is the ASCT2/LAT1 which regulates the import of glutamine and export of glutamine in exchange for leucine. The imported leucine then activates mTOR signalling pathway (Dang 2013). The other interaction pathway between MYC and mTOR was found through the tumour suppressor eukaryotic translation initiation factor 4E binding protein 1 (4EBP1) and the oncogene eukaryotic translation initiation factor 4E (eIF4E) (Pourdehnab et al. 2013). The mTOR-4EBP1-eIF4E-MYC axis has been recognised as an important common node for the survival of cancers from MYC-dependent tumorigenesis or mTOR-dependent tumorigenesis (Pourdehnab et al. 2013). The phosphorylation of 4EBP1 by mTOR prevents 4EBP1 suppression on eIF4E and it is essential for MYC-driven tumour development. eIF4E, in the meantime, can be transcriptionally activated by MYC. This activation of eIF4E together with the inhibition of 4EBP1 is required for mTOR-dependent tumorigenesis.

The mentioned roles of MYC show the importance of this oncogene in the regulation of cellular metabolism. Individual expression of MYC or Ras protects healthy cells from transforming into cancerous ones by supporting the two main barriers of tumorigenesis: apoptosis and senescence. MYC activates apoptosis (Zindy et al. 1998) and Ras stimulates senescence (Serrano et al. 1997). On the other hand, the co-expression of MYC together with its fellow oncogenic gene Ras initiate tumour

development by suppressing the two main hurdles of tumour development. The cooperativity of MYC and Ras leads to tumorigenesis and the mechanisms behind this process were reported by Larsson and Henriksson and Land et al (Land et al. 1983; Larsson and Henriksson 2010). These studies showed that Ras inhibits MYC-induced apoptosis via the PI3K/Akt pathway and the phosphorylation of MYC by Cdk2 kinase suppresses Ras-induced senescence. Cdk2 and MYC interact with each other and form an initial loop in mediating MYC-repressed senescence. Hydbring et al found that Ser62 MYC is the main site for MYC phosphorylation by Cdk2 (Hydbring et al. 2010). The small loop of Cdk2 and MYC then joined in a bigger autostimulatory loop of MYC-RAS in suppression of senescence and apoptosis (Fig. 6.1). MYC stimulates Cdk2, which subsequently phosphorylates MYC to suppress senescence and promote tumour growth. The importance of Cdk2 on MYC phosphorylation and tumour development makes this kinase a desirable target for cancer therapy.

The aim of this chapter is to examine the cellular effect of Cdk2 inhibition by CYC065 (Cyclacel) on glucose and glutamine metabolism in MYC overexpressing cancer cell lines, Kelly and VMRC-LCD. ^{1}H-MRS was firstly used to assess the changes in cellular D-glucose and L-glutamine metabolism following CYC065 treatment in these cancer cells. Subsequently, the *in vitro* uptake assays of 4-[^{18}F]fluoroglutamine and [^{18}F]FDG were carried out to investigate whether the outcomes obtained from this radiotracer uptake study were consistent with the observed changes of L-glutamine and D-glucose uptake measured by ^{1}H-MRS. The results obtained from this *in vitro* uptake assay will serve as the first step towards establishing the use of 4-[^{18}F]fluoroglutamine PET imaging to monitor tumour response following treatment with CYC065 *in vivo* and in future clinical trials.

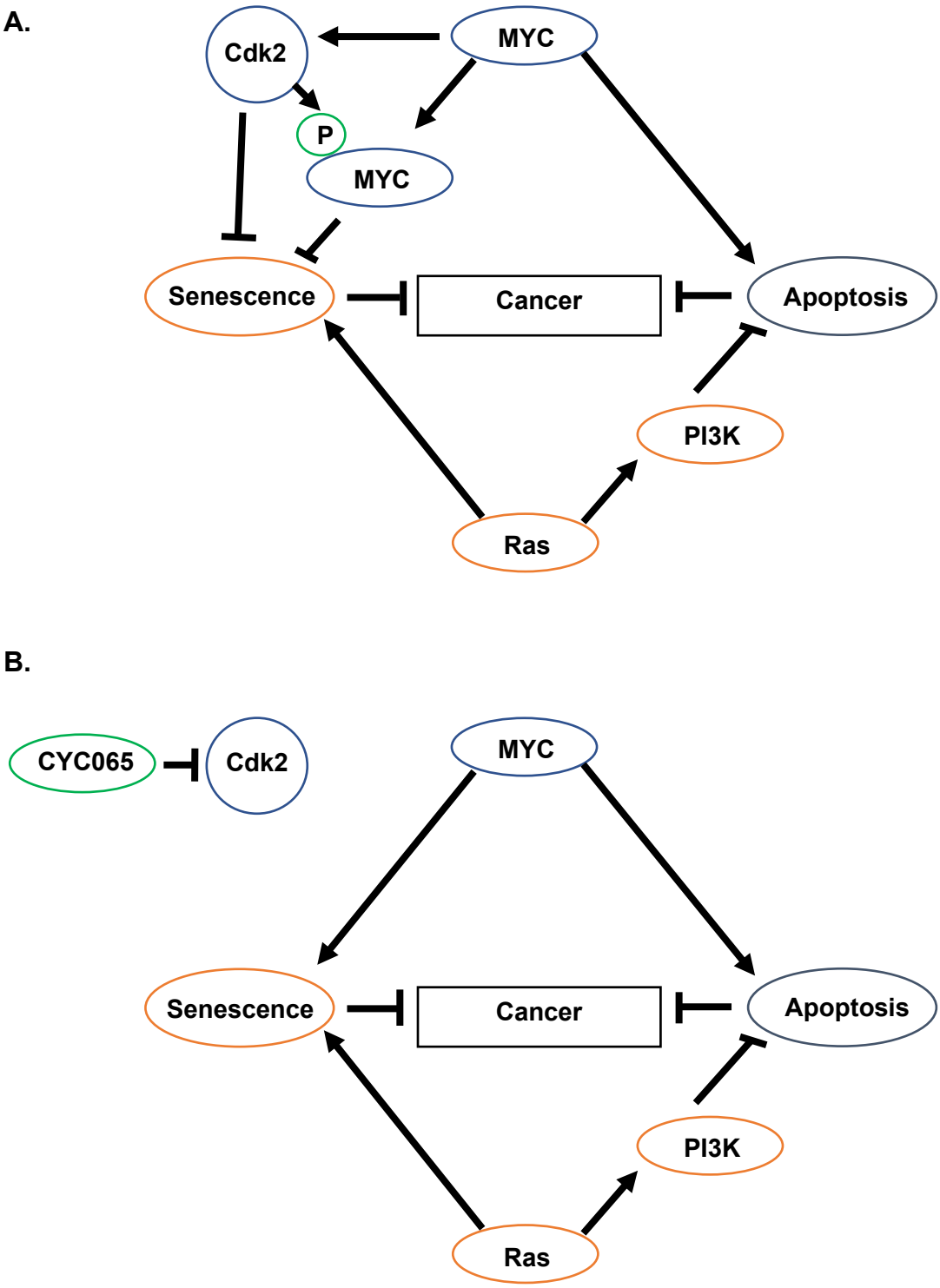

Figure 6.1. The autostimulatory loop of MYC and RAS. A. Co-expression of the two oncogenic genes MYC and Ras suppresses two barriers of cancer initiation: apoptosis and senescence, respectively. The MYC phosphorylation by Cdk2 represses Ras-induced senescence and Ras inhibits Myc-induced apoptosis via the PI3K/Akt pathway. **B.** Inhibition of Cdk2 kinase by CYC065 might potentially turn MYC into an inducer of senescence and subsequently a tumour suppressor. Figure modified from Hydbring and Larsson (2010).

6.2. Experiments and Results

6.2.1. Kelly WT and Kelly CYC065R cell growth inhibition following treatment with Cdk2 inhibitor CYC065

MYC overexpressing neuroblastoma cancer cell lines Kelly WT and CYC065 resistant Kelly (CYC065R) were treated for 24 hours with 250 nM Cdk2 inhibitor CYC065. Following the treatment, there was a 25% decrease of cell number in the CYC065 treated group of Kelly WT cell line when compared with the vehicle-treated control ($p<0.01$; Fig. 6.2A). There was no significant changes of cell growth in the CYC065 treated group of Kelly CYC065R cell line when compared with the vehicle-treated control (Fig. 6.2B)

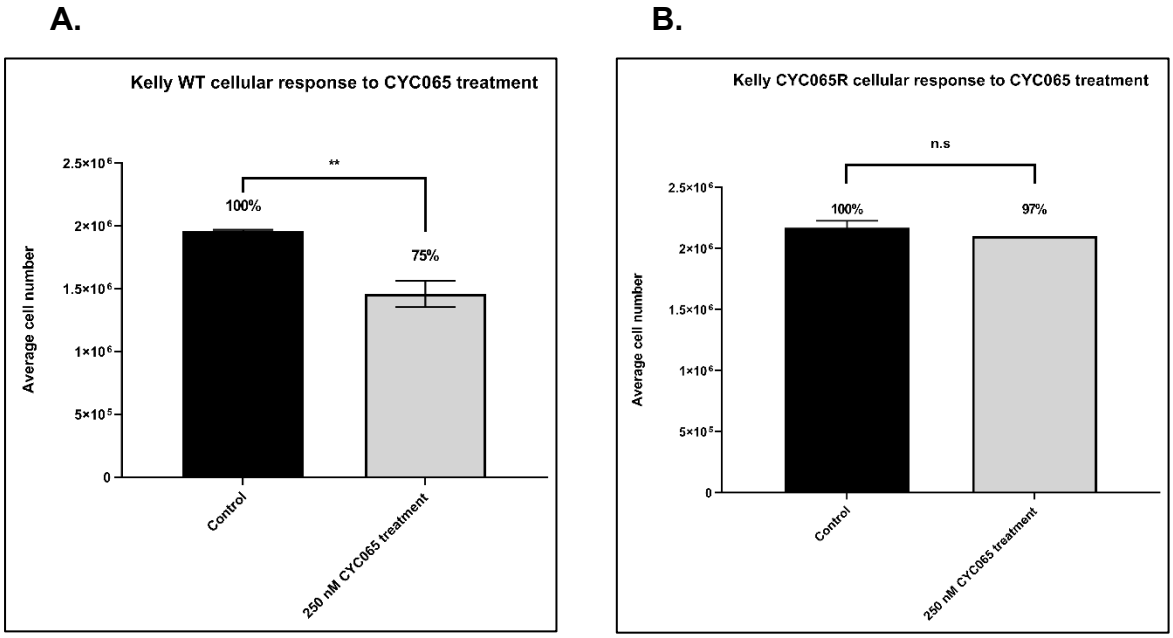

Figure 6.2. Cellular response of Kelly WT and Kelly CYC065R cell lines following treatment with CYC065. A. Cell growth response of Kelly WT cell line following treatment with 250 nM CYC065. **B.** Cell growth response of Kelly CYC065R cell line following treatment with 250 nM CYC065. Data are expressed as mean ± SD, n = 3. The significance was assessed with unpaired Student's t-test. P values: ** - <0.01, n.s = not significant.

6.2.2. ^{1}H-MRS study of metabolic changes in Kelly WT and Kelly CYC065R cells following CYC065 treatment

In order to examine the effect of Cdk2 inhibition on cellular glucose and glutamine metabolism, Kelly WT and CYC065 resistant Kelly (CYC065R) cells were treated with 250 nM Cdk2 inhibitor CYC065 for 24 hours. ^{1}H-MRS spectroscopy was used to analyse the cell culture media and cell extracts. The rates of metabolite uptake or secretion were calculated as described in section 2.3.4. Following the treatment with CYC065, a trend decrease in glucose uptake was observed in CYC065-treated Kelly WT cells when compared with vehicle-treated controls (≈3.3-fold decrease, Fig. 6.3A). However, the result is not statistically significant due to large variabilities among the three replicates ($p=0.06$). There were no significant changes in the lactate secretion (Fig. 6.3A), cellular lactate, cellular glucose and ATP level (Fig. 6.3B) following CYC065 treatment when compared with controls. These results suggest that CYC065 had no significant effect on glucose uptake and metabolism in Kelly WT cells.

Significant decreases in glutamine uptake (≈2-fold decrease, $p<0.05$; Fig. 6.3A) and glutamate secretion (≈4.4-fold decrease, $p<0.01$; Fig. 6.3A) were observed in Kelly WT cells following CYC065 treatment when compared with controls. In addition, a decrease in cellular glutamate level was also found following CYC065 treatment (≈2.9-fold decrease, $p<0.05$; Fig. 6.3B). There is no significant change in the cellular glutamine level (Fig. 6.3B). These results suggest that the glutaminolysis pathway might be affected by the CYC065 treatment. Interestingly, it was noted that the CYC065-treated Kelly WT cells switched from alanine secretion to alanine uptake ($p<0.01$; Fig. 6.3A) to maintain cellular alanine level, as shown by the non-significant change in cellular alanine level following CYC065 treatment (Fig. 6.3B).

Furthermore, decreases in the uptake of branched chain amino acids were found in Kelly WT cells following CYC065 treatment when compared with controls (≈2.9-fold decrease, $p<0.05$ for leucine uptake; ≈1.5-fold decrease, $p<0.05$ for iso-leucine uptake, and ≈3.5-fold decrease, $p<0.01$ for valine uptake; Fig. 6.4A). This leads to decreases in the cellular levels of these branched chain amino acids (≈2-fold decrease, $p<0.05$ for cellular leucine; ≈2.3-fold decrease, $p<0.05$ for cellular iso-leucine, and ≈2-fold decrease, $p<0.05$ for cellular valine; Fig. 6.4B). These data indicate the negative impact from Cdk2 Kinase inhibition, and its subsequent MYC

phosphorylation, on glucose uptake, glutamine and branched chain amino acid uptake and metabolism in the Kelly WT cell line.

These metabolic changes were not observed in CYC065-treated CYC065 resistant Kelly (CYC065R) cells when compared with vehicle controls (Fig. 6.5 and Fig. 6.6). Example ^{1}H-MRS spectra illustrate the changes in glutamine and branched chain amino acid uptake by CYC065- and vehicle-treated Kelly WT and Kelly CYC065R cells are shown in Fig. 6.7 and 6.8, respectively.

A.

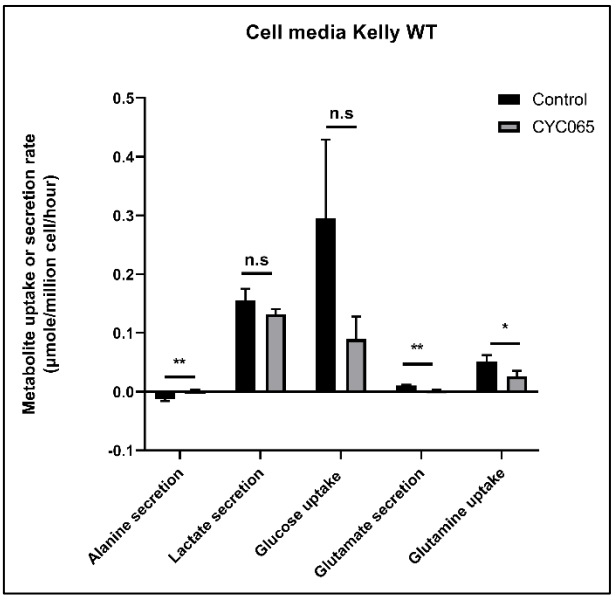

B.

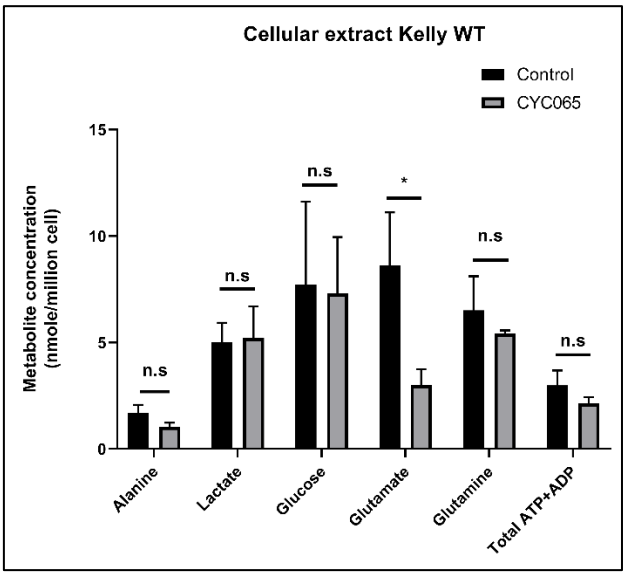

Figure 6.3. Metabolic changes in vehicle- and CYC065-treated Kelly WT cells measured by ^{1}H-MRS. A. Kelly cells were treated with 250nM of CYC065 for 24 hours, cell media were collected and analysed by ^{1}H-MRS. **B.** Kelly cells were treated with 250nM of CYC065 for 24 hours, cells were extracted by the dual phase extraction method and analysed by ^{1}H-MRS. Data are expressed as mean +/- SD, n = 3. Error bars represent +/- SD for 3 independent measurements. The significance level was assessed by two-tailed Student's t-test. P values: * - <0.05, ** - <0.01, n.s = not significant.

A.

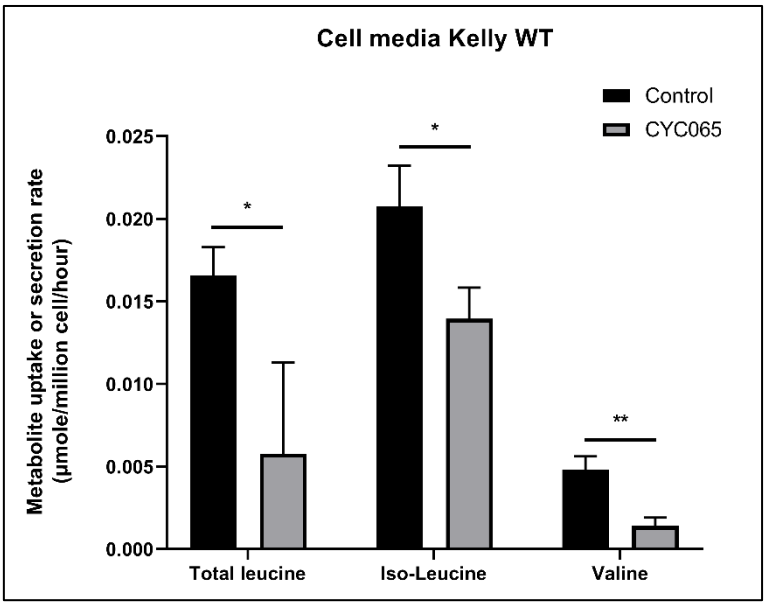

B.

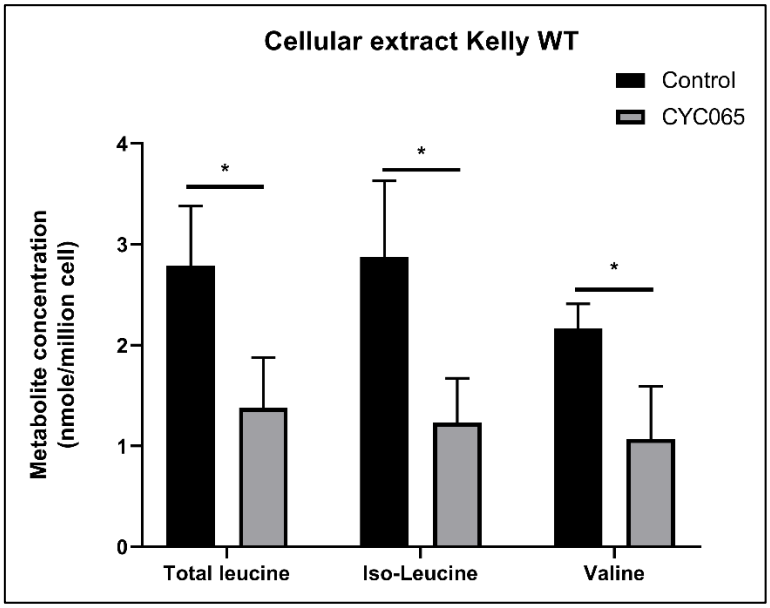

Figure 6.4. Changes in branch-chained amino acid metabolism in Kelly WT cells following vehicle or CYC065 treatment as measured by ^{1}H-MRS. A. Kelly cells were treated with 250nM of CYC065 for 24 hours, cell media were collected and analysed by ^{1}H-MRS. **B.** Kelly cells were treated with 250nM of CYC065 for 24 hours, cells were extracted by the dual phase extraction method and analysed by ^{1}H-MRS. Data are expressed as mean +/- SD, n = 3. Error bars represent +/- SD for 3 independent measurements. The significance level was assessed by two-tailed Student's t-test. P values: * - <0.05, ** - <0.01

A.

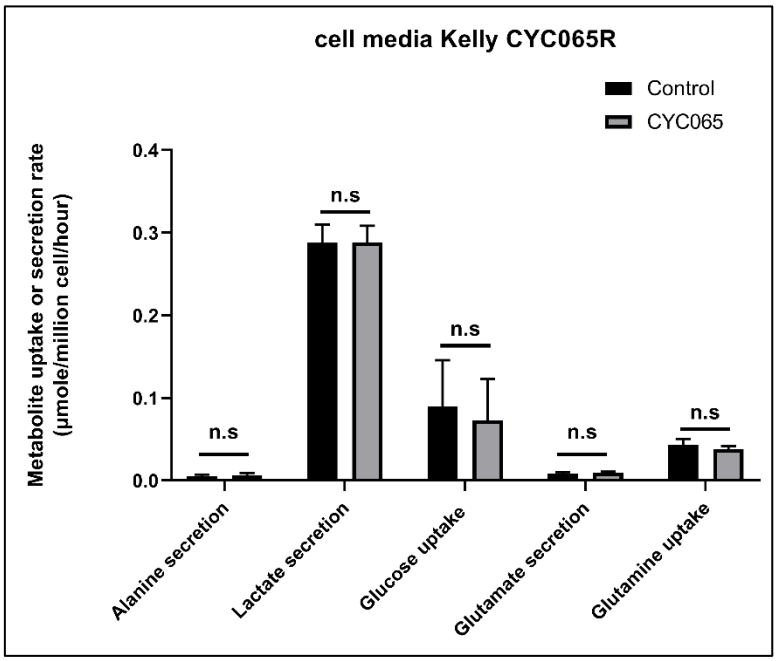

B.

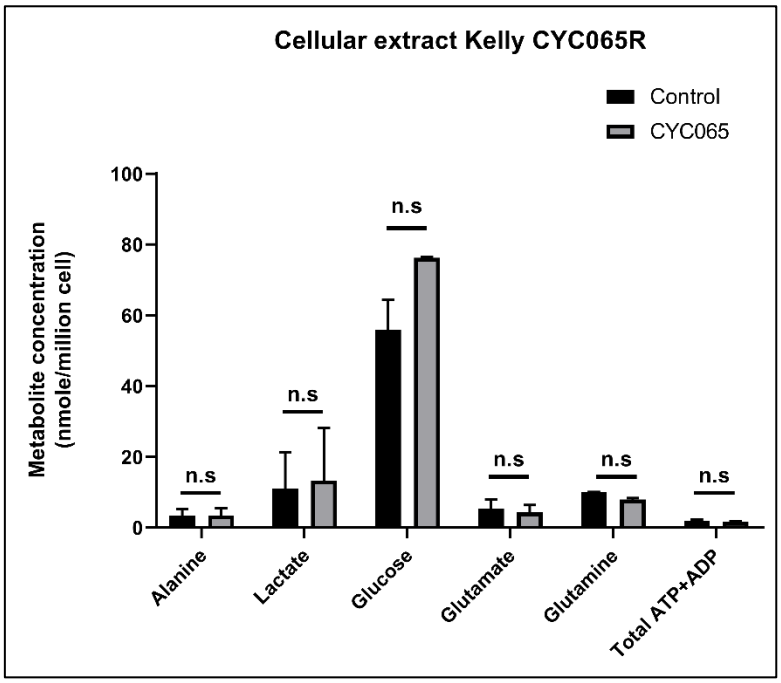

Figure 6.5. Metabolic changes in vehicle- and CYC065-treated Kelly CYC065R cells measured by ^{1}H-MRS. **A.** Kelly cells were treated with 250nM of CYC065 for 24 hours, cell media were collected and analysed by ^{1}H-MRS. **B.** Kelly cells were treated with 250nM of CYC065 for 24 hours, cells were extracted by the dual phase extraction method and analysed by ^{1}H-MRS. Data are expressed as mean +/- SD, n = 3. Error bars represent +/- SD for 3 independent measurements. The significance level was assessed by two-tailed Student's t-test. P values: n.s = not significant.

A.

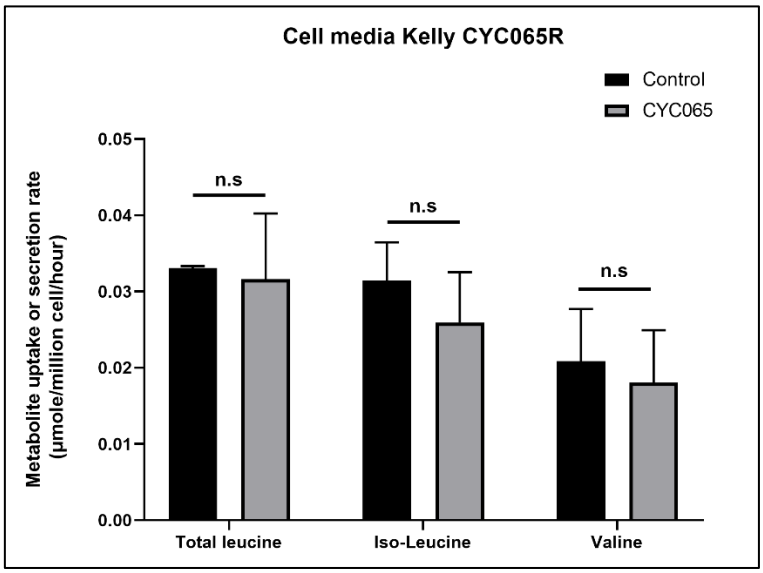

B.

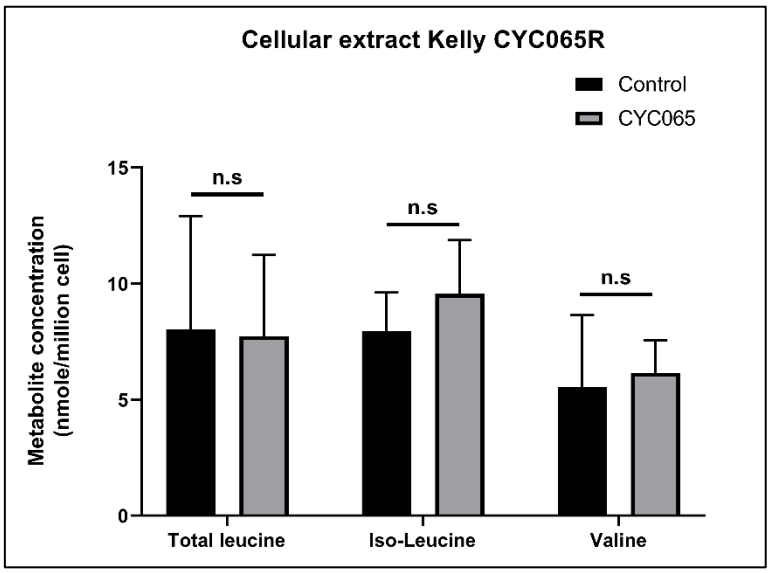

Figure 6.6. Changes in branch-chained amino acid metabolism in Kelly CYC065R cells following vehicle or CYC065 treatment as measured by ^{1}H-MRS. A. Kelly cells were treated with 250nM of CYC065 for 24 hours, cell media were collected and analysed by ^{1}H-MRS. **B.** Kelly cells were treated with 250nM of CYC065 for 24 hours, cells were extracted by the dual phase extraction method and analysed by ^{1}H-MRS. Data are expressed as mean +/- SD, n = 3. Error bars represent +/- SD for 3 independent measurements. The significance level was assessed by two-tailed Student's t-test. P values: n.s = not significant.

A.

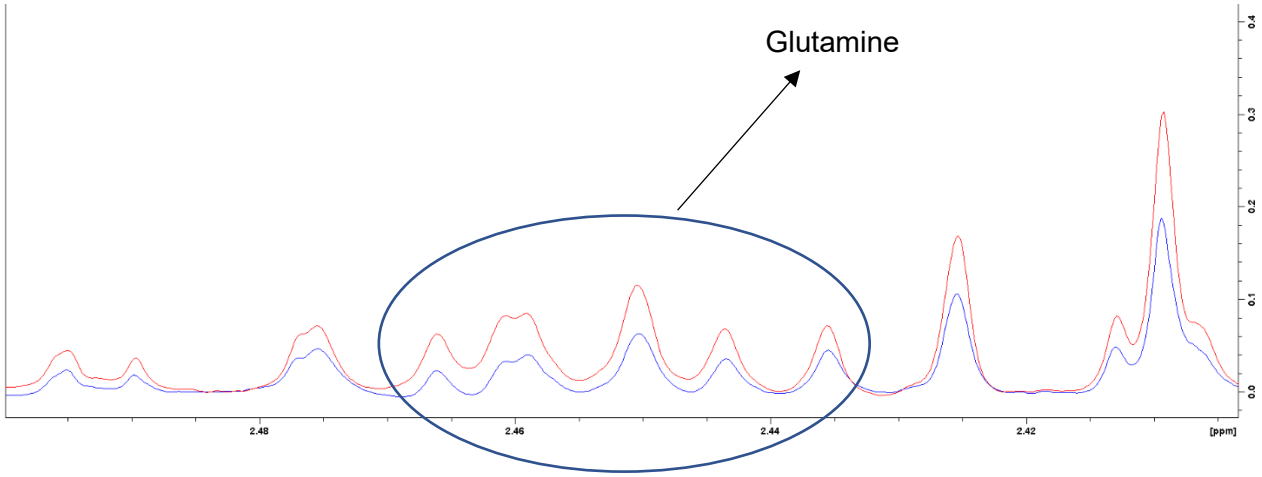

B.

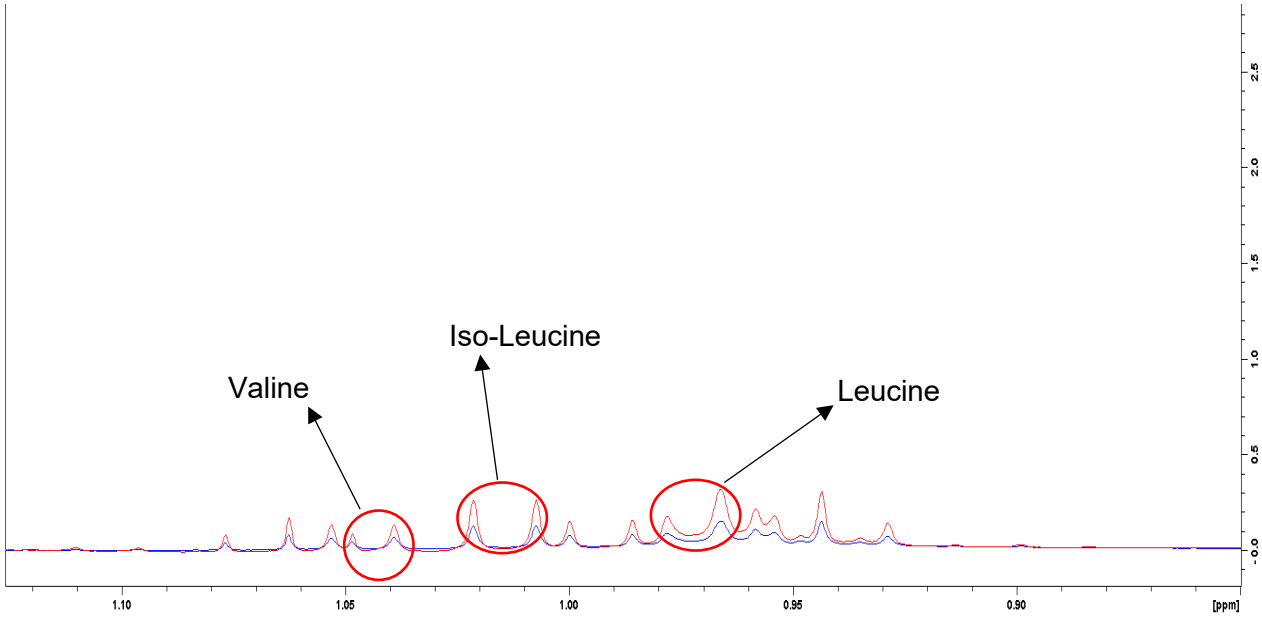

Figure 6.7. Example ^{1}H-MRS spectra of glutamine and branched chain amino acid (Leucine, iso-Leucine and Valine) uptake in Kelly WT cells. A. Changes in glutamine levels in culture media from vehicle- (blue) and CYC065-treated (red) Kelly WT cells. **B.** Changes in branched chain amino acid (Leucine, iso-Leucine and Valine) levels in culture media from vehicle- (blue) and CYC065-treated (red) Kelly WT cells. The decrease of amino acid uptake in Kelly WT cells following the treatment with CYC065 led to a higher level of remaining metabolites in the CYC065-treated cell culture media.

A.

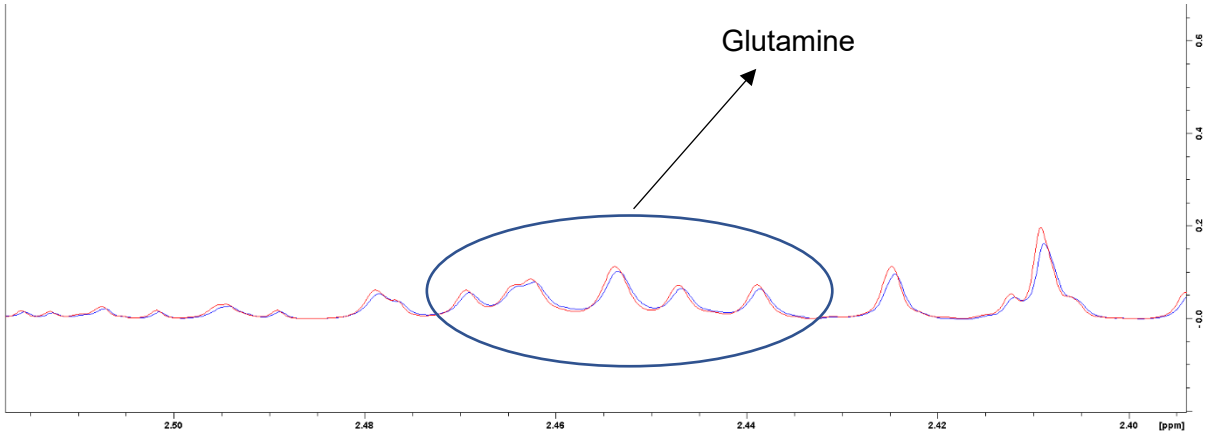

B.

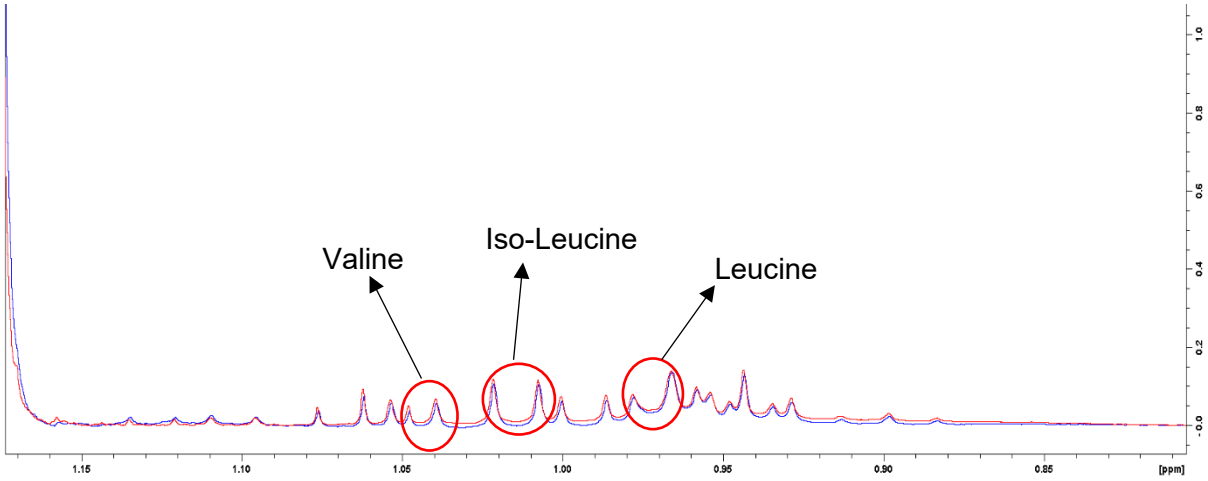

Figure 6.8. Example ^{1}H-MRS spectra of glutamine and branched chain amino acid (Leucine, iso-Leucine and Valine) uptake in Kelly CYC065R cells. A. Glutamine level in culture media from vehicle- (blue) and CYC065-treated (red) Kelly CYC065R cells**. B.** Branched chain amino acid (Leucine, iso-Leucine and Valine) levels in culture media from vehicle- (blue) and CYC065-treated (red) Kelly CYC065R cells**.** Both glutamine and branched chain amino acid uptake in Kelly CYC065R cells remain at a similar level between vehicle and CYC065 treatment. There was no significant changes in amino acid uptake between vehicle and CYC065 treatment.

6.2.3. [^{18}F]FDG and 4-[^{18}F]fluoroglutamine uptake changes in Kelly WT and Kelly CYC065R following CYC065 treatment

The *in vitro* uptake assays of 4-[^{18}F]fluoroglutamine and [^{18}F]FDG were carried out to investigate whether the outcomes obtained from these radiotracer uptake studies were consistent to the changes observed in L-glutamine and D-glucose uptake study by ^{1}H-MRS. Following the treatment with Cdk2 inhibitor, CYC065, significant decreases in [^{18}F]FDG and 4-[^{18}F]fluoroglutamine uptake were found in Kelly WT when compared with vehicle-treated controls (Fig. 6.9A). No significant changes of [^{18}F]FDG and 4-[^{18}F]fluoroglutamine uptake were observed in CYC065-treated Kelly CYC065R cells when compared with vehicle-treated controls (Fig. 6.9B). These results are consistent with the observed uptake changes of L-glutamine and D-glucose in the ^{1}H-MRS experiment.

6.2.4. Examination of glutamine transporter SLC1A5 (ASCT2), branched chain amino acid transporter SLC7A5 (LAT1) and glutaminase (GLS) enzyme expression following CYC065 treatment in Kelly WT and Kelly CYC065R cells

The mechanisms behind the decreases in branched chain amino acid uptake, glutamine uptake and glutamine metabolism in Kelly WT cells were further investigated by examining the protein changes following CYC065 treatment. The expressions of the specific glutamine transporter SLC1A5 (ASCT2), branched chain amino acid transporter SLC7A5 (LAT1) and the GLS enzyme were probed in CYC065-treated cells after 24 h. Following treatment with CYC065, decreases in the expression of ASCT2, LAT1 and glutaminase were found in Kelly WT cells (≈1.5-fold decrease for ASCT2, $p<0.01$; ≈2.9-fold decrease for LAT1, $p<0.0001$ and ≈1.9-fold decrease for glutaminase, $p<0.001$; Fig. 6.10) when compared with vehicle-treated controls. These decreases in the expression of ASCT2, LAT1 and glutaminase were not observed in CYC065-treated CYC065 resistant Kelly (CYC065R) cells when compared with vehicle controls (Fig. 6.11).

A.

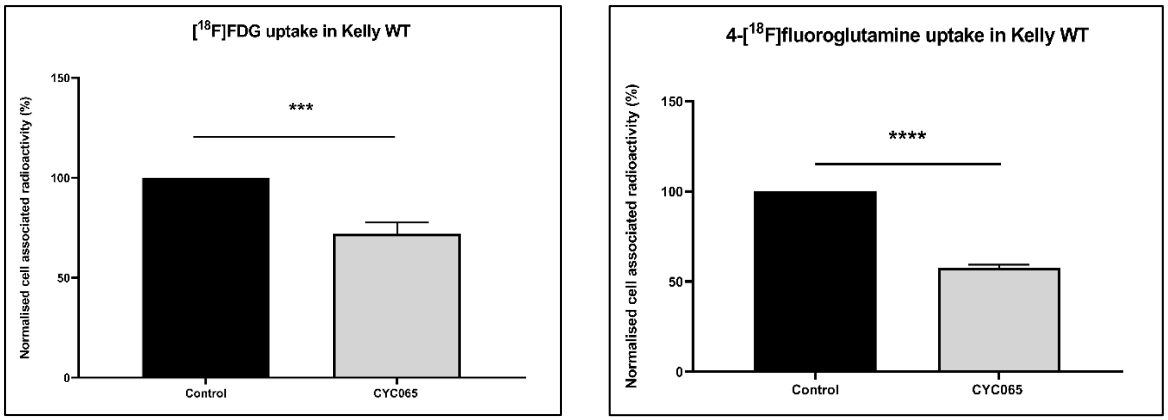

B.

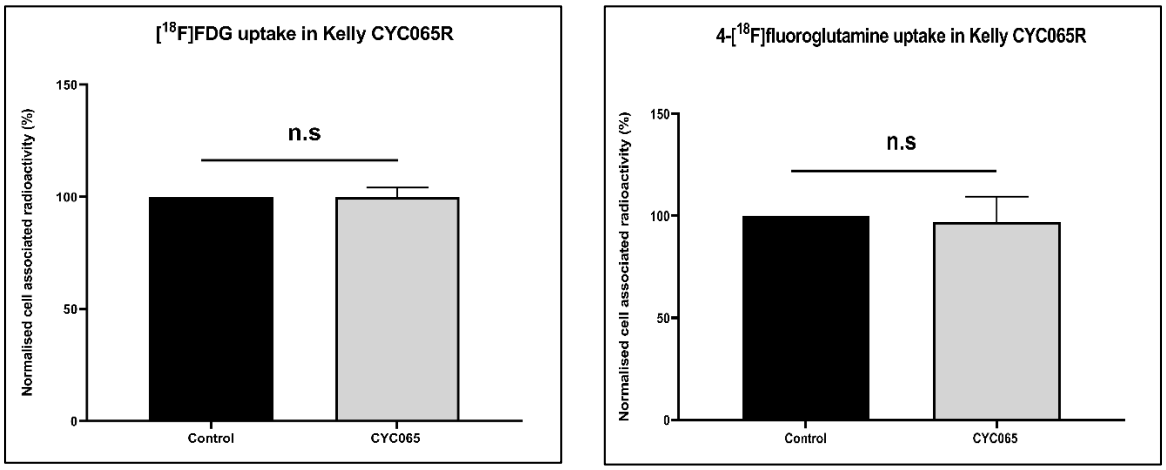

Figure 6.9. Changes in *in vitro* cell uptake of [^{18}F]FDG and 4-[^{18}F]fluoroglutamine in Kelly WT and Kelly CYC065R cells following CYC065 treatment. A. [^{18}F]FDG and 4-[^{18}F]fluoroglutamine uptake changes in Kelly WT following vehicle or CYC065 treatment. **B.** [^{18}F]FDG and 4-[^{18}F]fluoroglutamine uptake changes in Kelly CYC065R following vehicle or CYC065 treatment. Data are expressed as mean ± SD, n = 3. The significance level was assessed by two-tailed Student's t-test. P values: *** - <0.001, **** - <0.0001, n.s = not significant.

A.

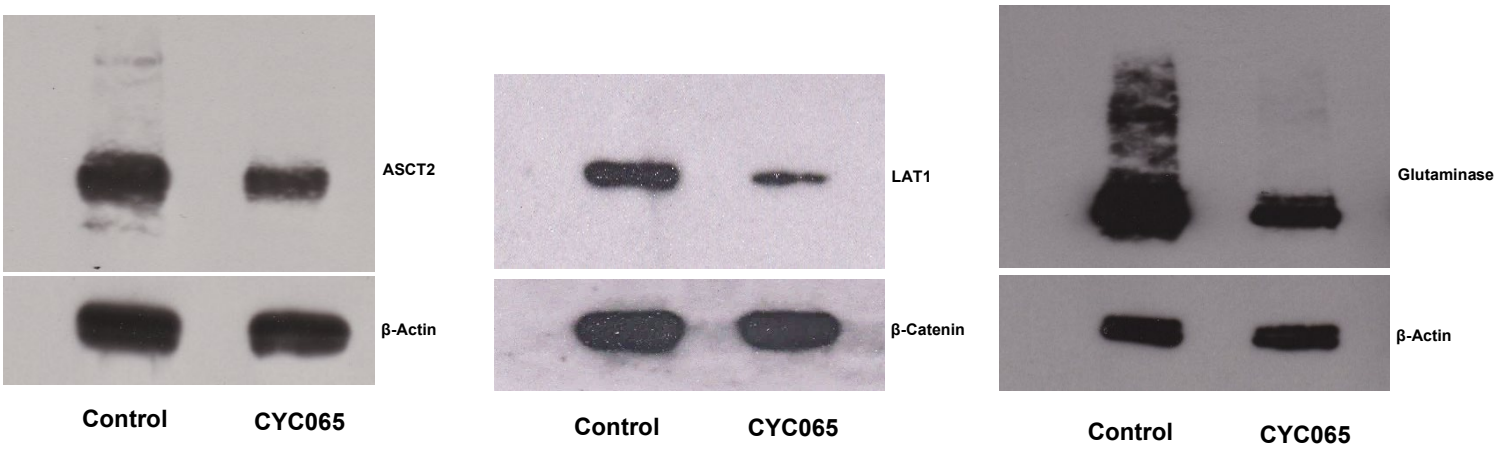

B.

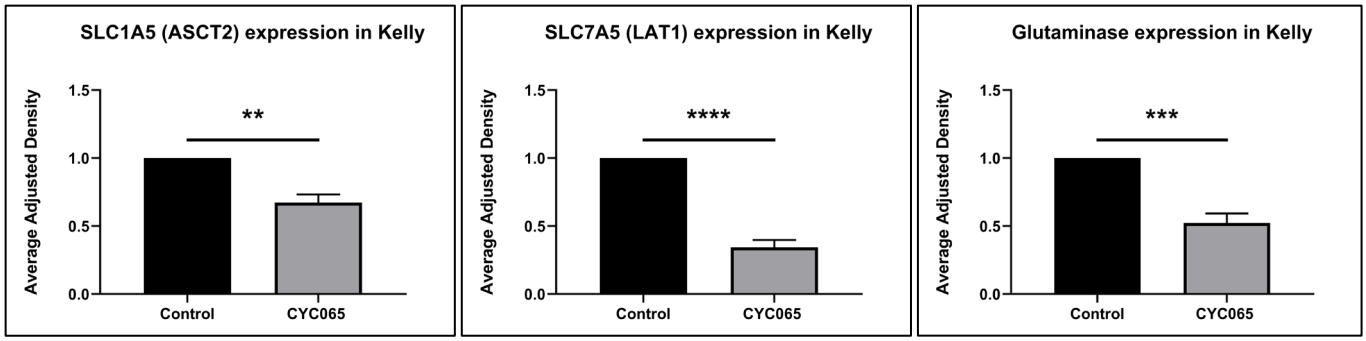

Figure 6.10. Changes in glutamine transporter SLC1A5 (ASCT2), branched chain amino acid transporter SLC7A5 (LAT1) and glutaminase enzyme expression in Kelly WT cell following CYC065 treatment. A. Significantly lower ASCT2, glutaminase and LAT1 expressions were found in CYC065-treated Kelly WT cells when compared with vehicle-treated controls. β-Actin was used as a loading control for ASCT2 and glutaminase. β-Catenin was used as a loading control for LAT1. **B.** Densitometry graphs showing the changes in ASCT2, LAT1 and Glutaminase expression in vehicle- and CYC065-treated Kelly WT cells. Data are expressed as mean ± SD, n = 3. The significance level was assessed by two-tailed Student's t-test. P values: ** - <0.01, *** - <0.001, **** - <0.0001.

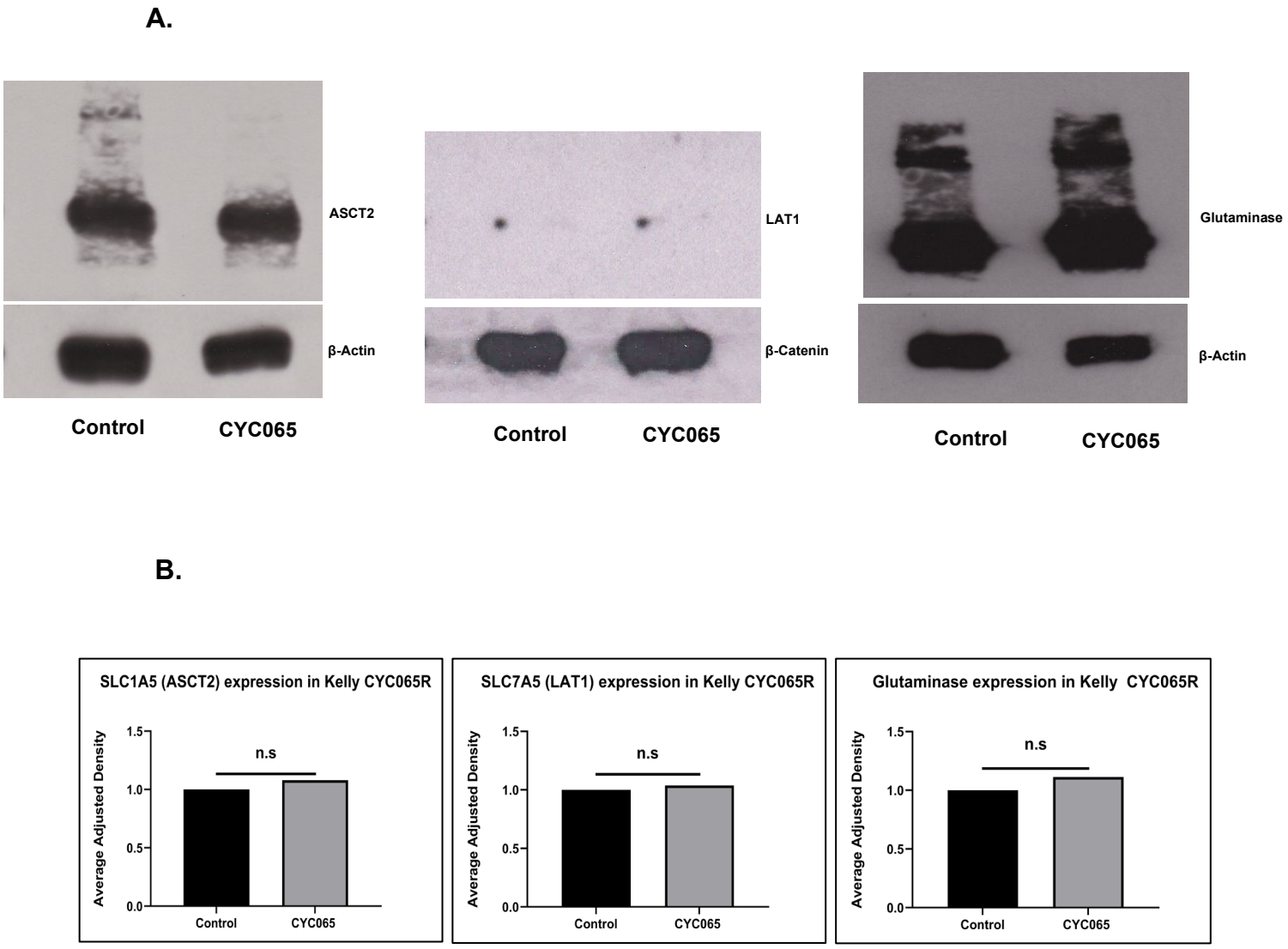

Figure 6.11. Glutamine transporter SLC1A5 (ASCT2), branched chain amino acid transporter SLC7A5 (LAT1) and glutaminase enzyme expression in Kelly CYC065R cell following CYC065 treatment. A. ASCT2, glutaminase and LAT1 expressions remain at a similar level in CYC065-treated Kelly CYC065R cells when compared with vehicle-treated controls. β-Actin was used as a loading control for ASCT2 and glutaminase. β-Catenin was used as a loading control for LAT1. **B.** Densitometry graphs showing the ASCT2, LAT1 and Glutaminase expressions in vehicle- and CYC065-treated Kelly CYC065R cells. The significance level was assessed by two-tailed Student's t-test. P values: n.s = not significant, n = 1.

6.2.5. VMRC WT and VMRC CYC065R cell growth inhibition following treatment with Cdk2 inhibitor CYC065

MYC overexpressing non-small cell lung cancer cell lines VMRC WT and CYC065 resistant VMRC (CYC065R) were treated for 24 hours with 250 nM Cdk2 inhibitor CYC065. Following the treatment, there was a 28% decrease of cell number in the CYC065 treated group of VMRC WT cell line when compared with the vehicle-treated controls ($p<0.001$; Fig. 6.12A). There was no significant changes of cell growth in the CYC065 treated group of VMRC CYC065R cell line when compared with the vehicle-treated controls (Fig. 6.12B).

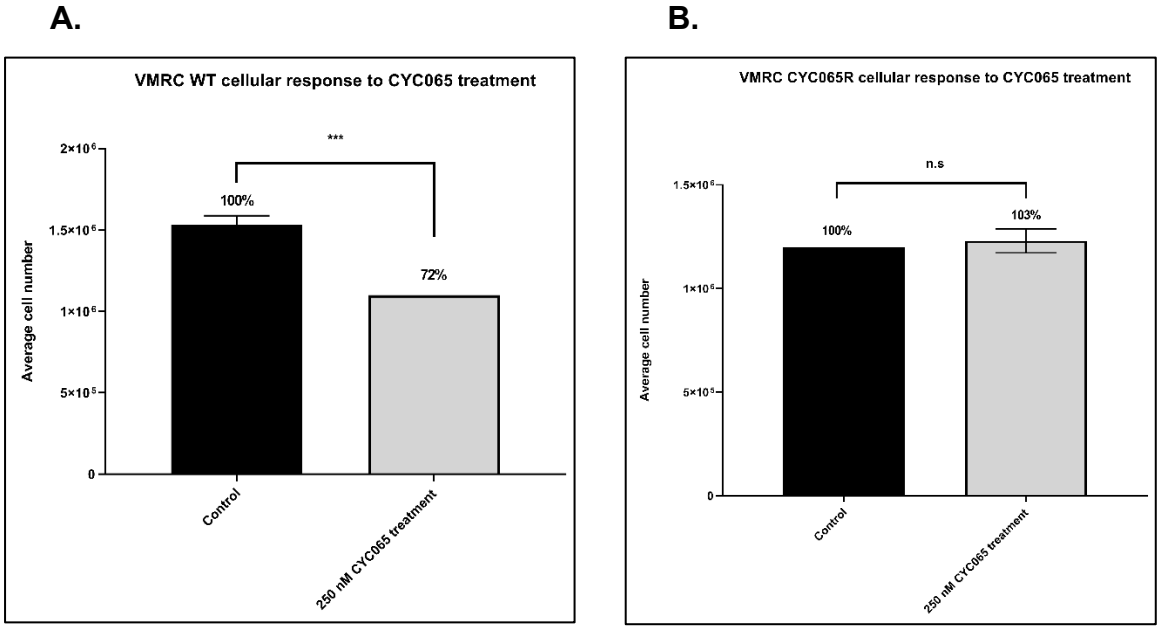

Figure 6.12. Cellular response of VMRC WT and VMRC CYC065R cell lines following treatment with CYC065. A. Cell growth response of VMRC WT cell line following treatment with 250 nM CYC065. **B.** Cell growth response of VMRC CYC065R cell line following treatment with 250 nM CYC065. Data are expressed as mean ± SD, n = 3. The significance was assessed with unpaired Student's t-test. P values: *** - <0.001, n.s = not significant.

6.2.6. ^{1}H-MRS study of metabolic changes in VMRC WT and VMRC CYC065R cells following CYC065 treatment

In order to examine the effect of CYC065 on cellular and glutamine metabolism, non-small cell lung cancer cell lines VMRC WT and CYC065 resistant VMRC (CYC065R) cells were treated with 250 nM Cdk2 inhibitor, CYC065, for 24 hours. ^{1}H-MRS spectroscopy was used to analyse the cell culture media and cell extracts. The rates of metabolite uptake or secretion were calculated as described in section 2.3.4. Following the treatment with CYC065, decreases in glucose uptake (≈6.8-fold, $p<0.0001$, Fig. 6.13A) and lactate secretion were observed (≈1.4-fold, $p<0.0001$, Fig. 6.13A) in the treated group of VMRC WT when compared with vehicle-treated control. No significant changes in cellular lactate and glucose levels were observed in the CYC065-treated group when compared with controls (Fig. 6.13B). However, the ATP level reduced following CYC065 treatment (≈1.8-fold decrease, $p<0.05$, Fig. 6.13B). These results indicate there might be a negative effect from the CYC065 treatment on glucose uptake and metabolism and subsequently on the ATP production from the glycolytic pathway.

Reduced glutamine uptake (≈3.6-fold, $p<0.0001$; Fig. 6.13A) and glutamate excretion (≈3.6-fold, $p<0.01$; Fig. 6.13A) were shown in VMRC WT cells following CYC065 treatment when compared with vehicle control group. In addition, decreases in cellular glutamine and glutamate levels were also observed following CYC065 treatment (≈1.4-fold, $p<0.01$ for cellular glutamine; and ≈2-fold, $p<0.05$ for cellular glutamate; Fig. 6.13B). Furthermore, decreases in alanine secretion (≈2.9-fold, $p<0.05$; Fig. 6.13A) and cellular alanine (≈2.1-fold, $p<0.001$; Fig. 6.13B) were also found in CYC065-treated cells when compared with vehicle controls. These results suggest that the glutaminolysis pathway was negatively impacted by CYC065 treatment, which could further explain the observed decrease of ATP level in CYC065-treated cells, as a portion of the cellular ATP is produced by glutamine metabolism in addition to glycolysis.

Furthermore, decreases in the uptake of three branched chain amino acids, leucine (≈1.5-fold, $p<0.001$), iso-leucine (≈2.8-fold, $p<0.001$) and valine (≈4.3-fold, $p<0.001$) were found in CYC065-treated cells when compared with vehicle-treated controls (Fig. 6.14A). This leads to a trend decrease in the cellular levels of these branched chain

amino acids (≈1.5-fold, p=0.06 for leucine; ≈2-fold, p=0.14 for iso-leucine, and ≈2-fold, p<0.05 for valine; Fig. 6.14B). However, the results of cellular leucine and iso-leucine are not statistically significant which could be due to large variabilities of the three replicates. These data indicate the inhibition of Cdk2 Kinase and its subsequent MYC phosphorylation had negative effects on glucose, glutamine and branched chain amino acid uptake and metabolism in the VMRC WT cell line.

These metabolic changes were not observed in the CYC065 resistant VMRC (CY065R) cell line (Fig. 6.15 and Fig. 6.16) following CYC065 treatment when compared with vehicle-treated controls. Example ^{1}H-MRS spectra illustrate the changes of glutamine uptake and branched chain amino acid uptake in CYC065- and vehicle-treated VMRC WT and VMRC CYC065R cells are shown in Fig. 6.17 and 6.18, respectively.

A.

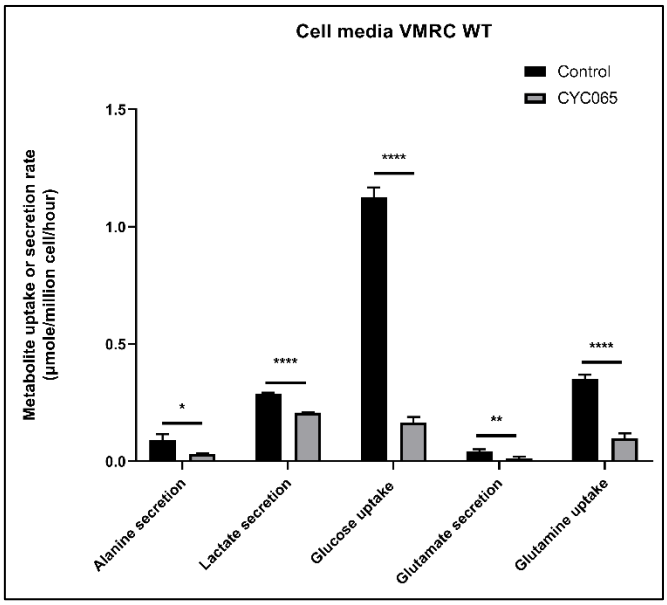

B.

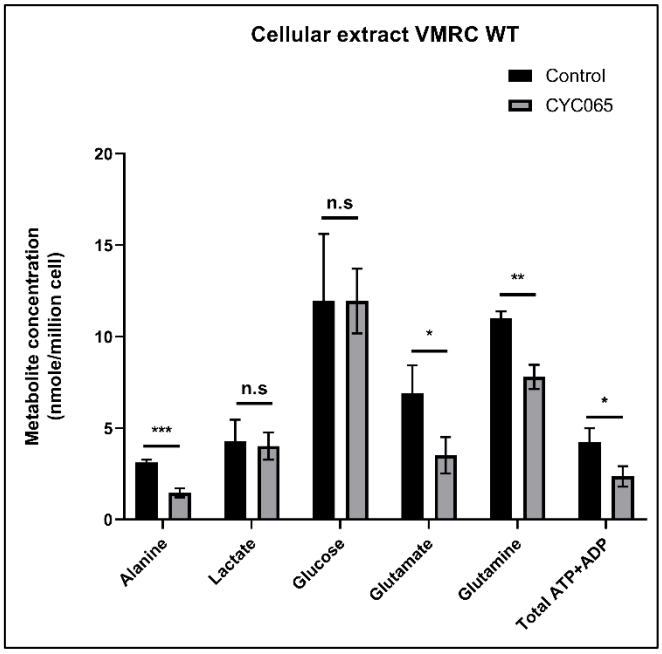

Figure 6.13. Metabolic changes in vehicle- and CYC065-treated VMRC WT cells measured by ^{1}H-MRS. A. VMRC cells were treated with 250nM of CYC065 for 24 hours, cell media were collected and analysed by ^{1}H-MRS. **B.** VMRC cells were treated with 250nM of CYC065 for 24 hours, cells were extracted by the dual phase extraction method and analysed by ^{1}H-MRS. Data are expressed as mean +/- SD, n = 3. Error bars represent +/- SD for 3 independent measurements. The significance level was assessed by 2-tailed Student's t-test. P values: * - <0.05, ** - <0.01, *** - <0.001, **** - <0.0001, n.s = not significant.

A.

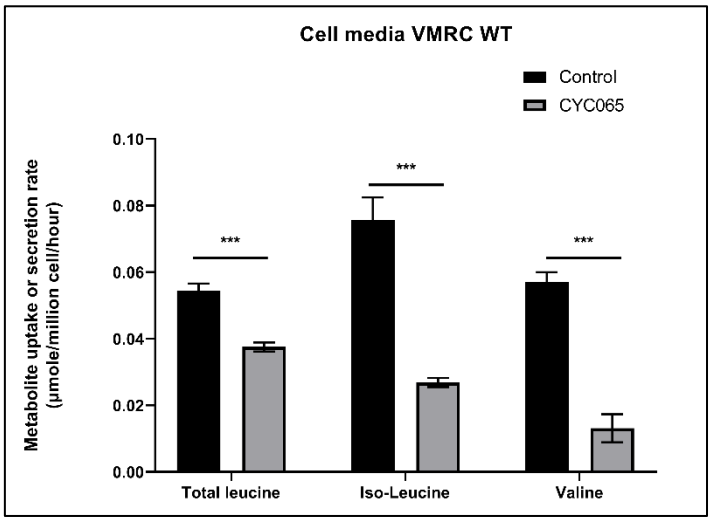

B.

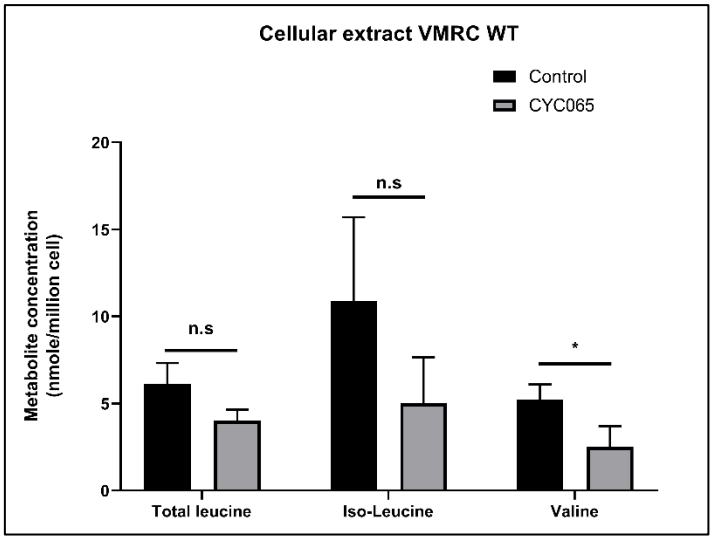

Figure 6.14. Branch-chain amino acid changes in vehicle- and CYC065-treated VMRC WT cells measured by ^{1}H-MRS. A. VMRC cells were treated with 250nM of CYC065 for 24 hours, cell media were collected and analysed by ^{1}H-MRS. **B.** VMRC cells were treated with 250nM of CYC065 for 24 hours, cells were extracted by the dual phase extraction method and analysed by ^{1}H-MRS. Data are expressed as mean +/- SD, n = 3. Error bars represent +/- SD for 3 independent measurements. The significance level was assessed by two-tailed Student's t-test. P values: * - <0.05, *** - <0.001, n.s = not significant.

A.

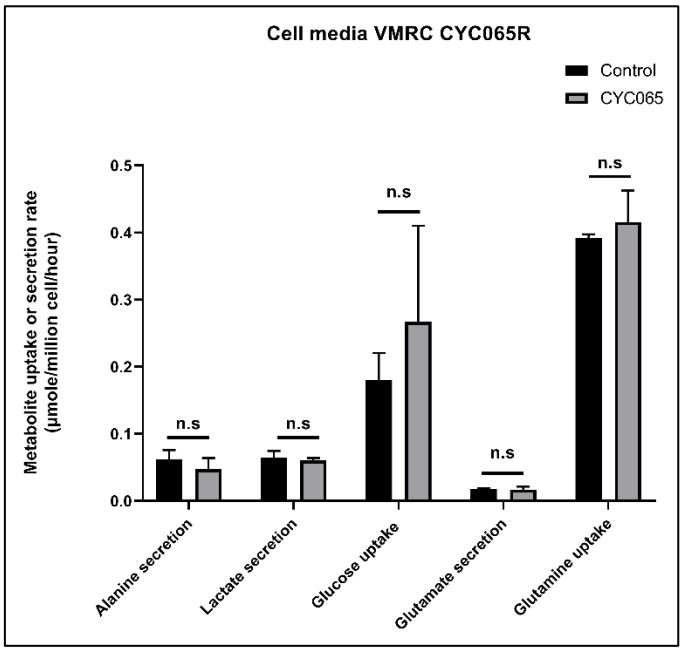

B.

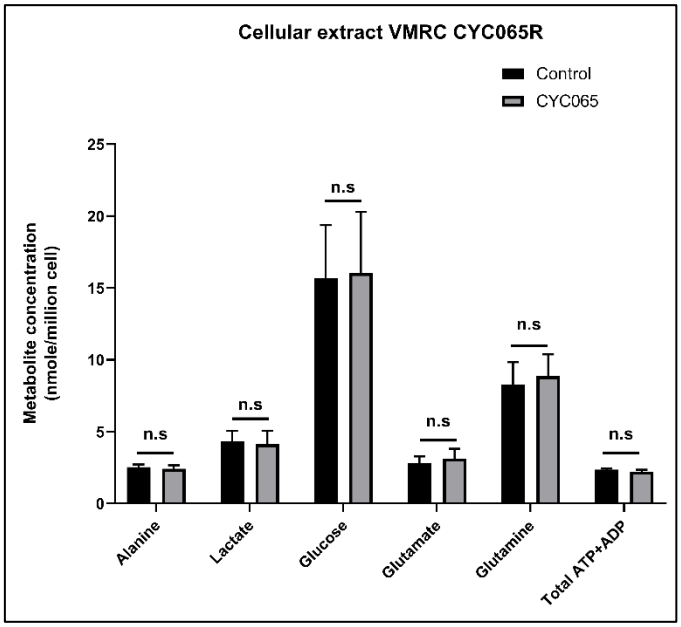

Figure 6.15. Metabolic changes in vehicle- and CYC065-treated VMRC CYC065R cells measured by ^{1}H-MRS. **A.** VMRC cells were treated with 250nM of CYC065 for 24 hours, cell media were collected and analysed by ^{1}H-MRS. **B.** VMRC cells were treated with 250nM of CYC065 for 24 hours, cells were extracted by the dual phase extraction method and analysed by ^{1}H-MRS. Data are expressed as mean +/- SD, n = 3. Error bars represent +/- SD for 3 independent measurements. The significance level was assessed by two-tailed Student's t-test. P values: n.s = not significant.

A.

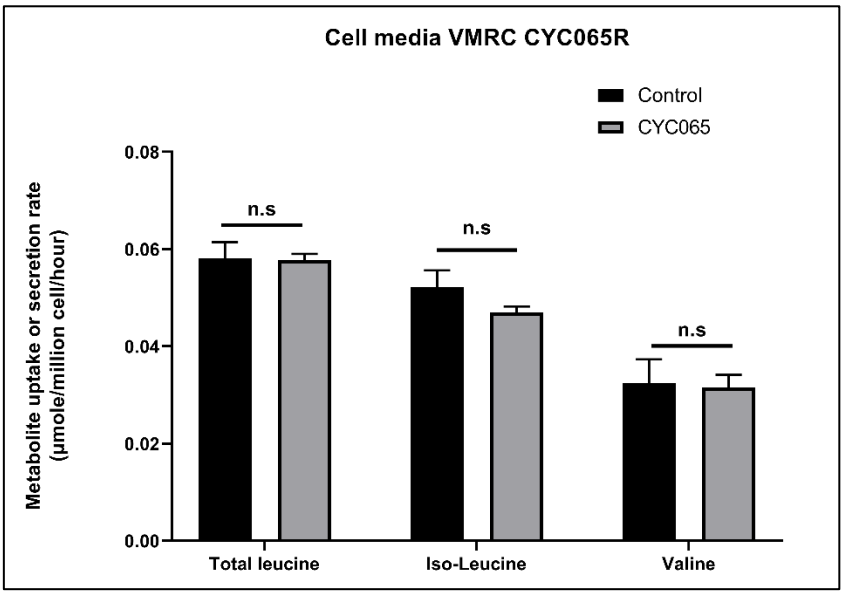

B.

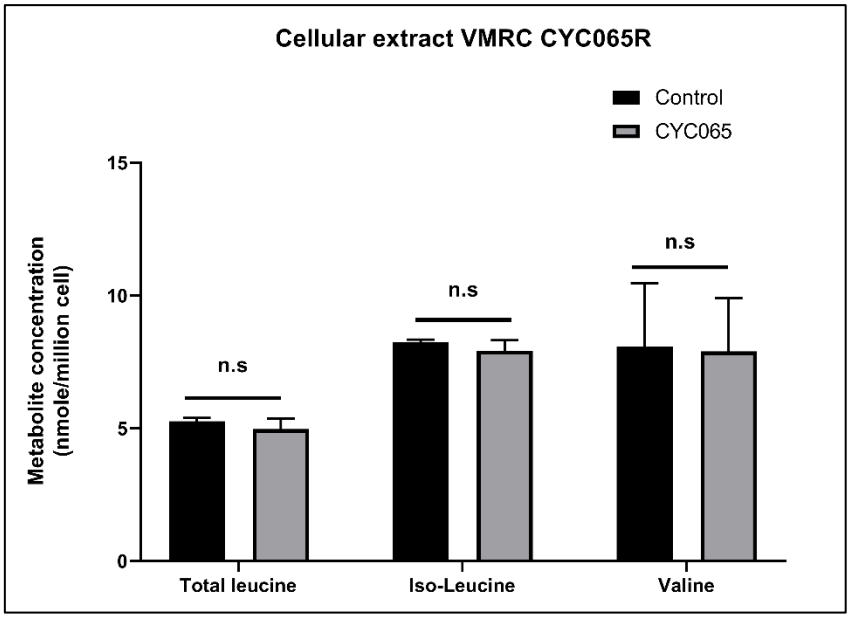

Figure 6.16. Branch-chained amino acid changes in vehicle- and CYC065-treated VMRC CYC065R cells measured by ^{1}H-MRS. A. VMRC cells were treated with 250nM of CYC065 for 24 hours, cell media were collected and analysed by ^{1}H-MRS. **B.** VMRC cells were treated with 250nM of CYC065 for 24 hours, cells were extracted by the dual phase extraction method and analysed by ^{1}H-MRS. Data are expressed as mean +/- SD, n = 3. Error bars represent +/- SD for 3 independent measurements. The significance level was assessed by two-tailed Student's t-test. P values: n.s = not significant.

A.

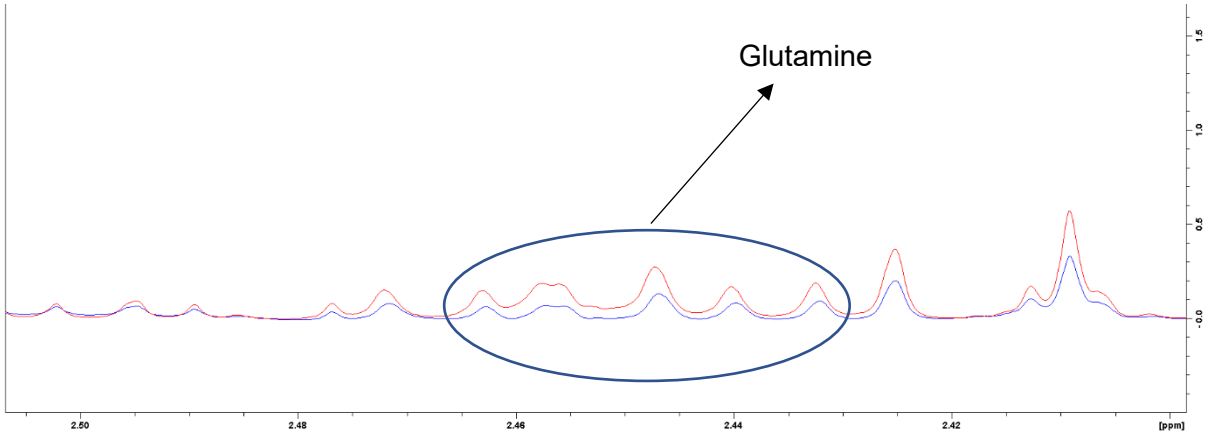

B.

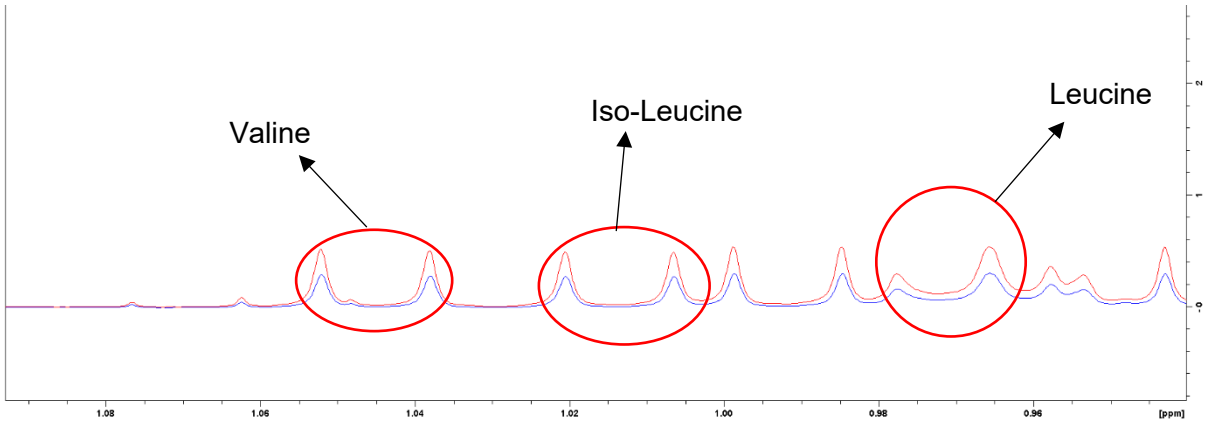

Figure 6.17. Example ^{1}H-MRS spectra of glutamine and branched chain amino acid (Leucine, iso-Leucine and Valine) uptake in VMRC WT cells. A. Changes in glutamine level in culture media from vehicle- (blue) and CYC065-treated (red) VMRC WT cells**. B.** Changes in branched chain amino acid levels (Leucine, iso-Leucine and Valine) in culture media from vehicle- (blue) and CYC065-treated (red) VMRC WT cells**.** The decrease of amino acid uptake in VMRC WT cells following the treatment with CYC065 led to a higher level of remaining metabolites in the CYC065-treated cell culture media.

A.

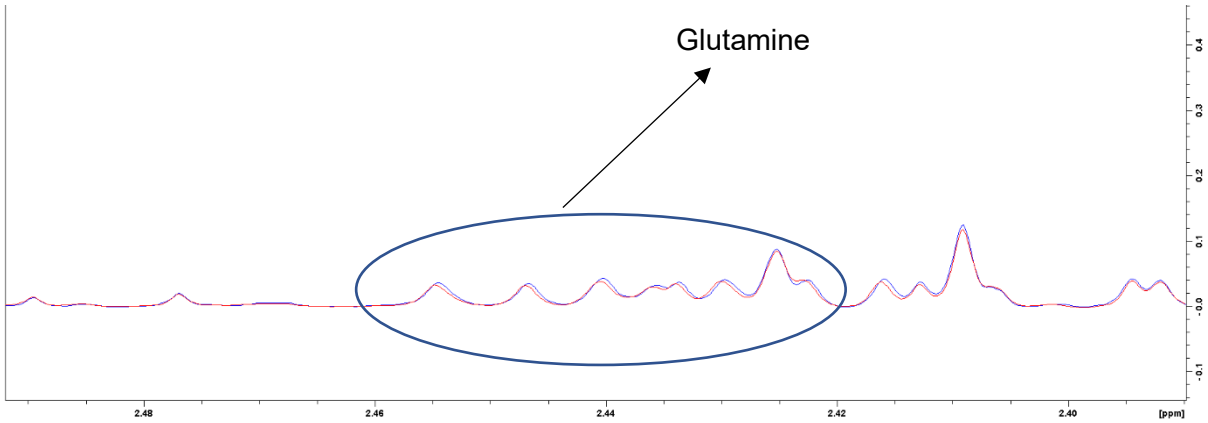

B.

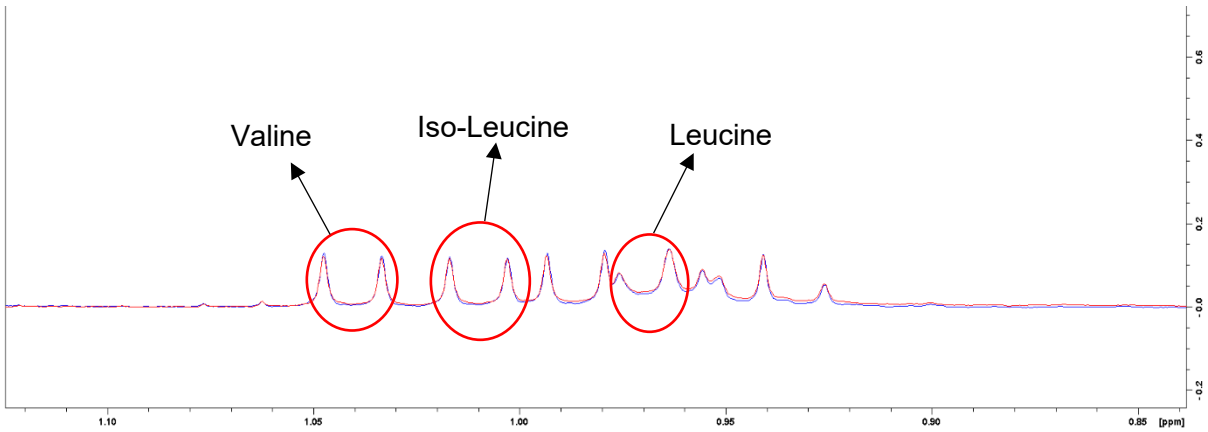

Figure 6.18. Example ^{1}H-MRS spectra of glutamine and branched chain amino acid (Leucine, iso-Leucine and Valine) uptake in VMRC CYC065R cells. A. Glutamine level in culture media from vehicle- (blue) and CYC065-treated (red) VMRC CYC065R cells**. B.** Branched chain amino acid levels (Leucine, iso-Leucine and Valine) in culture media from vehicle- (blue) and CYC065-treated (red) VMRC CYC065R cells**.** Both glutamine and branched chain amino acid uptake in VMRC CYC065R cells remain at a similar level between vehicle and CYC065 treatment. There was no significant changes in amino acid uptake between vehicle and CYC065 treatment.

6.2.7. [^{18}F]FDG and 4-[^{18}F]fluoroglutamine uptake changes in VMRC WT and VMRC CYC065R following CYC065 treatment

The *in vitro* uptake assays of 4-[^{18}F]fluoroglutamine and [^{18}F]FDG were carried out to investigate whether the outcomes obtained from this radiotracer uptake study were consistent to the changes of L-glutamine and D-glucose uptake in the ^{1}H-MRS experiment. Following treatment with the Cdk2 inhibitor CYC065, significant decreases of [^{18}F]FDG and 4-[^{18}F]fluoroglutamine uptake were found in VMRC WT cells when compared with vehicle-treated controls (Fig. 6.19A). No significant changes in [^{18}F]FDG and 4-[^{18}F]fluoroglutamine uptake were found in CYC065-treated VMRC CYC065R cells when compared with controls (Fig. 6.19B). These results are consistent with the observed uptake changes of L-glutamine and D-glucose in the ^{1}H-MRS studies.

6.2.8. Examination of glutamine transporter SLC1A5 (ASCT2), branched chain amino acid transporter SLC7A5 (LAT1) and glutaminase (GLS) enzyme expression following CYC065 treatment in VMRC WT and VMRC CYC065R cells

The mechanism behind the decreases in branched chain amino acid uptake, glutamine uptake and glutamine metabolism in VMRC WT cells were further investigated by examining the protein changes following CYC065 treatment. The expression of the specific glutamine transporter SLC1A5 (ASCT2), branched chain amino acid transporter SLC7A5 (LAT1) and the GLS enzyme were probed in VMRC cells after 24 h of CYC065 treatment. Following treatment with CYC065, a decrease in the expressions of ASCT2 (≈2.1-fold, $p<0.001$); LAT1 (≈22.5-fold, $p<0.0001$) and glutaminase (≈1.7-fold, $p<0.001$) was found in VMRC WT cells when compared with vehicle-treated controls (Fig. 6.20). These decreases in the expression of ASCT2, LAT1 and glutaminase were not observed in CYC065-treated CYC065 resistant VMRC (CYC065R) cells when compared with vehicle controls (Fig. 6.21).

A.

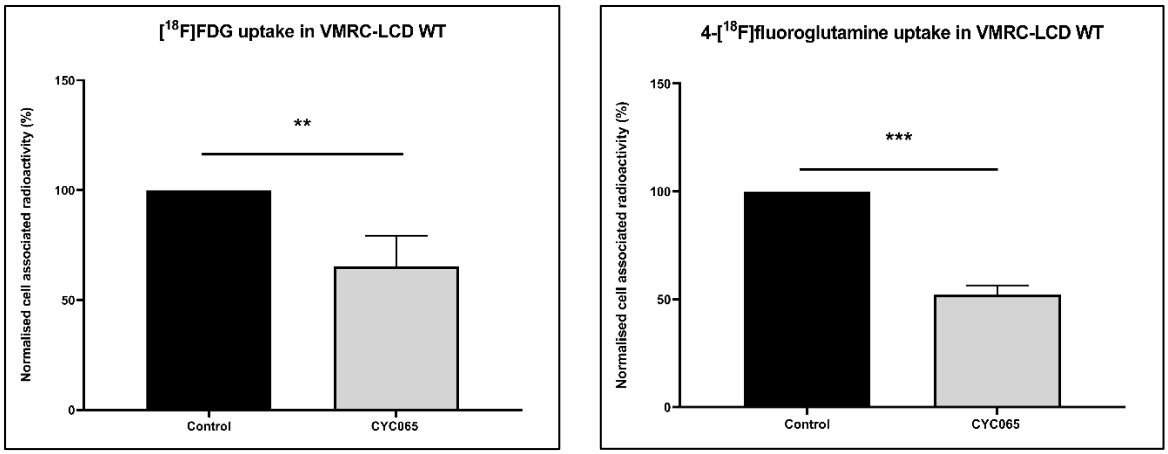

B.

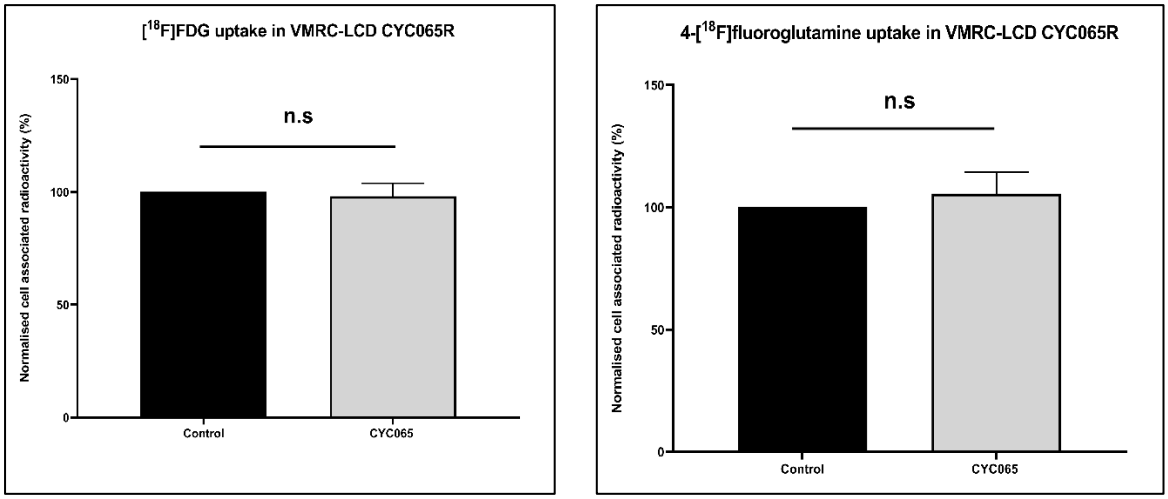

Figure 6.19. Changes in *in vitro* cell uptake of [^{18}F]FDG and 4-[^{18}F]fluoroglutamine in VMRC WT and VMRC CYC065R following CYC065 treatment. A. [^{18}F]FDG and 4-[^{18}F]fluoroglutamine uptake changes in VMRC WT cells following vehicle or CYC065 treatment. **B.** [^{18}F]FDG and 4-[^{18}F]fluoroglutamine uptake changes in VMRC CYC065R cells following vehicle or CYC065 treatment. Data are expressed as mean ± SD, n = 3. The significance level was assessed by two-tailed Student's t-test. P values: ** - <0.01, *** - <0.001, n.s = not significant.

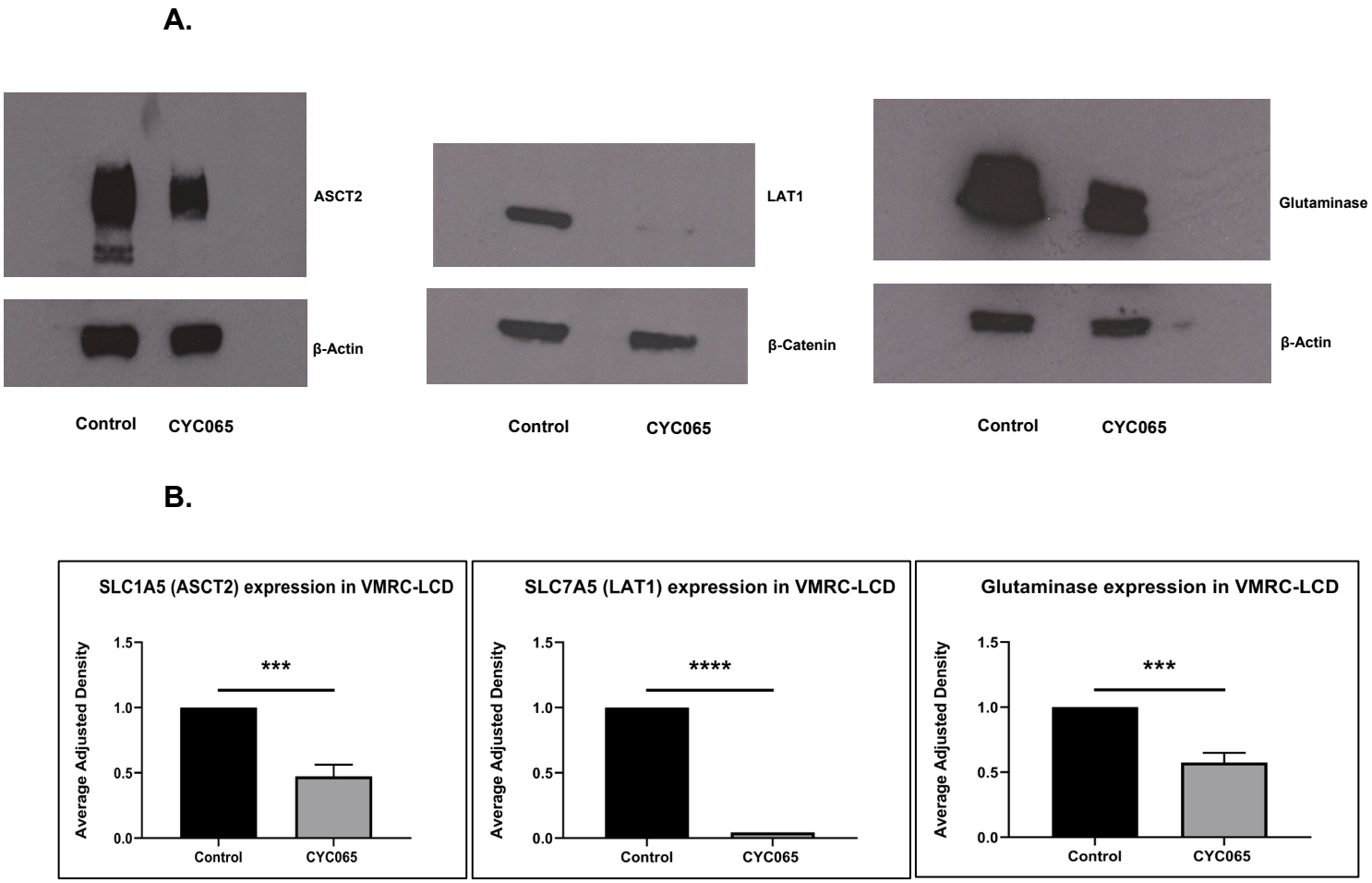

Figure 6.20. Changes in glutamine transporter SLC1A5 (ASCT2), branched chain amino acid transporter SLC7A5 (LAT1) and glutaminase enzyme expression in VMRC WT cells following CYC065 treatment. A. Significantly lower ASCT2, glutaminase and LAT1 expressions were found in CYC065-treated VMRC WT cells when compared with vehicle-treated controls. β-Actin was used as a loading control for ASCT2 and glutaminase. β-Catenin was used as a loading control for LAT1. **B.** Densitometry graphs showing the changes in ASCT2, LAT1 and Glutaminase expressions in vehicle- and CYC065-treated VMRC WT cells. Data are expressed as mean ± SD, n = 3. The significance level was assessed by two-tailed Student's t-test. P values: *** - <0.001, **** - <0.0001.

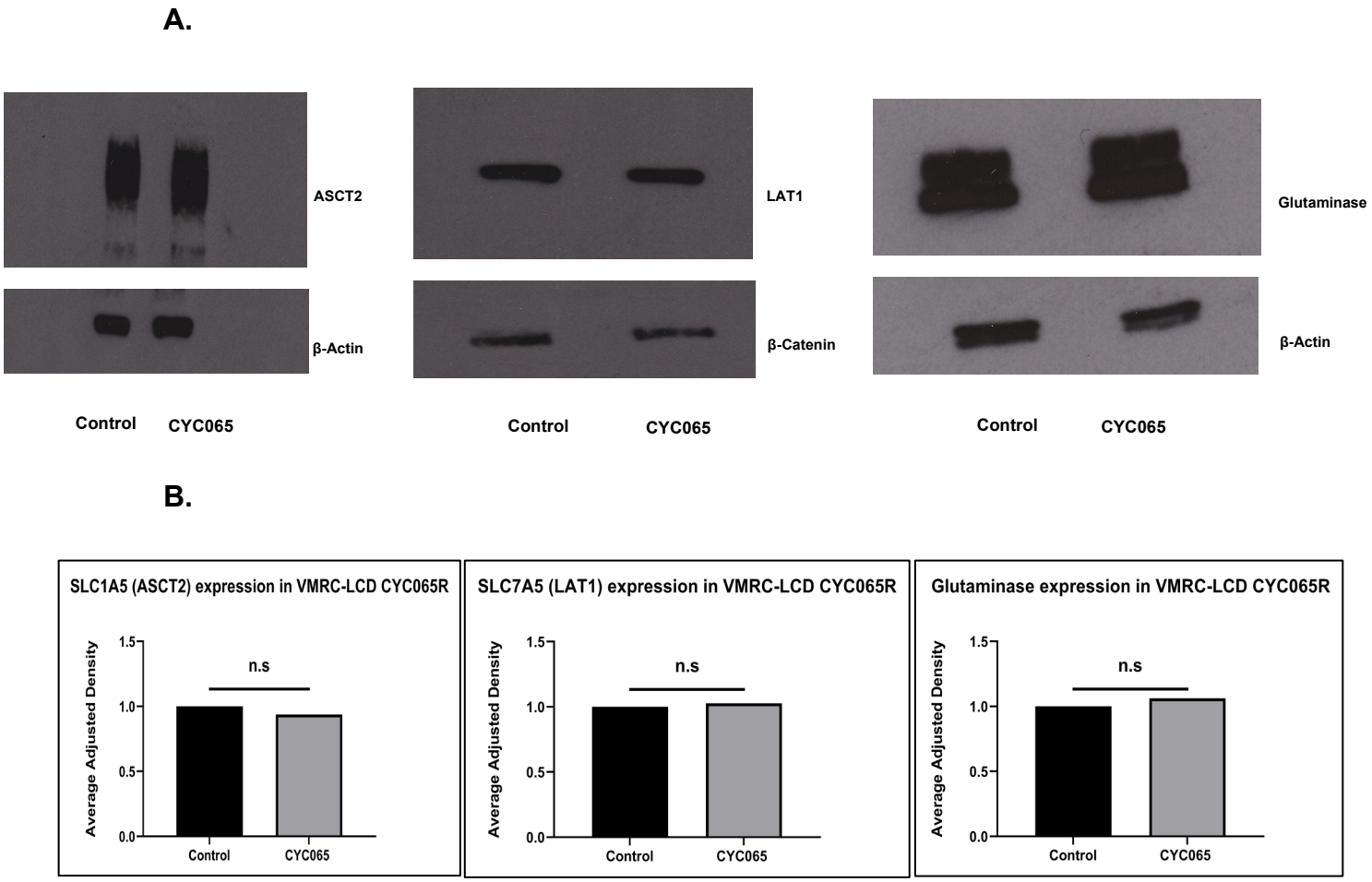

Figure 6.21. Glutamine transporter SLC1A5 (ASCT2), branched chain amino acid transporter SLC7A5 (LAT1) and glutaminase enzyme expression in VMRC CYC065R cells following CYC065 treatment. A. ASCT2, glutaminase and LAT1 expressions remain at a similar level in CYC065-treated VMRC CYC065R cells when compared with vehicle-treated controls. β-Actin was used as a loading control for ASCT2 and glutaminase. β-Catenin was used as a loading control for LAT1. **B.** Densitometry graphs showing the ASCT2, LAT1 and Glutaminase expressions in vehicle- and CYC065-treated VMRC CYC065R cells. The significance level was assessed by two-tailed Student's t-test. P values: n.s = not significant, n = 1.

6.3. Discussion

As described in a previous study by Hydbring and Larsson, Cdk2 is able to modulate the MYC capacity on suppression of senescence by phosphorylating MYC at Ser 62 (Hydbring and Larsson 2010). The loss of senescence might then lead to cancer initiation. Therefore, it was proposed that Cdk2 might become a potential target for future cancer treatment. It was initially shown that physiologic or pharmacologic inhibition of Cdk2 led to the suppression of subsequent MYC phosphorylation and turned MYC into an inducer of senescence which then prevents cancer initiation. Questions have then been raised on the detailed changes of cellular metabolites following Cdk2 inhibition and its effect on MYC, since it has been clearly demonstrated that MYC directly regulates many important metabolic pathways such as glycolysis and glutaminolysis.

In this chapter, ^{1}H-MRS was used to study the effect of Cdk2 inhibition by CYC065 on cellular metabolism, especially on the glutaminolysis pathway in MYC overexpressing cancer cell lines, Kelly and VMRC-LCD. The glutamine uptake decreased significantly following CYC065 treatment in both Kelly WT and VMRC WT cells. This is an expected outcome, as Cdk2 inhibition prevents the Cdk2-mediated phosphorylation of MYC and leads to the loss of MYC functions on cellular metabolism. It was clearly shown in a previous study that MYC directly induces the expression of important genes involved in glutamine metabolism, such as glutamine transporters ASCT2 and LAT1 (Deberardinis and Cheng 2010). This study also showed a reduction in the expression of these key glutamine transporters following Cdk2 and MYC inhibition. The decreased expression of LAT1 transporter could also lead to a fall in transporting branched side chain neutral amino acids into the cells, consistent with our observed decreases in leucine, iso-leucine and valine uptake following CYC065 treatment. The large reduction of glutamine uptake in VMRC WT cells contributed to a significant decrease in cellular glutamine level in this cell type. Consistent to the observed decrease in GLS expression level following Cdk2 and MYC inhibition, reductions in cellular glutamate and glutamate secretion were also seen in this study. This is not surprising since previous studies demonstrate that MYC controls the glutamine metabolism by upregulating the GLS enzyme (Wise et al. 2008; Gao et al. 2009).

In addition to the negative effect on glutaminolysis pathway following CYC065 treatment, the loss of MYC function caused by Cdk2 inhibition also led to a decrease

in glucose uptake in both cell types. However, the trend decrease in glucose uptake in Kelly WT is not statistically significant due to an inconsistent result in one of the three experiments and more experimental replicates are needed to confirm this result. The decrease in glucose uptake following CYC065 treatment can be explained by previous studies documenting that the activation of glucose metabolism pathway is one of the key functions of MYC (Osthus et al. 2000; Hu et al. 2011). MYC stimulates many glycolytic genes by binding to MYC consensus E-boxes (CACGTG) (Osthus et al. 2000; Kim et al. 2004). The results from this study suggest the importance of Cdk2 and MYC on glucose uptake and metabolism.

Interestingly, the cellular concentration of glucose and lactate remained unchanged in both Kelly WT and VMRC WT cells following CYC065 treatment despite a drop of glucose uptake. It was noted that Kelly WT cells changed metabolism from alanine secretion to uptake in order to maintain cellular alanine level during treatment. This phenomenon was not observed in VMRC WT cells. A previous study has found that some cancer cell types might alter metabolism to alanine dependence and convert alanine to glucose in glucose deprived conditions (Waterhouse et al.1979). Alanine can be converted by alanine aminotransferase enzyme (studied in Chapter 3) to pyruvate which then can enter the gluconeogenesis pathway to produce glucose to meet the high demand of cancer cell for glucose (Parker et al. 2020). It might also be a survival response to the effects of CYC065 treatment in Kelly WT cells. Adeva-Andany et al showed that cancer cells could use alanine cycle as an alternative pathway to insufficient glycolysis and glutaminolysis to support the TCA cycle and ATP production (Adeva-Andany et al. 2016). This might explain the unchanged level of ATP in Kelly WT cells, but not in VMRC WT cells in which a decrease of ATP level was observed. The mechanism by which the VMRC WT was able to utilize to maintain its cellular glucose level remains unknown. Beside alanine, there are other sources that can be used to generate glucose in mammalian cell lines, such as lactate, glycerol and glutamine (Garrett and Grisham 2002). Lactate can be a potential candidate in the case of VMRC since there was a decrease of lactate secretion, but not in intracellular level in this cell type. The cells might downregulate its lactate transporters (MCTs) to maintain its cellular lactate level and utilize lactate in a Cori cycle-like pathway to keep lactate and glucose at balance concentrations in adverse conditions (Halestrap 2013). Further experiments are needed to explain the exact roles of alanine and lactate in the

survival mechanism of Kelly WT and VMRC WT following treatment with CYC065. An application of ^{13}C-MRS using specific ^{13}C-labelled metabolites such as ^{13}C-alanine might be beneficial in providing a clearer picture of alanine cycle in which cancer cells utilize alanine to produce glucose or support TCA cycle and ATP production. ^{13}C-MRS has a wide chemical shift range which is typically 200 ppm, resulting in less spectral overlap and easier identification of interest metabolites (Clendinen et al. 2014). In addition, ^{13}C-Mass Spectrometry (^{13}C-MS) can also be applied in combination with ^{13}C-MRS in order to increase the number of detected metabolites or to analyse metabolites at low concentrations (picomole to femtomole) (Sumner et al. 2003; Bedair and Sumner 2008; Emwas 2015).

Taken together, the observed metabolic changes in the CYC065-treated wild-type cells remain unchanged in the CYC065-resistant cell lines following treatment, confirming that these observed metabolic changes are associated with the effect of CYC065 treatment. These results indicate that the Cdk2 inhibitor CYC065 provided some promising results on its effects on glucose and glutamine metabolism. However, it was also noted that cancer cells can still use other metabolic pathways to escape the effects of the inhibitor and survive. Further experiments are needed to provide a deeper understanding on the mechanism of this drug on cellular metabolism. The application of CYC065 as a single treatment or in combination with other therapies might depend on the type of tumour targeted and require further studies on different models of cancer. A combined therapy of CYC065 and alanine transporter inhibitors might be beneficial in the neuroblastoma Kelly cell line, as it adapted alanine metabolism for cell survival following CYC065 treatment. Parker et al suggested the alanine transporter SLC38A2 (SNAT2) plays an essential role in alanine uptake in cancer cells (Parker et al. 2020). Thus a concurrent inhibition of SNAT2 and Cdk2 kinase might have the desired anti-cancer effect on the Kelly cell line. Previous studies reported several SNAT2 inhibitors such as N-methylamino-isobutyric acid (Broer et al. 2016), or L-γ-glutamyl-p-nitroanilide (GPNA) (Broer et al. 2018) which might be applied in combination with CYC065 to treat neuroblastoma. A combination of CYC065 with dual mTOR inhibitors such as Vistusertib (AZD2014) (Pike et al. 2013; Basu et al. 2015; Guichard et al. 2015) or Sapanisertib (MLN0128) (Pourdehnab et al. 2013) which target the common node mTOR-4EBP1-eIF4E-MYC (Pourdehnab et al. 2013)

might also be considered as a potential cancer therapy for Myc-driven or mTOR-driven tumours.

In addition to investigate the effect of Cdk2 inhibition, by CYC065, on cancer cell metabolism, the studies reported in this chapter also examine the potential use of 4-[^{18}F]fluoroglutamine PET imaging to monitor tumour response following CYC065 treatment in future clinical trials. The *in vitro* uptake assays of 4-[^{18}F]fluoroglutamine and [^{18}F]FDG were initially carried out to investigate whether the outcomes obtained from this radiotracer uptake study were consistent with the observed changes of L-glutamine and D-glucose uptake from the ^{1}H-MRS study. This cell uptake experiment is a first step to confirm the inhibitor CYC065 also posed a similar effect on the uptake of PET radiotracers. Herein, the changes in 4-[^{18}F]fluoroglutamine and [^{18}F]FDG uptake are similar to the alterations of L-glutamine and D-glucose uptake in cancer cells following CYC065 treatment. Significant reductions in 4-[^{18}F]fluoroglutamine, [^{18}F]FDG, L-glutamine and D-glucose uptake were found in cancer cells following CYC065 treatment when compared with vehicle-treated control. The data again confirms the similar fate of these radiotracer analogues to their parental form. Further *in vivo* PET imaging trials can now be developed to examine the application of 4-[^{18}F]fluoroglutamine in monitoring the treatment response in tumour following the treatment with CYC065. Depending on the tumour type or stage of tumour growth, the use of either 4-[^{18}F]fluoroglutamine or [^{18}F]FDG should also be considered.

Chapter 7

Summary

7.1. Objectives and summary of the studies

- The first objective of this thesis has been to characterise the metabolic fate of the ^{18}F-glutamine based PET tracer called (2S, 4R)-4-[^{18}F]fluoroglutamine (4-[^{18}F]fluoroglutamine) in cancer cells and to confirm whether this radiotracer followed the same metabolic pathways as the L-glutamine (Chapter 3). The glutamine dependent colorectal cancer cell lines with a high expression of glutaminase enzyme HCT116 WT and HCT116 Bax-ko were used to study the metabolism of 4-[^{18}F]fluoroglutamine. The HCT116 Bax-ko cell line has an apoptosis accelerator Bax gene knocked out and subsequently has an impaired apoptosis pathway, which allows the evaluation of 4-[^{18}F]fluoroglutamine metabolism with minimal apoptosis signal following treatment with the inhibitors.
- The second objective has been to develop 4-[^{18}F]fluoroglutamine as an alternative non-invasive PET imaging method for [^{18}F]FDG undetected tumours (Chapter 4). Thirteen different cancer cell lines with different avidity for glucose and glutamine, HCT116 WT, HCT116 Bax-ko, PC3, Kelly, MDA-MB-231, TU8902, TU8988T, TU8988S, ASPC-1, T3M4, MIA PaCa-2, NCI-H508, DAN-G, were utilised to compare and investigate the potential use of 4-[^{18}F]fluoroglutamine as an alternative PET tracer to image [^{18}F]FDG undetected tumours.
- The third objective has been to examine 4-[^{18}F]fluoroglutamine PET as a potential strategy for the non-invasive monitoring of tumour response following therapy, such as the dual mTORC1/2 inhibitor AZD2014 as a single agent and in combination with Paclitaxel (Chapter 5) or the Cdk2 kinase inhibitor CYC065 (Chapter 6). The mTOR dependent and cisplatin-resistant ovarian (A2780cisR) and lung (H520) cancer cell lines were employed to examine the changes in 4-[^{18}F]fluoroglutamine uptake as a potential indicator for response following treatment with the dual mTORC1/2 inhibitor AZD2014 alone and in combination with Paclitaxel. The n-MYC overexpressing neuroblastoma cell line Kelly and c-MYC overexpressing non-small cell lung cancer cell line VMRC-LCD were

used to study the changes of L-glutamine and 4-[^{18}F]fluoroglutamine uptakes following treatment with CYC065, a Cdk2 kinase inhibitor.

A combination of MRS and PET imaging techniques were used to characterise the metabolism of 4-[^{18}F]fluoroglutamine and the metabolite changes associated with treatment response. In addition, biochemical assays, such as, cytotoxicity, *in vitro* radiotracer uptake and competitive inhibition assays and western blotting were also applied to support and complement the metabolic studies.

7.2. Overview of the chapters

7.2.1. Chapter 3: Evaluation of the metabolic pathways of 4-[^{18}F]fluoroglutamine PET tracer in cancer cells

In this chapter the metabolic pathways of 4-[^{18}F]fluoroglutamine were examined in HCT116 WT and HCT116 Bax-ko cells. The two main metabolic pathways of 4-[^{18}F]fluoroglutamine proposed by Cooper et al, which include the conversion of 4-[^{18}F]fluoroglutamine to 4-[^{18}F]fluoroglutamate by glutaminase and the γ-elimination of F^- from 4-[^{18}F]fluoroglutamate by alanine aminotransferase (Cooper et al. 2012), were examined by using the glutaminase inhibitor CB-839 and the alanine aminotransferase inhibitor L-cycloserine. ^{1}H-MRS was used to confirm the effectiveness of the chosen inhibitors on L-glutamine metabolism. A ^{19}F stable version of this PET tracer, 4-[^{19}F]fluoroglutamine has been synthesized by the Smith lab (ICR, Sutton, United Kingdom) for the metabolic study using ^{19}F-MRS. A significant increase in cellular glutamine and a decrease in glutamate were observed in both cell lines following glutaminase inhibition by CB-839 when compared to control, which is consistent with the mechanism of drug action. Similar results were also obtained with 4-[^{19}F]fluoroglutamine in which a significant increase of cellular 4-[^{19}F]fluoroglutamine and a decrease of cellular 4-[^{19}F]fluoroglutamate were found in CB-839-treated cells when compared with controls. Based on these findings, it could be concluded that 4-[^{18}F]fluoroglutamine can be enzymatically hydrolysed by the glutaminase enzyme in the same way as L-glutamine.

A significant increase in cellular glutamate was observed by ^{1}H-MRS following alanine aminotransferase inhibition by L-cycloserine. Interestingly, we found the cells changed their metabolism from alanine secretion to alanine uptake. This might be a response

of the cancer cells to rapidly replenish the depletion of cellular alanine level following L-cycloserine treatment. Cancer cells can upregulate alanine transporters such as SLC1A4 (ASCT1), SLC1A5 (ASCT2) and SLC38A2 (SNAT2) to maintain cellular alanine concentrations when alanine aminotransferase is inhibited (Parker et al. 2020). Hence, the intracellular alanine concentration remains unchanged after the drug treatment. Similar results were also observed with 4-[^{19}F]fluoroglutamate in which a significant increase of cellular 4-[^{19}F]fluoroglutamate was found.

Contrary to the hypothesis of this study, an increase in free F^- secretion following alanine aminotransferase treatment was found instead of a decrease. This finding suggests that the γ-elimination of F^- from 4-[^{19}F]fluoroglutamate might be taking place in other metabolic pathways, in addition to the catalysis by alanine aminotransferase as proposed by Cooper et al (Cooper et al. 2012). It might originate from a spontaneous non-enzymatic cellular degradation pathway of 4-[^{19}F]fluoroglutamate or other enzymatic pathways. These results confirmed 4-[^{19}F]fluoroglutamate, which is the downstream metabolic product of 4-[^{19}F]fluoroglutamine, can be metabolised by the alanine aminotransferase enzyme as L-glutamate. Further experiments will need to be carried out to fully determine the mechanisms behind the release of free F^- from the PET tracer 4-[^{18}F]fluoroglutamine.

Taken together, the observed changes indicate that similar to L-glutamine, 4-[^{19}F]fluoroglutamine can be metabolised in cancer cells by the glutaminase enzyme to yield 4-[^{19}F]fluoroglutamate, which further metabolised by the alanine aminotransferase enzyme. Beside the alanine aminotransferase pathway, the release of free fluoride from 4-[^{19}F]fluoroglutamate might be resulted from spontaneous cellular degradations of the compound or other enzymatic pathways.

7.2.2. Chapter 4: *In vitro* and *in vivo* uptake of 4-[^{18}F]fluoroglutamine and [^{18}F]FDG in a panel cancer cell lines

Chapter 4 provided an overview of different avidity for 4-[^{18}F]fluoroglutamine and [^{18}F]FDG as well as glucose and glutamine in thirteen different cell lines; HCT116 WT, HCT116 Bax-ko, PC3, Kelly, MDA-MB-231, TU8902, TU8988T, TU8988S, ASPC-1, T3M4, MIA PaCa-2, NCI-H508, DAN-G. This chapter confirmed 4-[^{18}F]fluoroglutamine produced a comparable signal intensity and tumour detection ability to [^{18}F]FDG in

glutamine dependent tumours PC3 without the need of fasting in mouse xenograft models. First, an *in vitro* uptake study was carried out in thirteen different cell lines. The 4-[^{18}F]fluoroglutamine uptake study showed a similar trend to the uptake study of L-glutamine by ^{1}H-MRS. In the case of [^{18}F]FDG and D-glucose uptake studies, most of the cell lines had a similar uptake trend for the two substrates. However, the Kelly cells had a much higher uptake of D-glucose than [^{18}F]FDG. It has been found that some cell types exhibited a high glutamine and 4-[^{18}F]fluoroglutamine influx, but low glucose and [^{18}F]FDG uptake (Kelly, TU8988S). Overall, these findings again confirmed the similar fate between 4-[^{18}F]fluoroglutamine and L-glutamine.

In order to investigate the intracellular level of radiotracers 4-[^{18}F]fluoroglutamine and [^{18}F]FDG over time, a time dependent cell uptake studies in glutamine dependent PC3 and glucose dependent HCT116 WT cell lines were also performed. Maximal cellular 4-[^{18}F]fluoroglutamine levels were reached at 1 hour before decreasing in both cell types, this could be due to the metabolism of 4-[^{18}F]fluoroglutamine after this time point or the efflux of 4-[^{18}F]fluoroglutamine to exchange for other amino acids. The dose dependent response to L-glutamine assay indicated that 4-[^{18}F]fluoroglutamine can enter the cell via the same transporters as L-glutamine, which is known as the substrate of glutamine import/export transporter systems N (SNAT5) and ASC (ASCT2) (Broer et al. 1999; Chaudhry et al. 1999). On the other hand, a maximal constant level of cellular [^{18}F]FDG was found in both cell lines after 1 hour. [^{18}F]FDG was found to be transported by GLUT-1 and GLUT-3, the same transporters as D-glucose (Brown and Wahl 1993; Reske et al. 1997; Brown et al. 1999).

Biodistribution and PET studies using 4-[^{18}F]fluoroglutamine and [^{18}F]FDG exhibited the expected higher tumour uptake of [^{18}F]FDG than 4-[^{18}F]fluoroglutamine in glucose avid HCT116 WT xenograft model. However, no significant difference in the uptake of the two radiolabelled tracers was found in PC3 tumours. This result is not consistent with the *in vitro* cell uptake studies in which PC3 cells showed a higher uptake 4-[^{18}F]fluoroglutamine than [^{18}F]FDG . Some of the factors that affect the uptake of 4-[^{18}F]fluoroglutamine *in vivo* could be due to the competition in uptake with L-glutamine, the influx/efflux rate of 4-[^{18}F]fluoroglutamine and the tumour metabolism of 4-[^{18}F]fluoroglutamine. The competition with normal substrate was minimised in [^{18}F]FDG imaging by fasting before the scans are taken.

The metabolism of 4-[^{18}F]fluoroglutamine in which alanine aminotransferase cleaved the C-F bond and produced free F^- might potentially cause problems with *in vivo* tumour diagnosis and image interpretation. The high uptake of free fluoride in bones might lead to high background signals and radiotracer accumulation in the skeleton which can hinder the analysis of tumours that are situated close to bones. An approach to increase the stability of 4-[^{18}F]fluoroglutamine is by replacing the hydrogen atoms on the β-carbon atom (close to the ^{18}F atom) with deuterium atoms. The activation energy of C-D bond in biochemical reactions is higher than the C-H bond. Hence, the cleavage of C-D bond is slower than the C-H bond in similar conditions (Kuchar and Mamat 2015).

High pancreas uptake of 4-[^{18}F]fluoroglutamine, which is due to the pancreas's exocrine function and high use of amino acids as precursors for protein and peptide synthesis (Lieberman et al. 2011), might also lead to a high background signal which can interfere with detecting tumours that are situated close to the pancreas or bladder. However, improvements have been made on PET/CT scanners to achieve better tumour detection capabilities by using new hardware, digital photomultipliers and faster electronics to implement better image reconstruction. PET sensitivity has also been enhanced by applying a larger axial field of view and 3D imaging (Slomka et al. 2016; Zhang et al. 2018). Hence, the high background signal in the pancreas might not be a critical issue of tumour diagnosis in the current era.

4-[^{18}F]fluoroglutamine PET imaging can be performed without fasting beforehand because glutamine is a non-essential amino acid which means the body is able to synthesize a sufficient amount for its own use when necessary and does not primarily rely on diet (Dunphy et al. 2018). Although 4-[^{18}F]fluoroglutamine did not produce a higher signal intensity than [^{18}F]FDG in the glutamine dependent PC3 tumour model, this glutamine PET tracer could still produce a comparable signal and tumour detection ability to [^{18}F]FDG in this glutamine dependent tumour model without the need of fasting. Thus, 4-[^{18}F]fluoroglutamine is ideal for patients with glutamine dependent tumour like PC3 prostate cancer model who might have difficulties with the fasting requirement, such as the diabetics.

Some cancer cell lines examined in this study, such as the neuroblastoma cancer cell line Kelly, demonstrated a very high uptake of 4-[^{18}F]fluoroglutamine. Hence, 4-

[^{18}F]fluoroglutamine may be an alternatively tool to [^{18}F]FDG for detecting glioma in patients, as [^{18}F]FDG has been shown to produce false positive signals due to a high uptake of [^{18}F]FDG in normal brain tissue (Hari et al. 2013). A previous study has shown 4-[^{18}F]fluoroglutamine produced a better tumour to brain ratio than [^{18}F]FDG (Zhu et al. 2017).

4-[^{18}F]fluoroglutamine can be used to monitor glutamine uptake and metabolic changes in tumours following treatment with inhibitors that target the glutaminolysis pathway. The effects of these inhibitors cannot be detected specifically by [^{18}F]FDG. 4-[^{18}F]fluoroglutamine can also be utilised as a complementary tool to [^{18}F]FDG, in order to provide broader information on cancer metabolism, as these radiotracers can assess different important metabolic pathways of cancer, namely glycolysis and glutaminolysis.

7.2.3. Chapter 5: PI3K/AKT/mTOR pathway and Glutamine Metabolism

In Chapter 5, the application of 4-[^{18}F]fluoroglutamine as a potential tool for assessment of treatment response in cancer was investigated. 4-[^{18}F]fluoroglutamine was used to monitor the glutamine uptake changes in mTOR dependent and cisplatin-resistant ovarian (A2780cisR) and lung (H520) cancer models following mTOR pathway inhibition by using AZD2014 as a single agent and in combination with Paclitaxel chemotherapy. The *in vitro* uptake assay of 4-[^{18}F]fluoroglutamine showed substantial increases in 4-[^{18}F]fluoroglutamine uptake and ASCT2 glutamine transporter expression in both A2780cisR and H520 cell lines following the treatments with AZD2014 alone and in combination with Paclitaxel when compared with controls. The increased glutamine uptake following mTOR inhibition was suggested to be a resistance mechanism of cancer cells against mTOR kinase inhibitors. Tanaka et al observed an increase of glutamine uptake and glutamine metabolism via the TCA cycle which promotes resistance to mTOR kinase inhibitors, rapamycin and PP242 (Tanaka et al. 2015).

Further *in vivo* PET imaging studies in tumour models can now be developed to examine the application of 4-[^{18}F]fluoroglutamine in monitoring tumour response to treatment with mTOR inhibitor, AZD2014, as a single agent and in combination with Paclitaxel chemotherapy. This study will provide information on the changes in 4-

[^{18}F]fluoroglutamine PET signal intensities before and after treatment and solidify necessary steps for the development of this imaging radiotracer in future clinical trials. It is expected that a similar trend to the *in vitro* uptake in which 4-[^{18}F]fluoroglutamine uptake increases following the treatment with AZD2014 alone and in combination therapy with Paclitaxel can be observed.

7.2.4. Chapter 6: Evaluating the effect of Cdk2 Kinase Inhibition on Glutamine Metabolism

Chapter 6 describes the application of 4-[^{18}F]fluoroglutamine as a potential tool for assessing treatment response in cancer following MYC signalling pathway inhibition of. 4-[^{18}F]fluoroglutamine was used to monitor the glutamine uptake changes in MYC dependent neuroblastoma (Kelly) and lung (VMRC-LCD) cancer models following Cdk2 kinase inhibition by CYC065. The phosphorylation of MYC by Cdk2 was shown to be essential in suppressing senescence and promoting tumour growth (Hydbring et al. 2010). ^{1}H-MRS was used to study the effect of Cdk2 inhibition by CYC065 on cellular metabolism, especially on the glutaminolysis pathway. Glutamine uptake decreased significantly following CYC065 treatment. This was an expected outcome since Cdk2 inhibition prevents Cdk2-mediated phosphorylation of MYC and leads to the loss of MYC function on cellular metabolism. MYC was previously known to induce the expression of important enzymes and transporters in the glutaminolysis pathway, such as glutaminase enzyme (Wise et al. 2008; Gao et al. 2009) and glutamine transporters ASCT2 (SLC1A5) and LAT1 (SLC7A5) (Deberardinis and Cheng 2010). It was found in this study that the expression of these important glutamine transporters and glutaminase reduced significantly following Cdk2 and MYC inhibition. The decreased expression of LAT1 transporter also led to a fall in its ability to transport large, branched side chain neutral amino acid into the cell.

In addition to the negative effect on glutamine and branched chain amino acid uptake, the loss of MYC function caused by Cdk2 inhibition also led to a decrease in glucose uptake. MYC was known to activate the glucose metabolism pathways (Osthus et al. 2000; Hu et al. 2011). Interestingly, the cellular concentration of glucose and lactate remained unchanged in both Kelly WT and VMRC WT cells following drug treatment despite a decrease in glucose uptake. It was noted that Kelly WT cells changed its

metabolism from alanine secretion to alanine uptake to maintain its cellular levels following CYC065 treatment. This phenomenon might be a survival response of cancer cells to Cdk2 and MYC inhibition by using alanine to maintain cellular glucose level and metabolism, as shown previously that cancer cells can convert alanine to glucose in a glucose deprived environment (Waterhouse et al.1979). In the case of VMRC WT cells, lactate can be a potential candidate to maintain cellular glucose level since there was a decrease of lactate secretion, but not in intracellular level in this cell type. The cell might downregulate its lactate transporters (MCTs) to maintain its cellular lactate level and utilize lactate in a Cori cycle like pathway to maintain glucose metabolism in adverse conditions (Halestrap 2013).

Taken together, these results indicate that the Cdk2 inhibitor CYC065 had a negative impact on glucose and glutamine metabolism in cancer cells. However, it was also noted that cancer cells can still utilise other pathways to survive the impacts from the inhibition. Further experiments are needed to provide a deeper understanding on the mechanism of this drug on cellular metabolism. The use of CYC065 as a single agent or in combination with other therapies might depend on the type of tumour targeted and require further studies on different models of cancer.

Similar to the L-glutamine uptake changes, a decrease in 4-[^{18}F]fluoroglutamine uptake was also found in cancer cells following treatment with the Cdk2 inhibitor CYC065. In addition, [^{18}F]FDG uptake also decreased following the drug treatment. These data were consistent with the results from ^{1}H-MRS study.

Further *in vivo* PET imaging studies in tumour models can now be developed to examine the use of 4-[^{18}F]fluoroglutamine in monitoring treatment response in tumours following treatment with the Cdk2 inhibitor CYC065. It is expected that a decrease of 4-[^{18}F]fluoroglutamine PET signal intensity, which is consistent with the *in vitro* uptake study, can be achieved after treatment. The information obtained from the *in vivo* experiments will be essential for the development of this imaging tool in future clinical trials.

7.3. Conclusions and future work

The work presented in this thesis contributes towards the understanding of how (2S, 4R)-4-[^{18}F]fluoroglutamine (4-[^{18}F]fluoroglutamine) is metabolised by cancer cells. The data described here also confirmed 4-[^{18}F]fluoroglutamine is a true surrogate for L-

glutamine and has potential applications in monitoring cancer, such as using as an alternative non-invasive PET imaging method for [^{18}F]FDG undetected tumours, or quantifying treatment response in tumours. Figure 7.1 summarizes the confirmed metabolic pathways of 4-[^{18}F]fluoroglutamine in cancer cells.

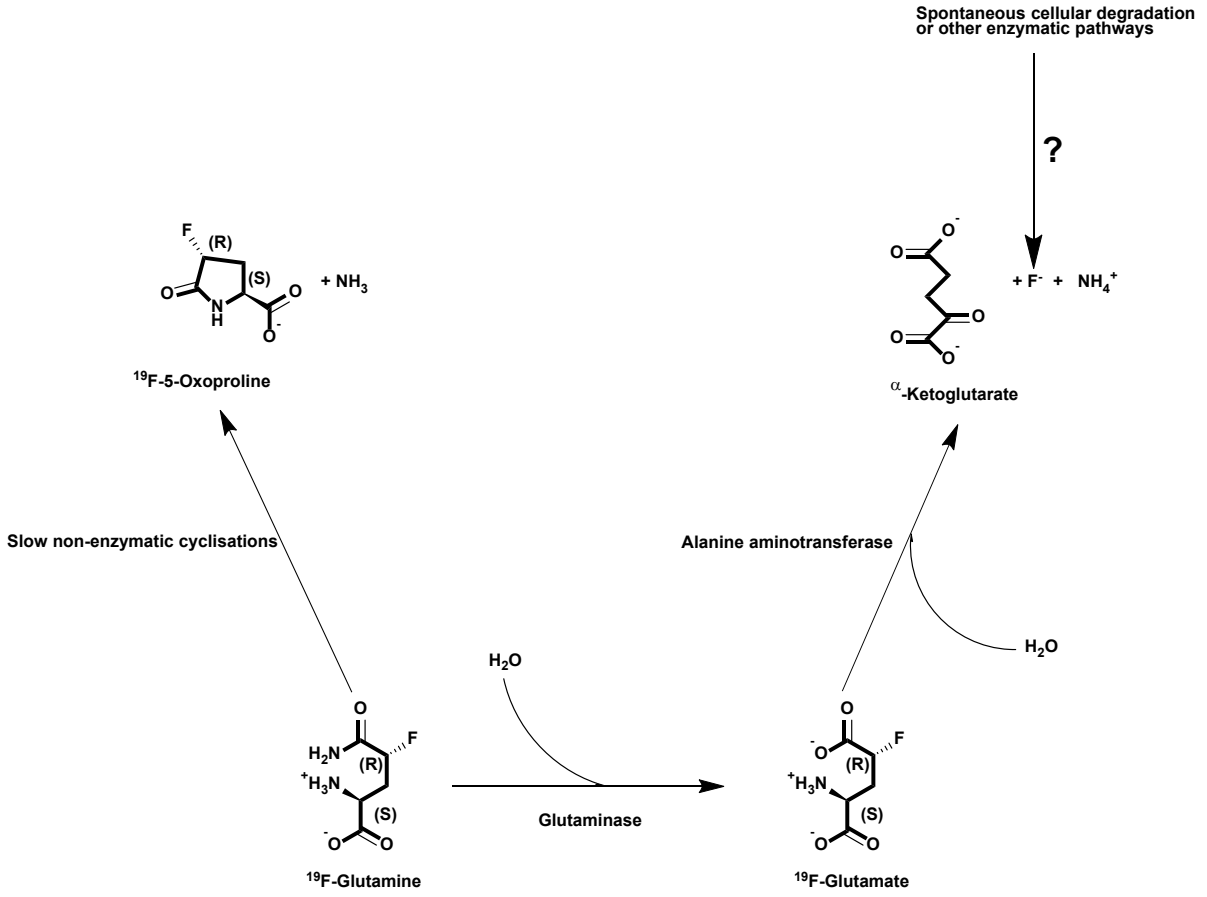

Figure 7.1. The proposed metabolic pathways of (2S, 4R)-4-[^{18}F]fluoroglutamine (4-[^{18}F]fluoroglutamine). 4-[^{18}F]fluoroglutamine can be enzymatically hydrolysed to 4-[^{18}F]fluoroglutamate by the glutaminase enzyme in the same way as L-glutamine. 4-[^{18}F]fluoroglutamate can be metabolised by the alanine aminotransferase enzyme as L-glutamate. Beside alanine aminotransferase enzyme, the defluorination of 4-[^{18}F]fluoroglutamine might also come from a spontaneous cellular degradation or other enzymatic pathways. Slow non-enzymatic cyclisations can lead to the formation of 4-^{18}F-5-oxoproline.

Previous findings in the metabolism of 4-[^{18}F]fluoroglutamine by Cooper et al, indicated the possible involvement of two key metabolic enzymes, glutaminase and alanine aminotransferase, in the glutamine metabolic pathway (Cooper et al. 2012). The metabolism of 4-[^{18}F]fluoroglutamine by these two enzymes in cancer cells were studied in detail in this research. The work in this thesis expanded the enzymology model study of Cooper et al by using a complex cellular system and confirmed 4-[^{18}F]fluoroglutamine follows a similar metabolic pathways as L-glutamine. However, the origin of the observed free F^- is not fully understood. 4-[^{19}F]fluoroglutamine and 4-[^{19}F]fluoroglutamate were found to be stable in cell culture media, as no free F^- was detected before cell incubation (Fig. 3.11A & B). The free F^- was only detected when 4-[^{19}F]fluoroglutamine was incubated with cells (Fig. 3.11C) and the γ-elimination of F^- from this glutamine analogue might be due to a spontaneous cellular degradation or other enzymatic pathways, in addition to the alanine aminotransferase catalytic pathway. Cooper et al also proposed that 4-[^{19}F]fluoroglutamate may be metabolised by glutamate dehydrogenase (converting normal mitochondrial glutamate to α-ketoglutarate) to form 4-Fluoro-α-ketoglutarate which might be another starting point for the γ-elimination of F^- ion (Cooper et al. 2012). As it has been found in this study, more free F^- was generated when a higher concentration of 4-[^{19}F]fluoroglutamate accumulated, which is the substrate of glutamate dehydrogenase enzyme. Further *in vitro* MRS experiments using glutamate dehydrogenase inhibitors are required to fully characterize the possible involvement of glutamate dehydrogenase enzyme in the release of free F^-. Glutamate dehydrogenase inhibitors such as (−)-Epigallocatechin-monogallate (EGCG), hexachlorophene (HCP) or bithionol (BTH) (Li et al. 2009; Whitelaw and Robinson 2013) can be used to assess whether a decrease in free F^- release can be observed in conjunction with an accumulation of 4-[^{19}F]fluoroglutamate. These studies can be performed in a similar fashion to the L-cycloserine studies, where ^{1}H-MRS can first be used to confirm the effectiveness of chosen inhibitors on L-glutamate metabolism in cancer cells and ^{19}F-MRS can then be carried out to monitor the changes of the free fluoride secretion following treatment with the inhibitors.

In this study, 4-[^{18}F]fluoroglutamine was also shown to have potential future application to patients who have difficulties with the fasting requirement of [^{18}F]FDG by producing a comparable signal intensity to the traditional [^{18}F]FDG PET imaging

without the need of fasting. It was, indeed, expected to achieve a better signal with 4-[^{18}F]fluoroglutamine than [^{18}F]FDG for the glutamine dependent cancer model PC3 in this research. However, our findings are consistent with previous studies by Dunphy et al and Zhu et al that 4-[^{18}F]fluoroglutamine produced a “comparable” but not “higher” signal intensity when compared with [^{18}F]FDG even in glutamine dependent cancer models (Dunphy et al. 2018; Zhu et al. 2019). These data reshaped future potential applications of 4-[^{18}F]fluoroglutamine. Patients with metabolic diseases, such as diabetes, are struggling with a non-caloric intake requirement for [^{18}F]FDG PET imaging. Hence, 4-[^{18}F]fluoroglutamine is beneficial for this group of patients.

Considering the plasticity of metabolism in different sizes and stages of tumour, further *in vivo* studies comparing the signal intensity of 4-[^{18}F]fluoroglutamine and [^{18}F]FDG in different developmental stages of tumour should be developed. This will help to establish a method of using either 4-[^{18}F]fluoroglutamine or [^{18}F]FDG to assess the correct stage of tumour growth. Alternatively, *in vivo* experiments which utilise longitudinal PET scannings to study different stages of tumour growth can be applied on the same cohort of animals to reflect the changes in cancer metabolism and associated radiotracer uptake.

The potential of applying 4-[^{18}F]fluoroglutamine in monitoring treatment response in cancer is promising. In this study, consistent results were obtained from the uptake studies of 4-[^{18}F]fluoroglutamine and glutamine uptake following treatment with a dual mTOR inhibitor, AZD2014, or a Cdk2 inhibitor, CYC065. These results suggest 4-[^{18}F]fluoroglutamine PET tracer can be used to monitor treatment response in tumours. Further *in vivo* studies of using 4-[^{18}F]fluoroglutamine PET imaging to examine the effect of AZD2014 and CYC065 on glutamine uptake in tumours are required for future clinical trial applications.

The pharmacologic inhibition of Cdk2 by CYC065 exhibited negative effects on glucose, glutamine, and branched chain amino acid uptake and metabolism in cancer cell lines (Kelly and VMRC-LCD). To identify and confirm whether these metabolic changes genuinely caused by the inhibition of Cdk2 and suppression of subsequent MYC phosphorylation, it is necessary to perform knockdown experiments of Cdk2 and MYC genes and utilize ^{1}H-MRS to measure the subsequent metabolic effects. Immunoblotting will also be carried out to quantify the protein expressions of relevant

transporters and enzymes such as ASCT2, LAT1, and glutaminase following the Cdk2 and MYC genes knockdown. As it was shown in previous studies, the activation of MYC increases the expression of genes involved in glutamine transport ASCT2 and LAT1 and glutaminase enzyme (Chang et al. 2008; Wise et al. 2008; Deberardinis and Cheng 2010; Dang 2013).

Further experiments will be needed to provide understanding on the application of CYC065 as a single treatment or in combination with other therapies. Despite the promising effects of CYC065 on glucose and glutamine uptake and metabolism, it was also noted that cancer cells can still use other metabolic pathways (e.g switching to alanine metabolism) to escape the effects of the inhibitor and survive. Further experiments are needed to exploit the exact role of alanine in the survival mechanism of cancer cells following treatment with CYC065. An application of ^{13}C-MRS using specific ^{13}C-labelled metabolites such as ^{13}C-alanine might be beneficial in providing a clearer picture of alanine cycle in which cancer cells utilize alanine to produce glucose or support TCA cycle and ATP production. ^{13}C-MRS has a wide chemical shift range which is typically 200 ppm, resulting in less spectral overlap and easier identification of metabolites of interest (Clendinen et al. 2014). In addition, ^{13}C-Mass Spectrometry (^{13}C-MS) can also be applied in combination with ^{13}C-MRS in order to increase the number of detected metabolites or to analyse metabolites at low concentrations (picomole to femtomole) (Sumner et al. 2003; Bedair and Sumner 2008; Emwas 2015).

A combined therapy of CYC065 and alanine transporter inhibitors might be beneficial in the case of cancer cells which altered its metabolism to alanine dependence. Parker et al suggested the alanine transporter SLC38A2 (SNAT2) plays an essential role in alanine uptake in cancer cells (Parker et al. 2020). Thus a concurrent inhibition of SNAT2 and Cdk2 kinase might provide a more effective treatment of cancer than Cdk2 kinase inhibition alone. Previous studies reported several SNAT2 inhibitors such as N-methylamino-isobutyric acid (Broer et al. 2016), or L-γ-glutamyl-p-nitroanilide (GPNA) (Broer et al. 2018) which might be applied in a combined therapy with CYC065.

The mTOR-4EBP1-eIF4E-MYC axis has been recognised as an important common node for the survival of cancers from MYC-dependent tumorigenesis or mTOR-dependent tumorigenesis (Pourdehnab et al. 2013). A combination of CYC065 with

dual mTOR inhibitors such as Vistusertib (AZD2014) (Pike et al. 2013; Basu et al. 2015; Guichard et al. 2015) or Sapanisertib (MLN0128) (Pourdehnab et al. 2013) which target the common node mTOR-4EBP1-eIF4E-MYC (Pourdehnab et al. 2013) might also be considered as a potential cancer therapy for Myc-driven or mTOR-driven tumours.

In conclusion, the studies in this thesis facilitates better understanding of 4-[^{18}F]fluoroglutamine metabolic fate and applications. It is a sensitive tool for studying glutamine transport and metabolism in cancer. Besides, this PET tracer can be further applied in multiple studies of normal glutamine metabolism in different human organs, specifically brain, muscle, liver, kidney and small intestine. 4-[^{18}F]fluoroglutamine PET imaging can be used as an alternative tool for [^{18}F]FDG undetected tumours, or for patients who have difficulties with the fasting requirement of the traditional [^{18}F]FDG PET imaging. 4-[^{18}F]fluoroglutamine can also be used as a complementary imaging method to [^{18}F]FDG to provide a more detailed picture of disease metabolism for a better diagnosis. The ability of 4-[^{18}F]fluoroglutamine to monitor treatment effects on cancer proves its importance in understanding therapies that target the glutamine metabolism and cannot be elucidated using [^{18}F]FDG.

References

1. Adeva-Andany, M.M., Pérez-Felpete, N., Fernández-Fernández, C., Donapetry-García, C., Pazos-García, C. (2016). Liver glucose metabolism in humans. *Biosci Rep*, 36, e00416.
2. Adler, L.P., Crowe, J.P., al-Kaisi, N.K., Sunshine, J.L. (1993). Evaluation of breast masses and axillary lymph nodes with [F-18] 2-deoxy-2-fluoro-D-glucose PET. *Radiology*, 187, 743–750.
3. Alfarouk, K.O., Verduzco, D., Rauch, C., Muddathir, A.K., et al. (2014). Glycolysis, tumor metabolism, cancer growth and dissemination. A new pH-based etiopathogenic perspective and therapeutic approach to an old cancer question. *Oncoscience*, 1, 777-802.
4. Almuhaideb, A., Papathanasiou, N., Bomanji, J. (2011). ^{18}F-FDG PET/CT Imaging In Oncology. *Ann Saudi Med*, 31, 3–13.
5. Al-Saffar, N.M.S., Marshall, L.V., Jackson, L.E., Balarajah, G. et al (2014). Lactate and choline metabolites detected *in vitro*by nuclear magnetic resonance spectroscopy and potential metabolic biomarkers for pi3k inhibition in pediatric glioblastoma. *Plos ONE*, 9, e103835.
6. Avril, N., Bense, S., Ziegler, S.I., Dose, J., Weber, W., Laubenbacher, C., Romer, W., Janicke, F., Schwaiger, M. (1997). Breast imaging with fluorine-18-FDG PET: quantitative image analysis. *J Nucl Med*, 38, 1186–1191.
7. Avril, N., Menzel, M., Dose, J., Schelling, M., Weber, W., Janicke, F., Nathrath, W., Schwaiger, M. (2001). Glucose metabolism of breast cancer assessed by 18F-FDG PET: histologic and immunohistochemical tissue analysis. *J Nucl Med*, 42, 9–16.
8. Avril, N., Rose, C.A., Schelling, M., Dose, J., Kuhn, W., Bense, S., Weber, W., Ziegler, S., Graeff, H., Schwaiger, M. (2000). Breast imaging with positron emission tomography and fluorine-18 fluorodeoxyglucose: use and limitations. *J Clin Oncol.*, 18, 3495–3502.
9. Babu, U.M., Johnston, R.B. (1976). Nuclear magnetic resonance studies of D2O-substrate exchange reactions catalyzed by glutamic pyruvic and glutamic oxaloacetic transaminases. *Biochemistry*, 15, 5671–5678.

10. Bader, A.G., Kang, S., Zhao, L., Vogt, P.K. (2005). Oncogenic PI3K deregulates transcription and translation. *Nat rev Cancer*, 5, 921-929.
11. Bae, S.U., Won, K.S., Song, B-I., Jeong, W.K., Baek, S.K., Kim, H.W. (2018). Accuracy of F-18 FDG PET/CT with optimal cut-offs of maximum standardized uptake value according to size for diagnosis of regional lymph node metastasis in patients with rectal cancer. *Cancer Imaging*, 18, 32.
12. Bailey, D.L, Townsend, D.W., Valk, P.E., Maisey, M.N. (2005). Positron Emission Tomography: Basic Sciences. Secaucus, NJ: Springer-Verlag.
13. Baird, F.E., Beattie, K.J., Hyde, A.R., Ganapathy, V., Rennie, M.J. and Taylor, P.M. (2004). Biodirectional substrate fluxes through the system N (SNAT5) glutamine transporter may determine net glutamine flux in rat liver. *J Physio.*, 559,367-381.
14. Baird, R.D., Tan, D.S., Kaye, S.B. (2010). Weekly paclitaxel in the treatment of recurrent ovarian cancer. *Nat Rev Clin Oncol*, 7, 575–582.
15. Barwick, T., Bencherif, B., Mountz, J.M., Avril, N. (2009). Molecular PET and PET/CT imaging of tumour cell proliferation using F-18 fluoro-L-thymidine: a comprehensive evaluation. *Nuclear Medicine communications*, 30.
16. Basu, B., Dean, E., Puglisi, M., Greystoke, A., et al. (2015). First-in-Human Pharmacokinetic and Pharmacodynamic Study of the Dual m-TORC 1/2 Inhibitor AZD2014. *Clin Cancer Res*, 21, 3412–3419.
17. Basu, B., Dean, E., Puglisi, M., Greystoke, A., et al. (2015). First-in-human pharmacokinetic and pharmacodynamic study of the dual m-TORC 1/2 inhibitor, AZD2014. *Clin Cancer Res*, 21, 3412–3419.
18. Basu, B., Krebs, M.G., Sundar, R., Wilson, R.H., et al. (2018). Vistusertib (dual m-TORC1/2 inhibitor) in combination with paclitaxel in patients with high-grade serous ovarian and squamous non-small-cell lung cancer. *Ann Oncol*, 29,1918-1925.
19. Baumann, M., Krause, M., Overgaard, J., Debus, J., Bentzen, S.M., Daartz, J., Richter, C., Zips, D., Bortfeld, T. (2016). Radiation oncology in the era of precision medicine. *Nature Reviews*, 16, 234-249.
20. Bedair, M., Sumner, L.W. (2008). Current and emerging mass-spectrometry technologies for metabolomics. *Trends Anal Chem*, 27, 238–250.
21. Belouche-Barbari, M., Chung, Y-L, Al-Saffar, N.M.S, Falck-Miniotis, M., Leach, M.O. (2010). Metabolic assessment of the action of targeted cancer

therapeutics using magnetic resonance spectroscopy. *British Journal of Cancer*, 102, 1-7.

22. Beykan, S., Dam, J.S., Eberlein, U., Kaufmann, J., et al. (2016). 177Lu-OPS201 targeting somatostatin receptors: in vivo biodistribution and dosimetry in a pig model. *EJNMMI Res*, 6, 1–9.
23. Bida, G.T., Satyamurthy, N., Barrio, J.R. (1984). The synthesis of 2-[F-18]fluoro-2-deoxy-D-glucose using glycals: a reexamination. *Journal of Nuclear Medicine*, 25, 1327-1334.
24. Blau, N., Duran, M., Gibson, K.M. (2008). Amino acids. In laboratory Guide to the Methods in Biochemical Genetics. *Springer Science & Business Media*.
25. Bolan, P.J., Meisamy, S., Baker, E.H., Lin, J., et al. (2003). In vivo quantification of choline compounds in the breast with 1H MR spectroscopy. *Magnetic Resonance in Medicine*, 50.
26. Bolzoni, M. *et al*. (2016). Dependence on glutamine uptake and glutamine addiction characterize myeloma cells: a new attractive target. *Blood*, 128, 667–79.
27. Bondi, A. (1964). van derWaals volumes and radii. *J Chem Phys*, 68, 441–664.
28. Boros, E., Pinkhasov, O.R., Caravan, P. (2018). Metabolite profiling with HPLC-ICP-MS as a tool for in vivo characterization of imaging probes. *EJNMMI radiopharm. chem*, 3, 2.
29. Bos, R., van Der Hoeven, J.J., van Der Wall, E., van Der Groep, P., et al. (2002). Biologic correlates of (18)fluorodeoxyglucose uptake in human breast cancer measured by positron emission tomography. *J Clin Oncol*, 20, 379–387.
30. Bott, A.J., Shen, J., Tonelli, C., Zhan, L. et al. (2019). Glutamine Anabolism Plays a Critical Role in Pancreatic Cancer by Coupling Carbon and Nitrogen Metabolism. *Cell Reports*, 29, 1287-1298.
31. Brachmann, S., Fritsch, C., Maira, S-M., García-Echeverría, C. (2009). PI3K and mTOR inhibitors—a new generation of targeted anticancer agents. *Current Opinion in Cell Biology*, 21, 194–8.
32. Bradford, M. (1976). A Rapid and Sensitive Method for the Quantification of Microgram Quantities of Protein Utilizing the Principle of Protein-Dye Binding. *Anal Biochem*, 72, 248.
33. Brasseur, K., Gevry, N., Asselin, E. (2016). Chemoresistance and targeted therapies in ovarian and endometrial cancers. *Oncotarget*, 8, 4008–4042.

34. Bray, F., Ferlay, J., Soerjomataram, I., Siegel, R.L., Torre, L.A., Jemal, A. Global Cancer Statistics 2018: GLOBOCAN Estimates of Incidence and Mortality Worldwide for 36 Cancers in 185 Countries. Lyon, France: International Agency for Research on Cancer. Available at: http://globocan.iarc.fr. Last accessed 23/01/2020.
35. Bray, F., Ferlay, J., Soerjomataram, I., Siegel, R.L., Torre, L.A., Jemal, A. (2018). Global cancer statistics 2018: GLOBOCAN estimates of incidence and mortality worldwide for 36 cancers in 185 countries. *CA Cancer J Clin*, 68, 394-424.
36. Broer, A., Brookes, N., Ganapathy, V., Dimmer, K., Wagner, C., Lang, F., Broer, S. (1999). The Astroglial ASCT2 Amino Acid Transporter as a Mediator of Glutamine Efflux. *Journal of Neurochemistry*, 73, 2184-2194.
37. Bröer, A., Fairweather, S., Bröer, S. (2018). Disruption of Amino Acid Homeostasis by Novel ASCT2 Inhibitors Involves Multiple Targets. *Front Pharmacol*, 9, 785.
38. Bröer, A., Rahimi, F., Bröer, S. (2016). Deletion of Amino Acid Transporter ASCT2 (SLC1A5) Reveals an Essential Role for Transporters SNAT1 (SLC38A1) and SNAT2 (SLC38A2) to Sustain Glutaminolysis in Cancer Cells. *J Biol Chem*, 291, 13194–13205.
39. Broer, A., Wagner, C., Lang, F. and Broer, S. (2000). Neutral amino acid transporter ASCT2 displays substrate-induced Na+ exchange and a substrate-gated anion conductance. *Biochem J*. 346, 705-710.
40. Broer, S. (2006). Amino acid Transport Across Mammalian Intestinal and Renal Epithelia. *Physiological Reviews*. 88, 249-286.
41. Broer, S. and Brookes, N. (2001). Transfer of glutamine between astrocytes and neurons. *J Neurochem*. 77, 705-719.
42. Bröer, S., and Bröer, A. (2017). Amino acid homeostasis and signalling in mammalian cells and organisms. *Biochem J*, 474, 1935–1963.
43. Brown, E.J., Beal, P.A., Keith, C.T., Chen, J., Shin, T.B., Schreiber, S.L. (1995). Control of p70 S6 kinase by kinase activity of FRAP *in vivo*. *Nature*, 377, 441–446.
44. Brown, R.S., Leung, J.Y., Kison, P.V., Zasadny, K.R., Flint, A., Wahl, R.L. (1999). Glucose Transporters and FDG Uptake in Untreated Primary Human Non-Small Cell Lung Cancer. *J Nucl Med*, 40, 556-565.

45. Brown, R.S., Wahl, R.L. (1993). Overexpression of Glut-1 glucose transporter in human breast cancer: an immunohistochemical study. Cancer, 72, 2979–2985.
46. Brush, J., Boyd, K., Chappell, F., Crawford, F., Dozier, M., Fenwick, E., et al. (2011). The value of FDG positron emission tomography/computerised tomography (PET/CT) in pre-operative staging of colorectal cancer: a systematic review and economic evaluation. *Health Technol Assess*, 15, 1–192.
47. Buchberger, A.R., DeLaney, K., Johnson, J., Li, L. (2018). Mass Spectrometry Imaging: A Review of Emerging Advancements and Future Insights. *Anal Chem*, 90, 240–265.
48. Buck, A., Schirrmeister, H., Kuhn, T., Shen, C., Kalker, T., Kotzerke, J., Dankerl, A., Glatting, G., Reske, S., Mattfeldt, T. (2002). FDG uptake in breast cancer: correlation with biological and clinical prognostic parameters. *Eur J Nucl Med Mol Imaging*, 29, 1317–1323.
49. Calnan, D.R., Brunet, A. (2008). The FoxO code. *Oncogene*, 27, 2276-2288.
50. Caraco, C., Aloj, L., Chen, L.Y., Chou, J.Y., Eckelman, W.C. (2000). Cellular release of [^{18}F]2-fluoro-2-deoxyglucose as a function of the glucose-6-phosphatase enzyme system. *J Biol* Chem, 275, 18489–18494.
51. Casneuf, V.F., Fonteyne, P., Van Damme, N., Demetter, P., et al. (2008). Expression of SGLT1, Bcl-2 and p53 in primary pancreatic cancer related to survival. *Cancer Invest*, 26, 852–859.
52. Castro, A.F., Rebhun, J.F., Clark, G.J., Quilliam, L.A. (2003). Rheb binds tuberous sclerosis complex 2 (TSC2) and promotes S6 kinase activation in a rapamycin- and farnesylation-dependent manner. *J Biol Chem*, 278, 32493-32496.
53. Chan, J.K., Brady, M.F., Penson, R.T., Huang, H., et al. (2016). Weekly vs. Every-3-Week Paclitaxel and Carboplatin for Ovarian Cancer. *N Engl J Med*, 374, 738–748.
54. Chaneton, B., Gottlieb, E. (2012). Rocking cell metabolism: Revised functions of the key glycolytic regulator PKM2 in cancer. *Trends Biochem Sci*, 37, 309–316.

55. Chaneton, B., Hillmann, P., Zheng, L., Martin, A.C., Maddocks, O.D., et al. (2012). Serine is a natural ligand and allosteric activator of pyruvate kinase M2. *Nature*, 491, 458–462.
56. Chang, C.H., Wu, H.C., Tsai, J.J., Shen, Y.Y., Changlai, S.P., Kao, A. (2003). Detecting metastatic pelvic lymph nodes by 18F-2-deoxyglucose positron emission tomography in patients with prostate-specific antigen relapse after treatment for localized prostate cancer. *Urol Int*, 70, 311-5.
57. Chang, J.M., Lee, H.J., Goo, J.M., Lee, H-Y, Lee, J.J, Chung, J-K, Im, J-G. (2006). False Positive and False Negative FDG-PET Scans in Various Thoracic Diseases. *Korean J Radiol*, 7, 57-69.
58. Chang, T.C., Yu, D., Lee, Y.S., Wentzel, E.A., et al. (2008). Widespread microRNA repression by Myc contributes to tumorigenesis. *Nat Genet*, 40, 43–50.
59. Chatterjee, A., Dasgupta, S., Sidransky, D. (2011). Mitochondrial subversion in cancer. *Cancer Prev. Res*, 4, 638–654.
60. Chaudhry, F.A., Reimer, R.J., Krizal, D., Barber, D., Storm-Mathisen, J., Copenhagen, D. R., Edwards, R. H. (1999). Molecular Analysis of System N Suggests Novel Physiological Roles in Nitrogen Metabolism and Synaptic Transmission. *Cell*, 99, 769–780.
61. Chen, A.P., Chu, W., Gu, Y-P., Cunningham, C.H. (2013). Probing early tumor response to radiation therapy using hyperpolarized [1-(13)C] pyruvate in MDA-MB-231 xenografts. *PLoS ONE*, 8, e56551.
62. Chen, R., Nishimura, M.C., Kharbanda, S., Peale, F., et al. (2014). Hominoid-specific enzyme GLUD2 promotes growth of IDH1R132H glioma. *Proc Natl Acad Sci*, 111, 14217-22.
63. Cheng, T., Sudderth, J., Yang, C., Mullen, A.R., Jin, E.S., Mates, J.M., DeBerardinis, R.J. (2011). Pyruvate carboxylase is required for glutamine-independent growth of tumor cells. *Proc Natl Acad Sci*, 108, 8674-8679.
64. Christensen, H.N. (1990). Role of amino acid transport and countertransport in nutrition and metabolism. *Physiol. Rev*, 70, 43–77.
65. Chughtai, K., Jiang, L., Greenwood, T.R., GLunde, K., Heeren, R.M.A. (2013). Mass Spectrometry images acylcarnitines, phosphatidylcholines, and sphingomyelin in MDA-MB-231 breast tumour models. *Journal of Lipid Research*, 54, 333-344.

66. Chung, Y-L, Griffiths, J.R. (2011). Metabolomic Studies on Cancer and on Anticancer Drugs by NMR Ex Vivo. *Encyclopedia of Magnetic Resonance*.
67. Chung, Y-L, Leach, M.O, Eykyn, T. (2017). Magnetic resonance spectroscopy to study glycolytic metabolism during autophagy. *Methods Enzymol*, 588, 133-153.
68. Clarke, R., Ressom, H.W., Wang, A., Xuan, J., Liu, M.C., Gehan, E.A., Wang, Y. (2008) The properties of high-dimensional data spaces: implications for exploring gene and protein expression data. *Nat Rev Cancer*, 8, 37-49.
69. Clendinen, C.S., Lee-McMullen, B., Williams, C.M., Stupp, G.S., Vandenborne, K., Hahn, D.A., Walter, G.A., Edison, A.S. (2014). 13C NMR Metabolomics: Applications at Natural Abundance. *Anal Chem*, 86, 9242–9250.
70. Codogno, P., Meijer, A.J. (2005). Autophagy and signaling: their role in cell survival and cell death. *Cell Death Differ*, 12 Suppl. 2, 1509-1518.
71. Cooper, A., Krasnikov, B., Pinto, J., Kung, H., Li, J., Ploessl, K. (2012). Comparative enzymology of (2S, 4R) 4-fluoroglutamine and (2S, 4R) 4-fluoroglutamate. *Comparative Biochemistry and Physiology*, 163, 108-120.
72. Cooper, A.J.L. (1976). Proton magnetic resonance studies of glutamate-alanine transaminase-catalyzed deuterium exchange. Evidence for proton conservation during prototropic transfer from the α carbon of L-alanine to the C4-position of pyridoxal 5′-phosphate. *J. Biol. Chem.*, 251, 1088–1096.
73. Cooper, A.J.L. (2012). The role of glutamine synthetase and glutamate dehydrogenase in cerebral ammonia homeostasis. *Neurochem. Res*, 37, 2439–2455.
74. Cooper, A.J.L., Nieves, E., Rosenspire, K.C., Filc-DeRicco, S., Gelbard, A.S., Brusilow, S.W. (1988). Short-term metabolic fate of 13N-labeled glutamate, alanine, and glutamine (amide) in rat liver. *J. Biol. Chem*, 263, 12268–12273.
75. Csibi, A., Fendt, S., Li, C., Poulogiannis, G., et al. (2013). The mTORC1 pathway stimulates glutamine metabolism and cell proliferation by repressing SIRT4. *Cell*, 153, 840-854.
76. Csibi, A., Lee, G., Yoon, S., Tong, H., et al. (2014). The mTORC1/S6K1 pathway regulates glutamine metabolism through the eIF4B-dependent control of c-Myc translation. *Current Biology*, 24, 2274-2280.
77. Dang, C.V. (2010). Glutaminolysis: Supplying carbon or nitrogen or both for cancer cells? *Cell Cycle.* 9, 3884-3886.

78. Dang, C.V. (2012). MYC on the path to cancer. *Cell*, 149, 22-35.
79. Dang, C.V. (2013). MYC, Metabolism, Cell Growth, and Tumorienesis. *Cold Spring Harb Perspect Med*, 3:a014217.
80. Dang, C.V., et al. (2006) The c-Myc target gene network. *Semin Cancer Biol*, 16, 253–264.
81. Dang, C.V., Hamaker, M., Sun, P., Le, A., Gao, P. (2011). Therapeutic targeting of cancer cell metabolism. *J. Mol. Med*, 89, 205–212.
82. David, C.J., Chen, M., Assanah, M., Canoll, P., Manley, J.L. (2010). HnRNP proteins controlled by c-Myc deregulate pyruvate kinase mRNA splicing in cancer. *Nature*, 463, 364–368.
83. Day, S.E., Kettunen, M.I., Gallagher, F.A., Hu, D-E., et al. (2007). Detecting tumour response to treatment using hyperpolarized 13C magnetic resonance imaging and spectroscopy. *Nature Medicine*, 13, 1382-1387.
84. De Castro, F., Benedetti, M., Antonaci, G., Del Coco, L., De Pascali, S.A., Muscella, A., Marsigliante, S., Fanizzi, F.P. (2018). Response of cisplatin resistant SKOV-3 cells to [Pt(*O,O*-acac)(γ-acac)(DMS)] Treatment revealed by a metabolomic ^{1}H-NMR study. *Molecules*, 23, 2301.
85. DeBerardinis, R.J., Cheng, T. (2010). Q's next: The diverse functions of glutamine in metabolism, cell biology and cancer. *Oncogene*, 29, 313–324.
86. DeBerardinis, R.J., Mancuso, A., Daikhin, E., Nissim, I., Yudkoff, M., Wehrli, S. (2007). Beyond aerobic glycolysis: transformed cells can engage in glutamine metabolism that exceeds the requirement for protein and nucleotide synthesis. *Proc Natl Acad Sci USA*, 104, 19345-19350.
87. DeBerardinis, R.J., Sayed, N., Ditsworth, D., Thompson, C.B. (2008). Brick by brick: Metabolism and tumour cell growth. *Curr Opin Genet Dev.* 18, 54-61.
88. DeFeo, E.M., Cheng, L.L. (2010). Characterizing human cancer metabolomics with ex vivo 1H HRMAS MRS. *Technology in Cancer Research & Treatment*, 9, 381-391.
89. DeLaBarre, B., Gross, S., Fang, C., Gao, Y. (2011). Full-length human glutaminase in complex with an allosteric inhibitor. *Biochemistry*, 50, 10764–10770.
90. Dennis, P.B., Jaeschke, A., Saitoh, M., Fowler, B., Kozma, S.C., Thomas, G. (2001). Mammalian TOR: a homeostatic ATP sensor. *Science*, 294, 1102-1105.

91. Dowling, C., Bollen, A.W., Noworolski, S.M., McDermott, M.W. (2001). Preoperative proton MR spectroscopic imaging of brain tumours: correlation with histopathologic analysis of resection specimens. *American Journal of Neuroradiology*, 22, 604-612.
92. Dumstorf, C.A., Konicek, B.W., McNulty, A.M., Parsons, S.H., et al. (2010). Modulation of 4E-BP1 function as a critical determinant of enzastaurin-induced apoptosis. *Mol Cancer Ther*, 9, 3158-3163.
93. Dunphy, M.P.S., Hardign. J.J., Venneti, S., Zhang, H., et al. (2018). In vivo PET assay of tumour glutamine flux and metabolism: In-Human trial of ^{18}F-(2S,4R)-4-Fluoroglutamine. *Radiology*, 287, 667-675.
94. Duran, R., Oppliger, W., Robitaille, A., Heiserich, L., et al. (2012). Glutaminolysis activates Rag-mTORC1 signalling. *Molecular Cell*, 47, 349-358.
95. Eberlin, L.S., Gabay, M., Fan, A.C., Gouw, A.M., Tibshirami, R.J., Felsher, D.W., Zare, R.N. (2014). Alteration of the lipid profile in lymphomas induced by MYC overexpression. *Proceedings of the National Academy of Sciences of the United States of America*, 111, 10450-10455.
96. Effert, P., Benniers, A.J., Tamimi, Y., Handt, S., Jakse, G. (2004). Expression of glucose transporter 1 (Glut-1) in cell lines and clinical specimens from human prostate adenocarcinoma. *Anticancer Res*, 24, 3057-3063.
97. Eilers, M., Eisenman, R.N. (2008). Myc's broad reach. *Genes Dev*, 22, 2755-2766.
98. El-tanani, M., Dakir, E., Raynor, B. and Morgan, R. (2016). Review Mechanisms of Nuclear Export in Cancer and Resistance to Chemotherapy. *Cancers*, 8, 35.
99. Emwas, A-H. (2015). The Strengths and Weaknesses of NMR Spectroscopy and Mass Spectrometry with Particular Focus on Metabolomics Research. Methods in molecular biology (Clifton, N.J.), 1277, 161-193.
100. Erickson, J.W., Cerione, R.A. (2010). Glutaminase: a hot spot for regulation of cancer cell metabolism? *Oncotarget*, 1, 734–740.
101. Eubank, W.B., Mankoff, D.A. (2005). Evolving role of positron emission tomography in breast cancer imaging. *Semin Nucl Med*., 35, 84–99.
102. Fan, T.W.M., Lane, A.N., Higashi, R.M., Farag, M.A., et al. (2009). Altered regulation of metabolic pathways in human lung cancer discerned by [13]C stable isotope-resolved metabolomics (SIRM). *Molecular Cancer*, 8, 41.

103. Ferlay, J., Shin, H.R., Bray F, Forman, D., Mathers C.D., Parkin, D. (2013). GLOBOCAN, Cancer Incidence and Mortality Worldwide: IARC CancerBase No. 11. Lyon, France: International Agency for Research on Cancer. Available at: http://globocan.iarc.fr. Last accessed 23/01/2020.

104. Finehout, E.J., Lee, K.H. (2004). An introduction to mass spectrometry applications om biological research. *Biochemistry and Molecular Biology Education*, 32, 93-100.

105. Fingar, D. and Blenis, J. (2004). Target of rapamycin (TOR): an integrator of nutrient and growth factor signals and coordinator of cell growth and cell cycle progression. *Oncogene*, 23, 3151-3171.

106. Foster, H., Coley, H.M., Goumenou, A., Pados, G., Harvey, A., Karteris, E. (2010). Differential expression of mTOR signalling components in drug resistance in ovarian cancer. *Anticancer Res*, 30, 3529–3534.

107. Fotiadis, D., Kanai, Y., and Palacin, M. (2013). The SLC3 and SLC7 families of amino acid transporters. *Mol. Aspects Med*, 34, 139–158.

108. Frias, M.A., Thoreen, C.C., Jaffe, J.D., Schroder, W., Sculley, T., Carr, S.A., Sabatini, D.M. (2006). mSin1 is necessary for Akt/PKB phosphorylation, and its isoforms define three distinct mTORC2s. *Curr. Biol*, 16, 1865-1870.

109. Fuchs, B. and Bode, B. (2005). Amino acid transporters ASCT2 and LAT1 in cancer: Partners in crime? *Seminars in Cancer Biology*, 15, 254-166.

110. Gadian, D. (1996). NMR and its Applications to Living Systems. Oxford: Oxford University Press, New York.

111. Gao, P., Tchernyshyov, I., Chang, T.C., Lee, Y.S., Kita, K., Ochi, T., et al. (2009). C-Myc suppression of miR-23a/b enhances mitochondrial glutaminase expression and glutamine metabolism. *Nature*, 458, 762-765.

112. Garami, A., Zwartkruis, F.J., Nobukuni, T., Joaquin, M., Roccio, M., Stocker, H., Kozma, S.C., Hafen, E., Bos, J.L., Thomas, G. (2003). Insulin activation of Rheb, a mediator of mTOR/S6K/4E-BP signaling, is inhibited by TSC1 and 2. *Mol Cell*, 11, 1457-1466.

113. Garcia, S., Jose, S., Jose, L., Dolores, A. and Heriberto, P. (2011). Tumour cell metabolism: An integral view. *Cancer Biology and Therapy*, 12, 939-948.

114. Garrett, R.H., Grisham, C.M. (2002). *Principles of Biochemistry with a Human Focus*. USA: Brooks/Cole, Thomson Learning. pp. 578, 585.

115. Gelbard, A.S., Benua, R.S., Laughlin, J.S., Rosen, G., Reiman, R.E., McDonald, J.M. (1979). Quantitative scanning of osteogenic sarcoma with nitrogen-13 labeled Lglutamate. *J. Nucl. Med*, 20, 782–784.

116. Gerber, F., Krummen, M., Potgeter, H., Roth, A., Siffrin, C., Spoendlin, C. (2004). Practical aspects of fast reversed-phase high-performance liquid chromatography using 3µm particle packed columns and monolithic columns in pharmaceutical development and production working under current good manufacturing practice. *Journal of Chromatography A*, 1036, 127–133.

117. Gillies, R.J., Robey, I., Gatenby, R.A. (2008). Causes and consequences of increased glucose metabolism of cancers. *J Nucl Med*, 49:24S-42S.

118. Gingras, A.C., Kennedy, S.G., O'Leary, M.A., Sonenberg, N., Hay, N. (1998). 4E-BP1, a repressor of mRNA translation, is phosphorylated and inactivated by the Akt(PKB) signalling pathway. *Genes Dev*, 12, 502-513.

119. Gingras, A.C., Raught, B., Sonenberg, N. (2001). Regulation of translation initiation by FRAP/mTOR. *Genes Dev*, 15, 807-826.

120. Glaholm, J., Leach, M.O., Collins, D., al Jehazi, B., Sharp, J.C., Smith, T.A., Adach, J., Hind, A., McCready, V.R., White, H. (1990). Comparison of 5-fluorouracil pharmacokinetics following intraperitoneal and intravenous administration using in vivo 19F magnetic resonance spectroscopy. *Br J Radiol*, 63, 547-553.

121. Glaudemans, A.J.M., Enting, R., Heesters, M.A.M., Dierckx, R.J.O., van Rheenen, R.J., Walenkamp, A.E., Slart, R.J.A. (2013). Value of 11C-Methionine PET in imaging brain tumours and metastases. *European Journal of Nuclear Medicine and Molecular Imaging*, 40, 615-635.

122. Glunde, K., Bhujwalla, Z.M., Ronen, S.M. (2011). Choline metabolism in malignant transformation. *Nature Reviews. Cancer*, 11, 835-848.

123. Goo, J.M., Im. J.G., Do, K.H., Yeo, J.S., et al. (2000). Pulmonary tuberculoma evaluated by means of FDG PET: findings in 10 cases. *Radiology*, 216:117-121.

124. Gort, E.H., Groot, A.J., van der Wall, E., van Diest, P.J., Vooijs, M.A. (2008). Hypoxic regulation of metastasis via hypoxia-inducible factors. *Curr Mol Med*, 8, 60-67.

125. Govindaraju, V., Young, K., Maudsley, A.A. (2000). Proton NMR chemical shifts and coupling constants for brain metabolites. *NMR in Biomedicine*, 13, 129-153.

126. Grandori, C, Cowley, S.M., James, L.P., Eisenman, R.N. (2000). The Myc/Max/Mad network and the transcriptional control of cell behaviour. *Annu Rev Cell Dev Biol*, 16, 653-699.

127. Grassi, I., Nanni, C., Allegri, V., Morigi, J.J., Montini, G.C., Castellucci, P., Fanti, S. (2012). The clinical use of PET with (11)C-acetate. *American Journal of Nuclear Medicine and Molecular Imaging*, 2, 33-47.

128. Green D (2011). Means to an End: Apoptosis and other Cell Death Mechanisms. Cold Spring Harbor, NY: Cold Spring Harbor Laboratory Press.

129. Grkovski, M., Goel, R., Krebs, S., Staton, K.D., et al. (2019). Pharmacokinetic assessment of 18F-(2S,4R)-4-fluoroglutamine in patients with cancer. *J Nucl Med*, 61, 357-366.

130. Guertin, D.A., Sabatini, D.M. (2007). Defining the Role of mTOR in Cancer. *Cancer Cell*, 12, 9-22.

131. Guichard, S.M., Curwen, J., Bihani, T., D'Cruz, C.M., et al. (2015). AZD2014, an Inhibitor of mTORC1 and mTORC2, Is Highly Effective in ER+ Breast Cancer When Administered Using Intermittent or Continuous Schedules. *Mol Cancer Ther*,14, 2508–2518.

132. Hahn-Windgassen, A., Nogueira, V., Chen, C.C., Skeen, J.E., Sonenberg, N., Hay, N. (2005). Akt activates mTOR by regulating cellular ATP level and AMPK activity. *J Biol Chem*, 280, 32081-9.

133. Halestrap, A.P. (2013). The SLC16 gene family - structure, role and regulation in health and disease. *Mol. Aspects Med*, 34, 337–349.

134. Hanahan, D., Weinberg, R.A. (2000). The Hallmarks of Cancer. *Cell*, 100, 57-70.

135. Hanahan, D., Weinberg, R.A. (2011.) Hallmarks of cancer: the next generation. *Cell*, 144, 646-674.

136. Hari, N., Frank, B., Giuseppe, E. (2013). False-Positive Finding of Brain Metastasis on ^{18}F-FDG PET Imaging Due to Early Subacute Ischemic Stroke. *Clinical Nuclear Medicine*, 38, 465-466.

137. Harwood, L.M., Moody, C.J., Percy, J.M. (2003). Experimental Organic Chemistry. UK: Blackwell Science Limited.

138. Hasler, G., Buchmann, A., Haynes, M., Müller, S.T., Ghisleni, C., Brechbühl, S., Tuura, R. (2019). Association between prefrontal glutamine levels and neuroticism determined using proton magnetic resonance spectroscopy. *Translational Psychiatry*, 9, 170.

139. Hassanein, M. *et al*. (2015). Targeting SLC1a5-mediated glutamine dependence in non-small cell lung cancer. *Int. J. Cancer*, 137, 1587–97.

140. Hawkins, R.A. (2009). The blood-brain barrier and glutamate. *Am. J. Clin. Nutr*, 90, 867S–874S.

141. Hawkins, R.A., Viña, J.R. (2016). How Glutamate Is Managed by the Blood-Brain Barrier. *Biology*, 5.

142. Heddleston, J.M., Li, Z., Lathia, J.D., Bao, S., Hjelmeland, A.B., Rich, J.N. (2010). Hypoxia inducible factors in cancer stem cells. *Br J Cancer*, 102, 789-795.

143. Higson, S.P. (2004). Analytical Chemistry. Oxford: Oxford University Press.

144. Holzmayer, T.A., Hilsenbeck, S., Von Hoff, D.D., Roninson, I.B. (1992). Clinical Correlates of MDR1 (P-glycoprotein) Gene Expression in Ovarian and Small-Cell Lung Carcinomas. *Journal of the National Cancer Institute*, 84, 1486–91.

145. Hsieh, A.C., Costa, M., Zollo, O., Davis, C., et al. (2010). Genetic Dissection of the Oncogenic mTOR Pathway Reveals Druggable Addiction to Translational Control via 4EBP-eIF4E. *Cancer Cell*, 17, 249-261.

146. Hu, S., Balakrishnan, A., Bok, R.A., Anderton, B., et al. (2011). 13C-pyruvate imaging reveals alterations in glycolysis that precede c-Myc-induced tumor formation and regression. *Cell Metab*,14, 131–142.

147. Hu, W., Zhang, C., Wu, R., Sun, Y., Levine, A., Feng, Z. (2010). Glutaminase 2, a novel p53 target gene regulating energy metabolism and antioxidant function. *Proc. Natl. Acad. Sci. U. S. A.*, 107, 7455–7460.

148. Hydbring, P., Bahram, F., Su, Y., et al. (2010). Phosphorylation by Cdk2 is required for Myc to repress Ras-induced senescence in cotransformation. *Proc Natl Acad Sci USA*, 107, 58-63.

149. Hydbring, P., Larsson, L-G. (2010). Tipping the balance: Cdk2 Enables Myc to Suppress Senescence. *Cancer Research*, 70, 6687-6691.

150. Imai, H., Kaira, K., Oriuchi, N., Shimizu, K., Tominaga, H., Yanagitani, N., Sunaga, N., Ishizuka, T., Nagamori, S., Promchan, K. (2010). Inhibition of L-type amino acid transporter 1 has antitumour activity in non-small cell lung cancer. *Anticancer Res*., 30, 4819-4828.

151. Imbert, L., Dulaurent, S., Mercerolle, M., Morichon, J., Lachâtre, G., Gaulier, J-M. (2014). Development and validation of a single LC–MS/MS assay following SPE for simultaneous hair analysis of amphetamines, opiates, cocaine and metabolites. *Forensic Sci Int*, 234, 132–138.

152. Inoki, K., Li, Y., Xu, T., Guan, K.L. (2003). Rheb GTPase is a direct target of TSC2 GAP activity and regulates mTOR signaling. *Genes Dev*, 17, 1829-1834.

153. Inoki, K., Zhu, T., Guan, K.L. (2003). TSC2 mediates cellular energy response to control cell growth and survival. *Cell*, 115, 577-590.

154. Jacinto, E., Facchinetti, V., Liu, D., Soto, N., Wei, S., Jung, S.Y., Huang, Q., Qin, J. and Su, B. (2006). SIN1/MIP1 maintains rictor-mTOR complex integrity and regulates Akt phosphorylation and substrate specificity. *Cell*, 127, 125-137.

155. Jacinto, E., Loewith, R., Schmidt, A., Lin, S., Ruegg, M.A., Hall, A., Hall, M. N. (2004). Mammalian TOR complex 2 controls the actin cytoskeleton and is rapamycin insensitive. *Nat. Cell Biol*, 6, 1122-1128.

156. Jadvar, H. (2012). Molecular imaging of prostate cancer: PET radiotracers. *AJR Am J Roentgenol*, 199, 278-291.

157. Jadvar, H., Desai, B., Ji, L., Conti, P.S., Dorff, T.B., Groshen, S.G., Pinski, J.K., Quinn, D.I. (2013) Baseline 18F-FDG PET/CT parameters as imaging biomarkers of overall survival in castrate-resistant metastatic prostate cancer. *J Nucl med*, 54, 1195-1201.

158. Janpipatkul, K., Suksen, K., Borwornpinyo, S., Jearawiriyapaisarn, N., Hongeng, S., Piyachaturawat, P., Chairoundua, A. (2014). Downregulation of LAT1 expression suppresses cholangiocarcinoma cell invasion and migration. *Cell Signal*, 26, 1668-1679.

159. Jemal, A., Bray, F., Melissa, M., Ferlay, J., Ward, E., Forman, D. (2011). Global Cancer Statistics. *CA: A Cancer Jounal for Clinicians*, 61, 69-90.

160. Jordan, M.A., Wilson, L. (2004). Microtubules as a target for anticancer drugs. *Nat Rev Cancer*, 4, 253–65.

161. Kaiser, L.G., Hirokazu, K., Fukunaga, M., Matson, G.B. (2016). Detection of glucose in the human brain with 1H MRS at 7 Tesla. *Magnetic Resonance in Medicine*, 76, 1653-1660.

162. Kamazawa, S., Kigawa, J., Kanamori, Y., Itamochi, H., Sato, S., Iba, T., Terakawa, N. (2002). Multidrug Resistance Gene-1 Is a Useful Predictor of Paclitaxel-Based Chemotherapy for Patients with Ovarian Cancer. *Gynecologic Oncology*, 86, 171–6.

163. Kanai, Y., Segawa, H., Ki, M, Uchino, H., et al. (1998). Expression cloning and characterization of a transporter for large neutral amino acids activated by the heavy chain of 4F2 antigen (CD98). *J Biol Chem*, 273, 23629-23632.

164. Kanazawa, Y., Umayahara, K., Shimmura, T., Yamashita, T. (1997). 19F NMR of 2-deoxy-2-fluoro-D-glucose for tumor diagnosis in mice. An NDP-bound hexose analog as a new NMR target for imaging. *NMR Biomed*, 10, 35-41.

165. Kang, S.A., Pacold, M.E., Lim, D., Lou, H.J., Ottina, K., Gray, N.S., et al. (2013). mTORC1 phosphorylation sites encode their sensitivity to starvation and rapamycin. *Science*, 341, 364-374.

166. Kim, D. K., Kanai, Y., Choi, H. W., Tangtrongsup, S., Chairoungdua, A., Babu, E., et al. (2002). Characterization of the system L amino acid transporter in T24 human bladder carcinoma cells. *Biochim Biophys Acta*, 1565, 112–121.

167. Kim, D-H, Sarbassov, D.D., Ali, S.M., King, J.E., Latek, R.R., Bromage, H.E., Tempst, P., Sabatini, D.M. (2002). mTOR Interacts with Raptor to Form a Nutrient-Sensitive Complex that Signals to the Cell Growth Machinery. *Cell*, 110, 163-175.

168. Kim, J.E., Chen, J. (2004). Regulation of peroxisome proliferator-activated receptor-gamma activity by mammalian target of rapamycin and amino acids in adipogenesis. *Diabetes*, 53, 2748-2756.

169. Kim, J.W.,Zeller, K.I., Wang, Y., Jegga, A.G., Aronow, B.J., O'Donnell, K.A., Dang, C.V. (2004). Evaluation of myc E-box phylogenetic footprints in glycolytic genes by chromatin immunoprecipitation assays. *Mol Cell Biol*, 24, 5923–5936.

170. Kim, S-J., Pak, K., Kim, K. (2019). Diagnostic performance of F-18 FDG PET/CT for prediction of KRAS mutation in colorectal cancer patients: a systematic review and meta-analysis. *Abdominal Radiology*, 44, 1703–1711.

171. Kiss, K., Baghy, K., Spisák, S., Szanyi, S., et al. (2015). Chronic Hyperglycemia Induces Trans-Differentiation of Human Pancreatic Stellate Cells and Enhances the Malignant Molecular Communication with Human Pancreatic Cancer Cells. *PLoS ONE*, 10(5): e0128059.

172. Kohl, N.E., Kanda, N., Schreck, R.R., Bruns, G., Latt, S.A., Gilbert, F., et al. (1983). Transposition and amplification of oncogene-related sequences in human neuroblastomas. *Cell*, 35, 359–67.

173. Kolmonen, M., Leinonen, A., Pelander, A., Ojanperä, I. (2007). A general screening method for doping agents in human urine by solid phase extraction and liquid chromatography/time-of-flight mass spectrometry. *Analytica Chimica Acta*, 585, 94–102.

174. Komarov, I.V., Afonin, S., Ulrich, A.S. (2019). ^{19}F-Labeled amino acids for NMR structure analysis of membrane-bound peptides. *Fluorine in Life Sciences: Pharmaceuticals, Medicinal Diagnostics, and Agrochemicals*, 349-395.

175. Koppenol, W.H., Bounds, P.L., Dang, C.V. (2011). Otto Warburg's contributions to current concepts of cancer metabolism. *Nat. Rev. Cancer*, 11, 325–337.

176. Kostakoglu, L., Agress, H., Goldsmith, S.J. (2003). Clinical role of FDG PET in evalutaion of cancer patients. *RadioGraphics*, 23, 315-340.

177. Kroemer, G., Pouyssegur, J. (2008). Tumor cell metabolism: cancer's Achilles' heel. *Cancer Cell*, 13, 472-482.

178. Kuchar, M., Mamat, C. (2015). Methods to Increase the Metabolic Stability of 18F-Radiotracers. *Molecules*, 20, 16186–16220.

179. Kumar, R., Alavi, A. (2004). Fluorodeoxyglucose-PET in the management of breast cancer. *Radiol Clin North Am*, 42, 1113–1122.

180. Kumar, R., Chauhan, A., Zhuang, H., Chandra, P., Schnall, M., Alavi, A. (2006). Clinicopathologic factors associated with false negative FDG-PET in primary breast cancer. *Breast Cancer Res Treat*, 98, 267–274.

181. Lai, M., Vassallo, I., Lanz, B., Poitry-Yamate, C., et al. (2018). In vivo characterization of brain metabolism by 1H MRS, 13C MRS and 18FDG PET

reveals significant glucose oxidation of invasively growing glioma cells. *Molecular Cancer Biology*, 143, 127-138.

182. Land, H., Parada, L.F., Weinberg, R.A. (1983). Tumorigenic conversion of primary embryo fibroblasts requires at least two cooperating oncogenes. *Nature*, 304, 596-602.

183. Lang, F., Pearce, D. (2016). Regulation of the epithelial Na+ channel by the mTORC2/SGK1 pathway. *Nephrol Dial Transplant*, 31, 200-205.

184. Langen, K.J., Braun, U., Rota Kops, E., et al. (1993). The influence of plasma glucose levels on fluorine-18-fluorodeoxyglucose uptake in bronchial carcinomas. *J Nucl Med*, 34, 355–359.

185. Laplante, M., Sabatini, D.M. (2009). mTOR signaling at a glance. *Journal of Cell Science*, 122, 3589-3594.

186. Larsson, L.G., Henriksson, M.A. (2010). The Yin and Yang functions of the Myc oncoprotein in cancer development and as targets for therapy. *Exp Cell Res*, 316, 1429-1437.

187. Lawal, I., Sathekge, M. (2016). F-18 FDG PET/CT imaging of cardiac and vascular inflammation and infection. *British Medical Bulletin*, 120, 55–74.

188. Le, A., Lane, A.N., Hamaker, M., Bose, S., et al. (2012). Glucose-independent glutamine metabolism via TCA cycling for proliferation and survival in B cells. *Cell Metab*, 15, 110–121.

189. Le, X.F., Hittelman, W.N., Liu, J., McWatters, A., Li, C., Mills, G.B., Bast, R.C.Jr. (2003). Paclitaxel induces inactivation of p70 S6 kinase and phosphorylation of Thr421 and Ser424 via multiple signaling pathways in mitosis. *Oncogene*, 22, 484– 497.

190. Leach, M.O., Verrill, M., Glaholm, J., Smith, T.A.D., et al. (1998). Measurements of human breast cancer using magnetic resonance spectroscopy: a review of clinical measurements and a report of localized 31P measurements of response to treatment. *NMR in Biomedicine*, 11, 314-340.

191. Levine, A.J., Puzio-Kuter, A.M. (2010). The control of the metabolic switch in cancers by oncogenes and tumor suppressor genes. *Science*, 330, 1340–1344.

192. Li, M., Smith, C.J., Walker, M.T., Smith, T.J. (2009). Novel Inhibitors Complexed with Glutamate Dehydrogenase ALLOSTERIC REGULATION BY CONTROL OF PROTEIN DYNAMICS. *J Biol Chem*, 284, 22988–23000.

193. Li, Y., Park, I., Nelson, S.J. (2015). Imaging Tumor Metabolism using *in vivo* MR Spectroscopy. *Cancer J*, 21, 123-128.

194. Lieberman, M. and Marks, A.D. (2009). Basic Medical Biochemistry a clinical approach. Lippincott Williams&Wilkins, Baltimore.

195. Lieberman, P., Ploessl, K., Wang, L., Qu, W., et al. (2011). PET Imaging of glutaminolysis in tumours by 18F-(2S, 4R)4-Fluoroglutamine. *J Nucl Med*, 52, 1947-1955.

196. Lin, E., Alessio, A. (2009). What are the basic concepts of temporal, contrast, and spatial resolution in cardiac CT? *J Cardiovasc Comput Tomogr*, 3, 403–408.

197. Lin, G., Chung, Y-L. (2014). Current opportunities and challenges of magnetic resonance spectroscopy, positron emission tomography, and mass spectrometry imaging for mapping cancer metabolism in vivo. *BioMed Research International*, 625095.

198. Listrom, C.D., Morizono, H., Rajagopal, B.S., McCann, M.T., Tuchman, M., Allewell, N.M. (1997). Expression, purification, and characterization of recombinant human glutamine synthetase. *Biochem. J*, 328, 159–163.

199. Liu, I.J., Zafar, M.B., Lai, Y.H., Segall, G.M., Terris, M.K. (2001). Fluorodeoxyglucose positron emission tomography studies in diagnosis and staging of clinically organ-confined prostate cancer. *Urology*, 57, 108-111.

200. Liu, Y.C., Li, F., Handler, J., Huang, C.R., Xiang, Y., Neretti, N., Sedivy, J.M., Zeller, K.I., Dang, C.V. (2008). Global regulation of nucleotide biosynthetic genes by c-Myc. *PLoS ONE*, 3, e2722.

201. Loven, J.,Orlando, D.A., Sigova, A.A., Lin, C.Y., Rahl, P.B., Burge, C.B., Levens, D.L., Lee, T.I., Young, R.A. (2012). Revisiting global gene expression analysis. *Cell*, 151, 476–482.

202. Lowe, S.W., Cepero, E., Evan, G. (2004). Intrinsic tumour suppression. *Nature*, 432, 307-315.

203. Lu, W., Helene, P. and Peng, H. (2010). Cancer metabolism: Is glutamine sweeter than glucose? *Cancer Cell.* 18, 199-200.

204. Luo, J., Solimini, N. L. & Elledge, S. J. (2009). Principles of cancer therapy: oncogene and non-oncogene addiction. *Cell* 136, 823–37.

205. Ma, X.M., Blenis, J. (2009). Molecular mechanisms of mTOR-mediated translational control. *Nat. Rev. Mol. Cell Biol*, 10, 307-318.

206. Maher, E.A., Marin-Valenci, I., Bachoo, R.M., Mashimo, T., et al. (2012). Metabolism of [U-13C]glucose in human brain tumors in vivo. *NMR in Biomedicine*, 25, 1234-1244.

207. Mahon, M.M, Cox, I.J., Dina, R., Soutter FRCOG, W.P., et al. (2004). 1H Magnetic resonance spectroscopy of preinvasive and invasive cervical cancer: In vivo-ex vivo profiles and effect of tumour load. *Journal of Magnetic Resonance Imaging*, 19, 356-364.

208. Mancuso, A., Sharfstein, S.T., Tucker, S.N., Clark, D.S., Blanch, H.W. (1994). Examination of primary metabolic pathways in a murine hybridoma with carbon-13 nuclear magnetic resonance spectroscopy. *Biotechnology and Bioengineering*, 44, 563-585.

209. Mankoff, D.A., Shields, A.F., Krohn, K.A. (2005). PET imaging of cellular proliferation. *Radiologic Clinics*, 43, 153-167.

210. Mannava, S., Grachtchouk, V., Wheeler, L.J., Im, M., Zhuang, D., Slavina, E.G., Mathews, C.K., Shewach, D.S., Nikiforov, M.A. (2008). Direct role of nucleotide metabolism in C-MYC dependent proliferation of melanoma cells. *Cell Cycle*, 7, 2392–2400.

211. Manning, B.D., Cantley, L.C. (2007). AKT/PKB signaling: navigating downstream. *Cell*, 129, 1261-1274.

212. Marien, E., Meister, M., Muley, T., Fieuws, S., et al. (2015). Non-small cell lung cancer is characterized by dramatic changes in phospholipid profiles. *International Journal of Cancer*, 137, 1539-1548.

213. Marin-Valenci, I., Yang, C., Mashimo, T., Cho, S. (2015). Analysis of tumour metabolism reveals mitochondrial glucose oxidation in genetically diverse human glioblastomas in the mouse brain in vivo. *Cell Metabolism*, 15, 827-837.

214. Maschauer, S., Prante, O., Hoffman, M., Deichen, J.T., Kuwert, T. (2004). Characterization of 18F-FDG uptake in human endothelial cells in vitro. *Journal of Nuclear Medicine*, 45, 455-460.

215. Mastroberardino, L., Spindler, B., Pfeiffer, R., Skelly, P. J., Loffing, J., Shoemaker, C. B., et al. (1998). Amino-acid transport by heterodimers of 4F2hc/CD98 and members of a permease family. *Nature*, 395, 288–291.

216. Matés, J.M., Segura, J.A., Campos-Sandoval, J.A., Lobo, C., Alonso, L., Alonso, F.J. (2009). Glutamine homeostasis and mitochondrial dynamics. *Int J Biochem Cell Biol*, 41, 2051-2061.

217. Mathew, R., White, E. (2011). Autophagy, stress, and cancer metabolism: what doesn't kill you makes you stronger. *Cold Spring Harbor Symposia on Quantitative Biology*, 76, 389-396.

218. Mathews, E.H., Stander, B.A., Joubert, A.M., Liebenberg, L. (2014). Tumor cell culture survival following glucose and glutamine deprivation at typical physiological concentrations. *Nutrition*, 30, 218-27.

219. Mayer, C., Zhao, J., Yuan, X., Grummt, I. (2004). mTOR-dependent activation of the transcription factor TIFIA links rRNA synthesis to nutrient availability. *Genes Dev*, 18, 423-434.

220. McIntyre, D.J.O., Howe, F.A., Ladroue, C., Lofts, F., Stubbs, M., Griffiths, J.R. (2011). Can localised (19)F magnetic resonance spectroscopy pharmacokinetics of 5FU in colorectal metastases predict clinical response? *Cancer Chemotherapy and Pharmacology*, 68, 29-36.

221. Medina, M.A. (2001). Glutamine and cancer. *J Nutr*, 131, 2539-2542.

222. Meng, D., Frank, A.R., Jewell, J.L. (2018). mTOR signaling in stem and progenitor cells. *Development*, 145, dev152595.

223. Micchelli, A., Tomassini, A., Puccetti, C., Valerio, M., et al. (2006). Metabolic profiling by 13C-NMR spectroscopy: [1,2-13C2]glucose reveals a heterogenous metabolism in human leukemia T cells. *Biochimie*, 88, 437-448.

224. Miyamoto, S., Hsu, C.C., Hamm, G., Darshi, M., et al. (2016). Mass Spectrometry Imaging Reveals Elevated Glomerular ATP/AMP in Diabetes/obesity and Identifies Sphingomyelin as a Possible Mediator. *EBioMedicine*, 7, 121–134.

225. Morrish, F., Isern, N., Sadilek, M., Jeffrey, M., Hockenbery, D.M. (2009). c-Myc activates multiple metabolic networks to generate substrates for cell-cycle entry. Oncogene, 28, 2485–2491.

226. Mukherji, S.K., Schiro, S., Castillp, M., Muller, K.E., Blackstock, W. (1997). Proton MR spectroscopy of squamous cell carcinoma of the extracellular head and neck: in vitro and in vivo studies. *American Journal of Neuroradiology*, 18, 1057-1072.

227. Mullen, A.R., Wheaton, W.W., Jin, E.S., Chen, P-H, et al. (2011) Reductive carboxylation supports growth in tumour cells with defective mitochondria. *Nature*, 481, 385-8.

228. Murayama, C., Kimura, Y., Setou, M. (2009). Imaging mass spectrometry: principle and application. *Biophys Rev*, 1, 131-139.

229. Nelson, B.S., Lin, L., Kremer, D.M., Sousa, C.M., et al. (2020). Tissue of origin dictates GOT1 dependence and confers synthetic lethality to radiotherapy. *Cancer & Metabolism*, 8(1).

230. Newsholme, P., Lima, M.M.R., Procopio, J., Pithon-Curi, T.C., Doi, S. Q., Bazotte, R.B., Curi, R. (2003). Glutamine and glutamate as vital metabolites. *Brazilian Journal of Medical and Biological Research*, 36, 153–163.

231. Nicklin, P., Bergman, P., Zhang, B., Triantafellow, E., et al. (2009). Bidirectional transport of amino acids regulates mTOR and autophagy. *Cell*, 136, 521-534.

232. Oppedisano, F., Pochini, L., Galluccio, M., Indiveri, C. (2006). The glutamine/amino acid transporter (ASCT2) reconstituted in liposomes: Transport mechanism, regulation by ATP and characterization of the glutamine/glutamate antiport. *BBA-Biomembranes*. 1768, 291-298.

233. Orr, G.A., Verdier-Pinard, P., McDaid, H., Horwitz, S.B. (2003). Mechanisms of Taxol resistance related to microtubules. *Oncogene*, 22, 7280–95.

234. Ortega, A.D., Sánchez-Aragó, M., Giner-Sánchez, D., Sánchez-Cenizo, L., Willers, I., Cuezva, J.M. (2009). Glucose avidity of carcinomas. *Cancer Lett*, 276, 125-135.

235. Osthus, R.C., Shim, H., Kim, S., Li, Q., Reddy, R., Mukherjee, M., Xu, Y., Wonsey, D., Lee, L.A., Dang, C.V. (2000)Deregulation of glucose transporter 1 and glycolytic gene expression by c-Myc. *J Biol Chem*, 275, 21797–21800.

236. Ozturk, S.S., Jorjani, P., Taticek, R., Lowe, B., Shackleford, S., Ladehoff-Guiles, D., Thrift, J., Blackie, J., Naveh, D. (1997). Kinetics of Glucose Metabolism and Utilization of Lactate in Mammalian Cell Cultures. In: Carrondo M.J.T., Griffiths B., Moreira J.L.P. (eds) Animal Cell Technology. Springer, Dordrecht.

237. Palacín, M., and Kanai, Y. (2004). The ancillary proteins of HATs: SLC3 family of amino acid transporters. *Pflugers Arch*, 447, 490–494.

238. Palacin, M., Nunes, V., Font-Llitjos, M., Jimenez-Vidal, M., Fort, J., Gasol, E., et al. (2005). The genetics of heteromeric amino acid transporters. *Physiology*, 112–124.

239. Panchal, II., Badeliya, S.N., Patel, R., Patel, A., Devaligar, A. (2019). In silico Analysis and Molecular Docking Studies of Novel 4-Amino-3- (Isoquinolin-4-yl)-1H-Pyrazolo[3,4-d]Pyrimidine Derivatives as Dual PI3-K/mTOR Inhibitors. *Current Drug Discovery Technologies*, 16, 297–306.

240. Park, I., Bok, R., Ozawa, T., Phillips, J.J., et al. (2011). Detection of early response to temozolomide treatment in brain tumors using hyperpolarized 13C MR metabolic imaging. *Journal of Magnetic Resonance Imaging*, 33, 1284-1290.

241. Parker, S.J., Amendola, C.R., Hollinshead, K.E.R., Yu, Q., et al. (2020). Selective alanine transporter utilization creates a targetable metabolic niche in pancreatic cancer. *Cancer Discov*, 10, 1-20.

242. Pelander, A., Ojanperä, I., Laks, S., Rasanen, I., Vuori, E. (2003). Toxicological screening with formula-based metabolite identification by liquid chromatography/time-of-flight mass spectrometry. *Analytical Chemistry*, 75, 5710–5718.

243. Peterson, T.R., Laplante, M., Thoreen, C.C., Sancak, Y., Kang, S.A., Kuehl, W.M., Gray, N.S., Sabatini, D.M. (2009). DEPTOR is an mTOR inhibitor frequently overexpressed in multiple myeloma cells and required for their survival. *Cell*, 137, 873-886.

244. Pike, K.G., Malagu, K., Hummersone, M.G., Menear, K.A., Duggan, H.M., Gomez, S., Martin, N.M., Ruston, L., Pass, S.L., Pass, M. (2013). Optimization of potent and selective dual mTORC1 and mTORC2 inhibitors: the discovery of AZD8055 and AZD2014. *Bioorg Med Chem Lett*, 23, 1212–1216.

245. Pioro, E.P., Majors, A.W., Mitsumoto, H., Nelson, D.R., Ng, T.C. (1999). 1H-MRS evidence of neurodegeneration and excess glutamate + glutamine in ALS medulla. *Neurology*, 53, 71-79.

246. Ploessl, K., Wang, L., Lieberman, B.P., Qu, W., Kung, H.F. (2012). Comparative evaluation of 18F-labeled glutamic acid and glutamine as tumor metabolic imaging agents. *J. Nucl. Med*, 53, 1616-1624.

247. Pochini, L., Scalise, M., Galluccio, M., and Indiveri, C. (2014). Membrane transporters for the special amino acid glutamine: structure/function relationships and relevance to human health. *Front Chem*, 2:61.

248. Podo, F. (1999). Tumour phospholipid metabolism. *NMR in Biomedicine*, 12, 413-439.

249. Pompella, A., Visvikis, A., Paolicchi, A., De Tata, V., Casini, A.F. (2003). The changing faces of glutathione, a cellular protagonist. *Biochemical Pharmacology*, 66, 1499–503.

250. Porstmann, T., Santos, C.R., Griffiths, B., Cully, M., Wu, M., Leevers, S., Griffiths, J.R., Chung, Y.L., Schulze, A. (2008). SREBP activity is regulated by mTORC1 and contributes to Akt-dependent cell growth. *Cell Metab*, 8, 224-236.

251. Pourdehnab, M., Truitt, M.L., Siddiqi, I.M., Ducker, G.S., Shokat, K.M., Ruggero, D. (2013). Myc and mTOR converge on a common node in protein synthesis control that confers synthetic lethality in Myc-driven cancers. *PNAS*, 110, 11988-11993.

252. Prasad, P. D., Wang, H., Huang, W., Kekuda, R., Rajan, D. P., Leibach, F. H., et al. (1999). Human LAT1, a subunit of system L amino acid transporter: molecular cloning and transport function. *Biochem. Biophys. Res* Commun, 255, 283–288.

253. Pujade-Lauraine, E., Hilpert, F., Weber, B., Reuss, A., et al. (2014). Bevacizumab combined with chemotherapy for platinum-resistant recurrent ovarian cancer: The AURELIA open-label randomized phase III trial. *J Clin Oncol*, 32, 1302–1308.

254. Qing, G., Li, B., Vu, A., Skuli, N., et al. (2012). ATF4 regulates MYC-mediated neuroblastoma cell death upon glutamine deprivation. *Cancer Cell*, 22, 631-44.

255. Qing,G., , Li,B., Vu, A., Skuli, N. et al. (2012). ATF4 Regulates MYC-mediated Neuroblastoma Cell Death upon Glutamine Deprivation. *Cancer Cell*, 22631–644.

256. Qu, W., Zha, Z., Ploessl, K., et al. (2011). Synthesis of optically pure 4-fluoro-glutamine as potential metabolic imaging agents for tumours. *J Am Chem Soc*, 133, 1122-1133.

257. Rajagopalan, K.N., DeBerardinis, R.J. (2011). Role of glutamine in cancer: therapeutic and imaging implications. *J Nucl Med*, 52, 1005-1008.

258. Ramadan, S., Lin, A., Stanwella, P. (2013). Glutamate and Glutamine: A Review of *In Vivo* MRS in the Human Brain. *NMR Biomed*, 26, 12.

259. Rana, P., Sripathy, G., Varshney, A., Kumar, P., Memita Devi, M., Marwaha, R.K., Tripathi, R.P., Khushu S. (2012). Phosphorous magnetic resonance spectroscopy-based skeletal muscle bioenergetic studies in subclinical hypothyroidism. *J Endocrinol Invest*, 35, 129-34.

260. Ransohoff, D.F. (2004). Rules of evidence for cancer molecular-marker discovery and validation. *Nat Rev Cancer*, 4, 309-314.

261. Rapp, U.R., Korn, C., Ceteci, F., Karreman, C., Luetkenhaus, K., et al. (2009). Myc Is a Metastasis Gene for Non-Small-Cell Lung Cancer. *PLOS* ONE, 4(6): e6029.

262. Rata, M., Giles, S.L., deSouza, N.M., Leach, M.O., Payne, G.S. (2014). Comparison of three reference methods for the measurement of intracellular pH using 31P MRS in healthy volunteers and patients with lymphoma. *NMR Biomed*, 27, 158-162.

263. Reed, J. C. (1994), Bcl-2 and the regulation of programmed cell death. *J. Cell Biol*, 124, 1-6.

264. Reiman, R.E., Huvos, A.G., Benua, R.S., Rosen, G., Gelbard, A.S., Laughlin, J.S. (1981). Quotient imaging with N-13 L-glutamate in osteogenic sarcoma: correlation with tumor viability. *Cancer*, 48, 1976–1981.

265. Reiman, R.E., Rosen, G., Gelbard, A.S., Benua, R.S., Laughlin, J.S. (1982). Imaging of primary Ewing sarcoma with N-13 L-glutamate. *Radiology*, 142, 495–500.

266. Rempel, A., Mathupala, S.P., Griffin, C.A., Hawkins, A.L., Pedersen, P.L. (1996). Glucose catabolism in cancer cells: amplification of the gene encoding type II hexokinase. *Cancer* Res, 56, 2468–2471.

267. Ren, P. *et al*. (2015). ATF4 and N-Myc coordinate glutamine metabolism in MYCN-amplified neuroblastoma cells through ASCT2 activation. *J. Pathol*, 235, 90–100.

268. Reske, S.N., Grillenberger, K.G., Glatting, G., et al. (1997). Overexpression of glucose transporter 1 and increased FDG uptake in pancreatic carcinoma. *J Nucl Med*, 38, 1344–1348.

269. Ritter, P. (1996). Biochemistry A foundation. Ch. 11. Brooks/Cole. Pacific Grove.

270. Robertson, J.P., Faulkner, A., Vernon, R.G. (1982). Regulation of glycolysis and fatty acid synthesis from glucose in sheep adipose tissue. *Biochem J*, 206, 577–586.

271. Robey, I.F, Stephen, R.M, Brown, K.S, Baggett, B.K, Gatenby, R.A, Gillies, R.J. (2008). Regulation of the Warburg effect in early-passage breast cancer cells. *Neoplasia*, 10, 745-756.

272. Rodrik-Outmezguine, V.S., Chandarlapaty, S., Pagano, N.C., Poulikakos, P.I., Scaltriti, M., Moskatel, E., et al. (2011) mTOR kinase inhibition causes feedback-dependent biphasic regulation of AKT signaling. *Cancer Discov*, 3, 248-259.

273. Roivainen, A., Kähkönen, E., Luoto, P., Borkowski, S., et al. (2013). Plasma pharmacokinetics, whole-body distribution, metabolism, and radiation dosimetry of 68Ga bombesin antagonist BAY 86-7548 in healthy men. *J Nucl Med*, 54, 867–72.

274. Ronen, S.M., Jackson, L.E., Belouche, M., Leach, M.O. (2001). Magnetic resonance detects changes in phosphocholine associated with Ras activation and inhibition in NIH 3T3 cells. *British Journal of Cancer*, 84, 691-696.

275. Ronen, S.M., Leach, M.O. (2001). Breast imaging technology: Imaging biochemistry-applications to breast cancer. *Breast Cancer Research*, 3, 36-40.

276. Rostom, A.Y., Powe, J., Kandil, A., Ezzat, A., Bakheet, S., el-Khwsky, F., el-Hussainy, G., Sorbris, R., Sjoklint, O. (1999). Positron emission tomography in breast cancer: a clinicopathological correlation of results. *Br J Radiol.*, 72, 1064–1068.

277. Roussel, T., Frydman, L., Bihan, D.L., Ciobanu, L. (2019). Brain sugar consumption during neuronal activation detected by CEST functional MRI at ultra-high magnetic fields. *Scientific Reports*, 9, 4423.

278. Ruvinsky, I., Meyuhas, O. (2006). Ribosomal protein S6 phosphorylation: From protein synthesis to cell size. *Trends Biochem Sci*, 31, 342-348.

279. Salminen, E., Hogg, A., Binns, D., Frydenberg, M., Hicks, R. (2002). Investigations with FDG-PET scanning in prostate cancer show limited value for clinical practice. *Acta Oncol*, 41, 425-429.

280. Saranovic, D.S., Stojiljkovic M. (2020) FDG PET/CT in TB: Mimics, Pitfalls, and Limitations. In: Sobic Saranovic D., Vorster M., Gambhir S., Pascual T. (eds) PET/CT in Tuberculosis. Clinicians' Guides to Radionuclide Hybrid Imaging. Springer, Cham.

281. Sarbassov, D.D., Ali, S.M., Kim, D.H., Guertin, D.A., Latek, R.R., Erdjument-Bromage, H., Tempst, P., Sabatini, D.M. (2004). Rictor, a novel binding partner of mTOR, defines a rapamycin-insensitive and raptorindependent pathway that regulates the cytoskeleton. *Curr. Biol*, 14, 1296-1302.

282. Sarbassov, D.D., Guertin, D.A., Ali, S.M., Sabatini, D.M. (2005). Phosphorylation and regulation of Akt/PKB by the rictor-mTOR complex. *Science*, 307, 1098-1101.

283. Schmidt, E.V. (2004). The role of c-myc in regulation of translation initiation. *Oncogene*, 23, 3217-3221.

284. Schneider, J., Centeno, M., Rodriguez-Escudero, F., Efferth, T., Mattern, J., Volm, M. (1993). High rate of expression of multidrug resistance-associated P-glycoprotein in human endometrial carcinoma and normal endometrial tissue. *European Journal of Cancer*, 29, 554–8.

285. Schulte, M.L., Fu, A., Zhao, P., Li, J., et al. (2018). Pharmacological Blockade of ASCT2-dependent Glutamine Transport Leads To Anti-tumor Efficacy in Preclinical Models. *Nat Med*, 24, 194–202.

286. Schwab, M., Alitalo, K., Klempnauer, K.H., Varmus, H.E., Bishop, J.M., Gilbert, F., et al. (1983). Amplified DNA with limited homology to myc cellular oncogene is shared by human neuroblastoma cell lines and a neuroblastoma tumour. *Nature*, 305, 245–8.

287. Semenza, G.L. (2008). Tumor metabolism: cancer cells give and take lactate. *J Clin Invest*, 118, 3835-3837.

288. Sener, A. and Malaisse, W. (1980). L-leucine and a nonmetabolized analogue activate pancreatic islet glutamate dehydrogenase. *Nature*, 288, 187-189.

289. Serrano, M., Lin, A.W., McCurrach, M.E., Beach, D., Lowe, S.W. (1997). Oncogeneic ras provokes premature cell senescence associated with accumulation of p53 and p16INK4a. *Cell*, 88, 593-602.

290. Shanware, N.P., Mullen, A.R., DeBerardinis, R.J., Abraham, R.T. (2011). Glutamine: pleiotropic roles in tumor growth and stress resistance. *J Mol Med*, 89, 229-236.

291. Shen, G., Liu, J., Jiang, X., Li, F., Zeng, H., Huang, R., Kuang, A. (2018). ^{18}F-FDG PET/CT is still a useful tool in detection of metastatic extent in patients with high risk prostate cancer. *Int J Clin Exp Med*, 11, 6905-6913.

292. Shroff, E.H., Eberlin, L.S., Dang, V.M., Gouw, A.M., et al. (2015). MYC oncogene overexpression drives renal cell carcinoma in a mouse model through glutamine metabolism. *Proceedings of the National Academy of Sciences*, 112, 6539-6544.

293. Simon-Manso, Y., Lowenthal, M.S., Kilpatrick, L.E., Sampson, M.L., et al. (2013). Metabolite profiling of a NIST standard reference material for human plasma (SRM 1950): GC-MS, LC-MS, NMR, and clinical laboratory analyses, libraries, and web-based resources. *Anal Chem*, 85, 11725–31.

294. Sitter, B., Sonnewald, U., Spraul, M., Fjosne, H.E., Gribbestad, I.S. (2002). High-resolution magic angle spinning MRS of breast cancer tissue. *NMR in Biomedicine*, 15, 327-337.

295. Skehan, P., Storeng, R., Scudiero, D., Monks, A., et al. (1990). New colorimetric cytotoxicity assay for anticancer-drug screenin. *J Natl Cancer Inst*, 82, 1107-1112.

296. Slomka, P.J., Pan, T., Germano, G. (2016). Recent advances and future progress in PET instrumentation. *Semin Nucl Med*, 46, 5–19.

297. Snyder, L.R., Kirkland, J.J., Dolan, J.W. (2009). Introduction to Modern Liquid Chromatography. John Wiley & Sons, New York.

298. Sonenberg, N., Hinnebusch, A.G. (2009). Regulation of translation initiation in eukaryotes: Mechanisms and biological targets. *Cell*, 136, 731-745.

299. Sonveaux, P., Végran, F., Schroeder, T., Wergin, M.C., Verrax, J., Rabbani, Z.N. (2008). Targeting lactate-fueled respiration selectively kills hypoxic tumor cells in mice. *J Clin Invest*, 118, 3930-3942.

300. Stanwell, P., Gluch, L., Clark, D., Tomanek, B., et al. (2005). Specificity of choline metabolites for in vivo diagnosis of breast cancer using 1H MRS at 1.5 T. *European Radiology*, 15, 1037-1043.

301. Steinberg, J.D., Vogel, W., Vegt, E. (2017). Factors influencing brown fat activation in FDG PET/CT: a retrospective analysis of 15,000+ cases. *Br J Radiol*, 90(1075), 20170093.

302. Stevens, A.N. (1987). NMR Spectroscopy: Application to Metabolic Research. *Functional Studies Using NMR*, 61-84.

303. Stewart, G.D., Gray, K., Pennington, C.J., Edwards, D.R., Riddick, A.C., Ross, J.A., Habib, F.K. (2008). Analysis of hypoxia-associated gene expression in prostate cancer: lysyl oxidase and glucose transporter-1 expression correlate with Gleason score. *Oncol Rep*, 20, 1561-1567.

304. Sumner, L.W., Mendes, P., Dixon, R.A. (2003). Plant metabolomics: large-scale phytochemistry in the functional genomics era. *Phytochemistry*, 62:817–836.

305. Sun, H., Yu, T., Li, J. (2011). Co-administration of perifosine with paclitaxel synergistically induces apoptosis in ovarian cancer cells: more than just AKT inhibition. *Cancer Lett*, 310, 118–128.

306. Sunaga, N., Oriuchi, N., Kaira, K., Yanagitani, N., et al. (2008). Usefulness of FDG-PET for early prediction of the response to gefitinib in non-small cell lung cancer. *Lung cancer*, 59, 203-210.

307. Suzuki, S., Tanaka, T., Poyurovsky, M.V., Nagano, H., et al. (2010). Phosphate-activated glutaminase (GLS2), a p53- inducible regulator of glutamine metabolism and reactive oxygen species. *Proc. Natl. Acad. Sci. U. S. A*., 107, 7461–7466.

308. Świątkiewicz, M., Fiedorowicz, M., Orzeł, J., Wełniak-Kamińska, M., Bogorodzki, P., Langfort, J., Grieb, P. (2017). ncreases in Brain ^{1}H-MR Glutamine and Glutamate Signals Following Acute Exhaustive Endurance Exercise in the Rat. *Front Physiol*, 8, 19.

309. Sze, D.Y., Jardetzky, O. (1990). Characterization of lipid composition in stimulated human lymphocytes by 1H-NMR. *Biochimica et Biophysica Acta (BBA) – Molecular Cell Reseach*, 1054, 198-206.

310. Szeliga, M., Obara-Michlewska, M. (2009). Glutamine in neoplastic cells: focus on the expression and roles of glutaminases. *Neurochem Int*, 55,71-75.

311. Tanaka, K., Sasayama, T., Irino, Y., Takata, K., et al. (2015). Compensatory glutamine metabolism promotes glioblastoma resistance to mTOR inhibitor treatment. *The journal of Clinical Investigation*, 125, 1591-1602.

312. Tanneeru, K., Guruprasad, L. (2011). Ligand-based 3-D pharmacophore generation and molecular docking of mTOR kinase inhibitors. *Journal of Molecular Modeling*, 18, 1611–24.

313. Tennant, D., Duran, R., Boulahbel, H. and Gottlieb, E. (2009). Metabolic transformation in cancer. *Carcinogenesis*, 30, 1269-1280.

314. Thomas, M.A., Nagarajan, R., Huda, A., Margolis, D., et al. (2014). Multidimensional MR spectroscopic imaging of prostate cancer in vivo. *NMR in Biomedicine*, 27, 53-66.

315. Thompson, C. (2009). Metabolic enzymes as oncogenes or tumor suppressors. *N Engl J Med*, 360, 813-815.

316. Tognarelli, J.M., Dawood, M., Shariff, M.I.F., Grover, V.P.B., Crossey, M.M.E., Cox, I.J., Taylor-Robinson, S.D., McPhail, M.J.W. (2015). Magnetic Resonance Spectroscopy: Principles and Techniques: Lessons for Clinicians. *Journal of Clinical and Experimental Hepatology*, 5, 320-328.

317. Tong, X., Zhao, F., Thompson, C.B. (2009). The molecular determinants of de novo nucleotide biosynthesis in cancer cells. *Curr Opin Genet Dev*, 19, 32-37.

318. Torizuka, T., Clavo, A.C., Wahl, R.L. (1997). Effect of hyperglycemia on in vitro tumor uptake of tritiated FDG, thymidine, L-methionine and L-leucine. *J Nucl Med*, 38, 382–386.

319. Torizuka, T., Tamaki, N., Inokuma ,T., et al. (1995). In vivo assessment of glucose metabolism in hepatocellular carcinoma with FDG-PET. *J Nucl Med*, 36, 1811–1817.

320. Trukington, T.G., Coleman, R.E. (2002). Clinical oncologic PET: An Introduction. *Semin Roentgenol*, 37, 102-109.

321. Tsai, I-L, Weng, T-I., Tseng, Y.J., Tan, H.K-L, Sun, H-J, Kuo, C-H. (2013). Screening and confirmation of 62 drugs of abuse and metabolites in urine by ultra-high-performance liquid chromatography-quadrupole time-of-flight mass spectrometry. *Journal of Analytical Toxicology*, 37, 642–651.

322. Tsunoda, Y., Ito, M., Fujii, H., Kuwano, H., Saito, N. (2008). Preoperative diagnosis of lymph node metastases of colorectal cancer by FDG-PET/CT. *Jpn J Clin Oncol*, 38, 347–53.

323. Tyagi, R.K., Azrad, A., Degani, H., Salomon, Y. (1996). Simultaneous extraction of cellular lipids and water-soluble metabolites: Evaluation by NMR spectroscopy. *Magnetic Resonance in Medicine*, 35, 194-200.

324. Uehara, T., Kikuchi, H., Miyazaki, S., Iino, I., et al. (2015). Overexpression of lysophosphatidylcholine acyltransferase 1 and concomitant lipid alterations in gastric cancer. *Annals of Surgical Oncology*, 1-8.

325. Vaalburg, W., Coenen, H.H., Crouzel, C., Elsinga, P.H., Långström, B., Lemaire, C., Meyer, G.J. (1992). Amino acids for the measurement of protein synthesis in vivo by PET. Int. *J. Rad. Appl. Instrum. B*, 19, 227–237.

326. Vali, R., Loidl, W., Pirich, C., Langesteger, W., Beheshti, M. (2015). Imaging of prostate cancer with PET/CT using (18)F-Fluorocholine. *American Journal of Nuclear Medicine and Molecular Imaging*, 5, 96-108.

327. van der Hoeven, J.J., Hoekstra, O.S., Comans, E.F., Pijpers, R., Boom, R.P., van Geldere, D., Meijer, S., Lammertsma, A.A., Teule, G.J. (2002). Determinants of diagnostic performance of [F-18]fluorodeoxyglucose positron emission tomography for axillary staging in breast cancer. *Ann Surg*., 236, 619–624.

328. Vaysse, P-M, Heeren, R.M.A., Portaand, T., Balluff, B. (2017). Mass spectrometry imaging for clinical research – latest developments, applications, and current limitations. *Analyst*, 142, 2690-2712.

329. Venneti, S., Dunphy, M.P., Zhang, H., et al. (2015). Glutamine-based PET imaging facilitates enhanced metabolic evaluation of gliomas in vivo. *Sci Transl Med*, 7, 274ra17.

330. Verrey, F., Closs, E. I., Wagner, C. A., Palacin, M., Endou, H., and Kanai, Y. (2004). CATs and HATs: the SLC7 family of amino acid transporters. *Pflugers Arch*, 447, 532–542.

331. Viglianti, B.L., Wong, K.K., Gross, M.D., Wale, D.J. (2018). Common Pitfalls in Oncologic FDG PET/CT Imaging. *J Am Osteopath Coll Radiol*, 7, 5-17.

332. Vöö S., Bomanji J. (2019) ^{18}F-FDG PET/CT Indications, Pitfalls and Limitations in Brain Imaging. In: Fraioli F. (eds) PET/CT in Brain Disorders. Clinicians' Guides to Radionuclide Hybrid Imaging. Springer, Cham.

333. Wagner, C. A., Lang, F., and Broer, S. (2001). Function and structure of heterodimeric amino acid transporters. *Am J Physiol Cell Physiol*, 281, C1077–C1093.

334. Wahl, R.L., Cody, R.L., Hutchins, G.D., Mudgett, E.E. (1991). Primary and metastatic breast carcinoma: initial clinical evaluation with PET with the radiolabeled glucose analogue 2-[F-18]-fluoro-2-deoxy-d-glucose. *Radiology*, 179, 765–770.

335. Wahl, R.L., Henry, C.A., Ethier, S.P. (1992). Serum glucose: effects on tumor and normal tissue accumulation of 2-[F-18]-fluoro-2-deoxy-D-glucose in rodents with mammary carcinoma. *Radiology*, 183, 643–647.

336. Wang, J., Qiu, S., Chen, S., Xiong, C., et al. (2015). MALDI-TOF MS imaging of metabolites with a N-(1-naphthyl) ethylenediamine dihydrochloride matrix and its application to colorectal cancer liver metastasis. *Analytical Chemistry*, 87, 422-430.

337. Wang, J.B., Erickson, J.W., Fuji, R., Ramachandran, S., et al. (2010). Targeting mitochondrial glutaminase activity inhibits oncogenic transformation. *Cancer Cell*, 18, 207–219.

338. Wang, Q., Hardie, R.A., Hoy, A.J., van Geldermalsen, M., Gao, D., Fazli, L., Sadowski, M.C., Balabanm S., Schreuder, M., Nagarajah, R., et al. (2015). Targeting ASCT2-mediated glutamine uptake blocks prostate cancer growth and tumour development. J. Pathol., 236, 278-289.

339. Wang, X., Proud, C.G. (2006) The mTOR pathway in the control of protein synthesis. *Physiology (Bethesda)*, 21, 362–369.

340. Waterhouse, C., Jeanpretre, N., Keilson, J. (1979). Gluconeogenesis from Alanine in Patients with Progressive Malignant Disease. *Cancer Res*, 39, 1968-1972.

341. Wellner, V.P., Zoukis, M., Meister, A. (1966). Activity of glutamine synthetase toward the optical isomers of α-aminoadipic acid. *Biochemistry*, 5, 3509–3514.

342. Wendel, H., Stanchina, E., Fridman, J., Malina, A., et al. (2004) Survival signalling by Akt and eIF4E in oncogenesis and cancer therapy. *Nature*, 428, 332–337.

343. White, M.A., Lin, C., Rajapakshe, K., Dong, J. et al. (2017). Glutamine Transporters Are Targets of Multiple Oncogenic Signaling Pathways in Prostate Cancer. *Mol Cancer* Res, 15, 1017-1028.

344. Whitelaw, B.S., Robinson, M.B. (2013). Inhibitors of glutamate dehydrogenase block sodium-dependent glutamate uptake in rat brain membranes. *Front. Endocrinol*, 4, 123.

345. Wilson, D.M., Keshari, K.R., Larson, P.E.Z., Chen, A.P. et al. (2010). Multi-compound polarization by DNP allows simultaneous assessment of multiple enzymatic activities in vivo. *Journal of Magnetic Resonance*, 205, 141-147.

346. Wise, D.R and Thompson, C.B. (2010). Glutamine addiction: a new therapeutic target in cancer. *Trends Biochem Sci.*, 35, 427-433.

347. Wise, D.R., DeBerardinis, R.J., Mancuso, A., Sayed, N., Zhang, X-Y, Pfeiffer, H.K., et al. (2008). Myc regulates a transcriptional program that stimulates mitochondrial glutaminolysis and leads to glutamine addiction. *Proc Natl Acad Sci*, 105, 18782-18787.

348. Wishart, D.S., Jewison, T., Guo, A.C., Wilson, M., et al. (2013). HMDB 3.0 – The Human Metabolome Database in 2013. *Nucleic Acids Research*, 41, D801-D807.

349. Wishart, D.S., Knox, C., Guo, A.C., Eisner, R., et al. (2009). HMDB: a knowledgebase for the human metabolome. *Nucleic Acids Research*, 37, D603-D610.

350. Witney, T.H., Kettunen, M.I., Brindle, K.M. (2011). Kinetic modelling of hyperpolarized 13C label exchange between pyruvate and lactate in tumour cells. *Journal of Biological Chemistry*, 286, 24572-24580.

351. Wolf, W., Presant, C.A., Servis, K.L., el-Tahtawy, A., Albright, M.J., Barker, P.B., Ring, R., Atkinson, D., Ong, R., King, M. (1990). Tumor trapping of 5-fluorouracil: in vivo 19F NMR spectroscopic pharmacokinetics in tumor-bearing humans and rabbits. *PNAS*, 87, 492-496.

352. Wolf, W., Presant, C.A., Waluch, V. (2000). ^{19}F-MRS studies of fluorinated drugs in humans. *Advanced Drug Delivery Reviews*, 41, 55–74.

353. Wolfson, R.L., Chantranupong, L., Saxton, R.A., Shen, K., Scaria, S.M., Cantor, J.R., Sabatini, D.M. (2016). Sestrin2 is a leucine sensor for the mTORC1 pathway. *Science*, 351, 43–48.

354. Wong, A-C.T.F, Thavasu, P., Gagrica, S., Swales, K.E., et al. (2017). Evaluation of the combination of the dual m-TORC1/2 inhibitor vistusertib (AZD2014) and paclitaxel in ovarian cancer models. *Oncotarget*, 8, 113874-113884.

355. Wong, D.T., Fuller, R.W., Molloy, B.B. (1973). Inhibition of amino acid transaminases by L-cycloserine. *Advances in Enzyme Regulations*, 11, 139-154.

356. Workman, P., Aboagye, E.O., Balkwill, F., Balmain, A., et al. (2010). Guidelines for the welfare and use of animals in cancer research. *British Journal of Cancer*

357. World Health Organisation (2011). The Global Burden of Disease: 2004 Update. Geneva.

358. Wu, W., Platoshyn, O., Firth, A.L., Yuan, J.X. (2007). Hypoxia divergently regulates production of reactive oxygen species in human pulmonary and coronary artery smooth muscle cells. *Am J Physiol Lung Cell Mol Physiol*, 293, L952–959.

359. Yanagida, O., Kanai, Y., Chairoungdua, A., Kim, D., et al. (2001). Human L-type amino acid transporter 1 (LAT1): characterization of function and expression in tumour cell lines. *Biochim Biophys Acta*, 1514, 291-302.

360. Yang, C., Sudderth, J., Dang, T., Bachoo, R.M., McDonald, J.G., DeBerardinis, R.J. (2009). Glioblastoma cells require glutamate dehydrogenase to survive impairments of glucose metabolism or Akt signaling. *Cancer Res*, 69, 7986–93.

361. Yecies, J. and Manning, B. (2011). mTOR links oncogenic signalling to tumour cell metabolism. *J. Mol. Med*, 89, 221-228.

362. Yernool, D., Boudker, O., Yan, J. and Eric, G. (2004). Structure of a glutamate transporter homologue from Pyrococcus horikoshii. *Nature.* 431, 811-818.

363. Yu, X., Li, X., Song, X., Dai, D., Zhu, L., Zhu, Y., Wang, J., Zhao, H., Xu, W. (2016). Advantages and disadvantages of F-18 fluorodeoxyglucose positron emission tomography/computed tomography in carcinoma of unknown primary. *Onco Lett*, 12, 3785–3792.

364. Yuneva, M.O., Fan, T.W., Allen, T.D., Higashi, R.M., et al. (2012). The metabolic profile of tumors depends on both the responsible genetic lesion and tissue type. *Cell Metab*, 15, 157–170.

365. Zaytsevaa, Y.Y., Valentino, J.D., Gulhati, P., Eversab, B.M. (2012). mTOR inhibitors in cancer therapy. *Cancer Letters*, 319, 1-7.

366. Zeller, K.I., Jegga, A.G., Aronow, B.J., O'Donnell, K.A., Dang, C.V. (2003). An integrated database of genes responsive to the Myc oncogenic transcription factor: Identification of direct genomic targets. *Genome Biol*, 4, pR69.

367. Zhang, J., Maniawski, P., Knopp, M.V. (2018). Performance evaluation of the next generation solid-state digital photon counting PET/CT system. *EJNMMI Res*, 8, 97.

368. Zhang, Y-J., Duan, Y., Zheng, X.F.S. (2011). Targeting the mTOR kinase domain: The second generation of mTOR inhibitors". *Drug Discovery Today*, 16, 325–31.

369. Zhao, X., Han, Q., Gang, X., Wang, G. (2018). Altered brain metabolites in patients with diabetes mellitus and related complications – evidence from ^{1}H MRS study. *Biosci Rep*, 38, BSR20180660

370. Zhou R, Pantel A, Li S, Lieberman B, Ploessl K, Choi H, et al. (2017). [18F](2S,4R)4-Fluoroglutamine PET Detects Glutamine Pool Size Changes in Triple-Negative Breast Cancer in Response to Glutaminase Inhibition. *Cancer Res*, 77, 1476-1484.

371. Zhu, A., Lee, D., Shim, H. (2011). Metabolic PET imaging in cancer detection and therapy response. *Seminars in Oncology*, 38, 55-69.

372. Zhu, H., Xu, X., Liu, T., Guo, X., et al. (2019). Comparison between (2S,4R)4-[^{18}F]fluoroglutamine and [^{18}F]-FDG PET imaging of liver cancer from HepG-2 cell to patient. *J Nucl Med*, 60, 1409S.

373. Zhu, L., Ploessl, K., Zhou, R., Mankoff, D., Kung, H.F. (2017). Metabolic Imaging of Glutamine in Cancer. *J Nucl Med*, 58, 533–537.

374. Zindy, F., Eischen, C.M., Randle, D.H., et al. (1998). Myc signalling via the ARF tumour suppressor regulates p53-dependent apoptosis and immortalization. *Genes Dev*, 12, 2424-2433.

375. Zoncu, R., Efeyan, A., Sabatini, D.M. (2010). mTOR: From growth signal integration to cancer, diabetes and ageing. *Nat Rev Mol Cell Biol*, 12, 21–35.

List of Conferences and Meetings

Conferences and Meetings	Year
London Metabolic Network Meeting	2017
Royal Society Chemical Biology Conference	2017
BCISMRM post-graduate meeting	2017
CRUK CIC Annual Imaging Conference	2017
ICR Annual Conference	2017
NCRI Conference	2018
ICR Annual Conference	2018
ICR Annual Conference	2019
WMIC Conference	2019
AACR Annual Virtual Meeting	2020
ICR Annual Virtual Conference	2020
WMIC Virtual Conference	2020